7848-5-Q

A STUDY OF AN INTERDIGITAL ARRAY ANTENNA

Fifth Quarterly Report
1 February through 31 March 1967

by

Pei Rin Wu

May 1967

A dissertation submitted in partial fulfillment
of the requirements for the degree of
Doctor of Philosophy in
The University of Michigan
1966

Contract No. AF 33(615)-3609
Project 6278, Task 01
O.E. Horton, Project Monitor
AVWE

Air Force Avionics Laboratory
Research and Technology Division
Air Force Systems Command
Wright-Patterson Air Force Base, Ohio

FOREWORD

This report, 7848-5-Q, was prepared by The University of Michigan Radiation Laboratory , Department of Electrical Engineering under the direction of Professor Ralph E. Hiatt and Professor John A. M. Lyon on Air Force Contract AF 33(615)-3609, under Task 627801 of Project 6278, "Study and Investigation of UHF-VHF Antennas (U)". The work was administered under the direction of the Air Force Avionics Laboratory, Wright-Patterson AFB, Ohio. The Task Engineer was Mr. Olin E. Horton, the Project Engineer, Mr. E. M. Turner.

This report covers the period 1 February through 31 March 1967

ACKNOWLEDGMENT

The author wishes to acknowledge the valuable help and encouragement of his thesis chairman, Professor John A. M. Lyon as well as the members of the committee for their helpful suggestions. The author is also indebted to Mr. P. H. Wilcox for the computations and Mr. U. E. Gilreath for assisting in the fabrication and measurement of the experimental models.

TABLE OF CONTENTS

LIST OF ILLUSTRATIONS

Chapter IV

ABSTRACT

An interdigital array antenna has been devised and studied in this work as a useful antenna for certain applications. The theory of the linear antenna was used in the theoretical analysis to obtain the dispersion relation for a source free infinite interdigital array. In carrying out this analysis, the antenna-wave theory concept was used. This is essential if Floquet's Theorem is to be applied along with the antenna theory. The approximate solutions were obtained numerically through the use of the digital computer. The input impedance and the radiation pattern were also formulated for a finite array of 2N+1 elements with a voltage source applied between the ground plane and the grounded end of the center element of the array. The expressions were then computed numerically, through the computer, for an approximate solution.

It is found that an interdigital array antenna has a fairly wide frequency band for its broadside radiation at low frequencies. The field is polarized in a plane parallel to the plane containing the elements and perpendicular to the axis of the array along which the elements are spaced. The input resistance has been found to be 500 ohms. However, when the frequency is increased and the length of each array element exceeds one quarter free space wavelength, the radiation pattern becomes twin lobed symmetrical about the broadside axis with the input resistance fluctuating between 50 and 100 ohms.

Several experimental models with 13, 14, 17 and 21 array elements were constructed and tested. The comparison between the theoretical dispersion characteristics and the experimental results after a correction for overall resonant length is close within the experimental error. The agreement between the theoretical solution and the experimental measurement of input impedance is reasonably good since the theory is based on an assumed current distribution. The vertical sections were not considered in the analysis. In view of this, an extended effort was given to experimental studies to determine the mechanism of the radiation and the input impedance characteristics for both broadside and twin lobe radiation.

CHAPTER I

INTRODUCTION AND STATEMENT OF THE PROBLEM

The main objective of the interdigital array antenna is to obtain a broadband low profile radiator of small electrical size and adaptable for possible airborne application. It is felt that if a structure can be constructed in such a manner that broadband radiation can be obtained when the structure is excited at one quarter-wave length instead of one half-wave length like the Yagi-Uda structures, then an electrically small antenna will be possible. The radiating property of the structure as an antenna should not be very much inferior to that of a Yagi-Uda structure.

The interdigital-line structure was first proposed by Fletcher[8] to be used as a slow wave device in a travelling wave amplifier for a reasonably wide band of operation. Later, it was compared with the other parallel line structures by Butcher[4], [5] and Pierce[24] for similar applications. Bolljahn and Matthaei[2] further developed the structure into a microwave band pass filter. However, all of the analyses were based on a closed structure, that is, between ground planes, and the possible use of such a structure as a radiator was not considered.

In treating the interdigital-line structure as an antenna, linear antenna theory[6], [9], [11], [16], [22], [29] is employed together with the methods developed by King and Sandler[12], King and Harrison[13], [14], Mailloux[19], [20] [21] and Tai[30], [31]. The concept of antenna-wave theory[19] was used to obtain the solution of an infinite interdigital array antenna which is essential if the Floquet's theorem is to be used. The outline of the present work is as follows. In Chapter II a source-free infinite array is analyzed and the dispersion characteristics are obtained by considering the periodic nature of the structure[1], [3], [25], [26], [28], [33]. Finite arrays of different elements are then analyzed in Chapter III, from which the impedance characteristics and the radiation patterns are obtained. Seven antennas were constructed and the experimental data are discussed in Chapter IV, including a comparison between theoretical and experimental results. Finally, the conclusion of the present work and comments on the future prospects are made in Chapter V.

CHAPTER II

A SOURCE-FREE INFINITE INTERDIGITAL ARRAY

2.1 Introduction.

The study of an infinite periodic structure by means of its dispersion characteristics is a powerful method for analyzing the performance of a finite length antenna structure[3], [25], [27], [28], [32], [33]. In order to understand the radiation property of the interdigital array antenna, it is, therefore, convenient to obtain the dispersion characteristics for a given set of parametric values. The basic assumptions made are:

(a) the infinite array is already excited by some external source and an unattenuated wave is propagated along the antenna surface;

(b) the field distribution near the surface of the structure is a TEM wave along the direction of the conductor;

(c) the line currents are induced along the axes of the cylindrical elements, and have a sinusoidal distribution which satisfies the interdigital boundary conditions;

(d) the vertical section of the conducting elements has negligible effect on the dispersion characteristics since they are much shorter in length and twice as far apart as the horizontal section of the conducting elements.

2.2 Formulation.

The geometry of an infinite interdigital array is shown in Figs. 2-1 and 2-2. It is seen that the interdigital array structure is a set of infinite parallel cylindrical conductors above the ground plane with alternate ends of the elements connected to the ground plane. At all points outside the conductor, the electric field may be expressed in terms of the scalar and vector potentials when the time dependence of $e^{j\omega t}$ is used:

$$\begin{aligned} E &= -\nabla\phi - j\omega A \\ &= -\frac{j\omega}{k_o^2}\left(\nabla\nabla\cdot A + k_o^2 A\right) \end{aligned} \tag{2.1}$$

where $k_o = \frac{\omega}{c} = \frac{2\pi}{\lambda}$, c = velocity of light in free space, λ=wave length, ω=angular

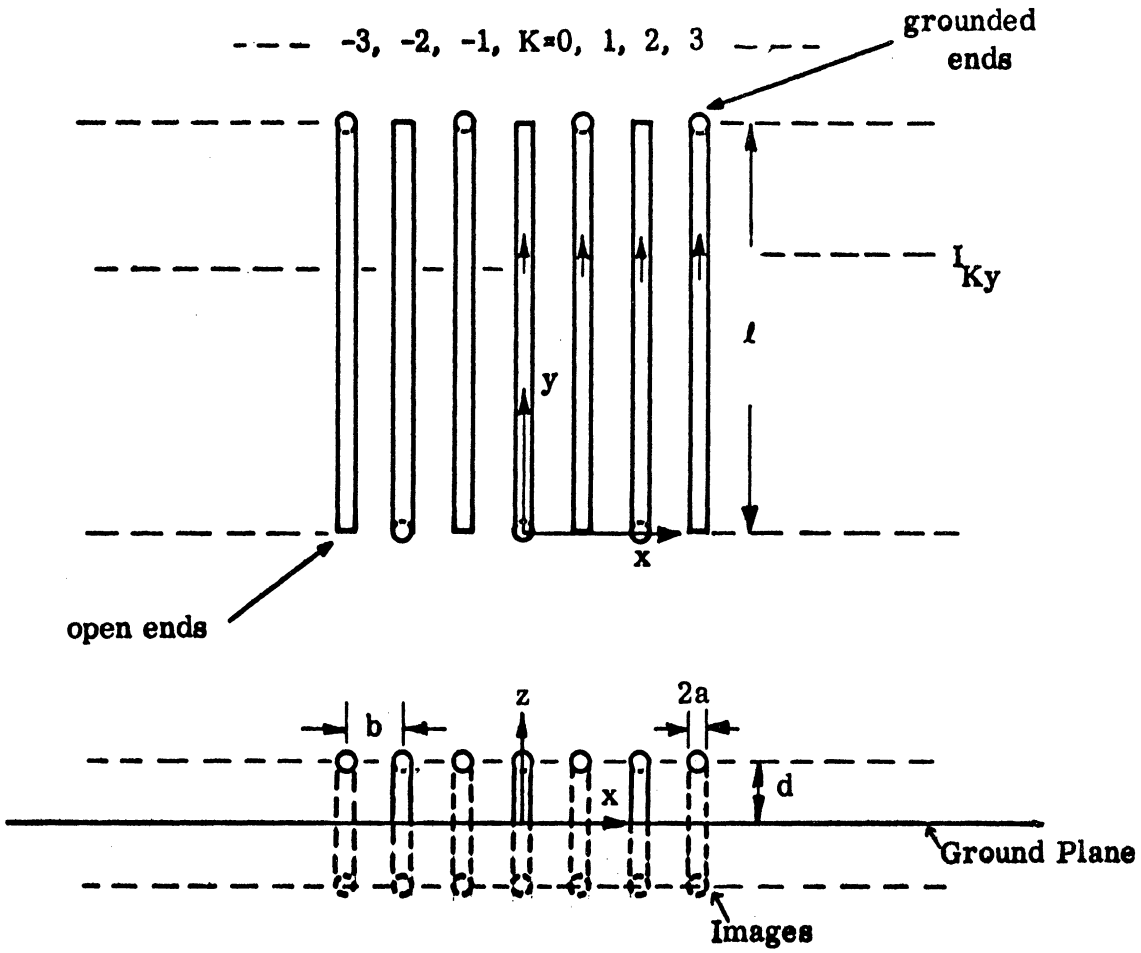

FIG. 2-1: A SOURCE FREE INFINITE INTERDIGITAL ARRAY ANTENNA.

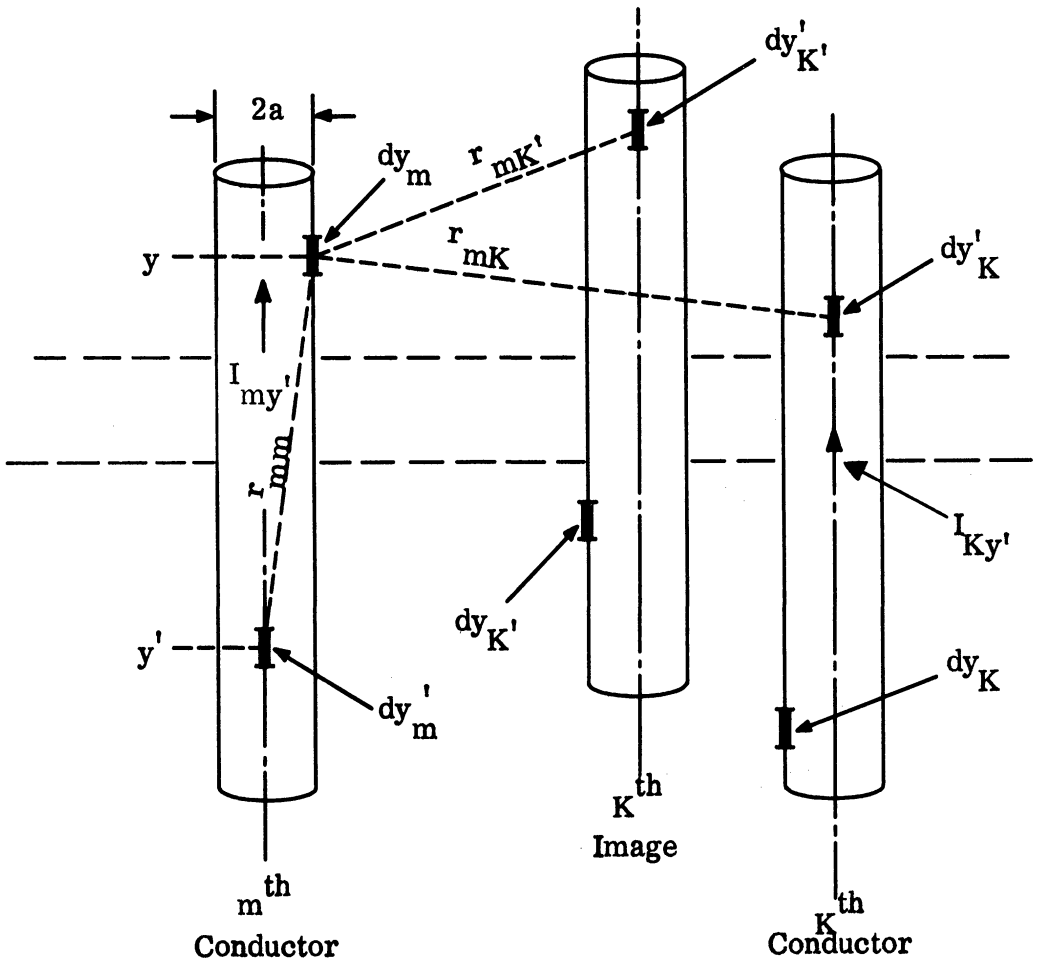

FIG. 2-2: THE GEOMETRY OF THE CONDUCTING ARRAY ELEMENTS.

frequency, ϕ = scalar potential, A = vector potential, and where use has been made of the definition

$$\nabla \cdot A + j\frac{k_o^2}{\omega}\phi = 0 \quad . \tag{2.2}$$

The y-component of (2.1) on the surface of the m^{th} antenna is

$$(E_{my})_{r=a} = -\frac{j\omega}{k_o^2}\left(\frac{\partial}{\partial y}\nabla \cdot A_m + k_o^2 A_{my}\right)_{r=a} \quad . \tag{2.3}$$

$$0 \leqslant y \leqslant \ell$$

Assuming a perfect conductor, the $(E_{my})_{r=a} = 0$ requirement gives

$$\frac{\partial}{\partial y}\nabla \cdot A_m + k_o^2 A_{my} = 0 \, . \tag{2.4}$$

This equation may be expanded into

$$\frac{\partial^2 A_{mx}}{\partial y \partial x} + \frac{\partial^2 A_{my}}{\partial y^2} + \frac{\partial^2 A_{mz}}{\partial y \partial z} + k_o^2 A_{my} = 0 \tag{2.5}$$

$$0 \leqslant y \leqslant \ell$$

For an idealized situation, both A_x and A_z are zero everywhere in space, so that (2.5) reduces to

$$\frac{\partial^2 A_{my}}{\partial y^2} + k_o^2 A_{my} = 0 \, , \qquad m=0, \pm 1, \pm 2, \ldots \tag{2.6}$$

at r=a

It is readily verified that

$$\left.\begin{aligned} A_{my}\Big|_{r=a} &= -\frac{j}{c}(C_m \cos k_o y + D_m \sin k_o y) \qquad \text{for m even,} \\ &= -\frac{j}{c}\left[C_m \cos k_o(\ell - y) + D_m \sin k_o(\ell - y)\right] \qquad \text{for m odd} \end{aligned}\right\} \tag{2.7}$$

are the solutions of (2.6); where C_m and D_m are arbitrary constants of integration. The factor $-\frac{j}{c}$ is included for later convenience, in order to make C_m and D_m have the dimensions of scalar potentials measured in volts. When the array is not excited by any voltage source, continuity of the scalar potential at y=0 for m even and $y=\ell$ for m odd requires that the D_m be zero. Thus, there results for an infinite source-free array:

$$\begin{aligned} A_{my}\Big|_{r=a} &= -\frac{j}{c} C_m \cos k_o y \qquad \text{for m even} \\ &= -\frac{j}{c} C_m \cos k_o(\ell - y) \qquad \text{for m odd} \end{aligned} \tag{2.8}$$

The vector potential at a point (a, y) just outside the surface of the m^{th} cylindrical conductor according to Hallén is approximately

$$A_{my} = \frac{\mu_o}{4\pi} \sum_{K=-\infty}^{K=\infty} \int_o^{\ell} I_{Ky'} \left(\frac{e^{-jk_o r_{mK}}}{r_{mK}} - \frac{e^{-jk_o r_{mK'}}}{r_{mK'}} \right) dy' \tag{2.9}$$

where, as shown in Fig. 2-2

$$r_{mK} = \sqrt{(y-y')^2 + (z-d)^2 + (x-Kb)^2}$$

$$r_{mK'} = \sqrt{(y-y')^2 + (z+d)^2 + (x-Kb)^2}$$

and $\mu_o = 4\pi \times 10^{-7}$ henry/meter, and where $I_{Ky'} = -I_{K'y}$ are the currents on K^{th} conductor and its image in the ground plane. Equations (2.8) and (2.9) form an infinite set of integral equations, viz.

$$A_{my}\Big|_{r=a} = \frac{\mu_o}{4\pi} \sum_{K=-\infty}^{K=\infty} \int_0^{\ell} I_{Ky'} \left(\frac{e^{-jk_o r_{mK}}}{r_{mK}} - \frac{e^{-jk_o r_{mK'}}}{r_{mK'}} \right) dy'$$

$$= -\frac{j}{c} \left[C_m \cos k_o y \right] \qquad \text{for } m \text{ even}$$

$$= -\frac{j}{c} \left[C_m \cos k_o (\ell - y) \right] \qquad \text{for } m \text{ odd} . \tag{2.10}$$

$$m = 0, \pm 1, \pm 2 \text{ -------}$$

The boundary conditions for an infinite interdigital array are given by

$$\left.\begin{aligned} I_{Ky}(y=0) &= 0 \qquad \text{for } K \text{ odd} \\ I_{Ky}(y=\ell) &= 0 \qquad \text{for } K \text{ even} . \end{aligned}\right\} \tag{2.11}$$

Now, assume that the infinite array has been excited by some external source and an unattenuated travelling wave is sustained on the surface of the array. Since the structure is periodic, Floquet's theorem[33] can be applied to relate the current induced in each conducting element; that is

$$I_{Ky}(y) = e^{-jK\psi} I_o f(y) \tag{2.12}$$

where 2ψ is the phase shift per section, I_o is the amplitude of the current induced on the zeroth element and $f(y)$ is the amplitude distribution function

of the current along the y-axis. Equation (2.12) shows that in a periodic structure, such as an infinite interdigital array, the current induced in each conducting element by an unattenuated wave propagating along the array can only be different by a constant phase shift per section, where each section contains a pair of cylindrical elements. This is a powerful theorem for wave phenomena in periodic structures. If (2.12) is applied to (2.9), the vector potential at a point (a, y) just outside the surface of the m^{th} cylindrical conductor is reduced to

$$A_y = \mu_o I_o \sum_{K=-\infty}^{K=+\infty} e^{-jK\psi} \int_o^{\ell} f(y')(G_{1y} - G_{2y})\, dy' \qquad (2.13)$$

where

$$\left.\begin{aligned} G_{1y} &= \frac{e^{-jk_o R_1}}{4\pi R_1} \\ G_{2y} &= \frac{e^{-jk_o R_2}}{4\pi R_2} \end{aligned}\right\} \qquad (2.14)$$

are free space Green's functions and where

$$\left.\begin{aligned} R_1 &= \sqrt{(y-y')^2 + a^2 + (Kb)^2} \\ R_2 &= \sqrt{(y-y')^2 + (a+2d)^2 + (Kb)^2} \end{aligned}\right\}$$

The subscript m was dropped from $A_{my}\big|_{r=a}$ because all such terms are identical once $f(y)$ is specified on a conducting element either by an actual distribution or by an assumed distribution.

The application of Floquet's theorem also makes the arbitrary constants C_m in (2.8) identical in each period, viz.

$$A_y = -\frac{j}{c}\left[C_e \cos k_o y\right] \quad \text{for m even}$$

$$= -\frac{j}{c}\left[C_o \cos k_o (\ell - y)\right] \quad \text{for m odd} \tag{2.15}$$

where C_e and C_o are arbitrary constants to be determined by the boundary conditions (2.11). Since the structure is symmetric about $y=\frac{\ell}{2}$, as can be seen from Eq. (2.15), the same result occurs whether m is odd or even, so the two solutions for (2.15) are identical, if they exist. In order to obtain a final form of the integral equation, the constants C_e and C_o must be evaluated. The boundary conditions given in (2.11) cannot be used directly because a small value of A_y exists at the end of the element even though $I_y=0$ is imposed. Therefore, it is assumed that the actual current I_y is proportional to $A_y - A_\ell$ when m is even and to $A_y - A_o$ when m is odd instead of just A_y alone[11] for a better approximation.

The evaluation of C_e and C_o can then proceed without actually solving the current I_y explicitly, using the method described by King[11], [15]. First form the functions $W_{ev}(y) = A_y - A_\ell$ and $W_{od}(y) = A_y - A_o$ to represent the distribution of the current along even and odd elements, respectively. A_ℓ and A_o can be obtained by letting $y=\ell$ for m even and $y=0$ for m odd in (2.13) and (2.15) as follows:

$$A_\ell\Big|_{m=even} = \mu_o I_o \sum_{K=-\infty}^{K=+\infty} e^{-jK\psi} \int_o^\ell f(y')(G_{1\ell} - G_{2\ell})\, dy'$$

$$= -\frac{j}{c}\left[C_e \cos k_o \ell\right] \tag{2.16}$$

and

$$A_o\Big|_{m=odd} = \mu_o I_o \sum_{K=-\infty}^{K=+\infty} e^{-jK\psi} \int_o^\ell f(y')(G_{1o} - G_{2o})\, dy'$$

$$= -\frac{j}{c}\left[C_o \cos k_o \ell\right] \tag{2.17}$$

where $G_{1\ell}$, $G_{2\ell}$, G_{1o} and G_{2o} are G_{1y}, G_{2y} as defined in (2.14) with all y's in the expressions been replaced by ℓ and o respectively.

From (2.16) and (2.17) the functions $W_{ev}(y)$ and $W_{od}(y)$ can be formed, that is,

$$W_{ev}(y) = A_y - A_\ell$$

$$= \mu_o I_o \sum_{K=-\infty}^{K=+\infty} e^{-jK\psi} \int_o^\ell f(y')(G_{1y} - G_{2y} - G_{1\ell} + G_{2\ell})\, dy'$$

$$= -\frac{j}{c} C_e \left[\cos k_o y - \cos k_o \ell\right] \tag{2.18}$$

and

$$W_{od}(y) = A_y - A_o$$

$$= \mu_o I_o \sum_{K=-\infty}^{K=+\infty} e^{-jK\psi} \int_o^{\ell} f(y')(G_{1y} - G_{2y} - G_{1o} + G_{2o})\, dy'$$

$$= -\frac{j}{c} C_o \left[\cos k_o(\ell - y) - \cos k_o \ell\right] \quad . \qquad (2.19)$$

The constants C_e and C_o are thus obtained from (2.18) and (2.19), respectively as follows

$$C_e = \frac{j\zeta_o I_o}{\cos k_o y - \cos k_o \ell} \sum_{K=-\infty}^{K=+\infty} e^{-jK\psi} \int_o^{\ell} f(y')(G_{1y} - G_{2y} - G_{1\ell} + G_{2\ell})\, dy' \qquad (2.20)$$

and

$$C_o = \frac{j\zeta_o I_o}{\cos k_o(\ell - y) - \cos k_o \ell} \sum_{K=-\infty}^{K=+\infty} e^{-jK\psi} \int_o^{\ell} f(y')(G_{1y} - G_{2y} - G_{1o} + G_{2o})\, dy' \qquad (2.21)$$

where $\zeta_o = \sqrt{\frac{\mu_o}{\epsilon_o}} = c\mu_o = 120\pi$.

Substituting (2.20) and (2.21) into (2.15) and combined with (2.13), there results

$$\sum_{K=-\infty}^{K=+\infty} e^{-jk\psi} \int_o^{\ell} f(y')(G_{1y} - G_{2y})\, dy'$$

$$= \frac{\cos k_o y}{\cos k_o y - \cos k_o \ell} \sum_{K=-\infty}^{K=+\infty} e^{-jK\psi} \int_o^{\ell} f(y')(G_{1y} - G_{2y} - G_{1\ell} + G_{2\ell})\, dy'$$

for m = even (2.22)

and

$$\sum_{K=-\infty}^{K=+\infty} e^{-jK\psi} \int_o^{\ell} f(y')(G_{1y} - G_{2y})\, dy'$$

$$= \frac{\cos k_o(\ell - y)}{\cos k_o(\ell - y) - \cos k_o y} \sum_{K=-\infty}^{K=+\infty} e^{-jK\psi} \int_o^{\ell} f(y')(G_{1y} - G_{2y} - G_{1o} + G_{2o})\, dy'$$

for m = odd (2.23)

Since (2.22) and (2.23) describe the symmetrical structure with the unknown phase shift constant ψ as a function of k_o and other physical parameters, and both expressions are interchangeable by shifting the reference coordinates, it is expected that they both will yield identical solutions, if the wave is to exist and be sustained along the array surface.

The current distribution function f(y) will have to be specified in order to solve (2.22) or (2.23). A sinusoidal distribution will be assumed for simplicity.

Let,

$$\begin{aligned} f(y) &= \sin k_o y && \text{for K odd,} \\ &= \sin k_o (\ell - y) && \text{for K even.} \end{aligned} \tag{2.24}$$

Substitution of (2.24) into (2.22) leads to the dispersion characteristics of the infinite interdigital array antenna. After many manipulations, the final forms of the dispersion relations are obtained.

$$\sum_{K=\text{ odd}} e^{-jK\psi} \Phi_{od} + \sum_{K=\text{ even}} e^{-jK\psi} \Phi_{ev} = 0 \tag{2.25}$$

where

$$\Phi_{od} = \frac{F_o(\ell)}{F_o(y)} \left[S_{b1}(\ell, y) - S_{b2}(\ell, y)\right] - S_{b1}(\ell, \ell) + S_{b2}(\ell, \ell) \tag{2.26}$$

$$\begin{aligned} \Phi_{ev} = \frac{F_o(\ell)}{F_o(y)} &\left\{G_o(\ell) \left[C_{b1}(\ell, y) - C_{b2}(\ell, y)\right]\right. \\ &\left. - F_o(\ell) \left[S_{b1}(\ell, y) - S_{b2}(\ell, y)\right]\right\} \\ &- G_o(\ell) \left[C_{b1}(\ell, \ell) - C_{b2}(\ell, \ell)\right] \\ &+ F_o(\ell) \left[S_{b1}(\ell, \ell) - S_{b2}(\ell, \ell)\right] \end{aligned} \tag{2.27}$$

$$\left.\begin{aligned} F_o(y) &= \cos k_o y \\ G_o(y) &= \sin k_o y \end{aligned}\right\} \tag{2.28}$$

$$\left.\begin{aligned} S_{b1}(\ell, y) &= \int_o^{\ell} \sin k_o y' \; G_{1y} \, dy' \\ 2 & \qquad\qquad\quad 2y \\ S_{b1}(\ell, \ell) &= \int_o^{\ell} \sin k_o y' \; G_{1\ell} \, dy' \\ 2 & \qquad\qquad\quad 2\ell \\ C_{b1}(\ell, y) &= \int_o^{\ell} \cos k_o y' \; G_{1y} \, dy' \\ 2 & \qquad\qquad\quad 2y \\ C_{b1}(\ell, \ell) &= \int_o^{\ell} \cos k_o y' \; G_{1\ell} \, dy' \\ 2 & \qquad\qquad\quad 2\ell \end{aligned}\right\} \tag{2.29}$$

2.3 The Numerical Results.

The dispersion relation (2.25) involves infinite summations. Therefore, unless the functions Φ_{od} and Φ_{ev} decrease rapidly as K is increased, the numerical solution will be very difficult. The examination of (2.26) and (2.27) shows that this is indeed the case since the sine and cosine integrals involved cancel out each other very rapidly as K increases. It can also be argued physically that the effect of the coupling from far-away elements tends to be nullified by the images of these far-away elements. Based on the above argument, the series of (2.25) was truncated at 20 and 30 terms and the equation was solved by Newton-Raphson method[23]. Let

$$F(\psi) = \sum_{K=\text{odd}} e^{-jK\psi} \Phi_{od} + \sum_{K=\text{even}} e^{-jK\psi} \Phi_{ev} \qquad (2.30)$$

be the sum of the dispersion relation (2.25) when an arbitrary value of the phase shift ψ is used for a given $k_o \ell$. The values of ψ which make $F(\psi)$ zero are the solutions of the dispersion relation (2.25). The null of the function $F(\psi)$ was attempted by using the first two terms in a Taylor's series expansion about $\psi^{(o)}$, a selected value of ψ. In this way, an increment $\delta\psi$ is found and the procedure is repeated, carrying out the expansion about the new value $\psi^{(1)} = (\psi^{(o)} + \delta\psi)$, and so on. Thus, the formula for the successive increments is found to be

$$\delta\psi = - \frac{F(\psi^{(i)}}{F'(\psi)\Big|_{\psi = \psi^{(i)}}} \qquad (2.31)$$

where $F'(\psi)$ denotes the derivative of $F(\psi)$, with respect to its argument, and $\psi^{(i)}$ are successive values of ψ obtained by carrying out i iterations. The results of a 20 - term solution and of a 30 - term solution do not differ significantly (identical within the third decimal point). It is therefore concluded that the result represents the solution of the expression (2.25) approximately and, thus, represents the dispersion characteristics of the infinite source free interdigital array. The curves are plotted in Figs. 2-3 through 2-18, with a wide range of parametric values.

The dashed lines are references corresponding to the limiting dispersion characterisitcs and are useful in establishing different regions. The $k_o \ell = \psi$ line bisects the plot into fast wave and slow wave regions as shown in Fig. 2-3. The dotted line represents the solution obtained from $b/\ell = 0.05$ alone in the forbidden

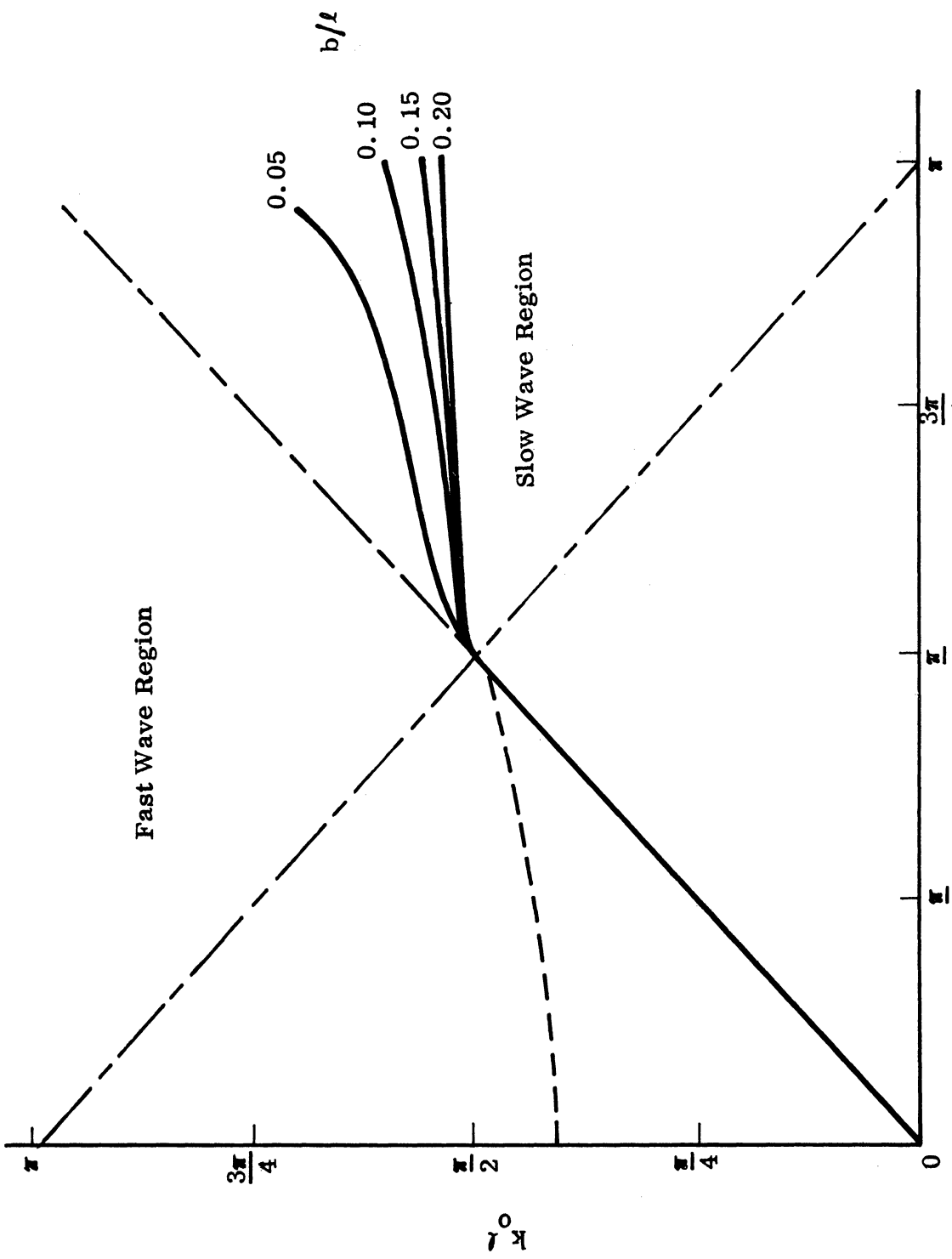

FIG. 2-3: THE DISPERSION CHARACTERISTICS FOR AN INFINITE INTERDIGITAL ARRAY, $a/\ell = 0.01$, $d/\ell = 0.075$.

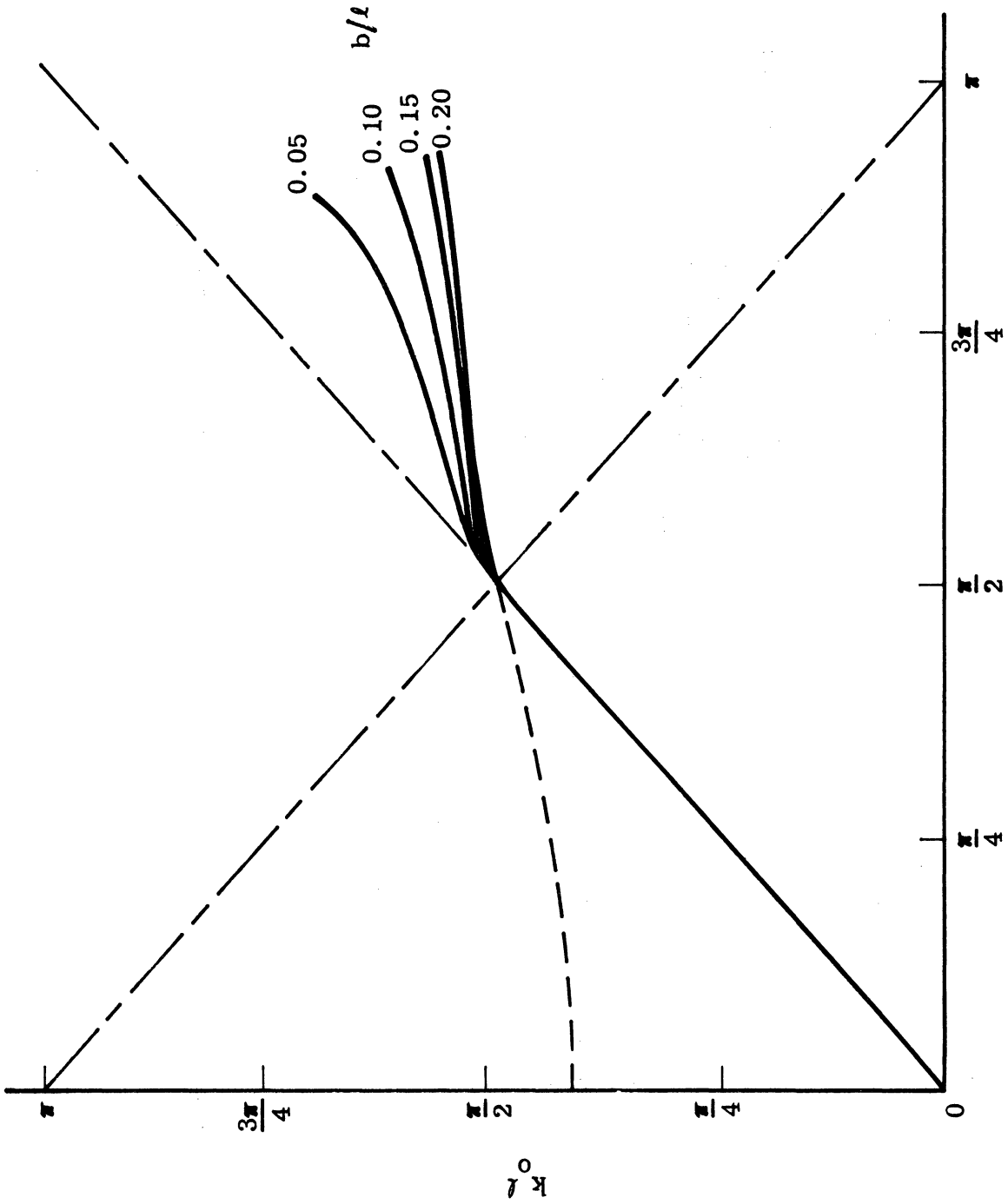

FIG. 2-4: THE DISPERSION CHARACTERISTICS FOR AN INFINITE INTERDIGITAL ARRAY, $a/\ell = 0.01$, $d/\ell = 0.125$.

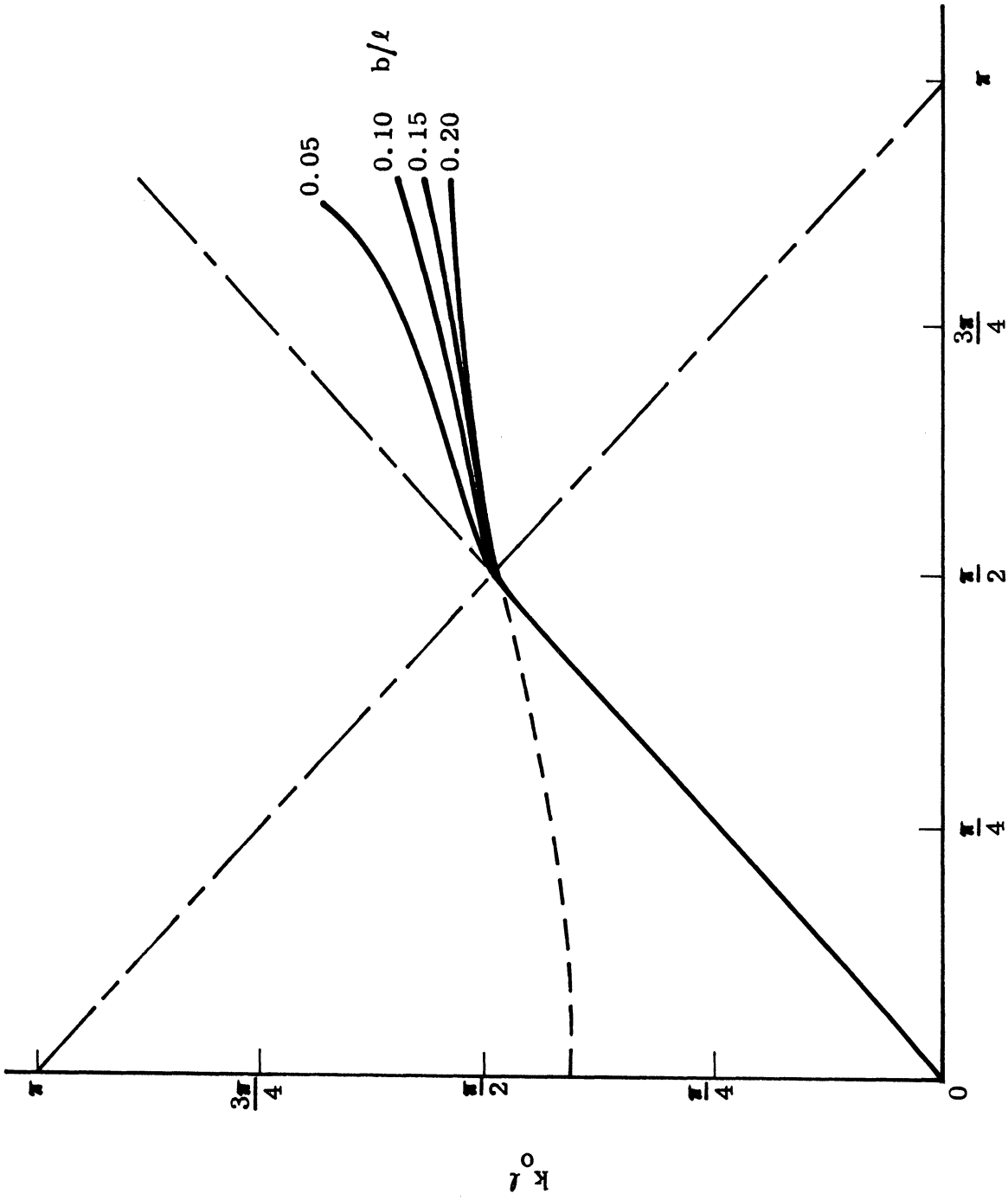

FIG. 2-5: THE DISPERSION CHARACTERISTICS FOR AN INFINITE INTERDIGITAL ARRAY, $a/\ell = 0.01$, $d/\ell = 0.175$.

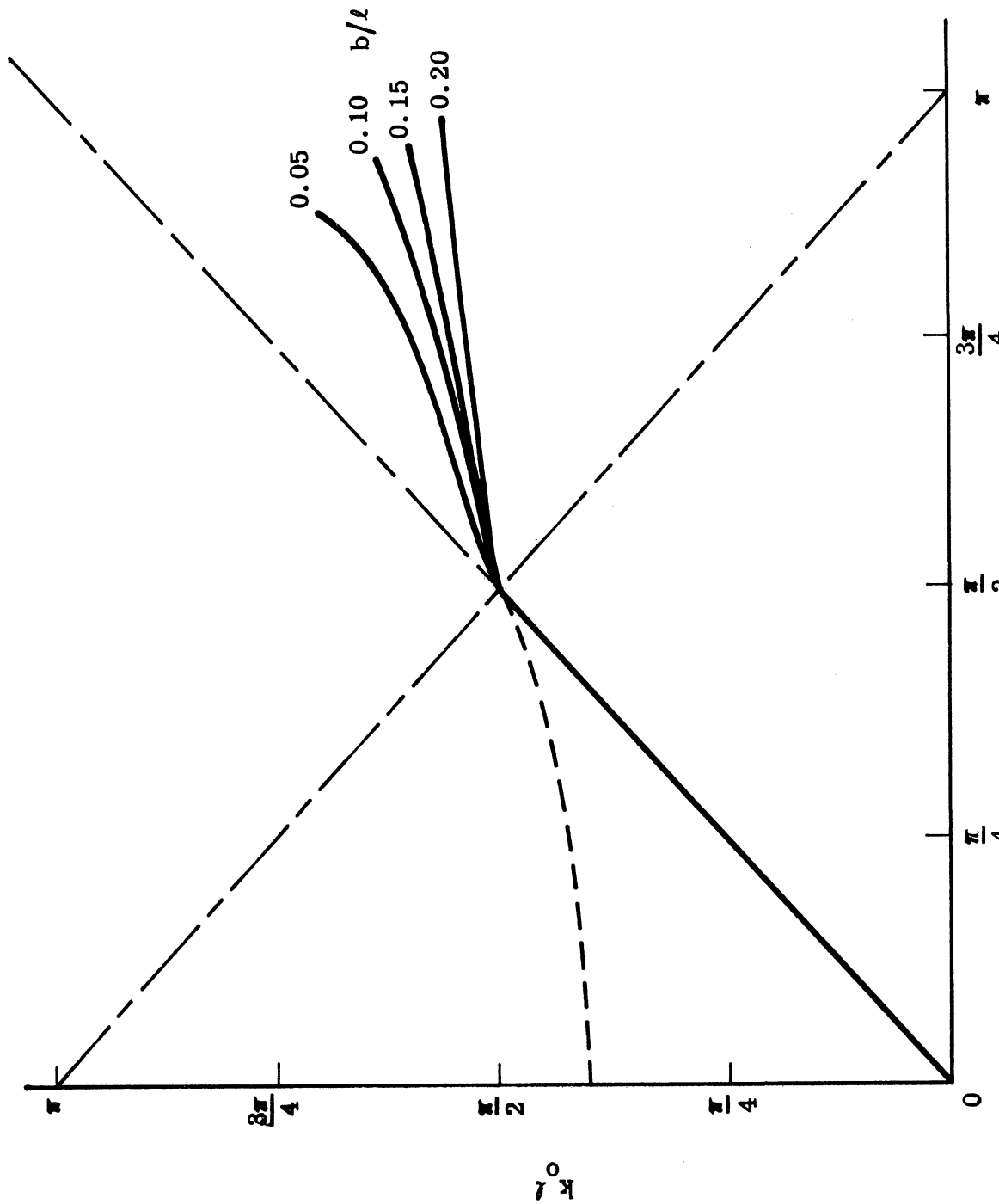

FIG. 2-6: THE DISPERSION CHARACTERISTICS FOR AN INFINITE INTERDIGITAL ARRAY, $a/\ell = 0.01$, $d/\ell = 0.225$.

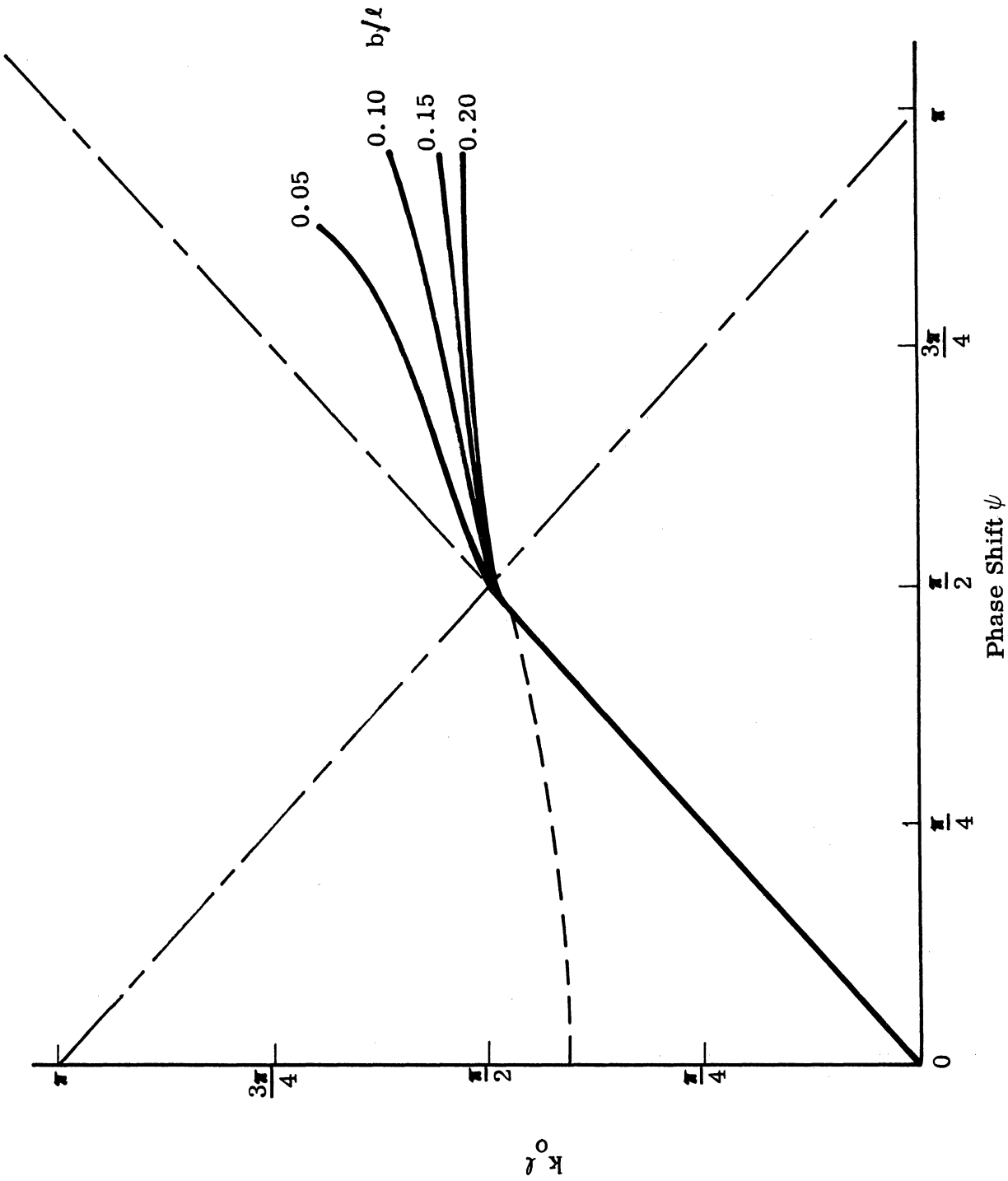

FIG. 2-7: THE DISPERSION CHARACTERISTICS FOR AN INFINITE INTERDIGITAL ARRAY, a/ℓ=0.015, d/ℓ=0.075.

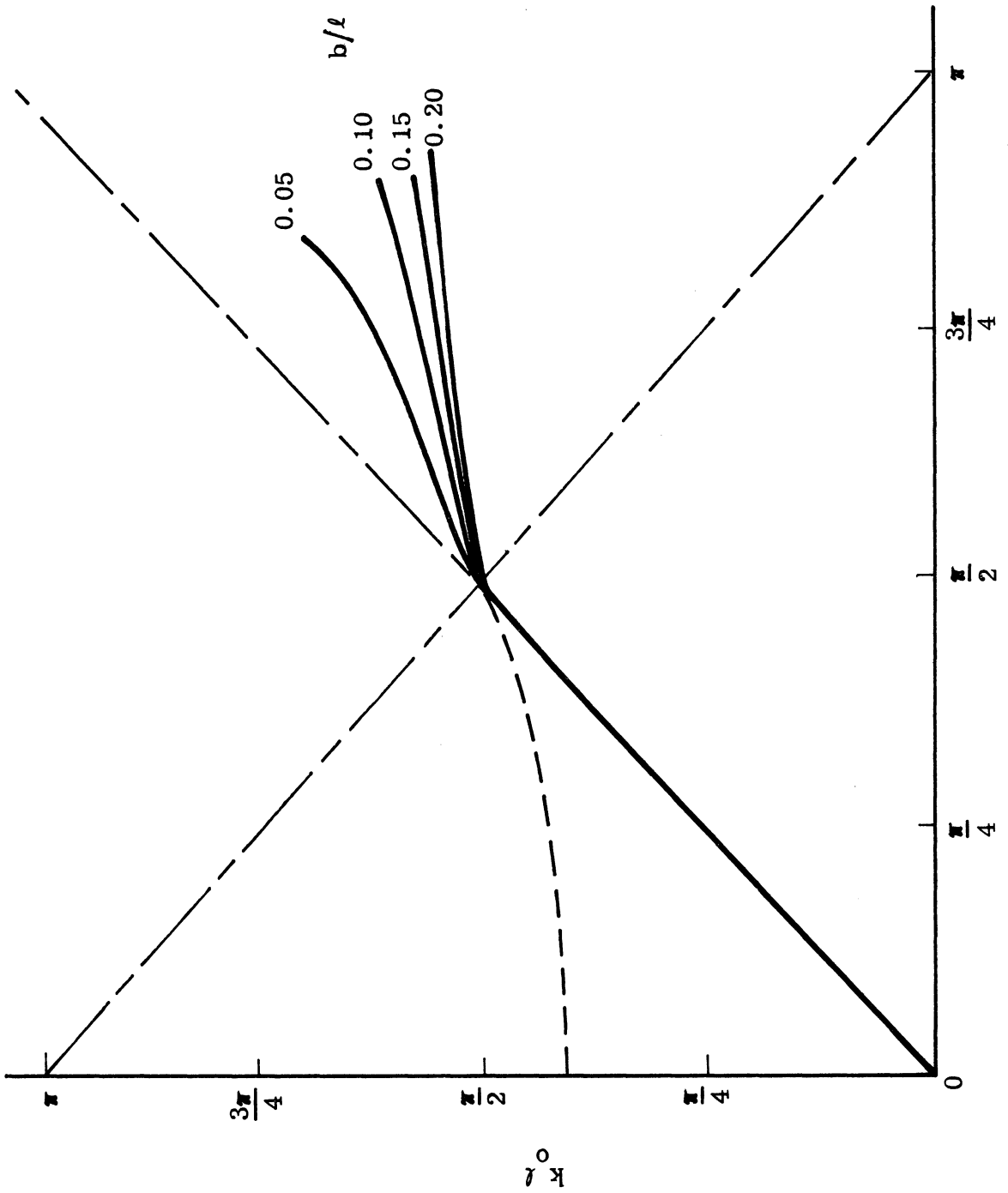

FIG. 2-8: THE DISPERSION CHARACTERISTICS FOR AN INFINITE INTERDIGITAL ARRAY, $a/\ell = 0.015$, $d/\ell = 0.125$.

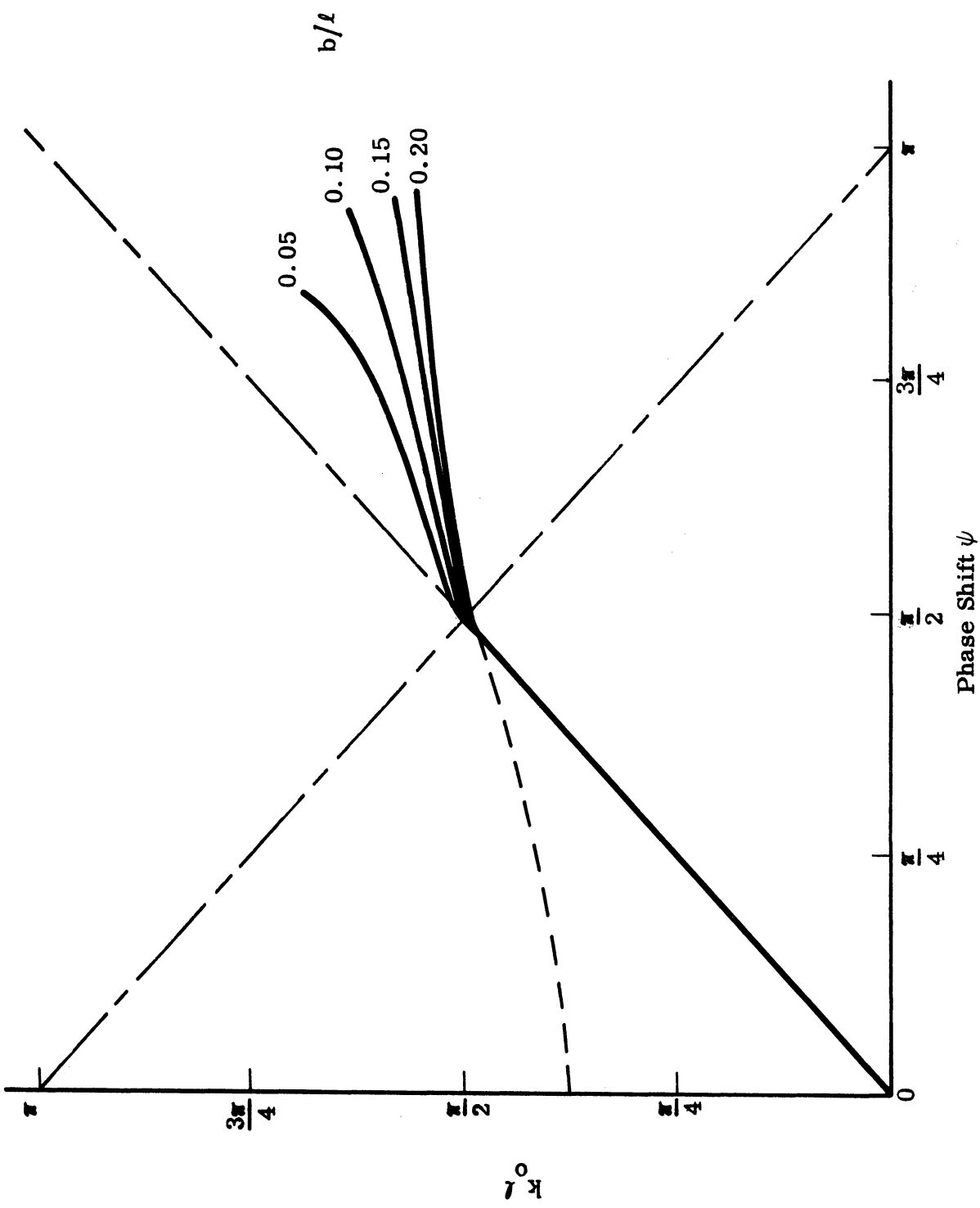

FIG. 2-9: THE DISPERSION CHARACTERISTICS FOR AN INFINITE INTERDIGITAL ARRAY, $a/\ell = 0.015$, $d/\ell = 0.175$.

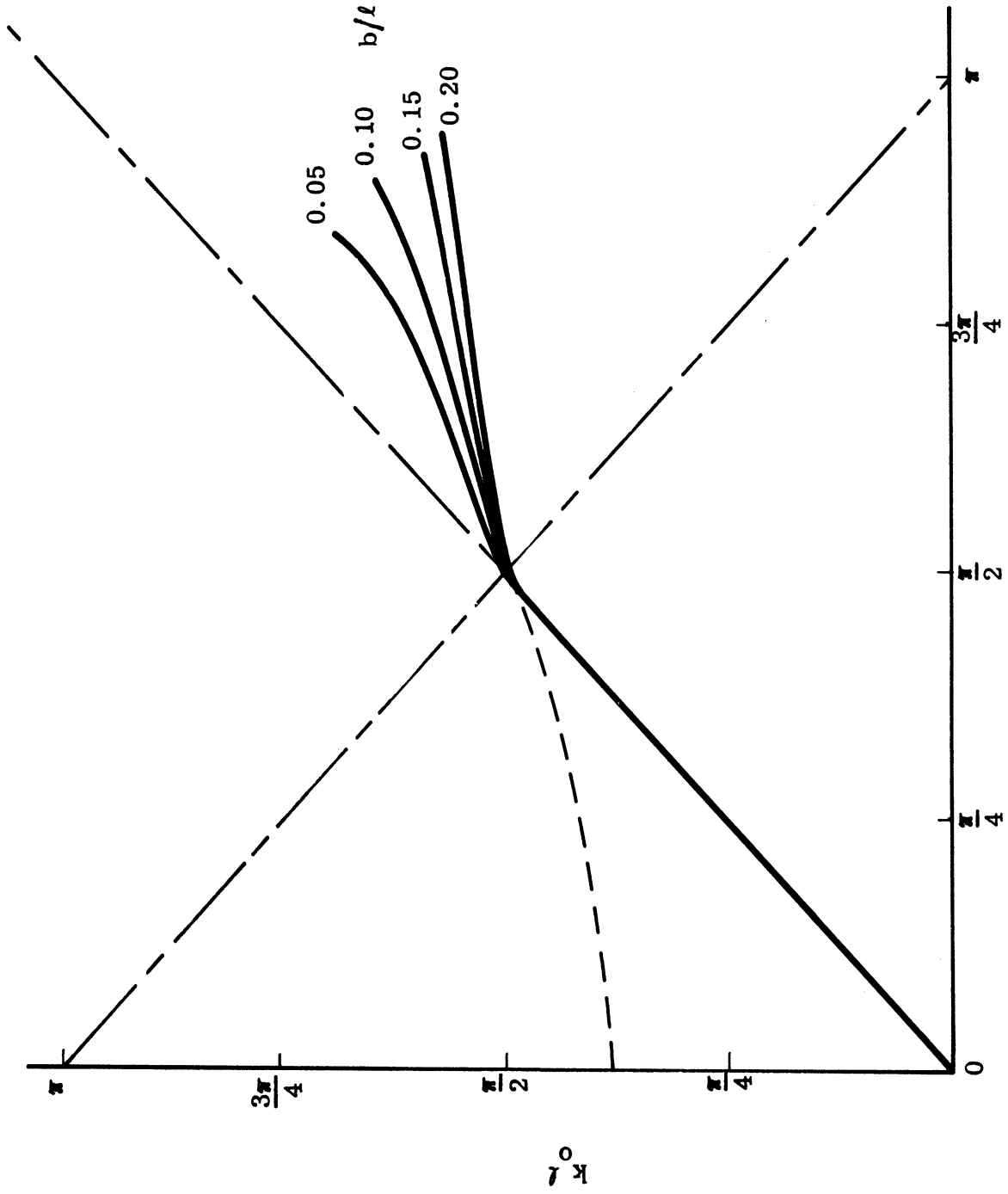

FIG. 2-10: THE DISPERSION CHARACTERISTICS FOR AN INFINITE INTERDIGITAL ARRAY, $a/\ell = 0.015$, $d/\ell = 0.225$.

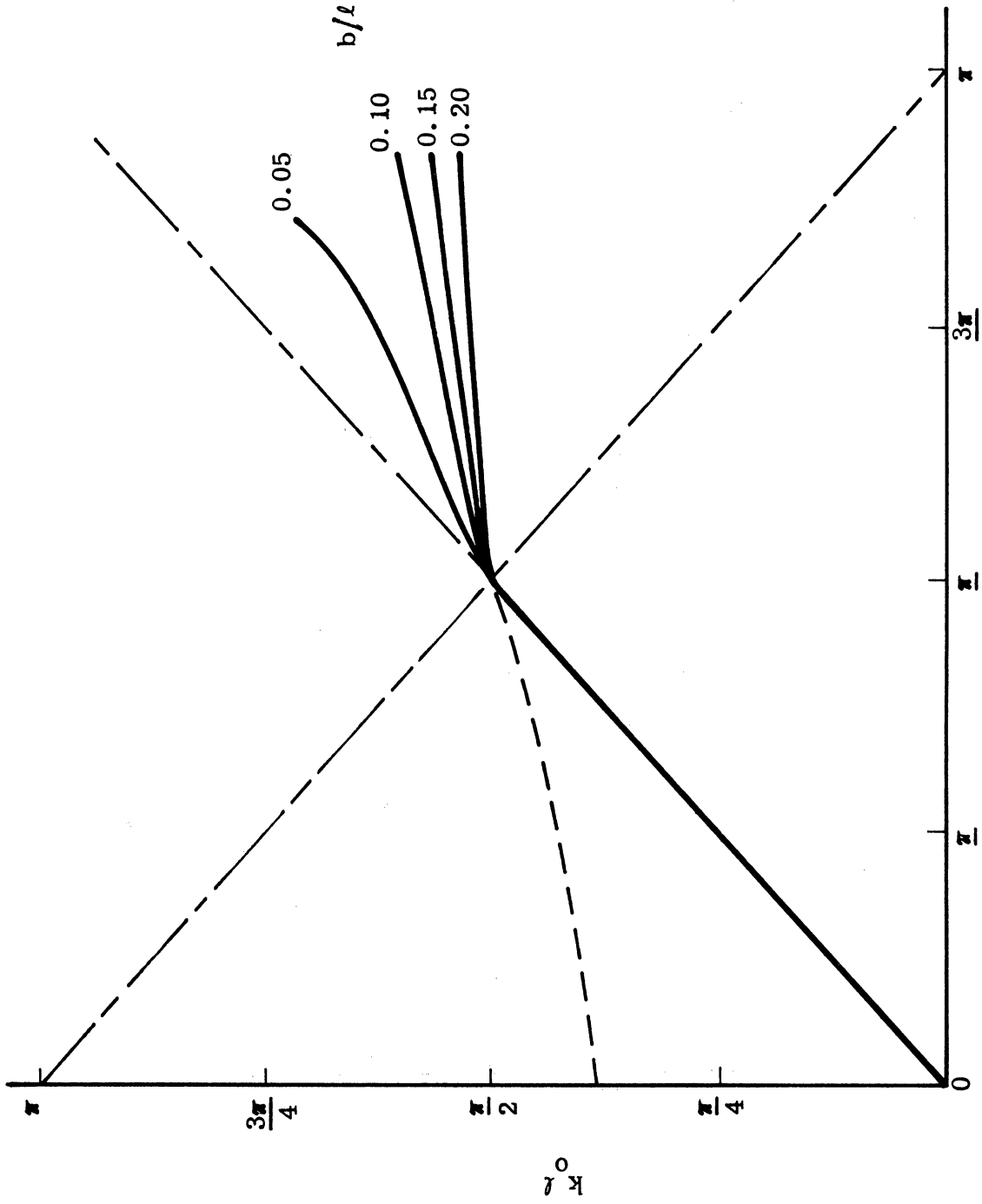

FIG. 2-11: THE DISPERSION CHARACTERISTICS FOR AN INFINITE INTERDIGITAL ARRAY, $a/\ell = 0.02$, $d/\ell = 0.075$.

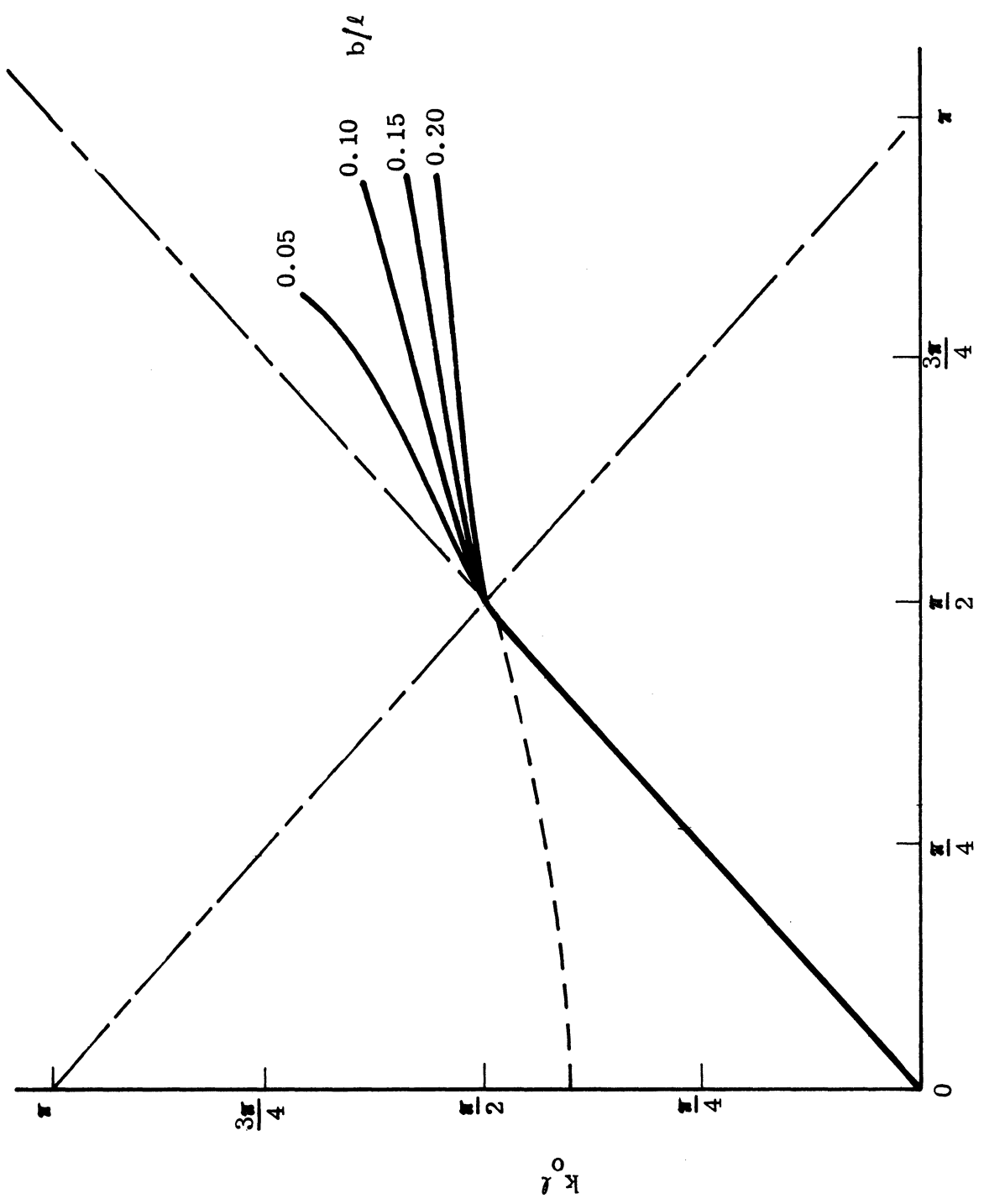

FIG. 2-12: THE DISPERSION CHARACTERISTICS FOR AN INFINITE INTERDIGITAL ARRAY, $a/\ell = 0.02$, $d/\ell = 0.125$.

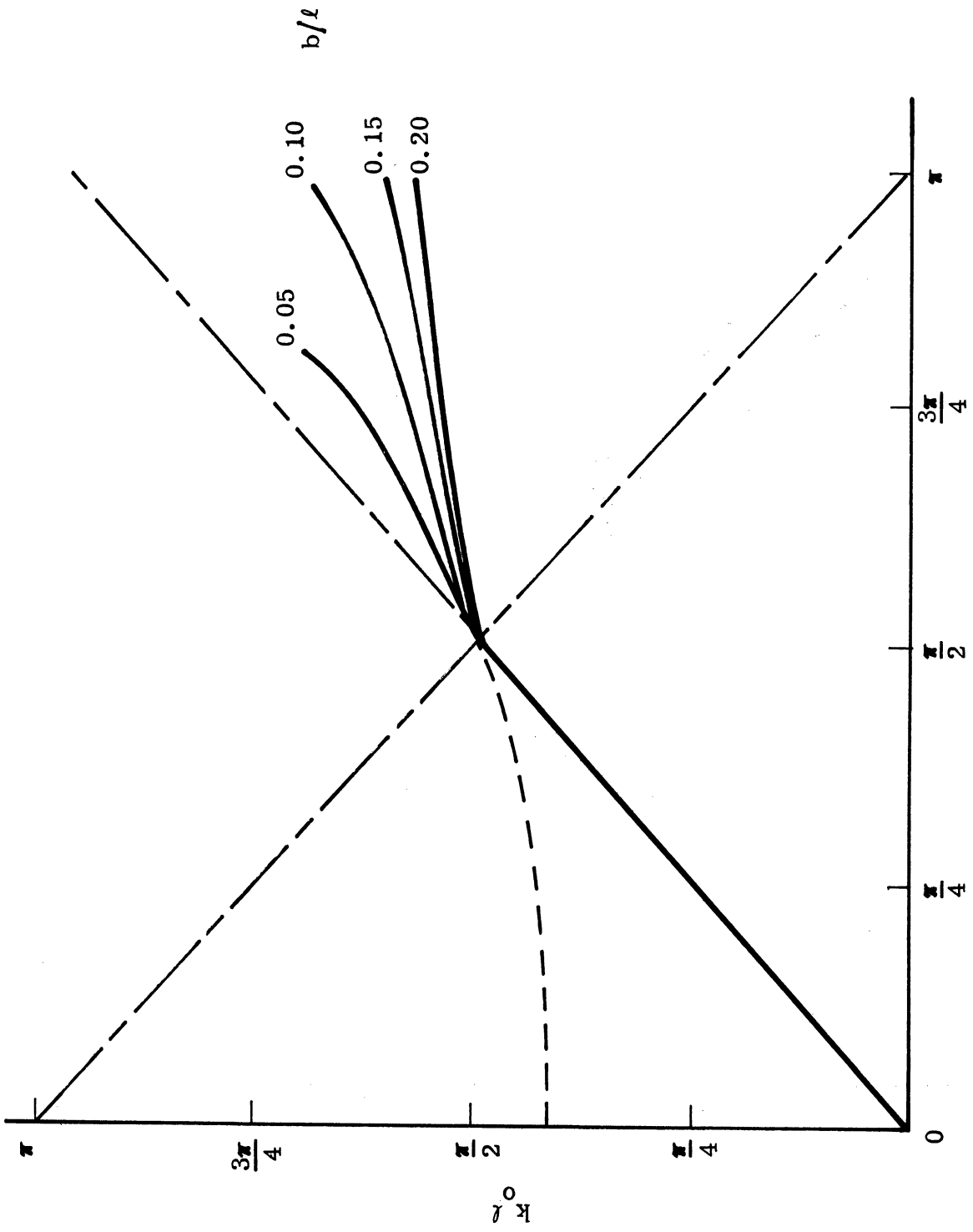

FIG. 2-13: THE DISPERSION CHARACTERISTICS FOR AN INFINITE INTERDIGITAL ARRAY, $a/\ell = 0.02$, $d/\ell = 0.175$.

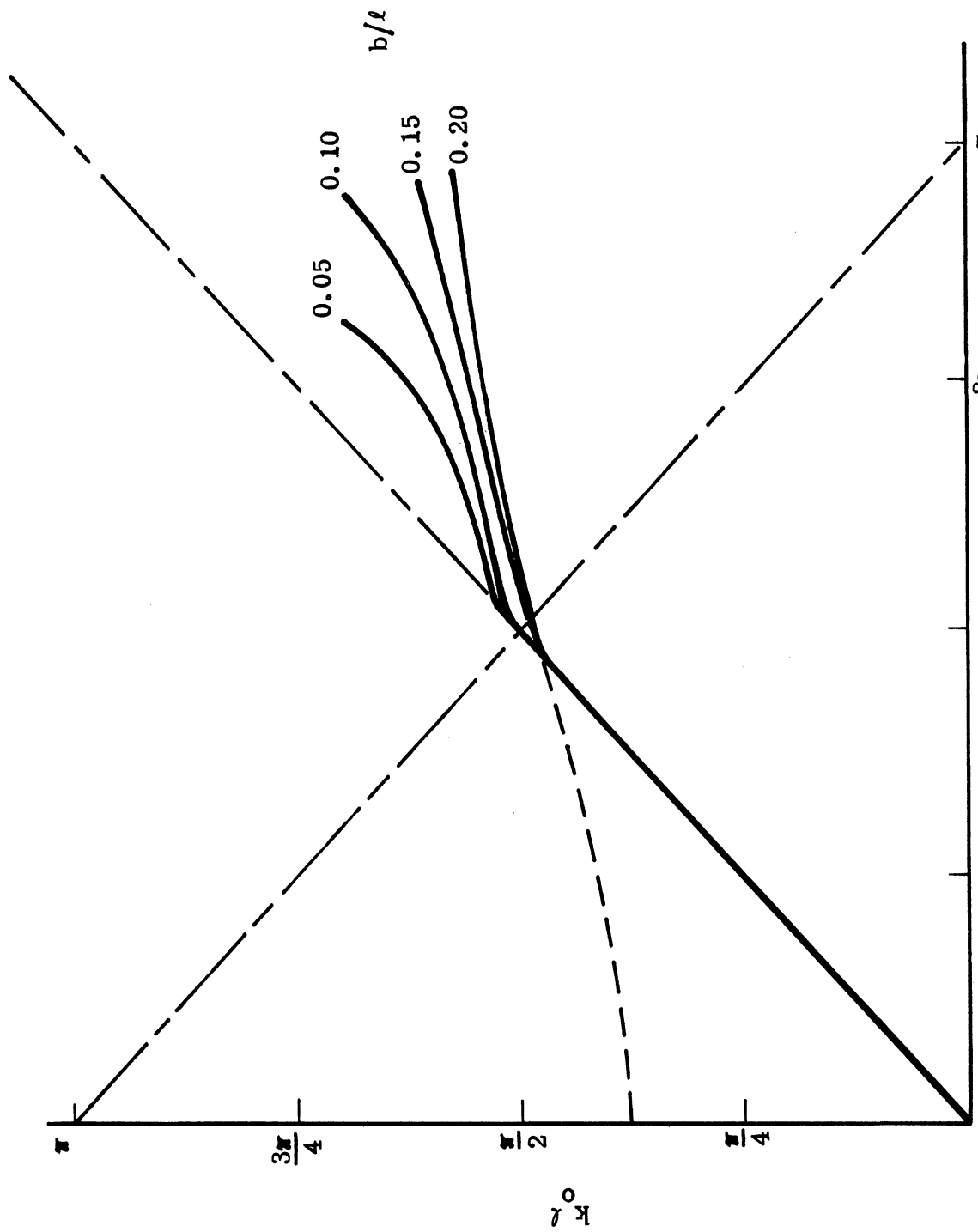

FIG. 2-14: THE DISPERSION CHARACTERISTICS FOR AN INFINITE INTERDIGITAL ARRAY, $a/\ell = 0.02$, $d/\ell = 0.225$.

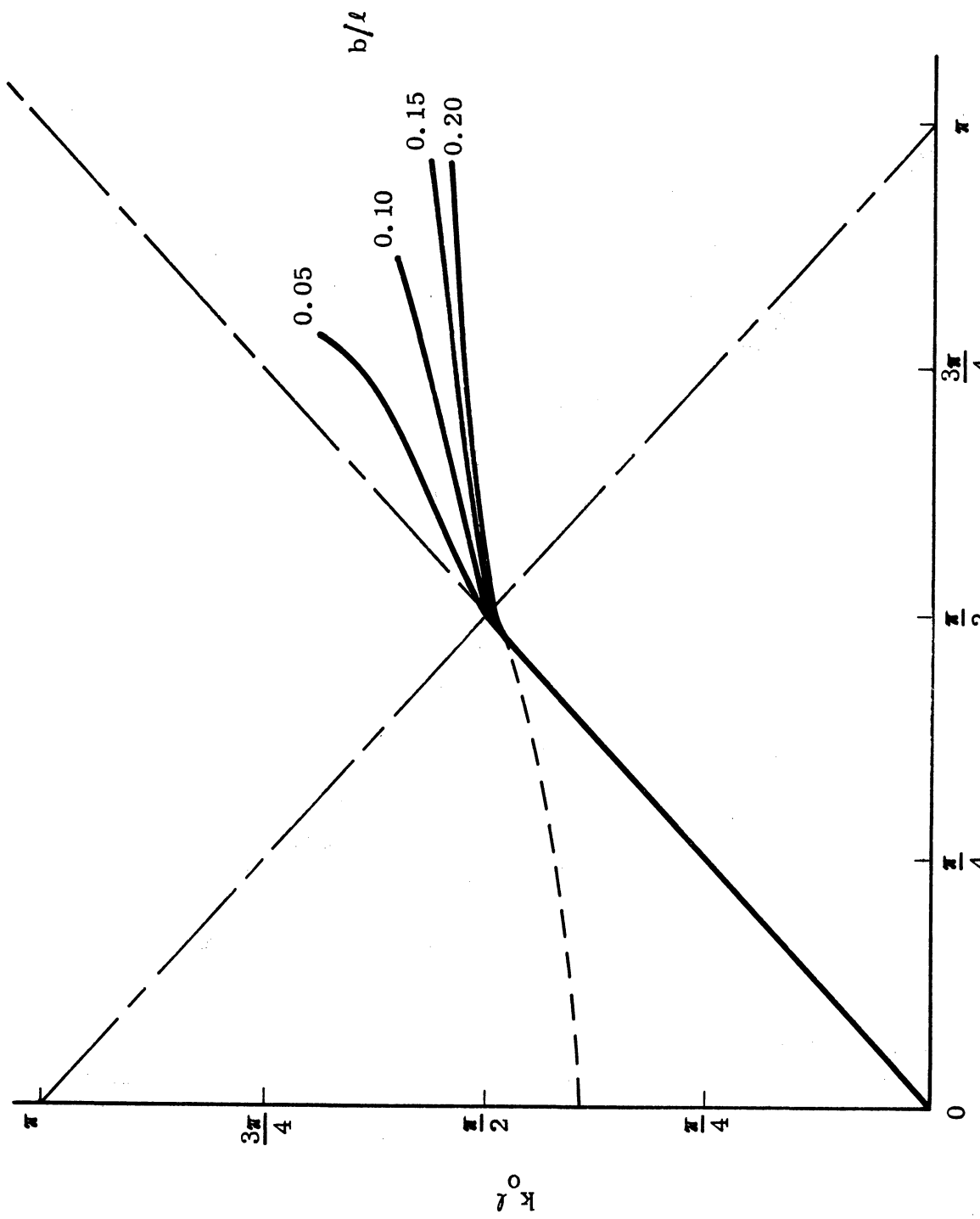

FIG. 2-15: THE DISPERSION CHARACTERISTICS FOR AN INFINITE INTERDIGITAL ARRAY, $a/\ell = 0.025$, $d/\ell = 0.075$.

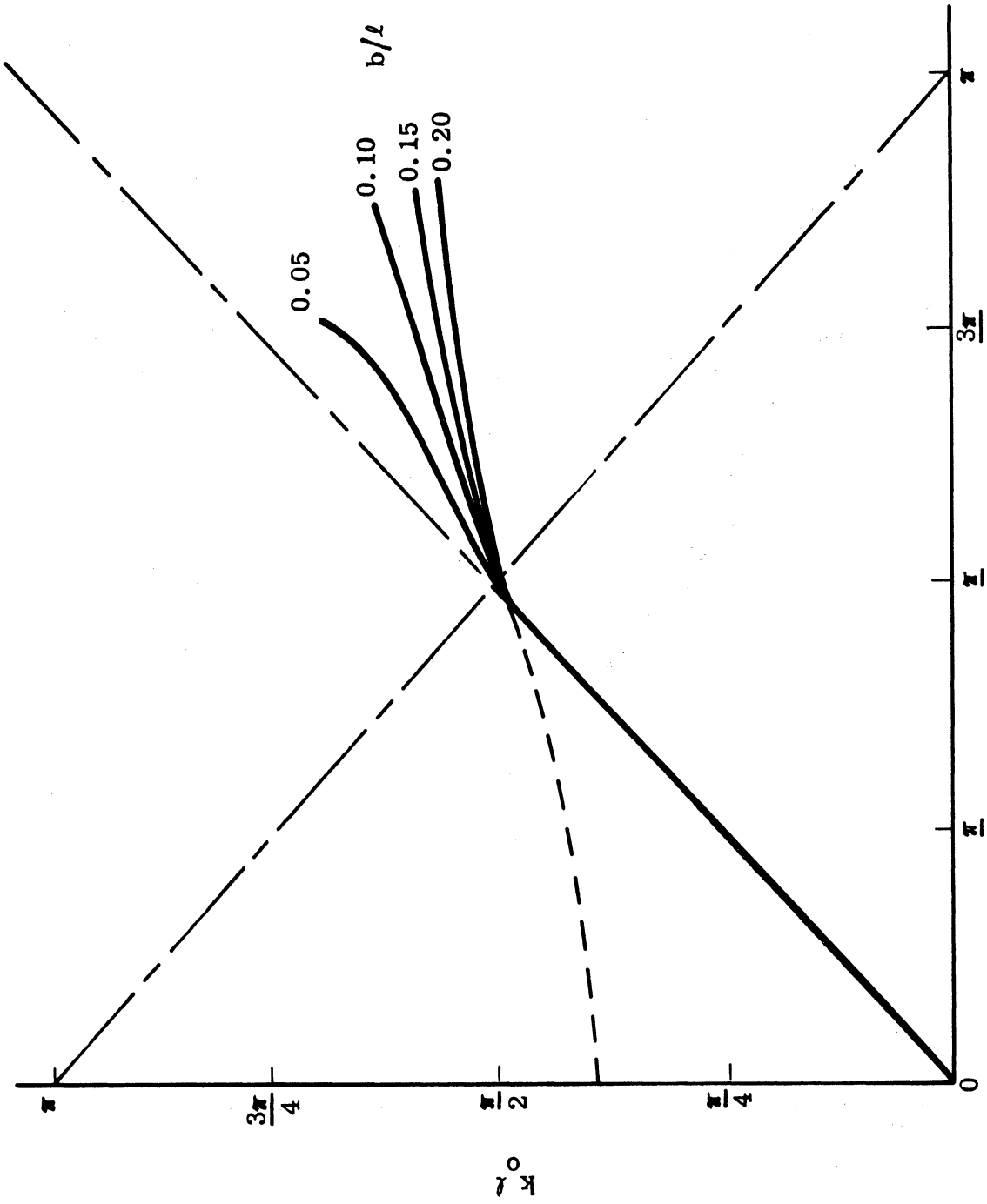

FIG. 2-16: THE DISPERSION CHARACTERISTICS FOR AN INFINITE INTERDIGITAL ARRAY, $a/\ell = 0.025$, $d/\ell = 0.125$.

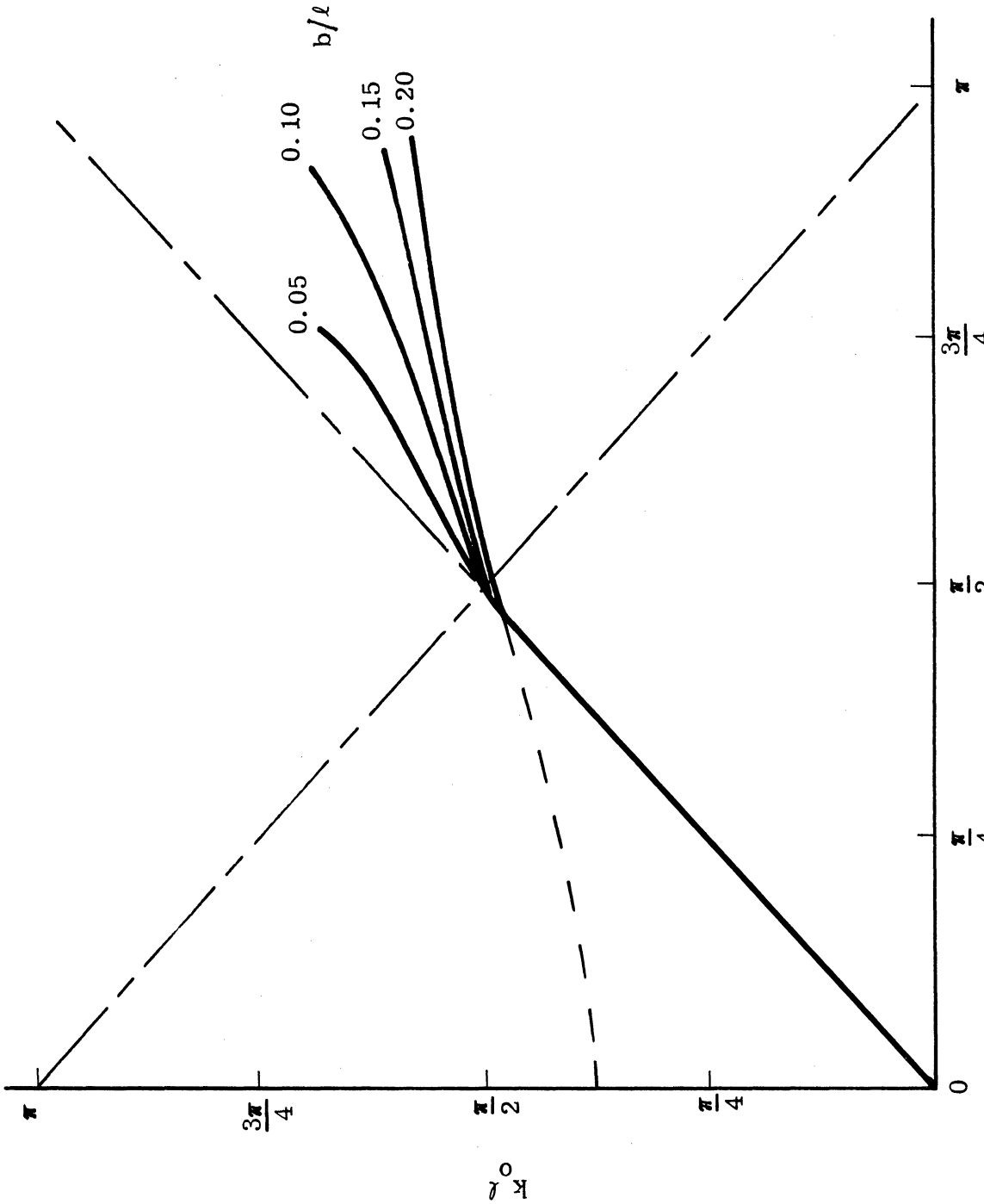

FIG. 2-17: THE DISPERSION CHARACTERISTICS FOR AN INFINITE INTERDIGITAL ARRAY, $a/\ell = 0.025$, $d/\ell = 0.175$.

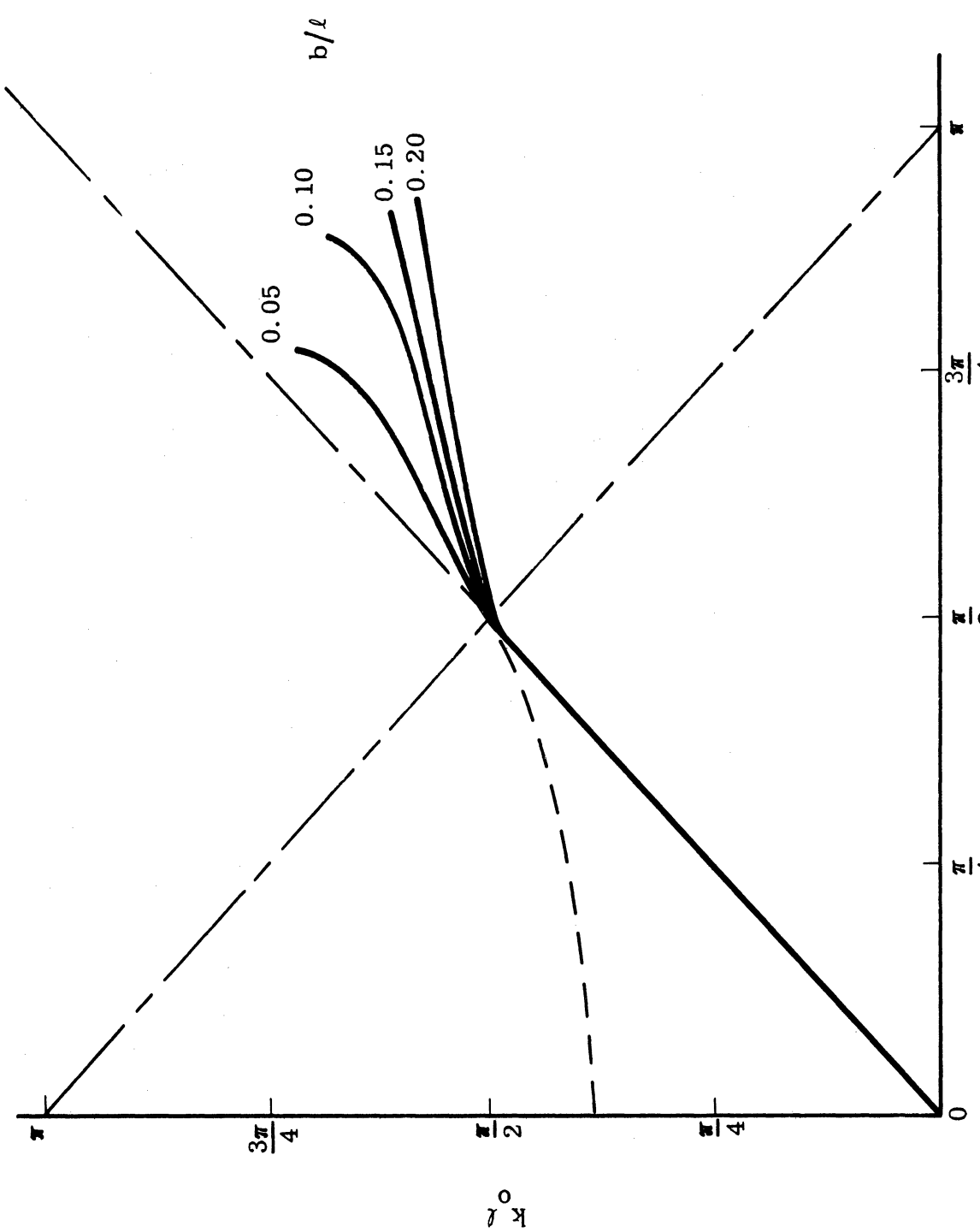

FIG. 2-18: THE DISPERSION CHARACTERISTICS FOR AN INFINITE INTERDIGITAL ARRAY, $a/\ell = 0.025$, $d/\ell = 0.225$.

region (or fast wave region), since it is expected that the solution indicated by the dotted line is not a valid one.

The reason for an invalid solution in a fast wave region is actually perceived through experimental measurement. If the solution in the fast wave region is valid, then since the slope of the curve is always positive, the direction of the phase velocity and the group velocity must be the same. This is found to be true through experiment in the slow wave region when the structure is excited by a source. But the phase velocity and the energy flow (associated with the group velocity) in the fast wave region are actually found to be in opposite directions. This phenomenon will be discussed in Chapter IV. Thus, a travelling wave radiation mechanism in the fast wave region cannot be excited physically for an interdigital array antenna. The behavior in the fast wave region then will have to be that of a leaky wave type. In other words, a complex solution must be assumed in the fast wave region for a better description of the structure. A numerical solution was tried for a complex root in the fast wave region but the solution was not satisfactory due to the complexity involved in double iteration and the slow and uncertain convergence of the root. However, it is likely[32] that when the radiation is of a leaky wave type in an open structure, the real part of the dispersion curve will follow very closely to that of a free-space one. Therefore, although the imaginary part is not known, it is expected that the real part of the dispersion curve will be approximately along the solid line $k_o \ell = \psi$ until $k_o \ell$ approaches or exceeds $\frac{\pi}{2}$; from there the slow wave solution takes over. The solutions obtained in the slow wave region are different for different parametric values, as shown by the solid lines in the plot. Figures 2-19 and 2-20 are the dispersion characteristics for varying distances from the ground plane and radii of the cylindrical elements. It is seen that the distance above the ground plane has only a slight effect on the dispersion curves while the increase in radii of the cylindrical elements seems to shift a curve toward the $k_o \ell = \psi$ line.

When the frequency is increased beyond $k_o \ell = \frac{\pi}{2}$, the assumption of the current distribution becomes less realistic and, therefore, the solutions in the

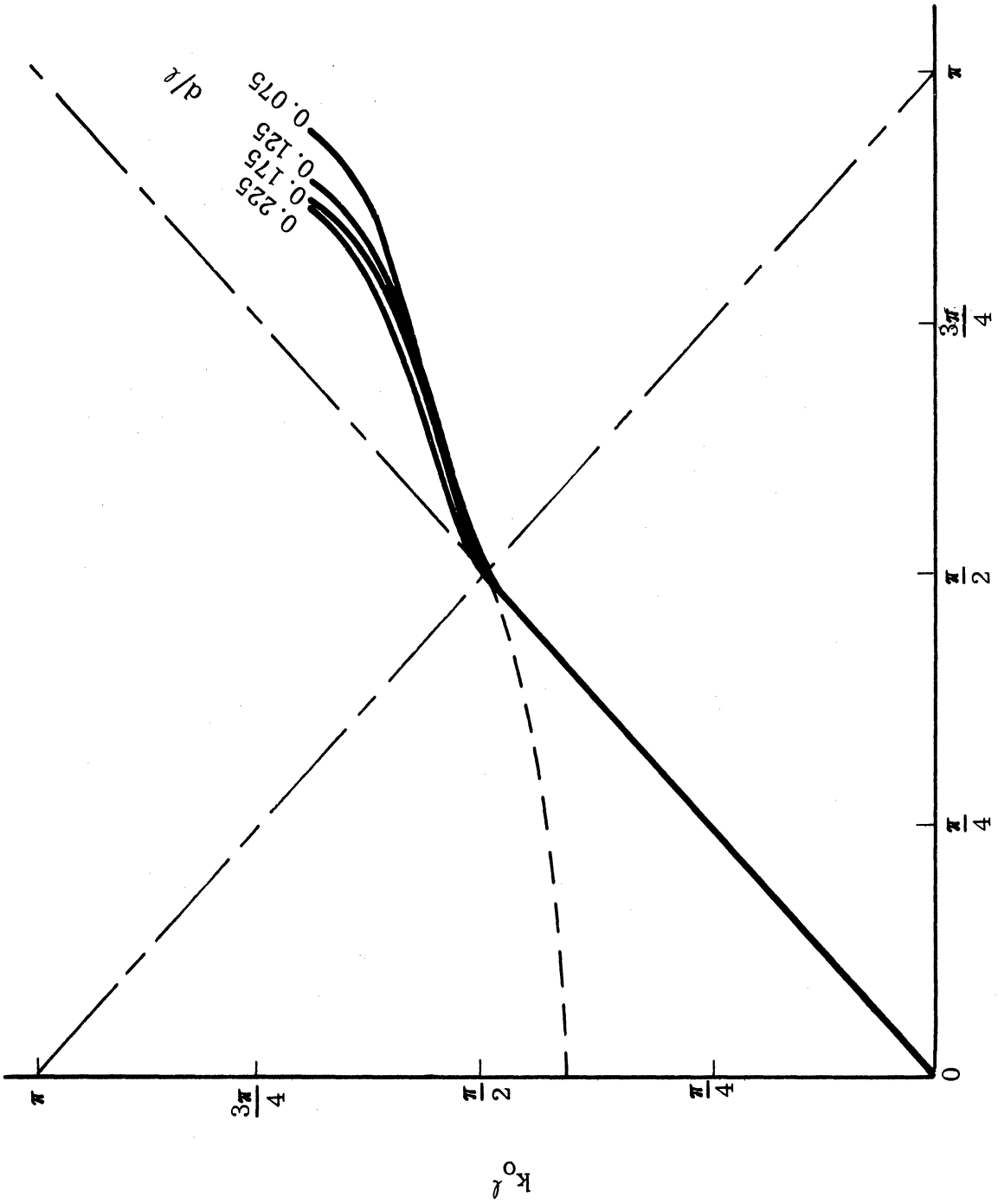

FIG. 2-19: THE DISPERSION CHARACTERISTICS FOR AN INFINITE INTERDIGITAL ARRAY, $a/\ell = 0.01$, $b/\ell = 0.05$.

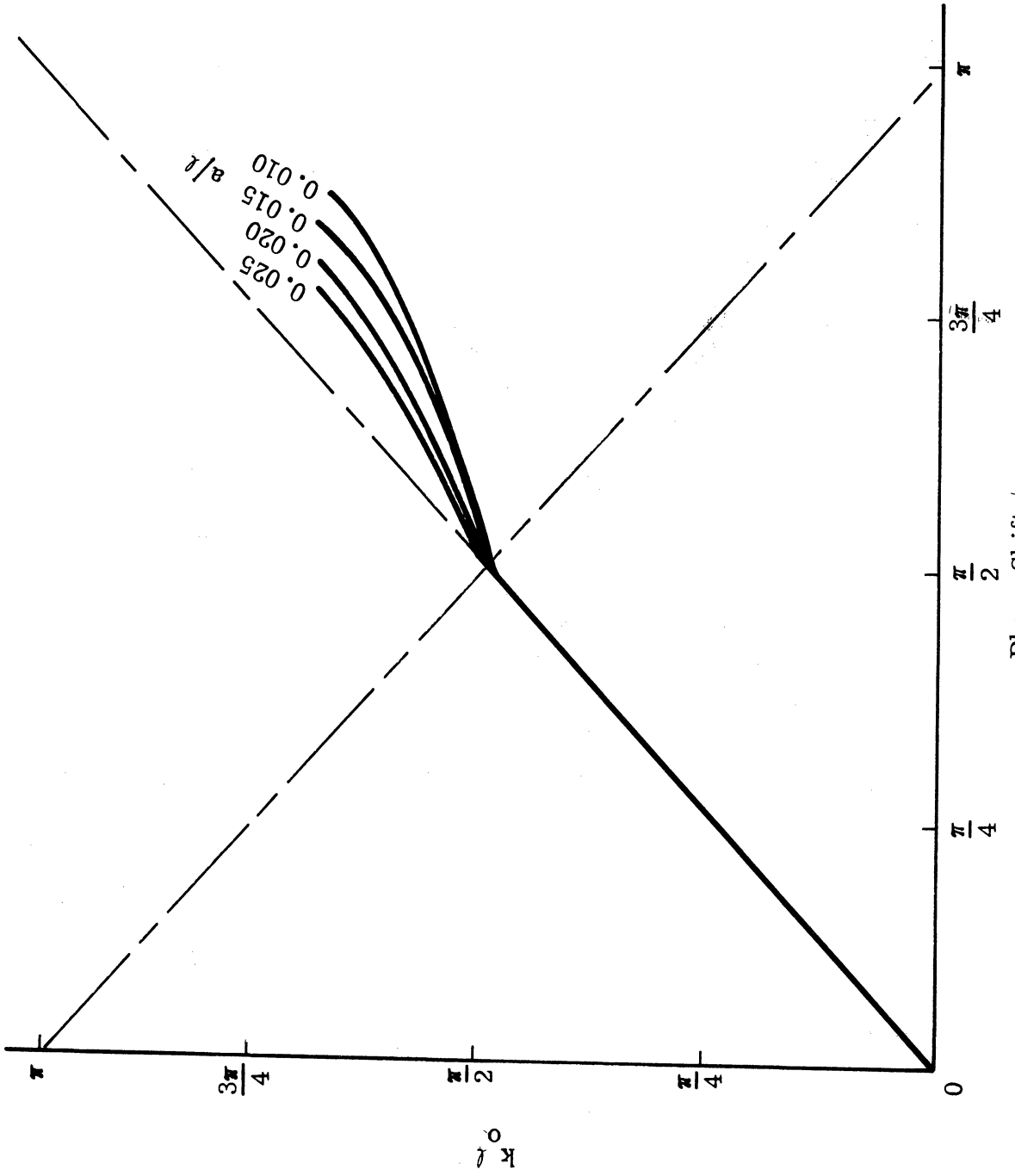

FIG. 2-20: THE DISPERSION CHARACTERISTICS FOR AN INFINITE INTERDIGITAL ARRAY, $b/\ell = 0.05$, $d/\ell = 0.175$.

higher frequency range become less accurate. The comparison of the present solution and those of other workers[2], [8] is shown in Fig. 2-21; a direct comparison is difficult because of the fact that (i) solutions obtained by Fletcher and others are in a closed structure, (ii) available dispersion characteristics are for a square conductor, instead of the circular one used in the present analysis, see Fig. 2-21a. The dispersion curves compare quite well near $k_o \ell = \frac{\pi}{2}$, but the solutions deviate gradually as soon as $k_o \ell$ is increased. The deviations are considered to be due to:

(a) A closed structure tends to reach cut-off frequency faster when $k_o \ell$ is increased, which implies that the curve will gradually "level off" when $k_o \ell$ is increased, while in an open structure a "cut-off" is reached more slowly and, thus, the curve goes up slightly. Then, it should shift toward
persion curve $k_o \ell = \psi$ with imaginary components when the "cut-off" is reached in order to satisfy the radiation condition in free space.

(b) As mentioned before, the assumed current distribution in the analysis may depart from the actual one. This could have contributed to the discrepancies between the two solutions.

(c) Possible differences in the computation procedures for the numerical solutions may have contributed to the deviation.

2.4 Discussion.

The study of the dispersion curves obtained shows that the interdigital array has a slow wave solution when the frequency is near and above the equivalent quarter wave length of the array element. In a lower frequency range, there will be an attenuated wave along the array, represented by a complex propagation constant along the array. This will contribute to a broadside pattern in the far zone if the antenna is fed at the center of the array. If the antenna is fed at one end of the array, the far zone pattern will tilt toward the feed end of the array in a typical "leaky wave" phenomena[32], [33].

If the frequency is increased until the slow wave region is reached, the finite array will become a travelling wave antenna which gives an oblique radiation

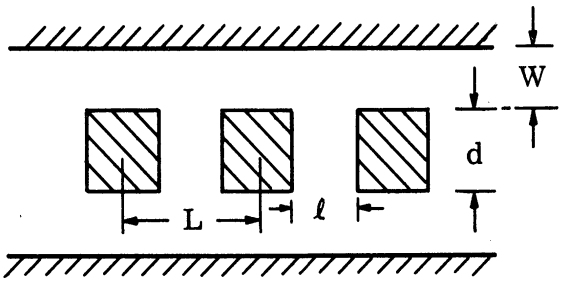

(a) Cross Sectional View of Fletcher's Rectangular Interdigital Line.

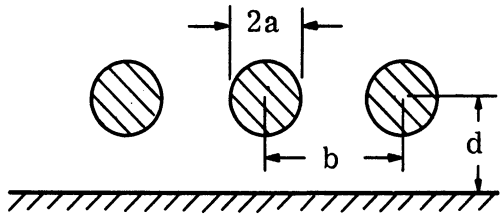

(b) Cross Sectional View of the Interdigital Array Antenna.

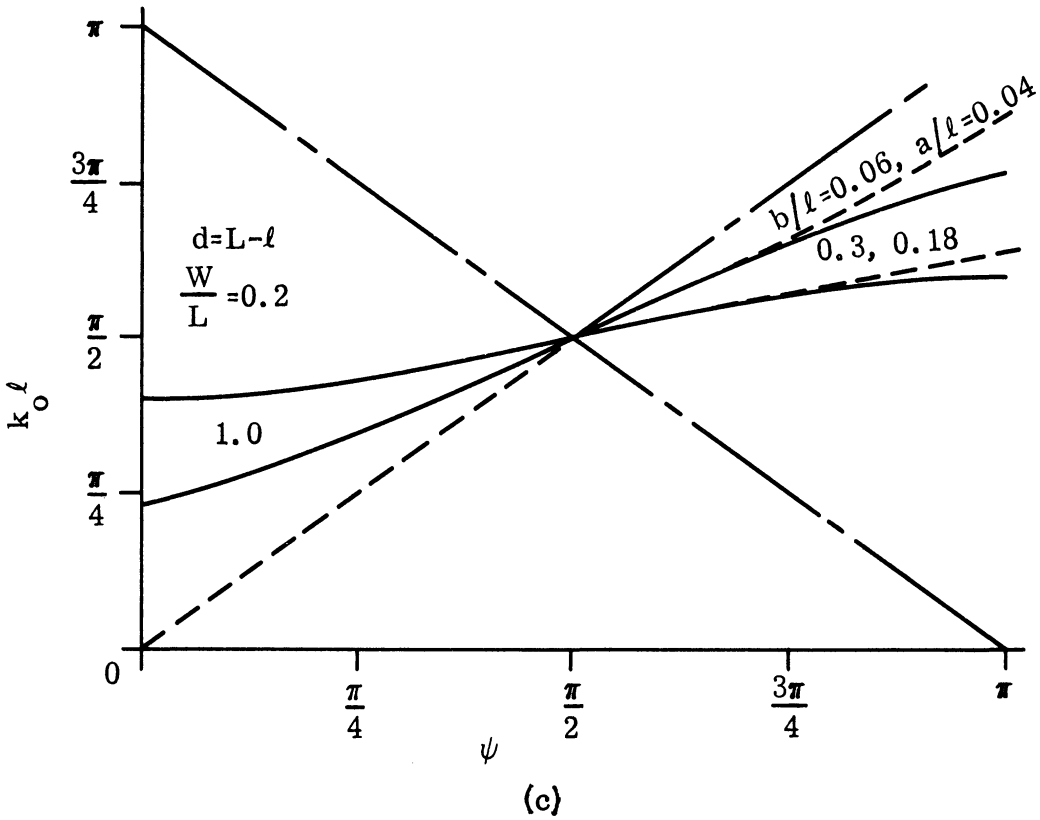

(c)

FIG. 2-21: THE DISPERSION CHARACTERISTICS OF FLETCHER'S SOLUTION (Solid Line, $\ell/L=0.4$) AND THE INTERDIGITAL ARRAY ANTENNA (Dashed Line, $d/\ell=0.06$) FOR THE EQUIVALENT PARAMETERS.

in the forward direction of the array. Thus, if the antenna is fed at the center of the array, an oblique radiation with two symmetrical beams, one toward each end of the array (i.e. a 'rabbit ear' pattern) will result. On the other hand, if the antenna is fed at one end, only a single oblique beam will occur along the direction of the array in a typical travelling wave antenna behavior[32].

It is also observed from these curves that for a given element size of radius "a" length "ℓ", and distant from the ground plane "d", the dispersion curves vary with the separation distance "b" in such a way that when they are very close together, say $b/\ell < 0.05$, the dispersion curves predict a wider bandwidth for the structure and therefore a wider bandwidth is anticipated for both broadside and oblique radiation patterns when the structure is properly fed. The wideband characteristics in the forbidden region can be utilized to operate the antenna over a wide frequency band in a broadside pattern or an oblique pattern, depending on whether the antenna is center-fed or end-fed. The curves become more dispersive as the separation b/ℓ is increased, indicating a narrower bandwidth for the structure. In view of the above, the upper limit of b/ℓ should be around 0.15 while the lower limit will be determined by the element radius and, perhaps, additional factors not readily deduced from the analysis of an infinite array.

The slow wave solutions of a Yagi-Uda array obtained by Mailloux[19], [20], [21], Sengupta[25], [26], Serracchioli and Levis[27] were also compared with the present solution. A direct comparison is difficult because of the difference in the array spacing of the two structures. In the Yagi-Uda array, the array spacing is at least 0.1λ while the array spacing of the interdigital array is at most 0.1λ. As will be discussed in later chapters, the interdigital spacing is made as small as possible for wider band applications. It is interesting to observe however, that when the element radius "a" is decreased toward a small value, the dispersion curve of the Yagi-Uda array tends to become the calculated free space dispersion curve with smaller bandwidth according to the solutions given in the references and as shown in Fig. 2-22a. The Yagi-Uda array is seen to be quite narrow banded compared with the interdigital array structure even for the array

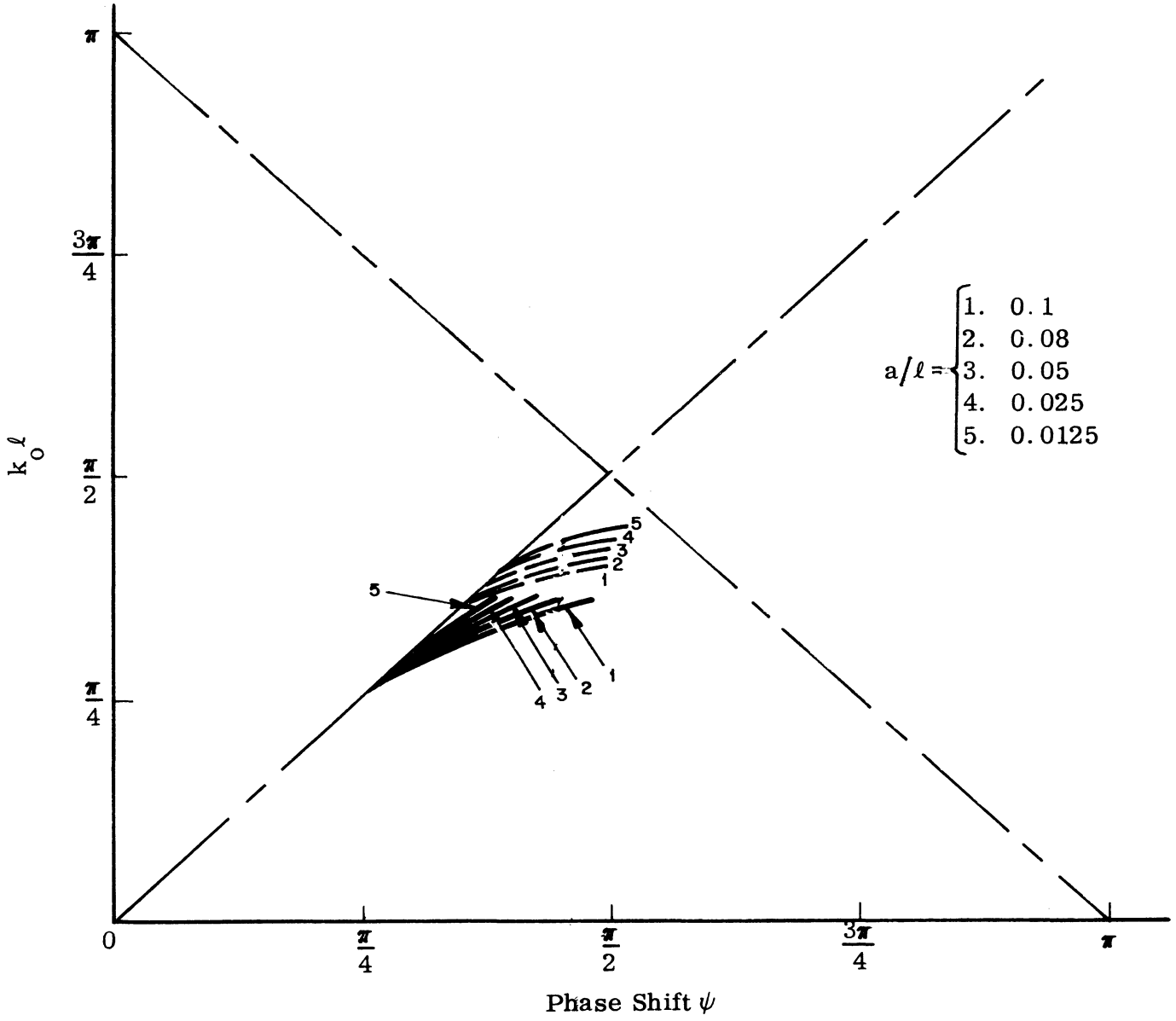

FIG. 2-22a: THE DISPERSION CHARACTERISTICS FOR AN INFINITE YAGI-UDA ARRAY (SERRACCHIOLI AND LEVIS) FOR $b/\lambda=0.1$ (—), AND $b/\lambda=0.4$ (---).

spacings of 0.1λ and 0.4λ. As the spacing is further decreased the trend is toward a narrower bandwidth with a lower resonant frequency for the elements. It is interesting to note from Fig. 2-22b that the dispersion curve for the combination of two parallel non-staggered Yagi-Uda arrays obtained by Mailloux[20] has a tendency to move up in frequency when they are fed out of phase (anti-symmetric case) and the spacing L_x between the array is decreased. However, the bandwidth becomes narrower, as seen from the plot.

It seems from the above comparisons that interdigital current distributions have helped to extend the dispersion curves and thus increase the bandwidth of the structure. No solution exists when the expression of (2.25) is solved separately for an even or an odd mode only, which seems to strengthen the statement made above concerning the wideband behavior of the interdigital array structure.

The frequency equivalent to the quarterwave length of the array element has been and will be used in discussions to account for the actual current distribution. The short vertical section will of course affect the resonant frequency of the array element. The measurement of the resonant frequency of a single element will be utilized to determine the equivalent length of each array element (see Chapter IV). The solution of Serracchioli and Levis[27] is not based upon a sinusoidal distribution of current along the dipole elements and thus the shift of the dispersion curve as a function of the dipole spacing is evident while no shift was obtained in the interdigital array solution. The solution of Mailloux also depended upon a sinusoidal current distribution and therefore a shift did not occur. Later his theoretical curve was adjusted to provide a better fit with the experimental data.

Attempts were also made to compare the interdigital structure with other parallel line structures as transmission networks. As pointed out by Bolljahn and Matthaei[2] the interdigital structure is a wideband structure although it is not as good as the Meander line or the zig-zag line which have all-pass characteristics.

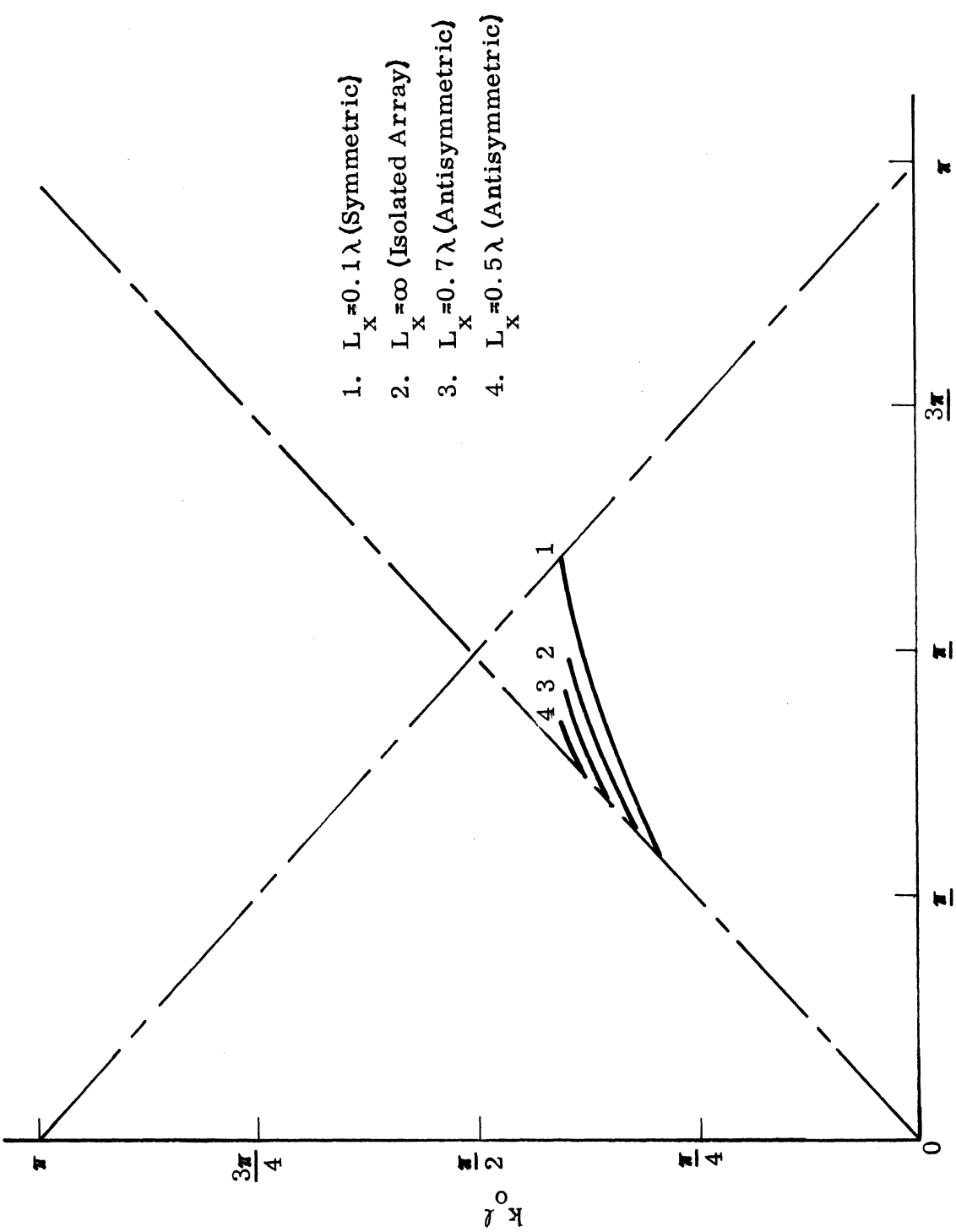

FIG. 2-22b: THE DISPERSION CHARACTERISTICS FOR A PARALLEL NONSTAGGER INFINITE YAGI-UDA ARRAYS (MAILLOUX[19]) FOR a/ℓ=0.05, b/ℓ=0.2, AND VARIOUS ARRAY SPACINGS L_x.

CHAPTER III

A FINITE INTERDIGITAL ARRAY WITH VOLTAGE SOURCE

3.1 Introduction.

In order to obtain a better understanding of a physically realizable interdigital array antenna, it is desired that the radiation patterns and the input impedance be known for a given set of parameters. In this chapter, an array of 2N+1 elements is studied. A voltage source is assumed at the center of the array and is applied across an infinitesimal gap at the grounded terminal of the 0^{th} array element. Some assumptions concerning the line current, its amplitude distribution, and the nature of the wave along the unexcited array elements carry over from the previous chapter. In order to estimate the input impedance, Hallén's first order current distribution is assumed on the 0^{th} element where the voltage is applied. Since these assumptions provide only a very crude analysis, it will be useful in predicting the antenna performance only if a reasonable agreement is obtained from the experimental measurement.

3.2 Formulation.

A finite interdigital array with 2N+1 elements is shown in Fig. 3-1. The voltage source is applied across a small gap δ between the vertical section of the 0^{th} element and the ground plane. Since the vector potential of the array is still described by (2.6), it must satisfy the equations

$$\frac{\partial^2 A_{my}}{\partial y^2} + k_o^2 A_{my} = 0, \qquad m=0, \pm 1, \pm 2, \text{ --- } \pm N \tag{3.1}$$

with the solutions

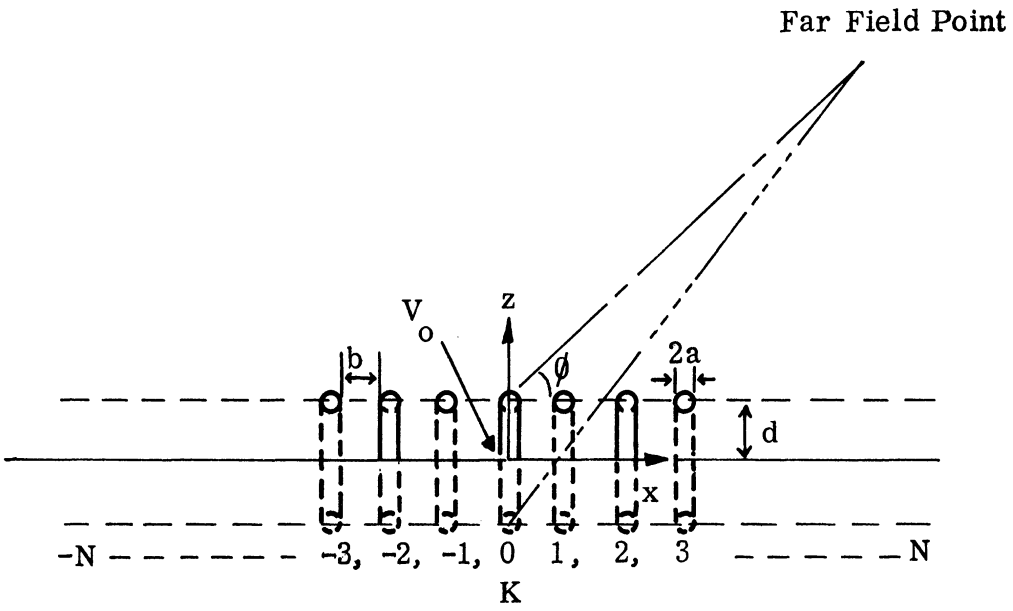

FIG. 3-1: A FINITE INTERDIGITAL ARRAY ANTENNA WITH VOLTAGE SOURCE V_o APPLIED AT THE GROUNDED END OF THE 0^{th} ELEMENT.

$$A_{my}\Big|_{r=a} = -\frac{j}{c}\,(C_m \cos k_o y + D_m \sin k_o y) \quad \text{for } m \text{ even}$$

$$= -\frac{j}{c}\,\left[C_m \cos k_o (\ell - y) + D_m \sin k_o (\ell - y)\right] \quad \text{for } m \text{ odd} \;. \qquad (3.2)$$

The scalar potential can be found from (2.2) once the vector potential is known, In other words,

$$\phi_m = \frac{j\omega}{k_o^2}\,\nabla \cdot A$$

$$= \frac{j\omega}{k_o^2}\,\frac{\partial A_{my}}{\partial y} \;. \qquad (3.3)$$

Substituting (3.2) into (3.3) there results:

$$\phi_m = \left[-C_m \sin k_o y + D_m \cos k_o y\right] \quad \text{for } m \text{ even}$$

$$= \left[C_m \sin k_o (\ell - y) - D_m \cos k_o (\ell - y)\right] \quad \text{for } m \text{ odd} \;. \qquad (3.4)$$

If the 0^{th} element of the array is excited across a small gap by a voltage source V_o, then

$$\left.\begin{aligned} \phi_o\Big|_{y=0} &= V_o = D_o \\ \phi_m\Big|_{y=0} &= 0 = D_m \qquad \text{for m even} \\ \phi_m\Big|_{y=\ell} &= 0 = D_m \qquad \text{for m odd} \quad . \end{aligned}\right\} \tag{3.5}$$

The integral equation of the finite array is thus describable by

$$\left.\begin{aligned} A_{oy} &= \mu_o \sum_{K=-N}^{K=+N} \int_o^{\ell} I_{Ky'} (G_{1y} - G_{2y})\, dy' \\ &= -\frac{j}{c} (C_o \cos k_o y + V_o \sin k_o y) \\ A_{my} &= \mu_o \sum_{K=-N}^{K=+N} \int_o^{\ell} I_{Ky'} (G_{1my} - G_{2my})\, dy' \\ &= -\frac{j}{c} \left[C_m \cos k_o y\right] \qquad \text{for m} = \text{even} \neq 0 \\ &= -\frac{j}{c} \left[C_m \cos k_o (\ell - y)\right] \qquad \text{for m} = \text{odd} \end{aligned}\right\} \tag{3.6}$$

where

$$G_{1my} = \frac{e^{-jk_o R_{1m}}}{4\pi R_{1m}}$$

$$G_{2my} = \frac{e^{-jk_o R_{2m}}}{4\pi R_{2m}}$$

are free space Green's functions with

$$R_{1m} = \sqrt{(y-y')^2 + a^2 + (K-m)^2 b^2}$$

$$R_{2m} = \sqrt{(y-y')^2 + (a+2d)^2 + (K-m)^2 b^2}$$

(3.7)

and where C_o and C_m are arbitrary constants to be determined.

The unknown constants C_o and C_m can be evaluated by the same method used in the previous chapter. It is necessary to form the functions:

$$W_o(y) = A_{oy} - A_{o\ell}$$

$$= \mu_o \sum_{K=-N}^{K=+N} \int_o^{\ell} I_{Ky'} (G_{1y} - G_{2y} - G_{1\ell} + G_{2\ell})\, dy' \qquad (3.8)$$

$$= -\frac{j}{c} \left[C_o (\cos k_o y - \cos k_o \ell) + V_o (\sin k_o y - \sin k_o \ell) \right]$$

$$W_{ev}(y) = A_{my} - A_{m\ell}$$

$$= \mu_o \sum_{K=-N}^{K=+N} \int_o^{\ell} I_{Ky'} (G_{1my} - G_{2my} - G_{1m\ell} + G_{2m\ell})\, dy' \qquad (3.9)$$

$$= -\frac{j}{c} C_m (\cos k_o y - \cos k_o \ell)$$

for m even .

$$W_{od}(y) = A_{my} - A_{mo}$$

$$= \mu_o \sum_{K=-N}^{K=+N} \int_o^{\ell} I_{Ky'} (G_{1my} - G_{2my} - G_{1mo} + G_{2mo})\, dy' \qquad (3.10)$$

$$= -\frac{j}{c} C_m \left[\cos k_o (\ell - y) - \cos k_o \ell\right] \quad \text{for m odd}$$

where G_{1mo}, G_{2mo}, $G_{1m\ell}$ and $G_{2m\ell}$ are as defined in (3.7) by letting y=0 and ℓ, respectively.

The expressions in (3.8), (3.9) and (3.10) give the values of C_o and C_m, respectively, as follows:

$$C_o = \frac{j\xi_o}{\cos k_o y - \cos k_o \ell} \sum_{K=-N}^{K=+N} \int_o^{\ell} I_{Ky'} (G_{1y} - G_{2y} - G_{1\ell} + G_{2\ell})\, dy'$$

$$- V_o \left(\frac{\sin k_o y - \sin k_o \ell}{\cos k_o y - \cos k_o \ell} \right) \qquad (3.11)$$

and

$$C_m = \frac{j\xi_o}{\cos k_o y - \cos k_o \ell} \sum_{K=-N}^{K=+N} \int_o^{\ell} I_{Ky'} (G_{1my} - G_{2my} - G_{1m\ell} + G_{2m\ell})\, dy'$$

for m even

$$= \frac{j\xi_o}{\cos k_o (\ell - y) - \cos k_o \ell} \sum_{K=-N}^{K=+N} \int_o^{\ell} I_{Ky'} (G_{1my} - G_{2my} - G_{1mo} + G_{2mo})\, dy'$$

for m odd. (3.12)

Substitution of C_o and C_m into (3.6) gives a set of $2N + 1$ integral equations which can be solved once the current $I_{Ky'}$ is specified for every K. The expression (3.6) becomes

$$\sum_{K=-N}^{K=+N} \int_o^{\ell} I_{Ky'} (G_{1y} - G_{2y})\, dy' + j \frac{V_o}{\xi_o} \left[\frac{\sin k_o (\ell - y)}{\cos k_o y - \cos k_o \ell} \right]$$

$$= \frac{\cos k_o y}{\cos k_o y - \cos k_o \ell} \sum_{K=-N}^{K=+N} \int_o^{\ell} I_{Ky'} (G_{1y} - G_{2y} - G_{1\ell} + G_{2\ell})\, dy' ,$$

$$\sum_{K=-N}^{K=+N} \int_o^{\ell} I_{Ky'} (G_{1my} - G_{2my})\, dy'$$

$$= \frac{\cos k_o y}{\cos k_o y - \cos k_o \ell} \sum_{K=-N}^{K=+N} \int_o^{\ell} I_{Ky'} (G_{1my} - G_{2my} - G_{1m\ell} + G_{2m\ell})\, dy'$$

for m even, $m \neq 0$

$$= \frac{\cos k_o (\ell - y)}{\cos k_o (\ell - y) - \cos k_o \ell} \sum_{K=-N}^{K=+N} \int_o^{\ell} I_{Ky'} (G_{1my} - G_{2my} - G_{1mo} + G_{2mo})\, dy'$$

for m odd

(3.13)

Since Floquet's theorem cannot be applied to a finite structure, it is necessary to assume the current $I_{Ky'}$ in each conducting element. A sinusoidal distribution is used in all elements except the excited element, where Hallén's first order distribution is assumed to match the voltage source. Thus, let

$$\left.\begin{aligned} I_{Ky} &= A_K \sin k_o y && \text{for } K = \text{odd} \\ &= A_K \sin k_o(\ell - y) && \text{for } K = \text{even and } K \neq 0 \\ &= A_o\left[\frac{\cos k_o y - \cos k_o \ell}{1 - \cos k_o \ell}\right] + jB_o \sin k_o(\ell - y) && \text{for } K = 0 \end{aligned}\right\} \quad (3.14)$$

be the current induced in the array elements. The real constants A_o and B_o and the complex constants A_K are to be determined from the integral equatic (3.13). Substitute (3.14) into (3.13) and, after some manipulations, one finally arrives at a set of $2N + 1$ simultaneous integral equations.

$$\left.\begin{aligned} &\sum_{K=\text{odd}}^{N} A_K \, \Phi_{odo} + \sum_{K=\text{even}}^{N} A_K \, \Phi_{evo} + A_o \, \Phi_{Ao} + jB_o \, \Phi_{Bo} \\ &\qquad = \frac{jV_o}{\xi_o} G_o(\ell - y) \\ &\sum_{K=\text{odd}}^{N} A_K \, \Phi_{odl} + \sum_{K=\text{even}}^{N} A_K \, \Phi_{evl} + A_o \, \Phi_{Al} + jB_o \, \Phi_{Bl} = 0 \\ &\qquad \vdots \\ &\sum_{K=\text{odd}}^{N} A_K \, \Phi_{odm} + \sum_{K=\text{even}}^{N} A_K \, \Phi_{evm} + A_o \, \Phi_{Am} + jB_o \, \Phi_{Bm} = 0 \end{aligned}\right\} \quad (3.15)$$

where

$$K = \pm 1,\ \pm 2,\ ----,\ \pm N$$

$$m = \pm 1,\ \pm 2,\ ---,\ \pm N$$

and where

$$\Phi_{odm} = \frac{F_o(\ell)}{F}\left[S_{b1m}(\ell, y) - S_{b2m}(\ell, y)\right]$$

$$- \left[S_{b1m}(\ell, f) - S_{b2m}(\ell, f)\right] \qquad (3.16)$$

$$\Phi_{evm} = \frac{F_o(\ell)\,G_o(\ell)}{F}\left[C_{b1m}(\ell, y) - C_{b2m}(\ell, y)\right]$$

$$- \frac{\left[F_o(\ell)\right]^2}{F}\left[S_{b1m}(\ell, y) - S_{b2m}(\ell, y)\right]$$

$$- G_o(\ell)\left[C_{b1m}(\ell, f) - C_{b2m}(\ell, f)\right]$$

$$+ F_o(\ell)\left[S_{b1m}(\ell, f) - S_{b2m}(\ell, f)\right] \qquad (3.17)$$

$$\Phi_{Am} = \frac{1}{1 - F_o(\ell)}\left\{F_o(\ell)\left[E_{b1m}(\ell, f) - E_{b2m}(\ell, f)\right]\right.$$

$$- \frac{\left[F_o(\ell)\right]^2}{F}\left[E_{b1m}(\ell, y) - E_{b2m}(\ell, y)\right]$$

$$- \left[C_{b1m}(\ell, f) - C_{b2m}(\ell, f)\right]$$

$$\left. + \frac{F_o(\ell)}{F}\left[C_{b1m}(\ell, y) - C_{b2m}(\ell, y)\right]\right\} \qquad (3.18)$$

$$\Phi_{Bm} = \Phi_{evm}\Big|_{K=0} \tag{3.19}$$

$$F = \begin{cases} F_o(y) & m \text{ even} \\ F_o(\ell - y) & m \text{ odd} \end{cases}$$

$$f = \begin{cases} \ell & m \text{ even} \\ 0 & m \text{ odd} \end{cases}$$

and where

$$\left.\begin{aligned} S_{\substack{b1m \\ b2m}}(\ell, y) &= \int_o^{\ell} \sin k_o y' \, G_{\substack{1my \\ 2my}} \, dy' \\ S_{\substack{b1m \\ b2m}}(\ell, \ell) &= \int_o^{\ell} \sin k_o y' \, G_{\substack{1m\ell \\ 2m\ell}} \, dy' \\ S_{\substack{b1m \\ b2m}}(\ell, o) &= \int_o^{\ell} \sin k_o y' \, G_{\substack{1mo \\ 2mo}} \, dy' \end{aligned}\right\} \tag{3.20}$$

$$\left.\begin{aligned} C_{\substack{b1m \\ b2m}}(\ell, y) &= \int_o^{\ell} \cos k_o y' \, G_{\substack{1my \\ 2my}} \, dy' \\ C_{\substack{b1m \\ b2m}}(\ell, \ell) &= \int_o^{\ell} \cos k_o y' \, G_{\substack{1mo \\ 2mo}} \, dy' \\ C_{\substack{b1m \\ b2m}}(\ell, o) &= \int_o^{\ell} \cos k_o y' \, G_{\substack{1mo \\ 2mo}} \, dy' \end{aligned}\right\} \tag{3.21}$$

$$\left.\begin{aligned} E_{\substack{b1m \\ b2m}}(\ell, y) &= \int_o^{\ell} G_{\substack{1my \\ 2my}}\, dy' \\ E_{\substack{b1m \\ b2m}}(\ell, \ell) &= \int_o^{\ell} G_{\substack{1m\ell \\ 2m\ell}}\, dy' \\ E_{\substack{b1m \\ b2m}}(\ell, o) &= \int_o^{\ell} G_{\substack{1mo \\ 2mo}}\, dy' \end{aligned}\right\} \quad (3.22)$$

The short vertical sections can be taken into consideration by assuming a constant current distribution on all vertical sections with amplitudes identical to the maximum value of the amplitude of the horizontal section. In other words, each short vertical section is taken to be a Hertzian dipole with a dipole moment of $2 I_K d$ and a radiation resistance of[16]

$$R_r = \frac{80\pi^2}{\lambda^2} (2d)^2 \quad . \quad (3.23)$$

The radiation pattern of these Hertzian dipoles can be considered to be similar to that of a pair of parallel Hertzian dipole arrays which give a vertically polarized endfire radiation along the array in both directions.

3.3 The Numerical Results.

Equation (3.15) was put into the digital computer for a numerical solution to yield the unknown coefficients A_o, B_o and A_K for a given set of parameters. The radiation pattern and the input impedance were computed from the computer output data.

3.3.1 The Input Impedance.

It is expected that the input impedance formulated below will be consistent only within the validity of linear antenna theory. The mathematical

model using a "delta" voltage source does not correspond to physical boundary conditions. Therefore the input impedance formulated on this basis is severely limited in accuracy.

The first order input impedance of a finite interdigital array looking from the voltage source is defined to be

$$Z_i = \frac{V_o}{I_o(y=0)} = \frac{V_o}{A_o + jB_o \sin k_o \ell} \quad . \tag{3.24}$$

Solving (3.15) by letting $y = \frac{\ell}{2}$ and $K = \pm 1, \text{----}, \pm N$ will yield $\left(\frac{A_o}{V_o}\right)$ and $\left(\frac{B_o}{V_o}\right)$ which can be used in (3.24) to obtain an approximate expression for the input impedance of the structure. The numerical results for N=6, and 10 are plotted in Figs. 3-2 through 3-15 for typical parameter values.

It is observed from these plots that the input resistance of the structure is fluctuating around 50Ω. The increase in b/ℓ, the separation between array elements seems to decrease the input resistance over all frequency ranges and the increase in d/ℓ, the distance of the array above the ground plane increases the input resistance over all frequency ranges by a significant amount. The above observation indicates an expected effect of a cylindrical antenna parallel above a ground plane. When the antenna is close to the ground plane, the radiation effect decreases since the radiation effect is proportional to the input resistance of the antenna when the antenna is near, or less than, a quarter wavelength of the frequency. The increase in b/ℓ decreases the coupling effect between the array elements, and, if the coupling is to increase the radiation effect, then the input resistance should decrease when b/ℓ is increased. This being the case noted here, it is believed that the coupling effect for the interdigital boundary condition is helpful in improving the radiation of the structure,

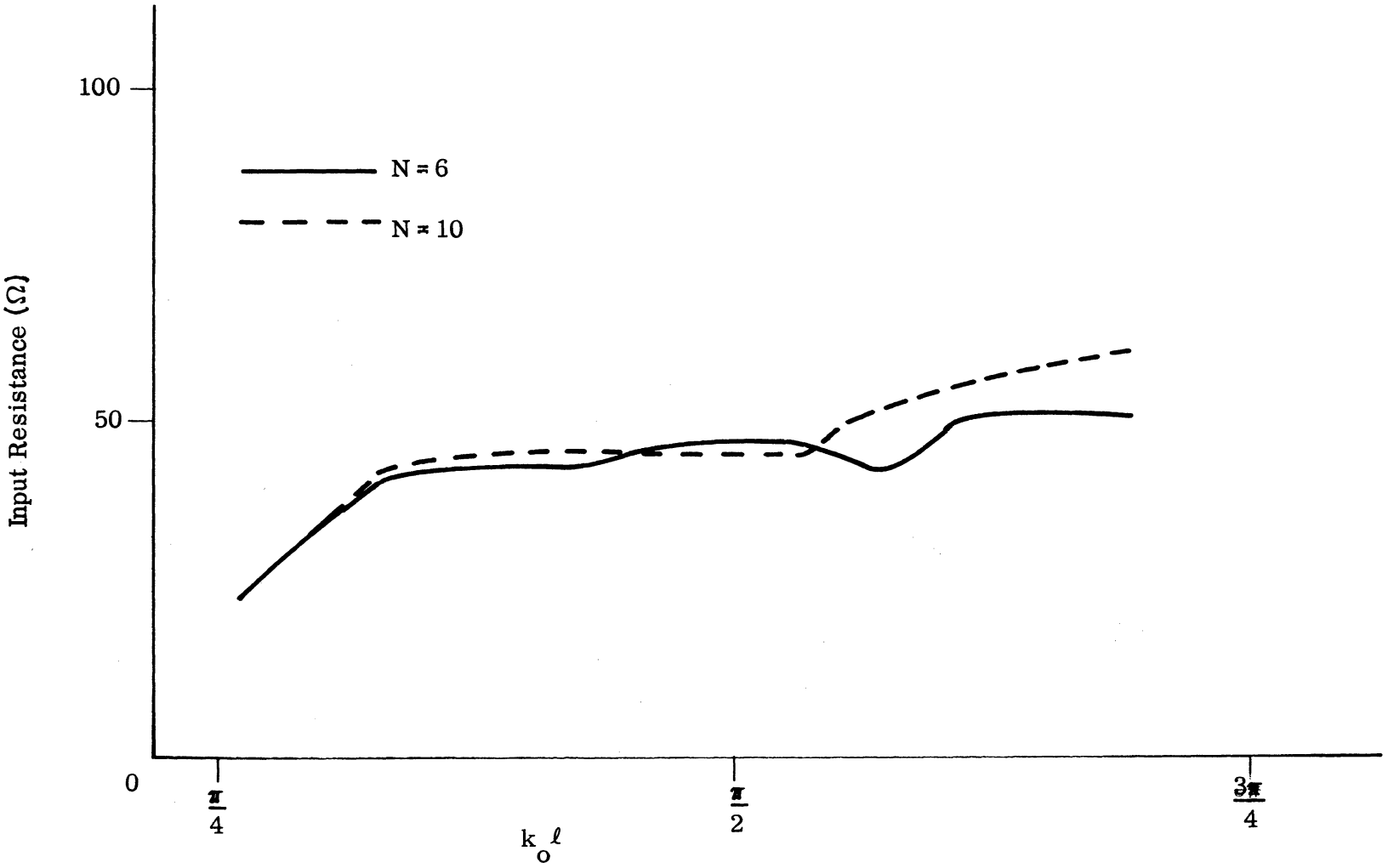

FIG. 3-2: THE INPUT RESISTANCE FOR $a/\ell = 0.01$, $b/\ell = 0.1$, $d/\ell = 0.075$.

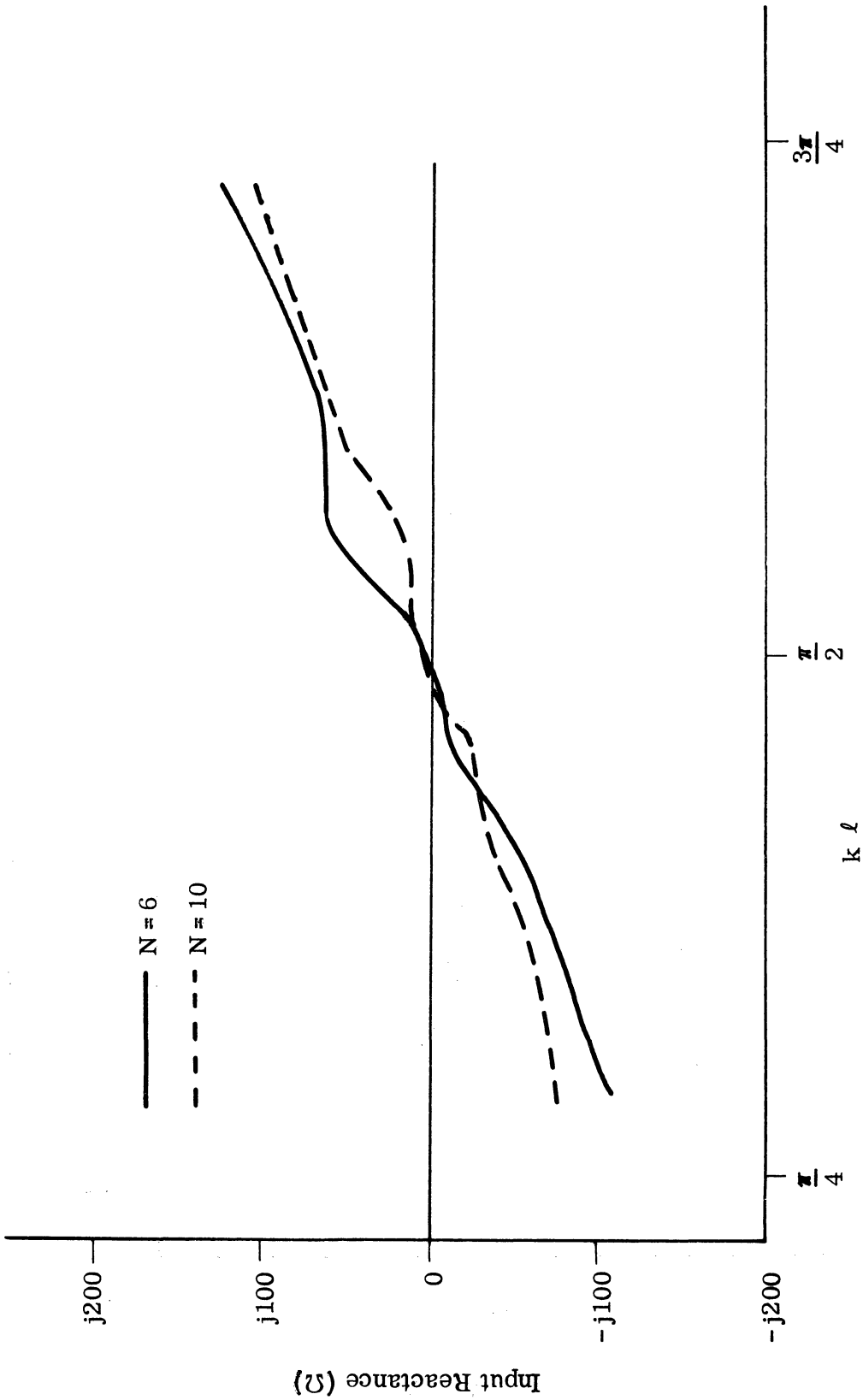

FIG. 3-3: THE INPUT REACTANCE FOR $a/\ell = 0.01$, $b/\ell = 0.1$, $d/\ell = 0.075$.

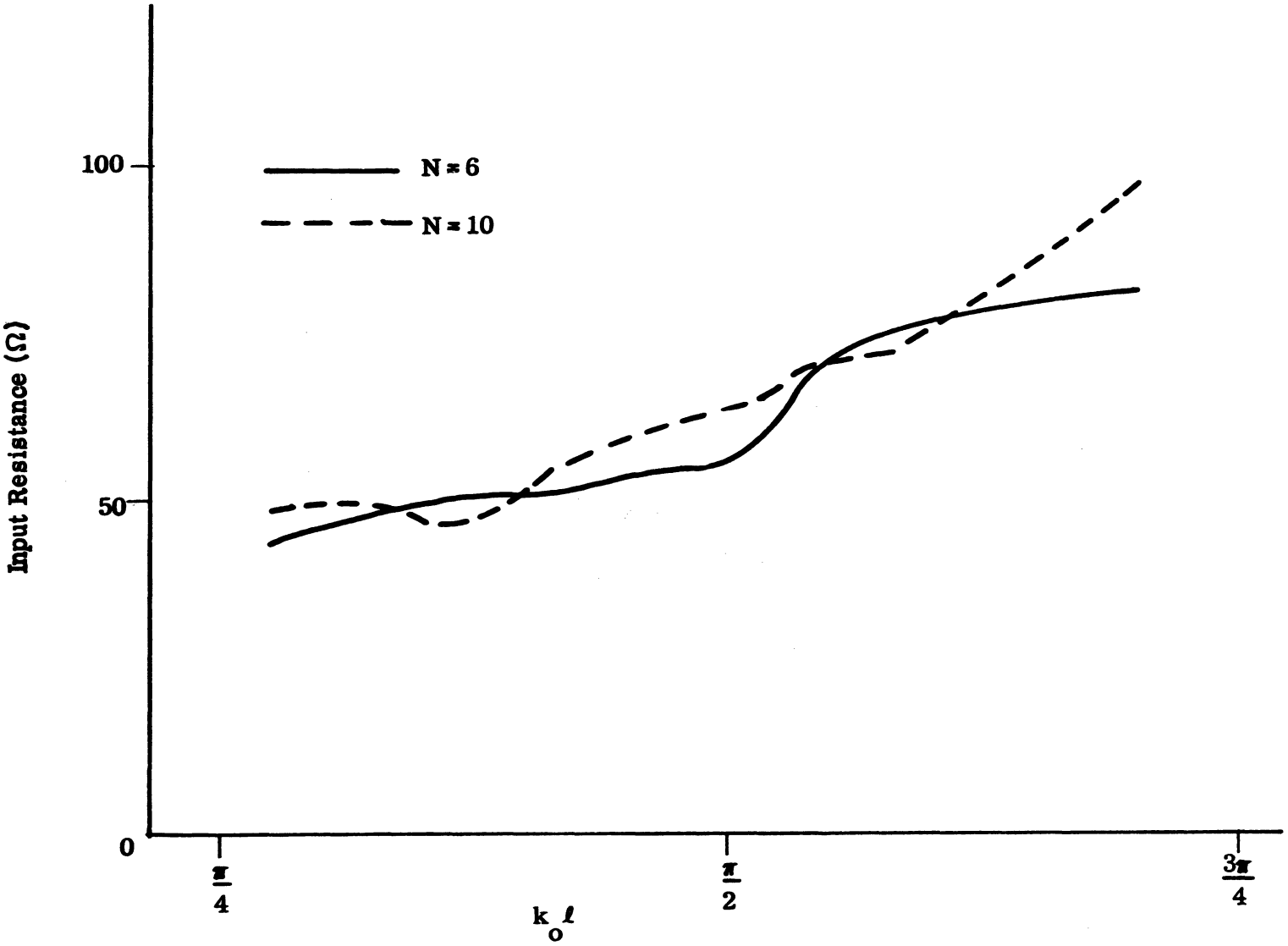

FIG. 3-4: THE INPUT RESISTANCE FOR $a/\ell = 0.01$, $b/\ell = 0.1$, $d/\ell = 0.225$.

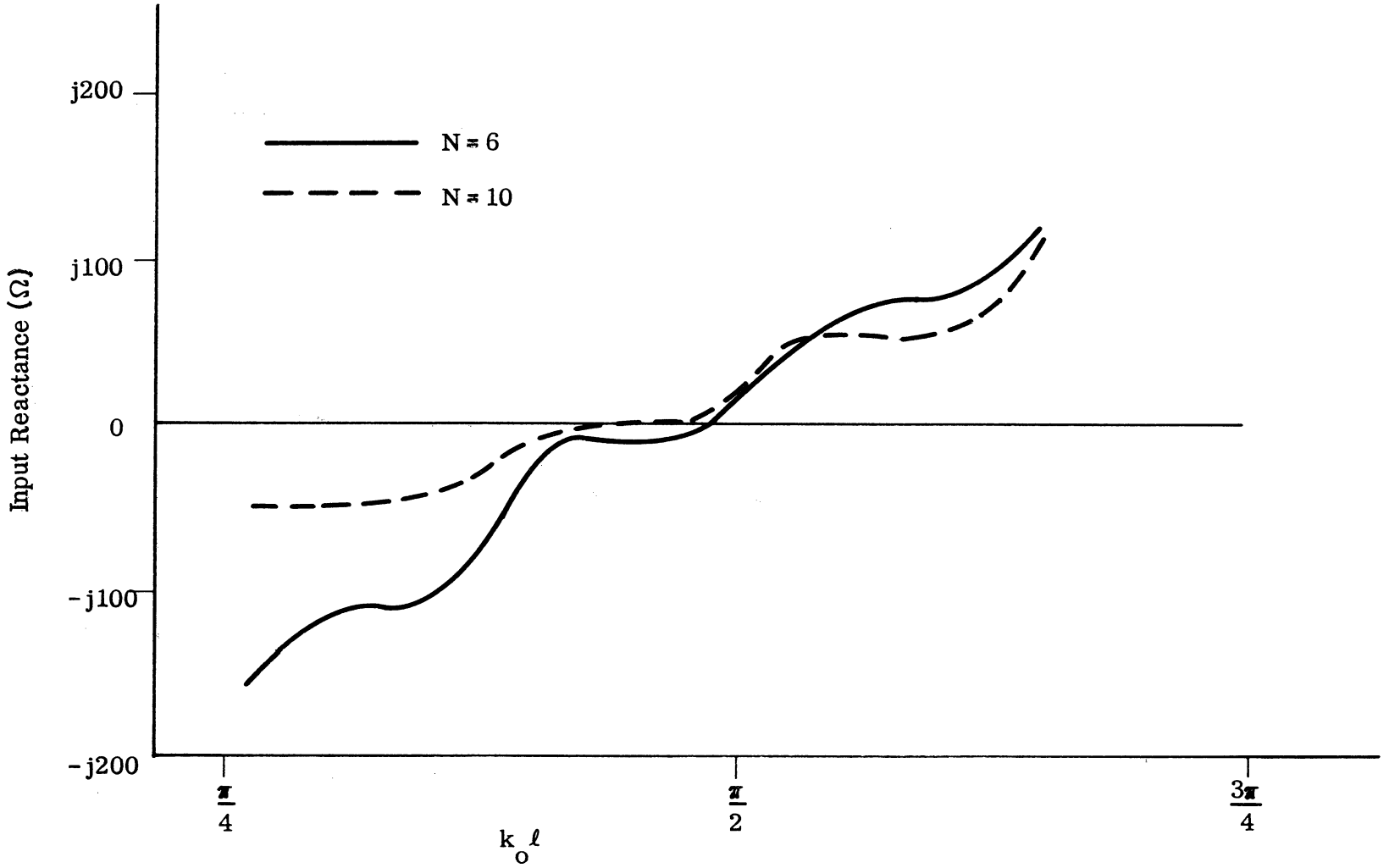

FIG. 3-5: THE INPUT REACTANCE FOR $a/\ell = 0.01$, $b/\ell = 0.1$, $d/\ell = 0.225$.

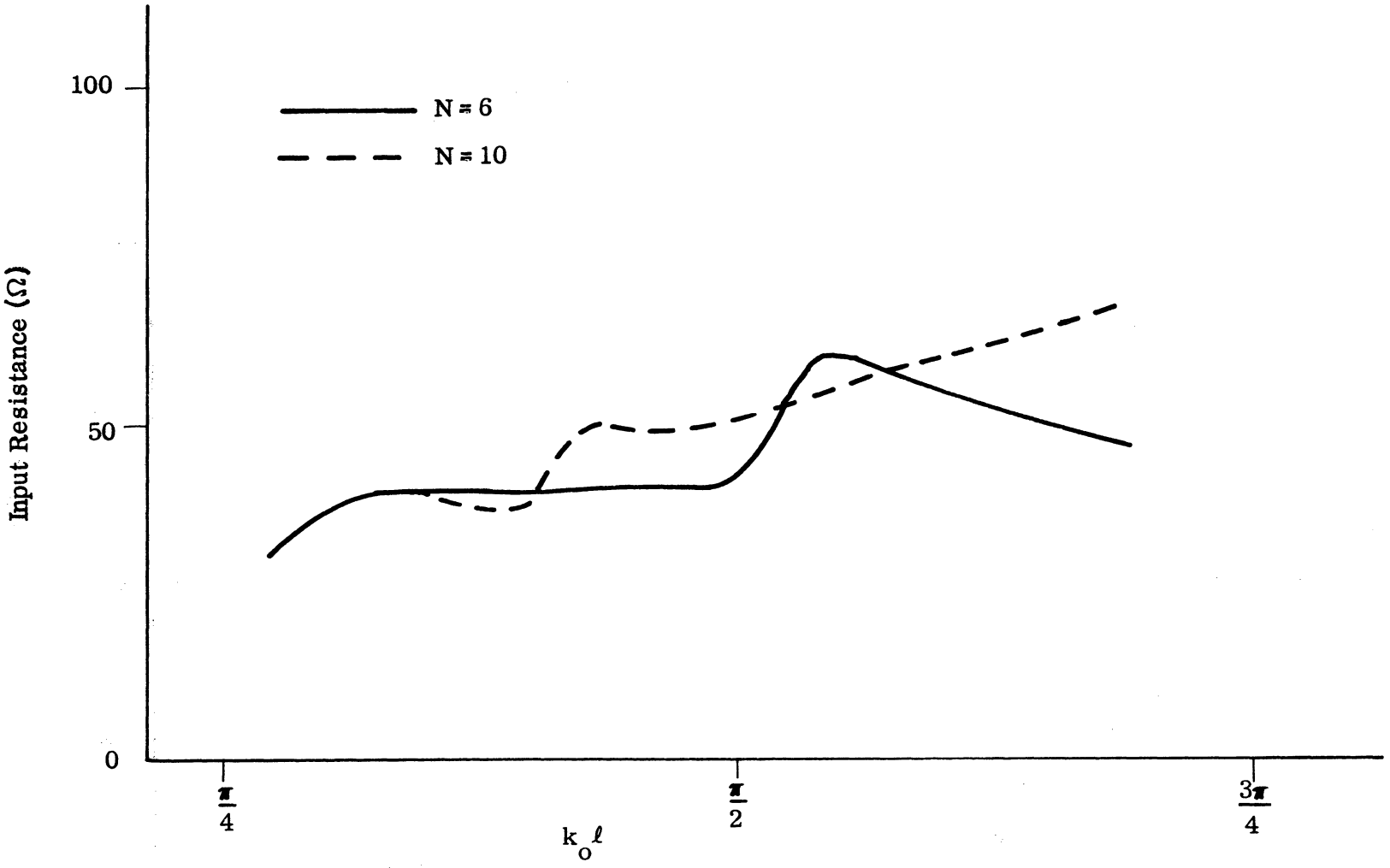

FIG. 3-6: THE INPUT RESISTANCE FOR $a/\ell = 0.01$, $b/\ell = 0.2$, $d/\ell = 0.075$.

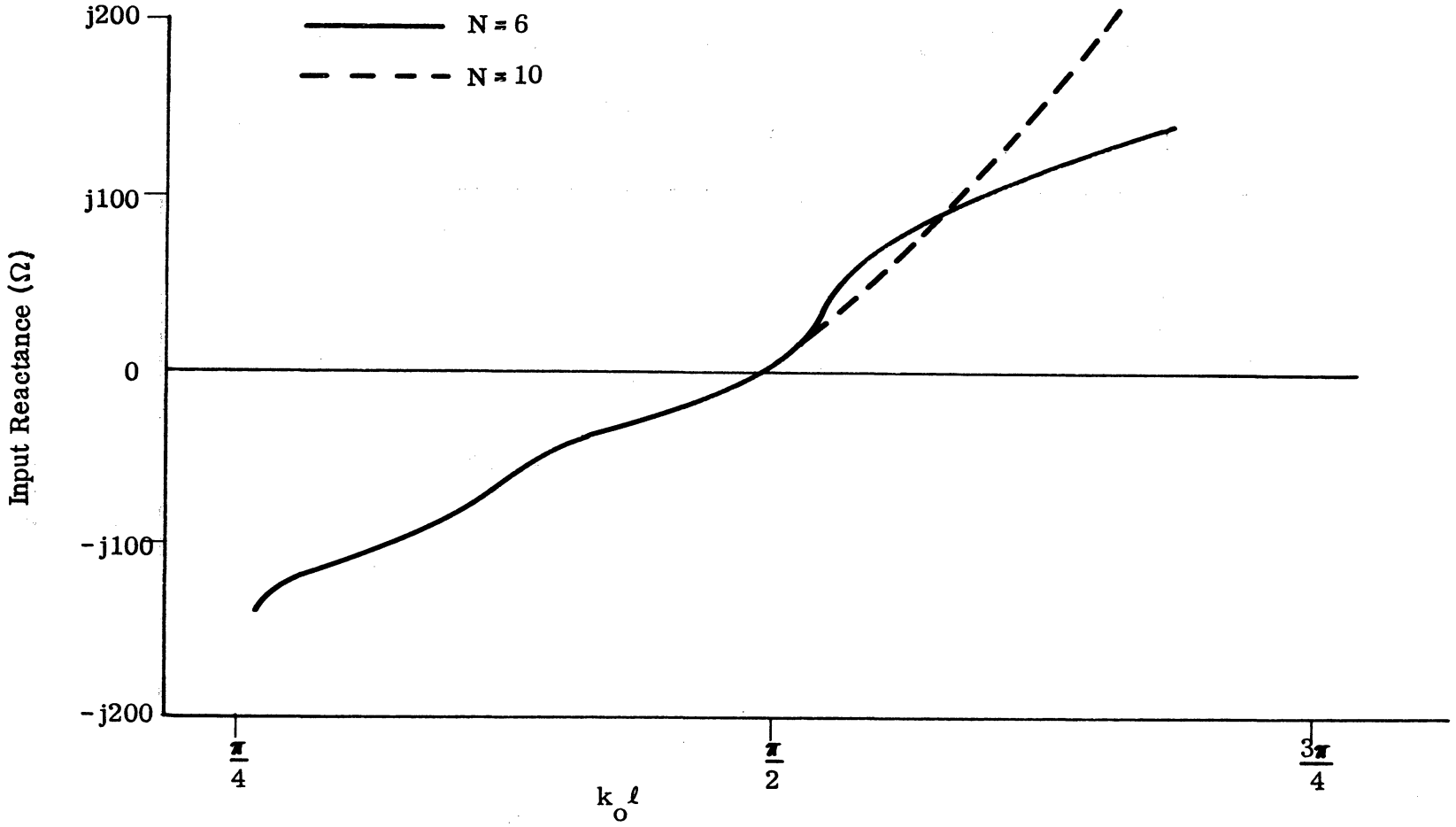

FIG. 3-7: THE INPUT REACTANCE FOR $a/\ell = 0.01$, $b/\ell = 0.2$, $d/\ell = 0.075$.

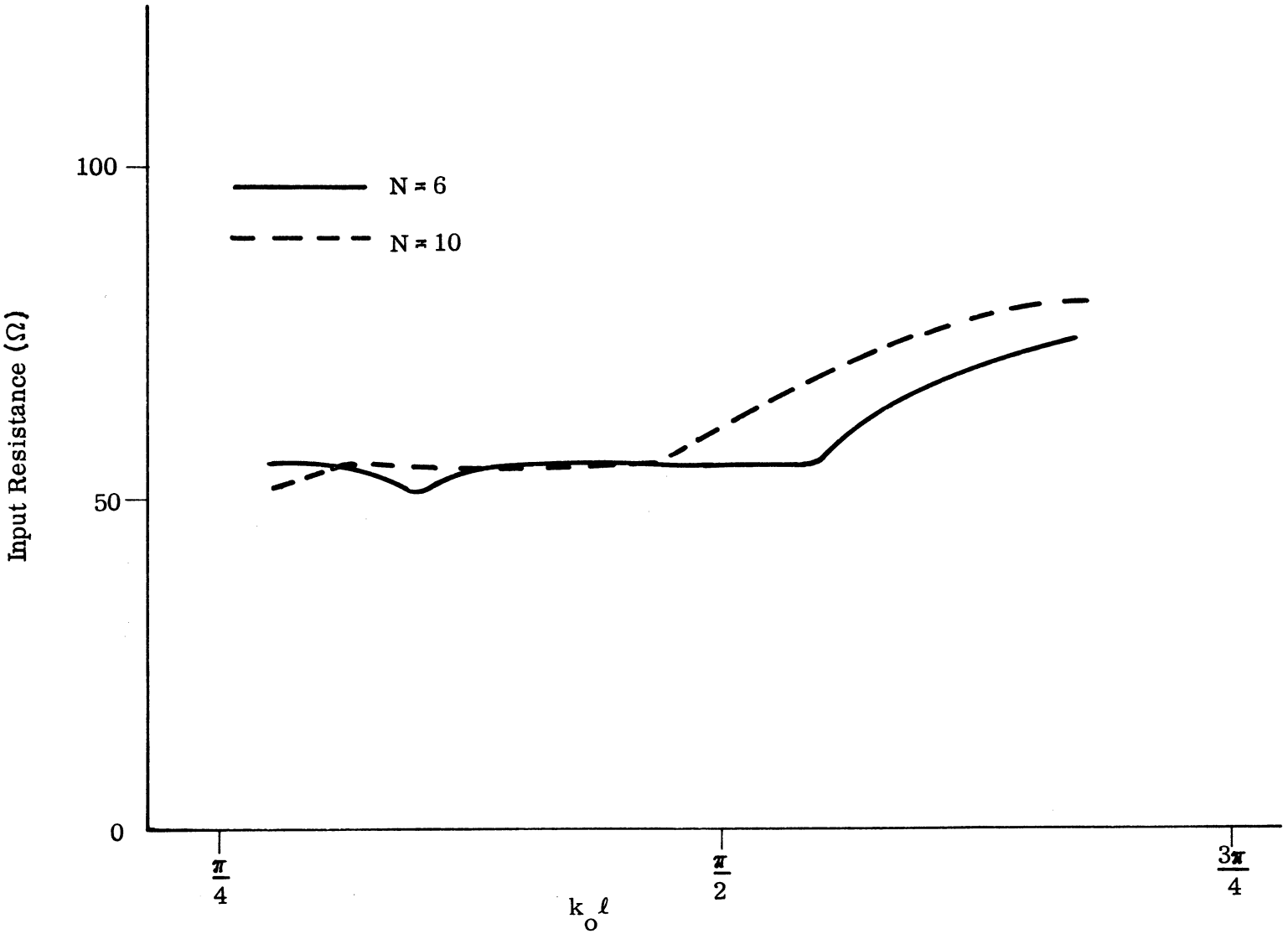

FIG. 3-8: THE INPUT RESISTANCE FOR $a/\ell = 0.01$, $b/\ell = 0.2$, $d/\ell = 0.225$.

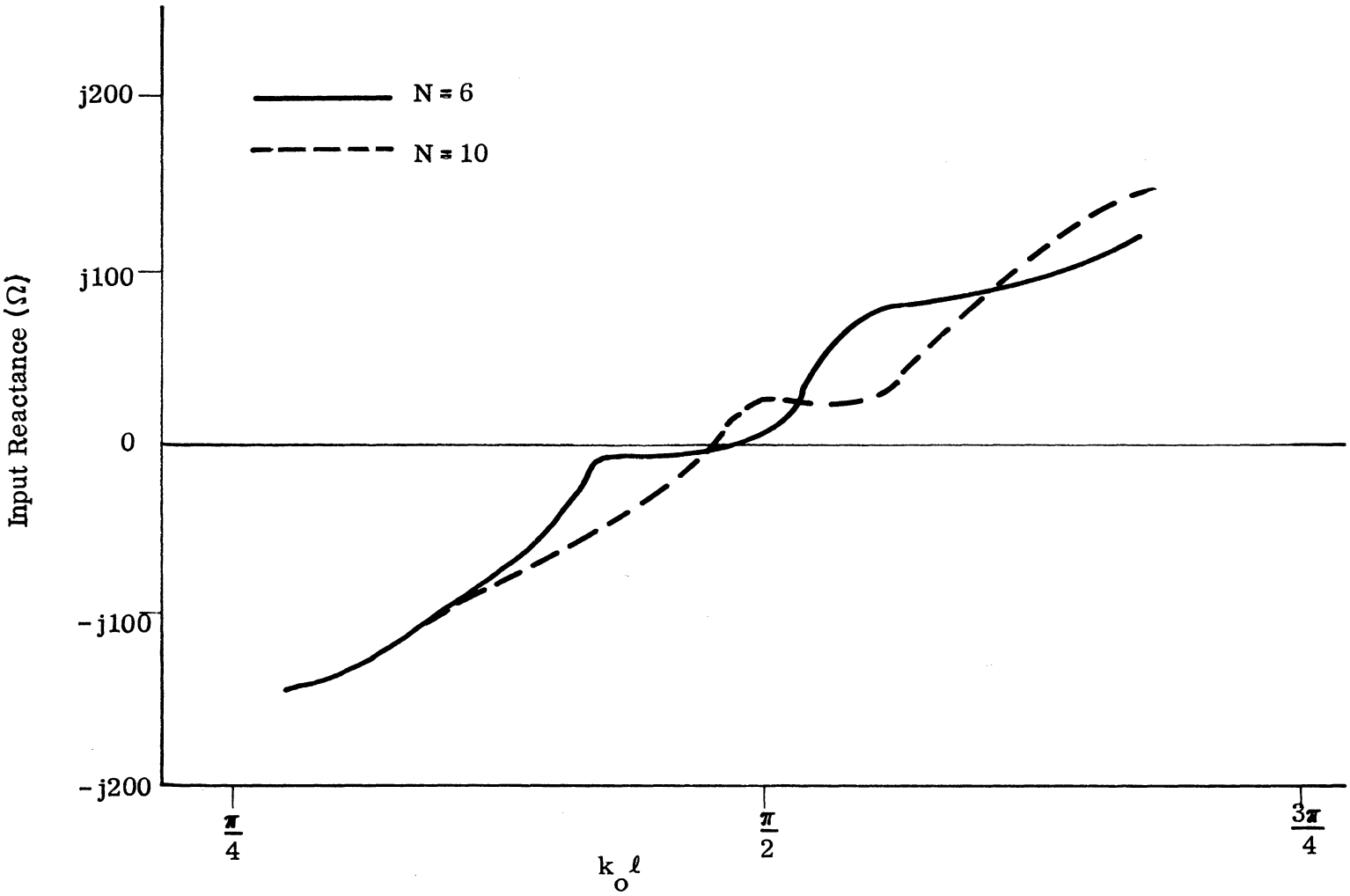

FIG. 3-9: THE INPUT REACTANCE FOR $a/\ell = 0.01$, $b/\ell = 0.2$, $d/\ell = 0.225$.

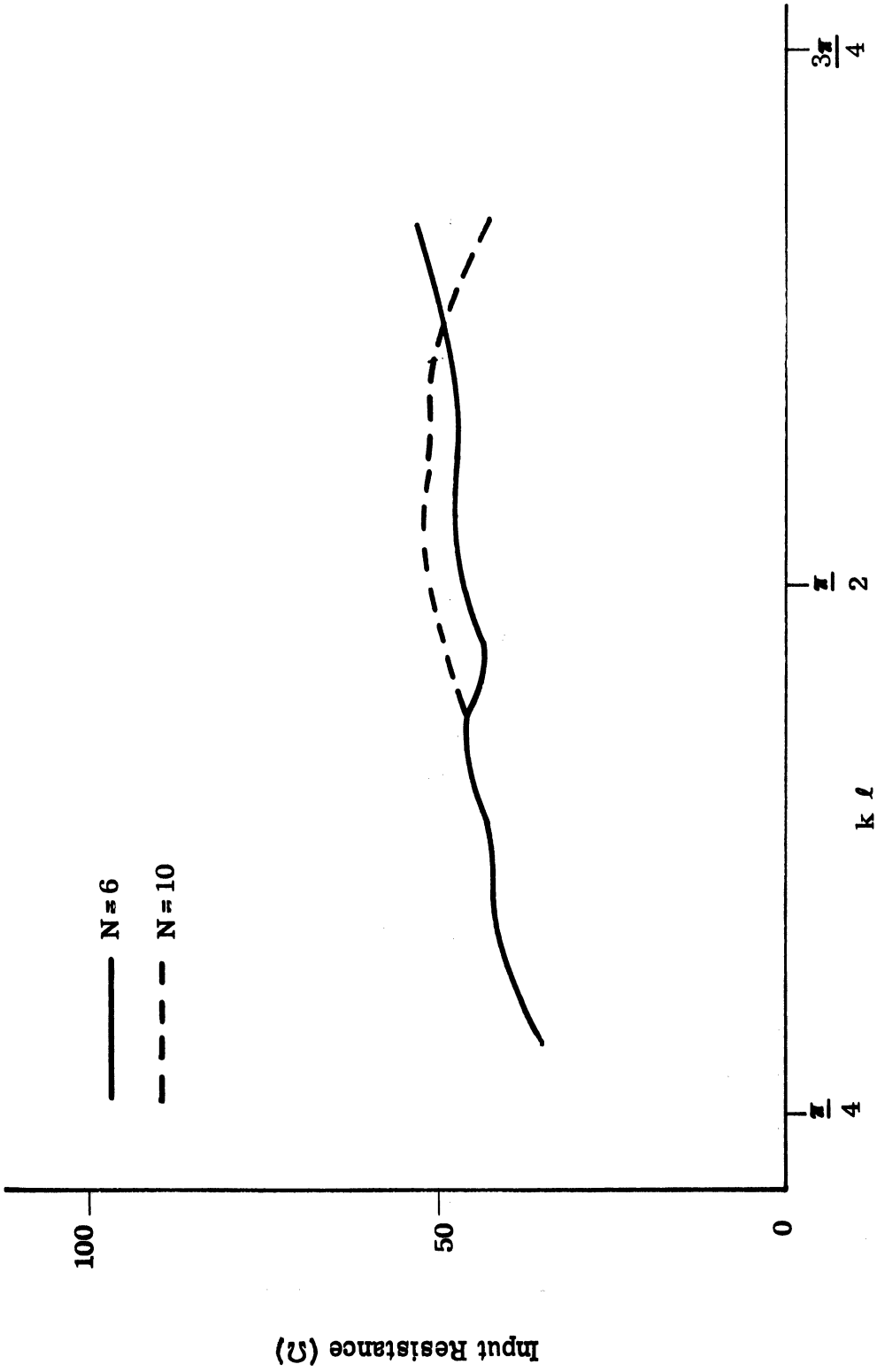

FIG. 3-10: THE INPUT RESISTANCE FOR $a/\ell = 0.02$, $b/\ell = 0.1$, $d/\ell = 0.075$.

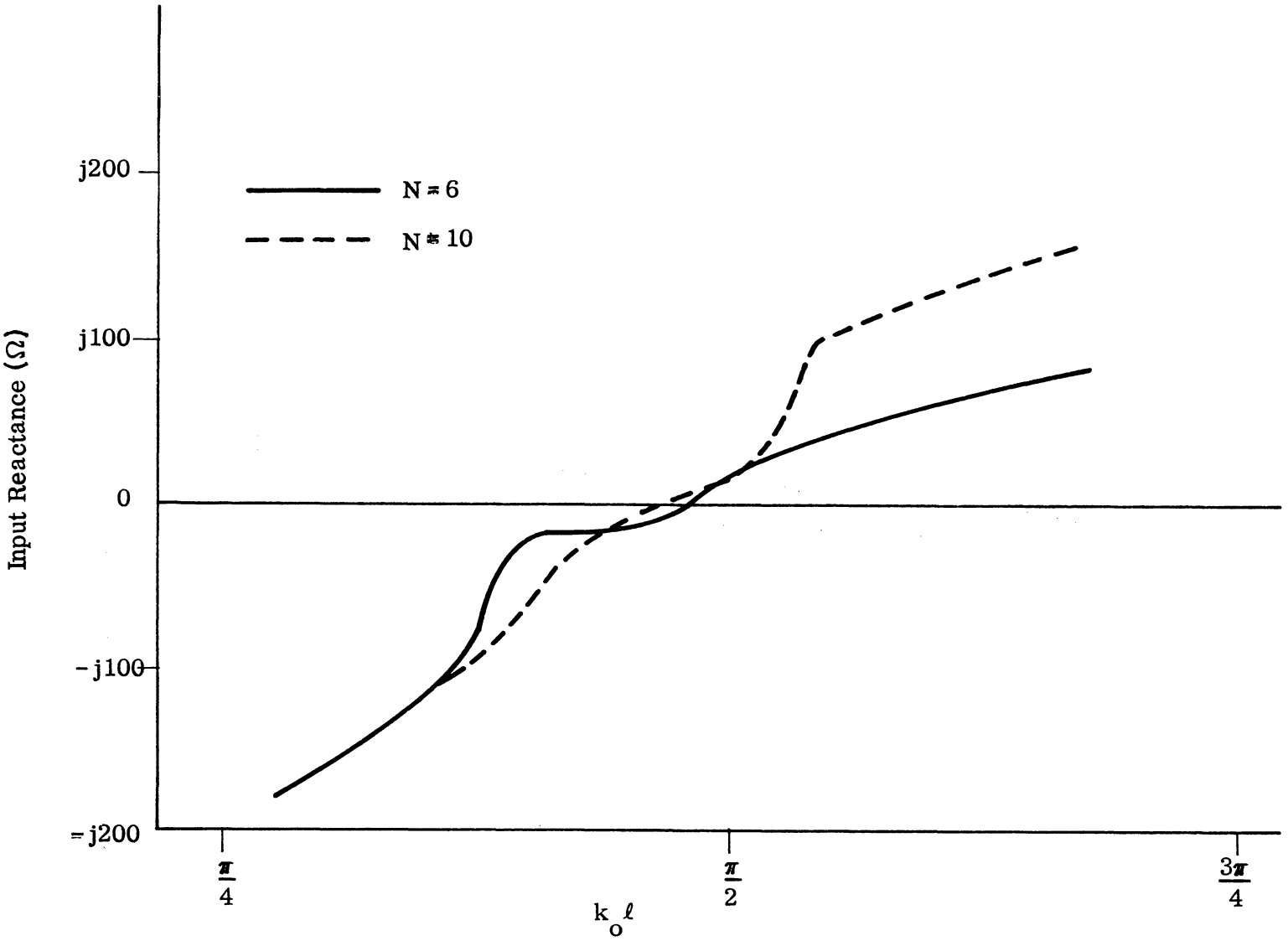

FIG. 3-11: THE INPUT REACTANCE FOR $a/\ell = 0.02$, $b/\ell = 0.1$, $d/\ell = 0.075$.

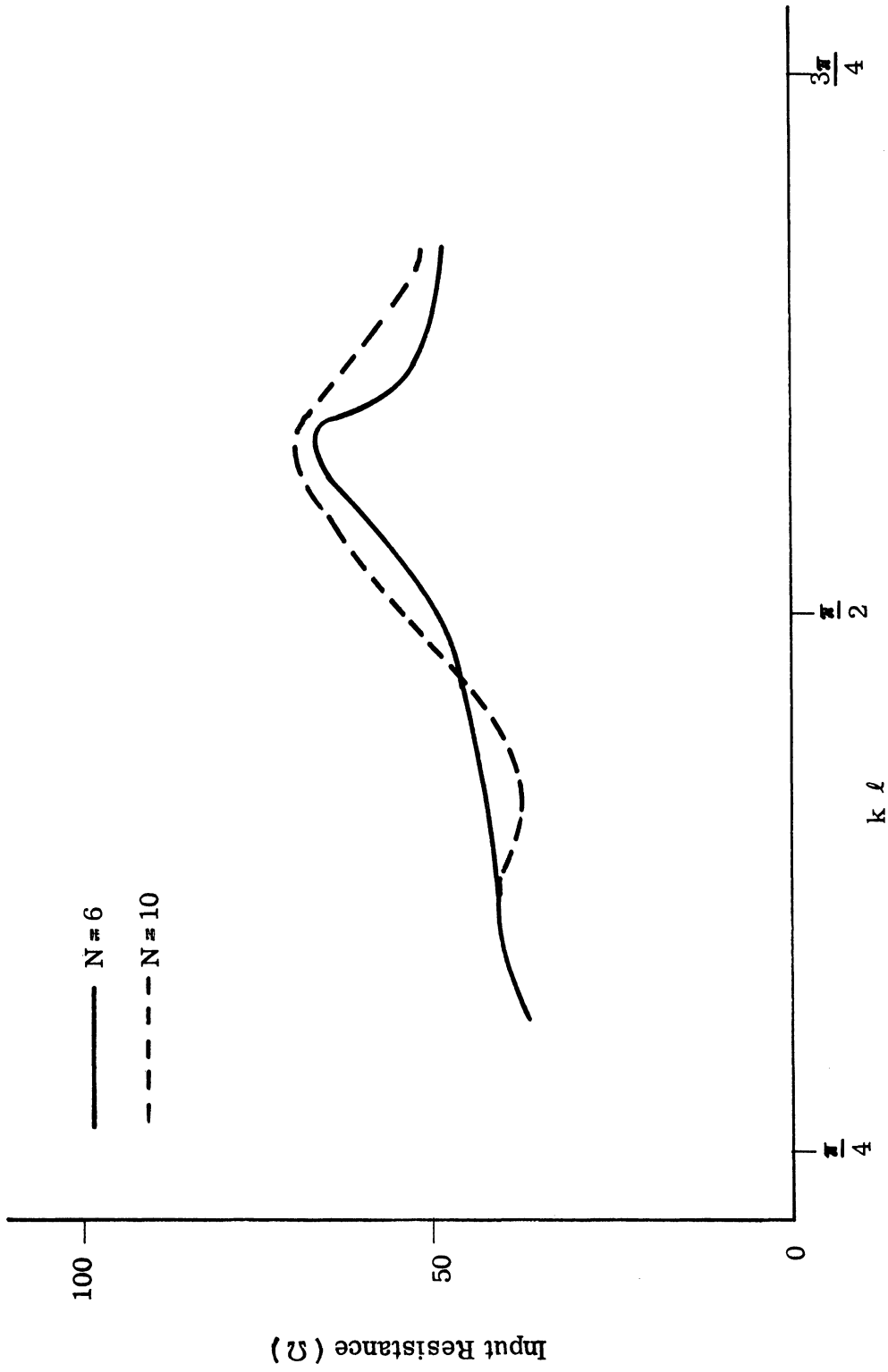

FIG. 3-12: THE INPUT RESISTANCE FOR $a/\ell = 0.02$, $b/\ell = 0.2$, $d/\ell = 0.075$.

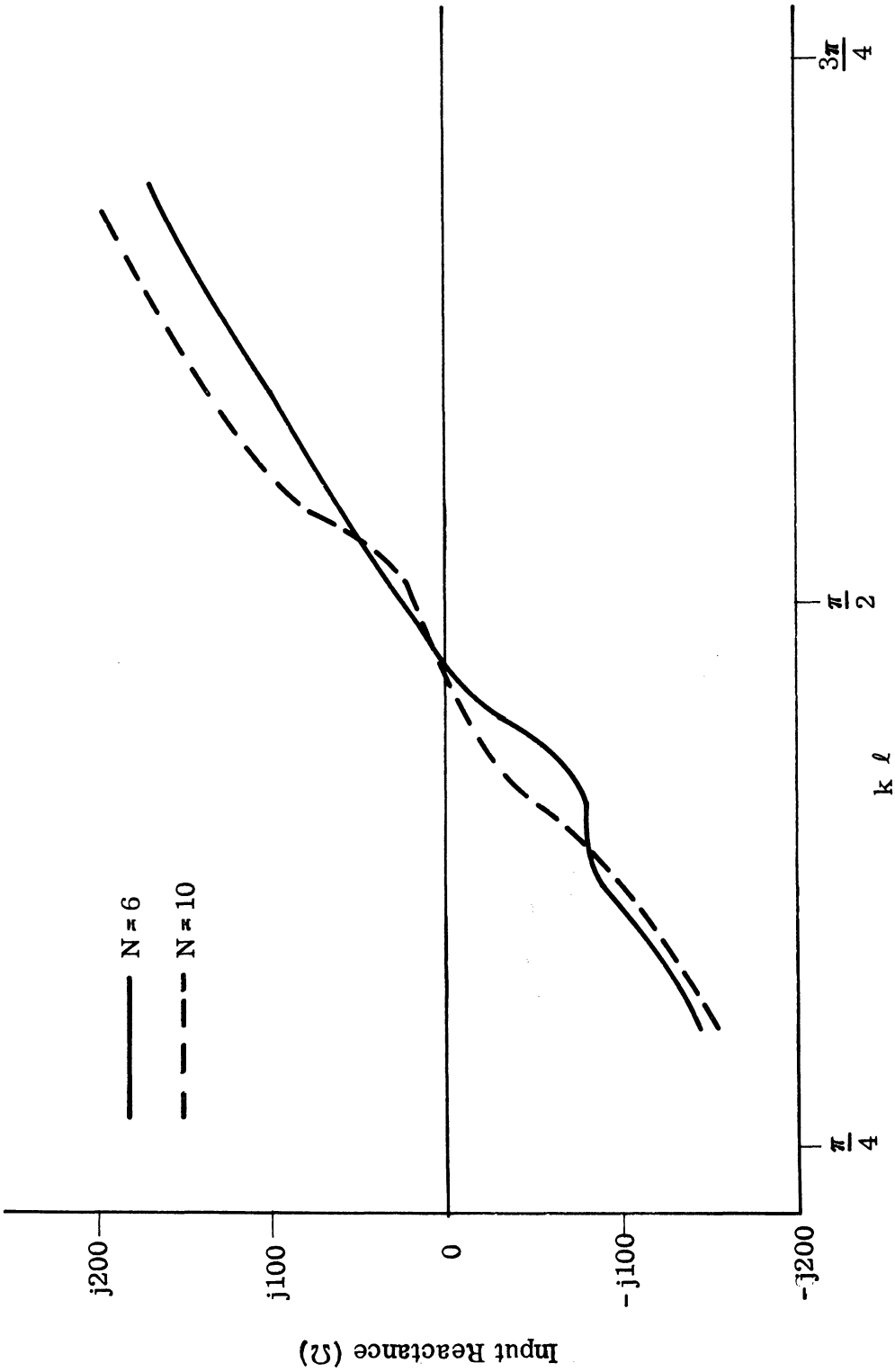

FIG. 3-13: THE INPUT REACTANCE FOR $a/\ell = 0.02$, $b/\ell = 0.2$, $d/\ell = 0.075$.

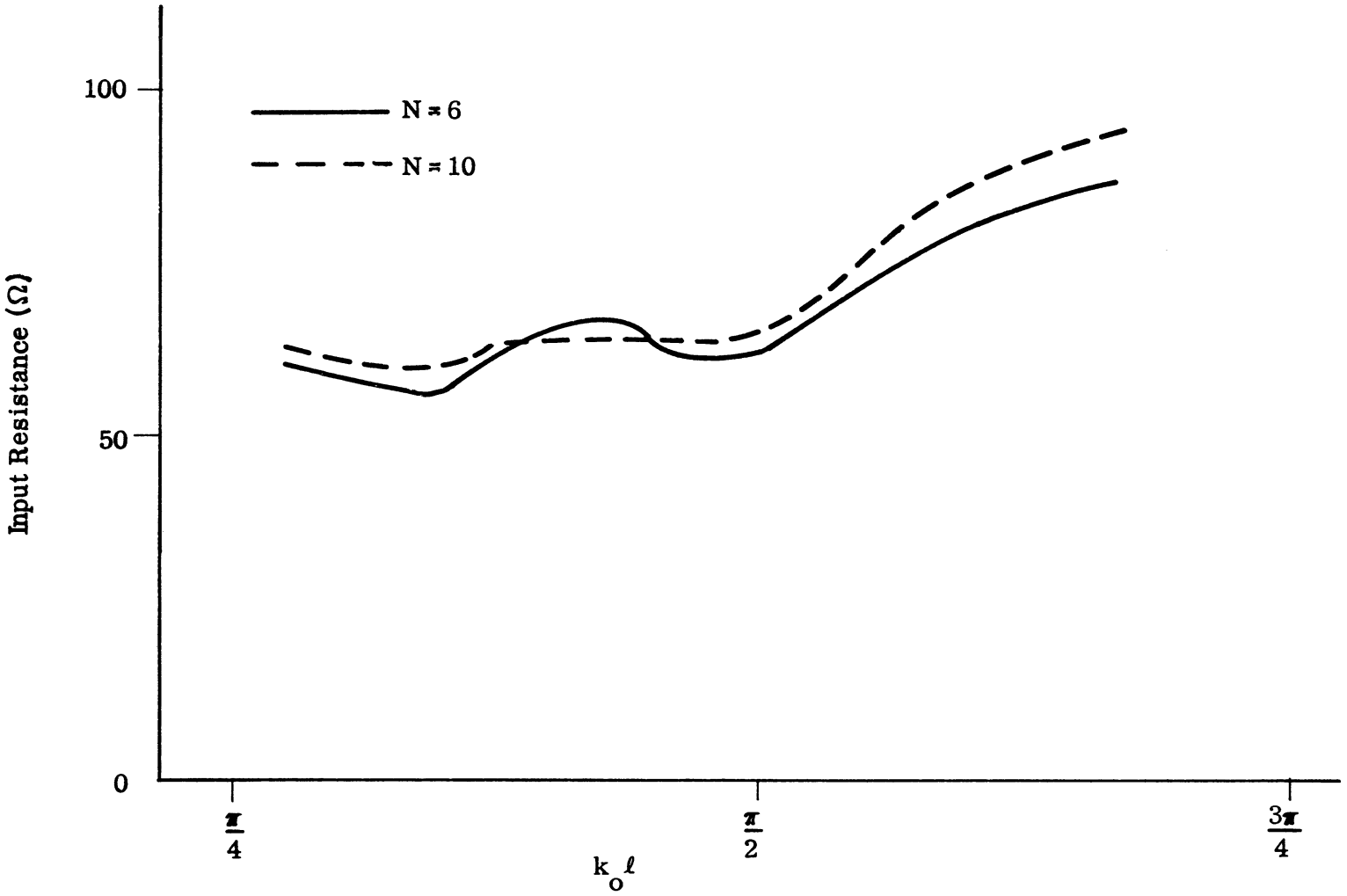

FIG. 3-14: THE INPUT RESISTANCE FOR $a/\ell = 0.02$, $b/\ell = 0.2$, $d/\ell = 0.225$.

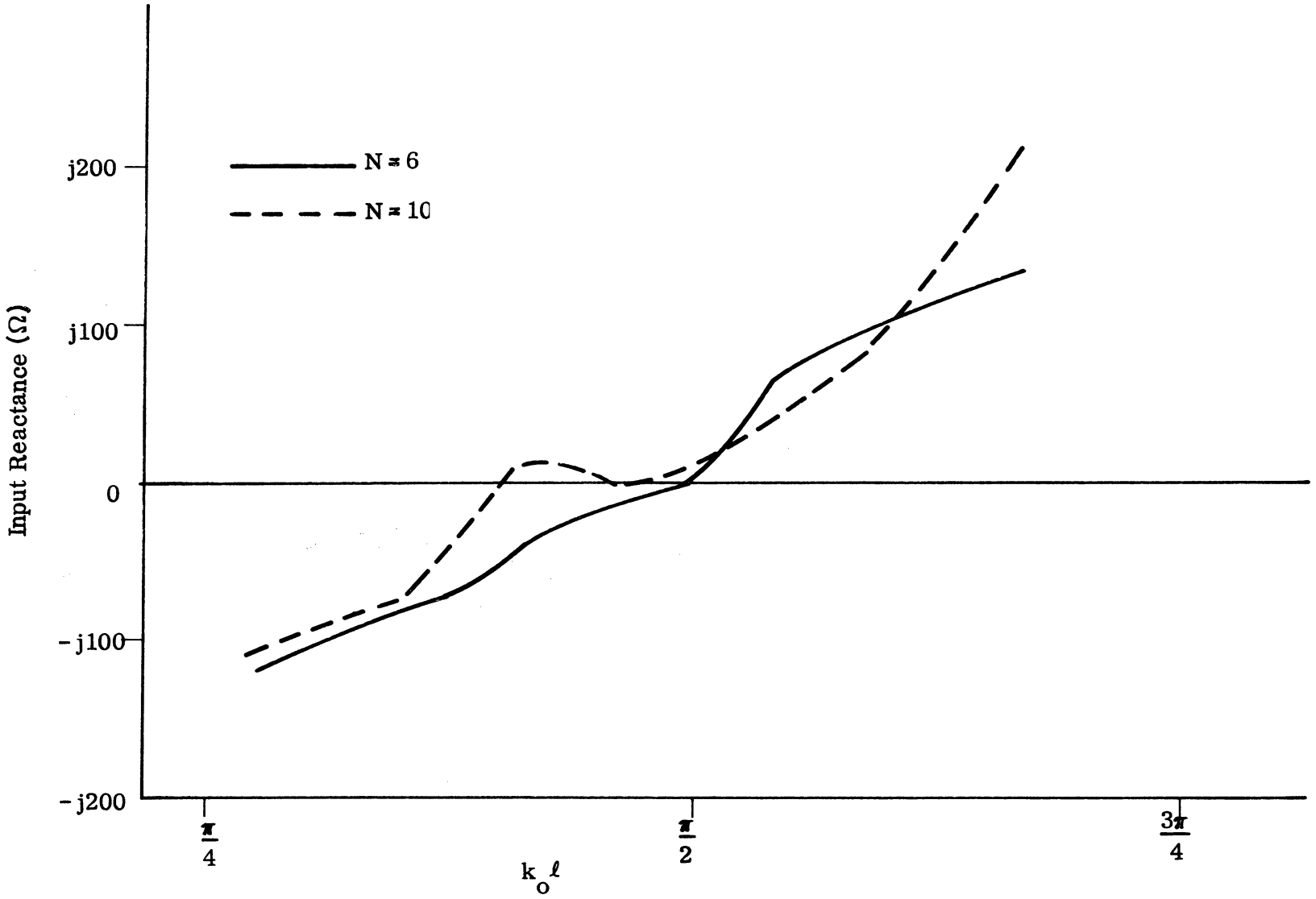

FIG. 3-15: THE INPUT REACTANCE FOR $a/\ell = 0.02$, $b/\ell = 0.2$, $d/\ell = 0.225$.

as will be confirmed through experiments in the next chapter.

If typical values of d/ℓ are used in (3.23), the radiation resistance of the vertical sections is found to be less than 5Ω; therefore, the effect of the vertical sections will be very small compared to that of the horizontal ones unless d/ℓ is increased very significantly.

However, the above discussion is only indicative of structure dependence and results must be checked by experiment, in particular since the analytical formulation is very crude.

3.3.2 The Radiation Pattern.

The radiation pattern can be computed by letting $y=\frac{\ell}{2}$ and $K=\pm 1, \pm 2, ----, \pm N$ in (3.15). With A_o, B_o, and A_K known, the complex space factor is found to be

$$F=(1-z_2)\left[\frac{A_o F_o(\frac{\ell}{2}) - F_o(\ell)}{G_o(\frac{\ell}{2})\left[1-F_o(\ell)\right]} + jB_o + z_1 A_1 + z_1^2 A_2 + ---- + z_1^K A_K\right] \tag{3.25}$$

where

$$z_1 = e^{jk_o b\cos\phi} \quad \text{for K positive}$$
$$= e^{-jk_o b\cos\phi} \quad \text{for K negative} \tag{3.26}$$
$$z_2 = e^{jk_o(2d)\sin\phi}$$

and where b, d, ϕ are as indicated in Fig. 3-1.

The magnitude of (3.25) is calculated for N=6 and 10 with various parameter values as shown in Figs. 3-16 through 3-29. From these, it is seen that a broadside pattern is obtained over a wide frequency range except for some frequencies where the array elements are the equivalent of a quarter-wavelength; here a beam split is noted for several cases. The comparison of the same parameter values

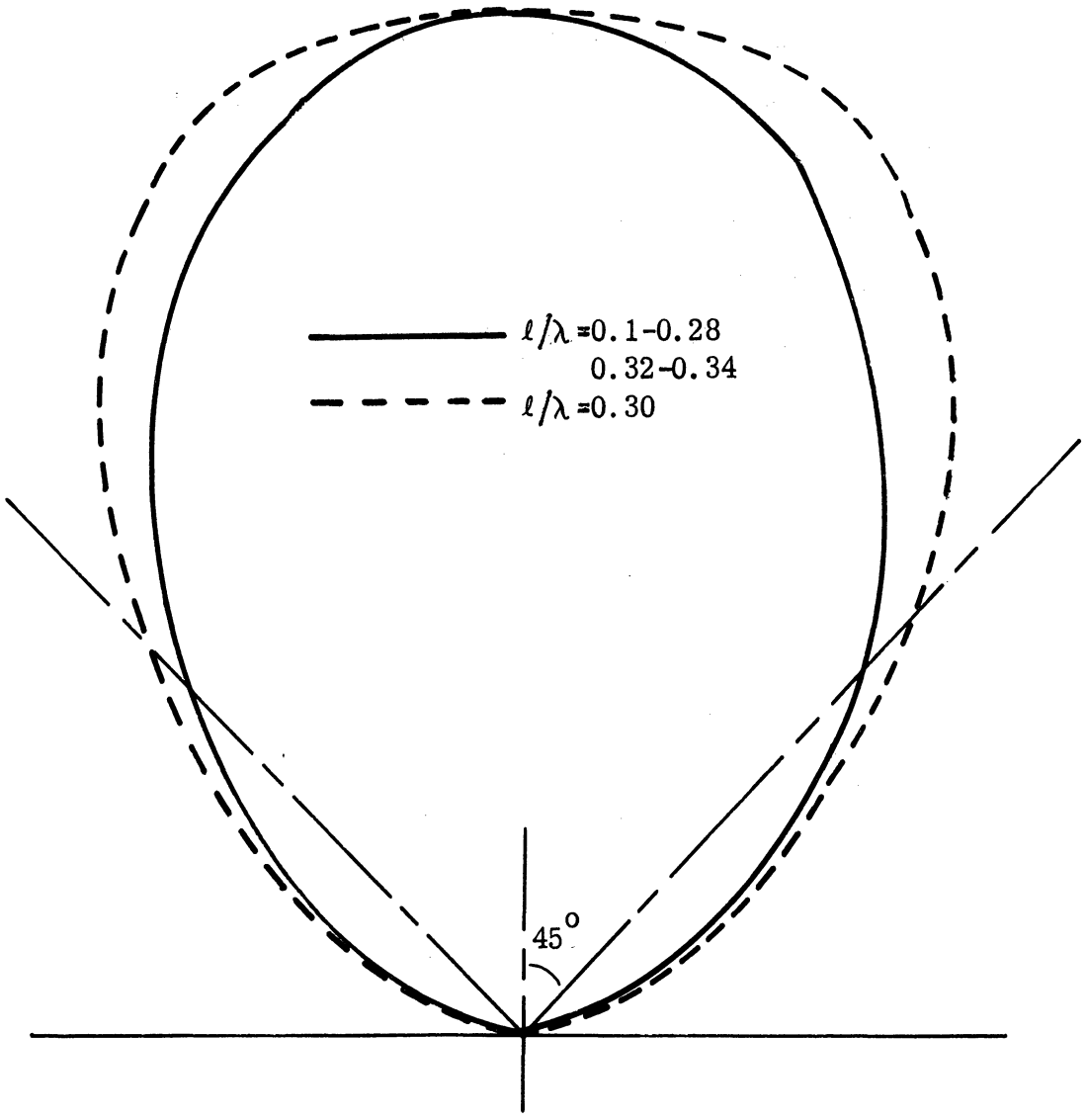

FIG. 3-16: THE FAR FIELD H-PLANE E_y-PATTERN FOR N=6, $a/\ell=0.01$, $b/\ell=0.1$, $d/\ell=0.075$.

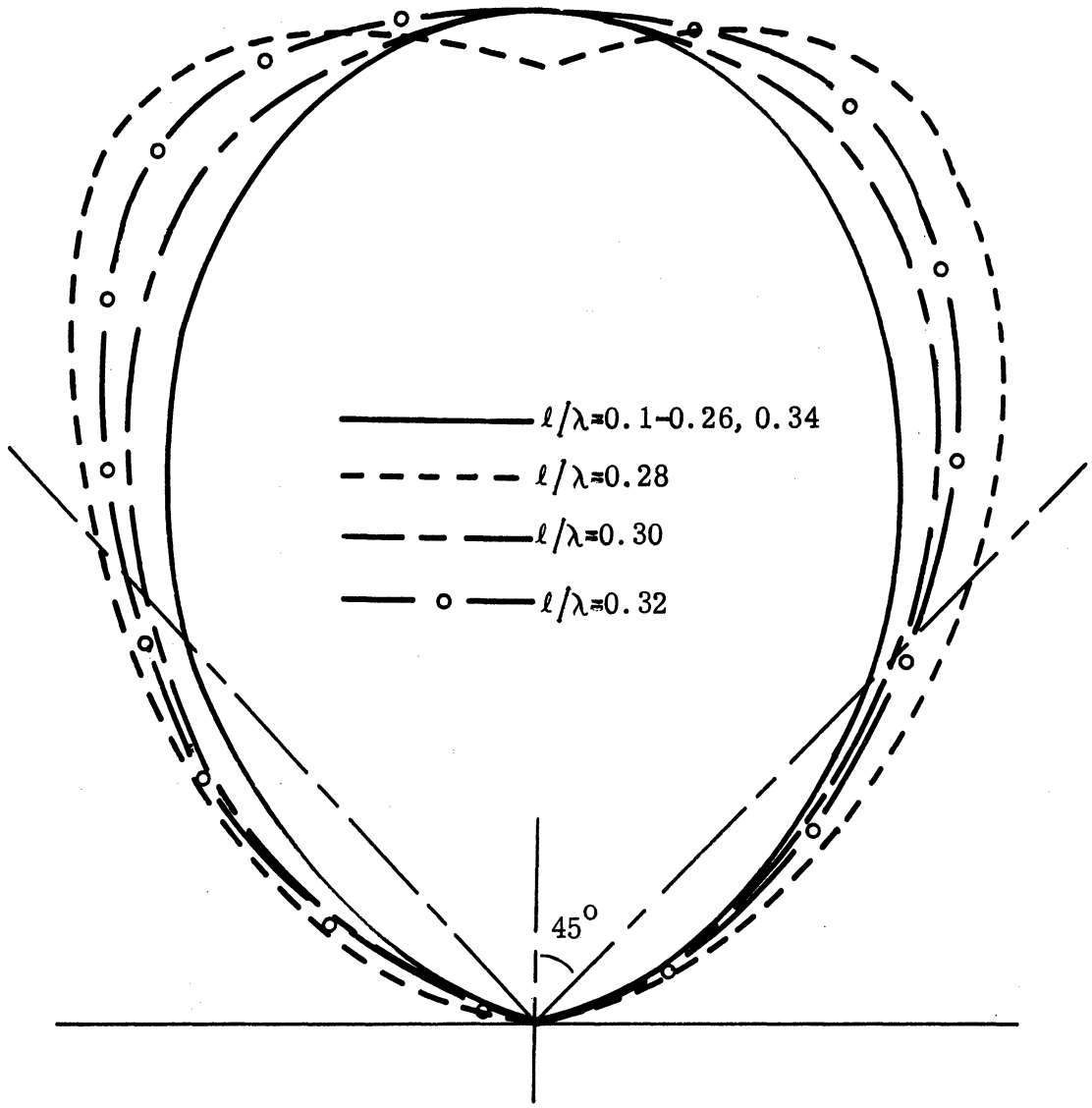

FIG. 3-17: THE FAR FIELD H-PLANE E_y-PATTERN FOR N=10, $a/\ell=0.01$, $b/\ell=0.1$, $d/\ell=0.075$.

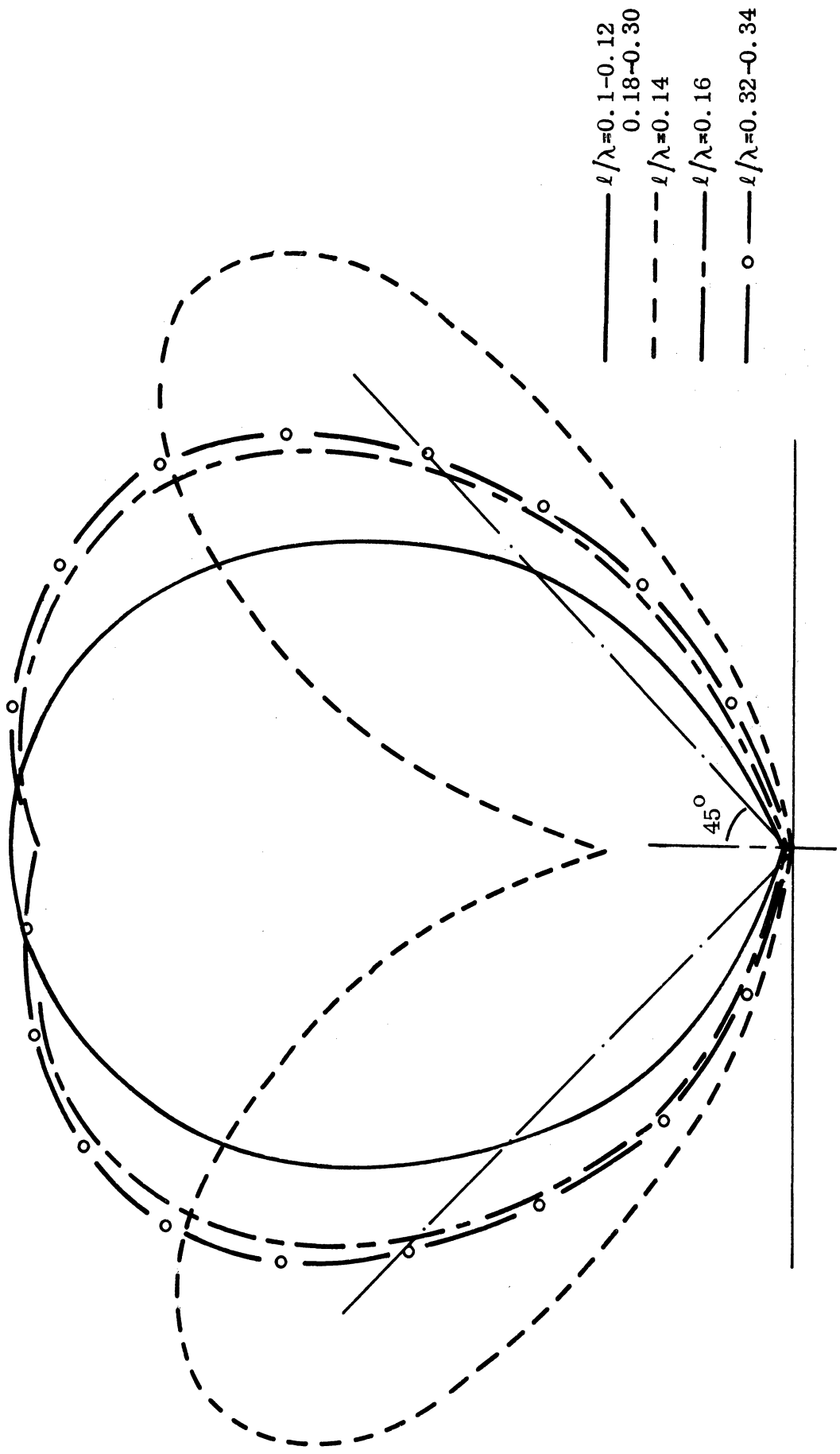

FIG. 3-18: THE FAR FIELD H-PLANE E_y-PATTERN FOR N=6, a/ℓ=0.01, b/ℓ=0.1, d/ℓ=0.225.

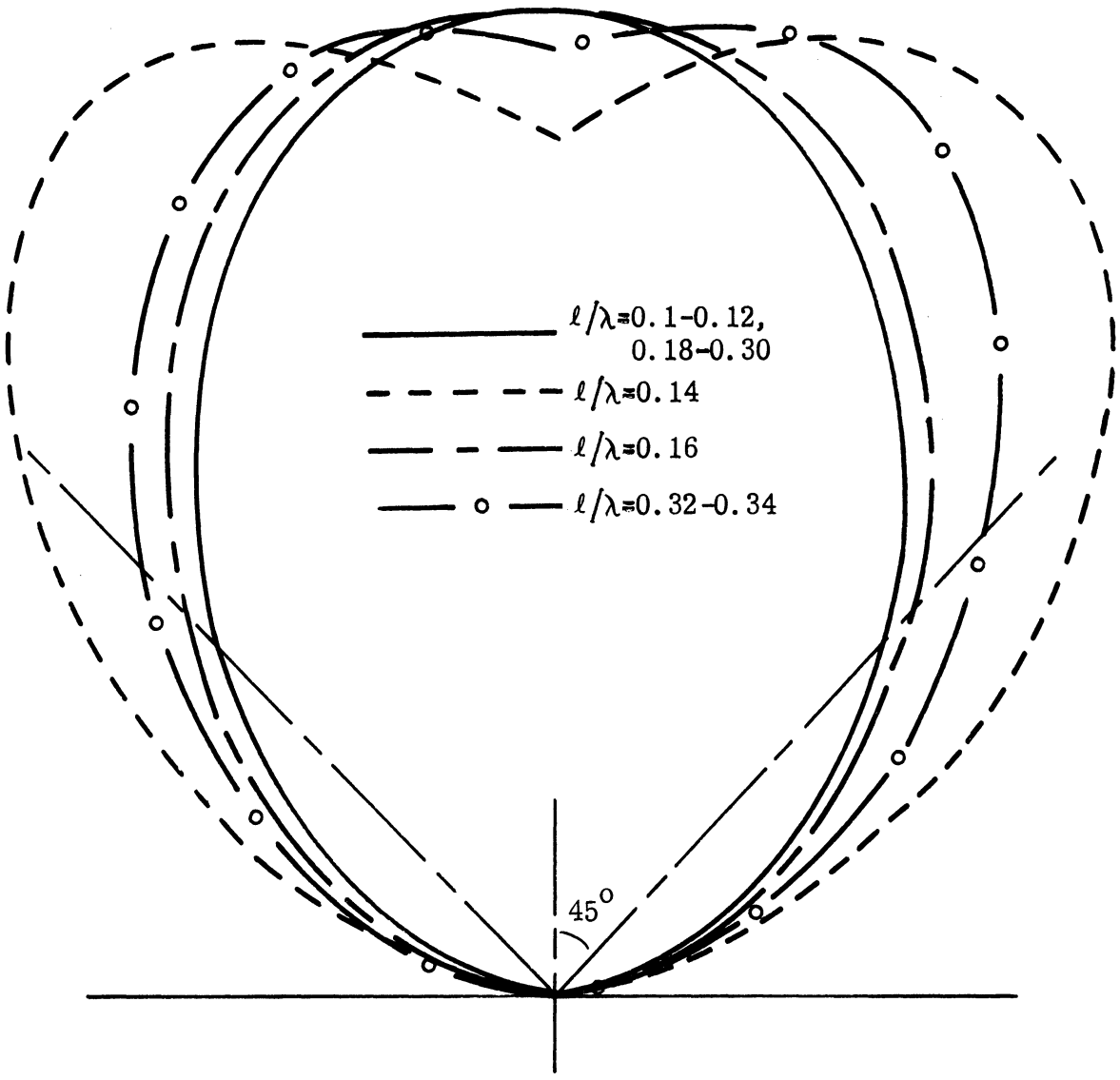

FIG. 3-19: THE FAR FIELD H-PLANE E_y-PATTERN FOR N=10, a/ℓ=0.01, b/ℓ=0.1, d/ℓ=0.225.

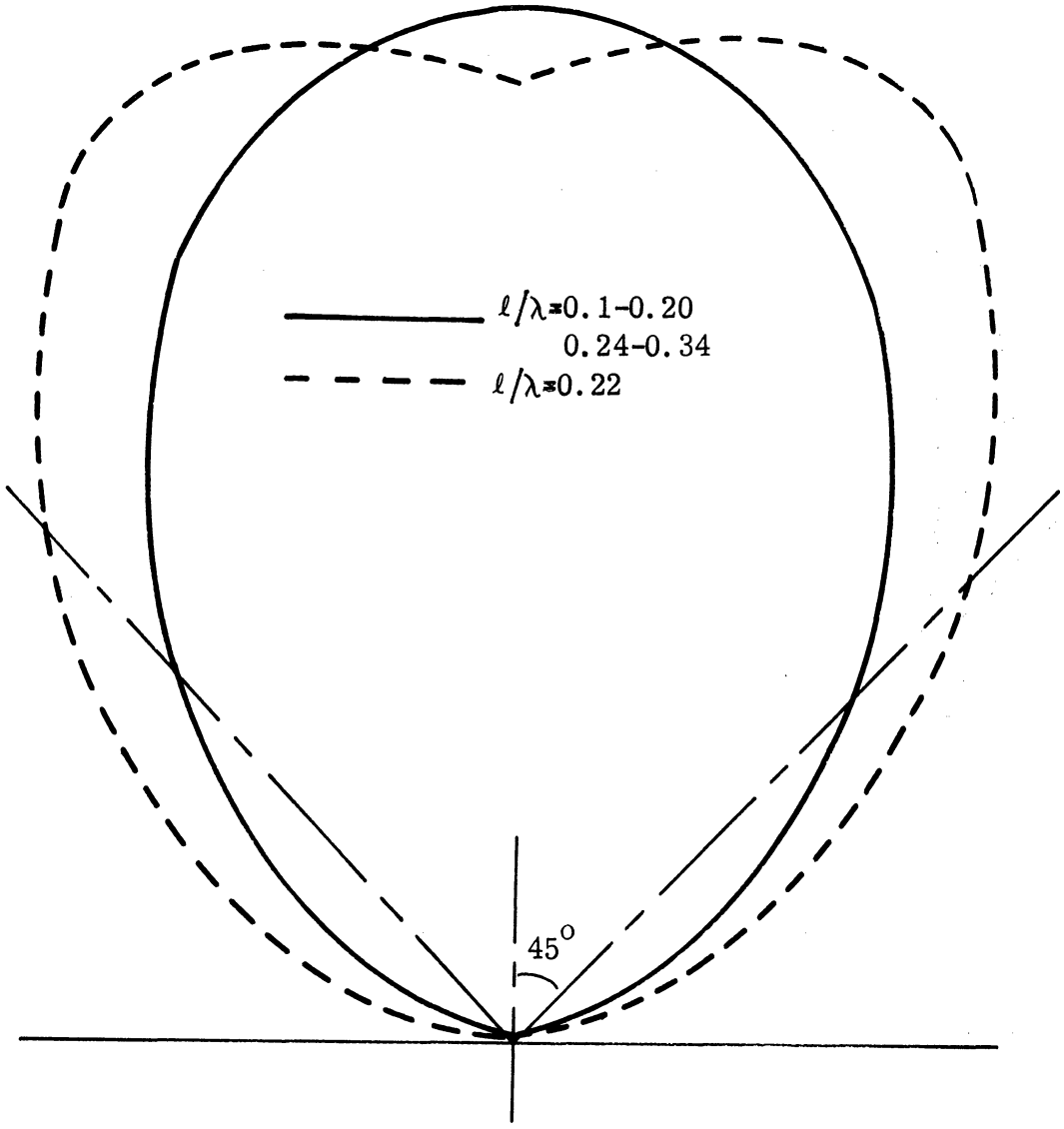

FIG. 3-20: THE FAR FIELD H-PLANE E_y-PATTERN FOR N=6, a/ℓ=0.01, b/ℓ=0.2, d/ℓ=0.075.

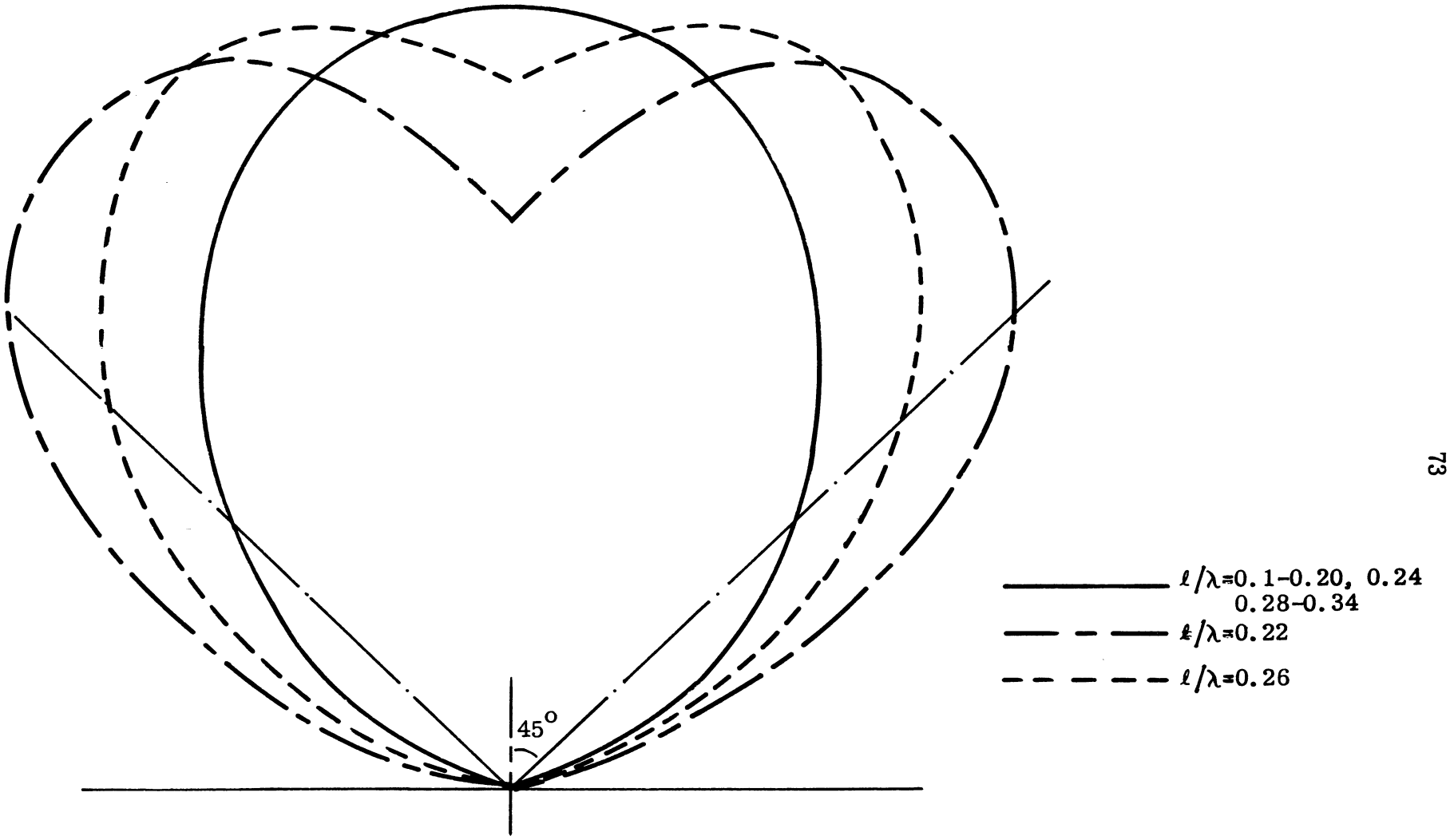

FIG. 3-21: THE FAR FIELD H-PLANE E_y-PATTERN FOR N=10, a/ℓ=0.01, b/ℓ=0.2, d/ℓ=0.075.

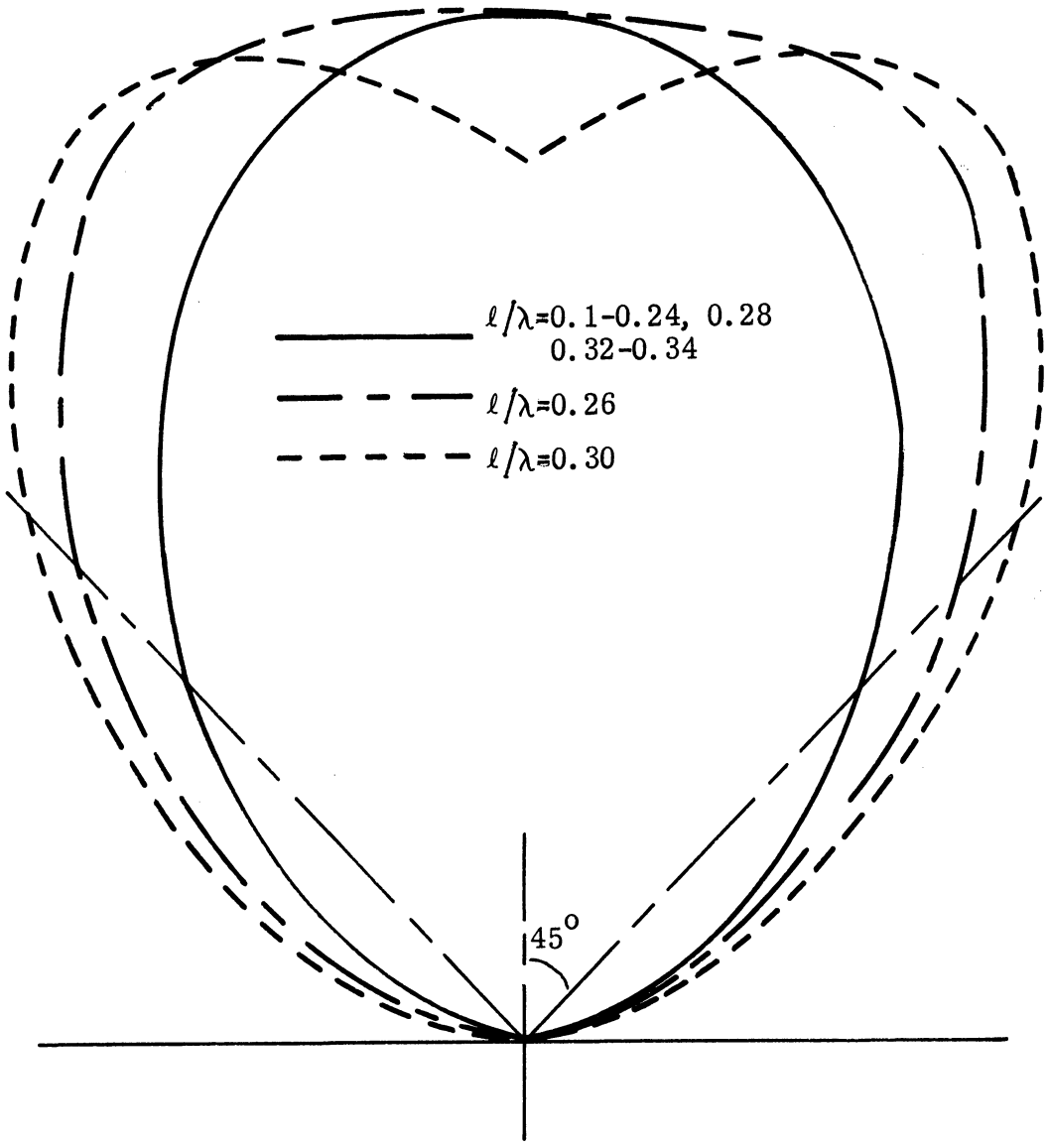

FIG. 3-22: THE FAR FIELD H-PLANE E_y-PATTERN FOR N=6, a/ℓ=0.01, b/ℓ=0.2, d/ℓ=0.225.

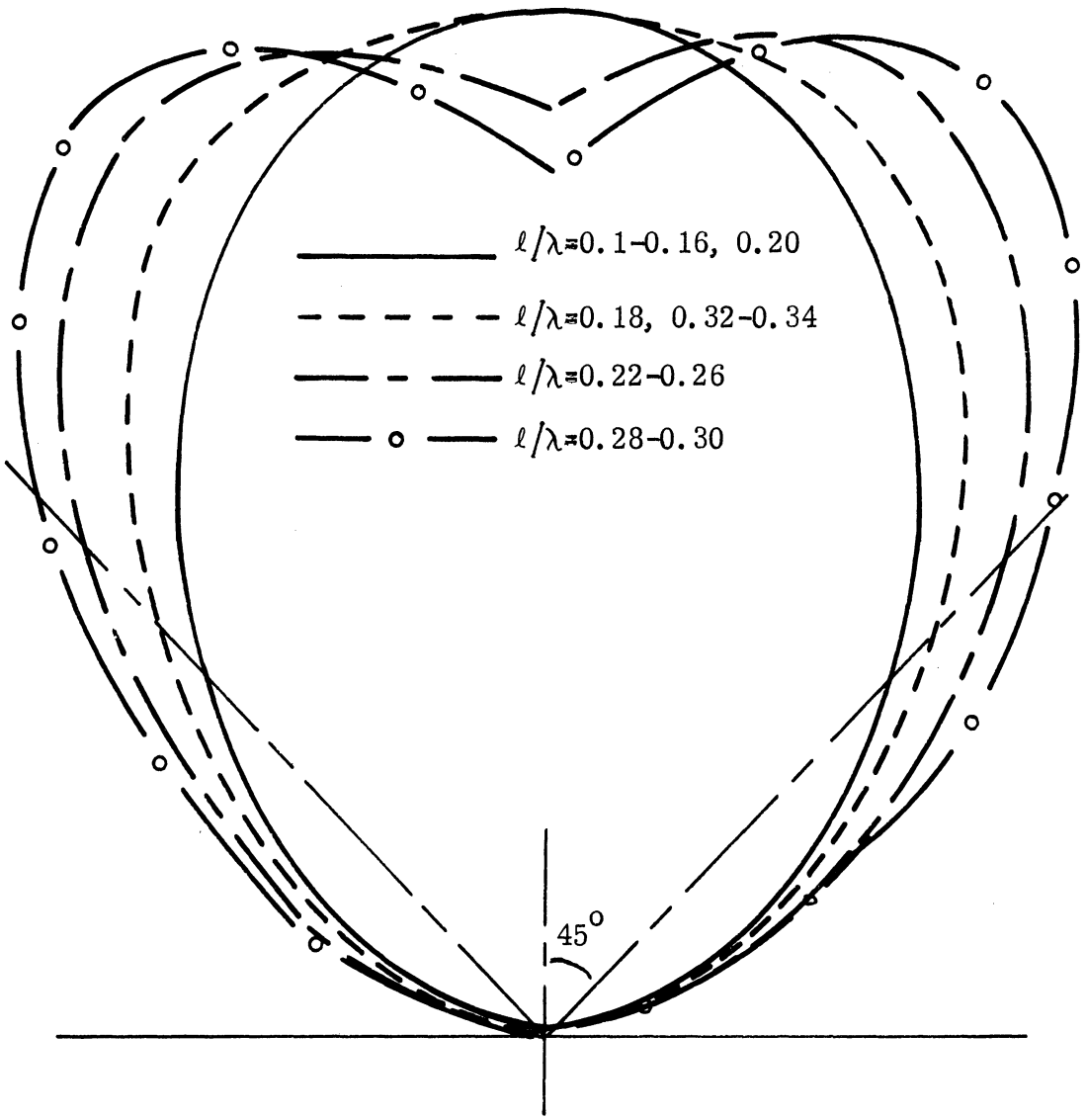

FIG. 3-23: THE FAR FIELD H-PLANE E_y-PATTERN FOR N=10, a/ℓ=0.01, b/ℓ=0.2, d/ℓ=0.225.

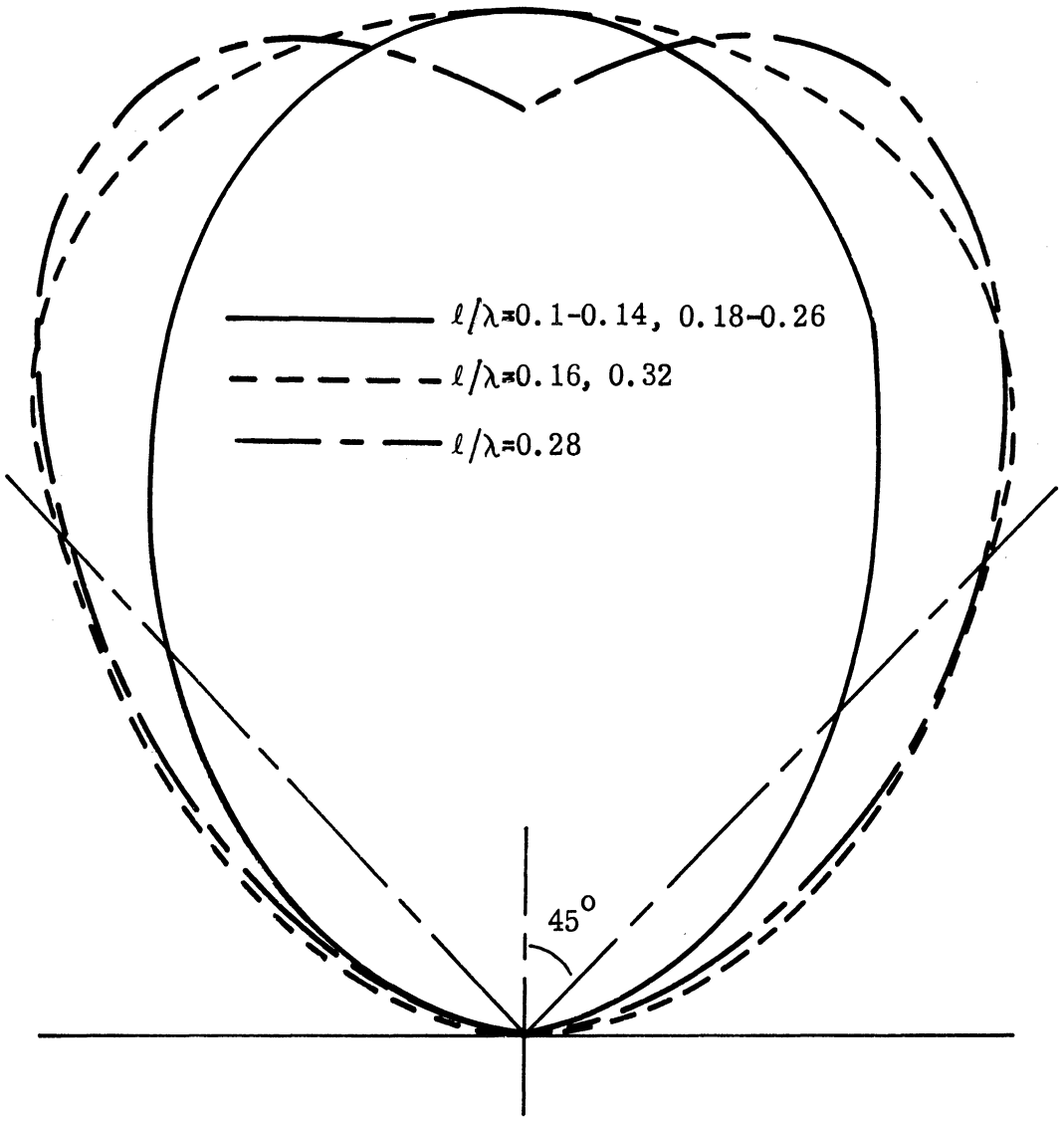

FIG. 3-24: THE FAR FIELD H-PLANE E_y-PATTERN FOR N=6, $a/\ell=0.02$, $b/\ell=0.1$, $d/\ell=0.075$.

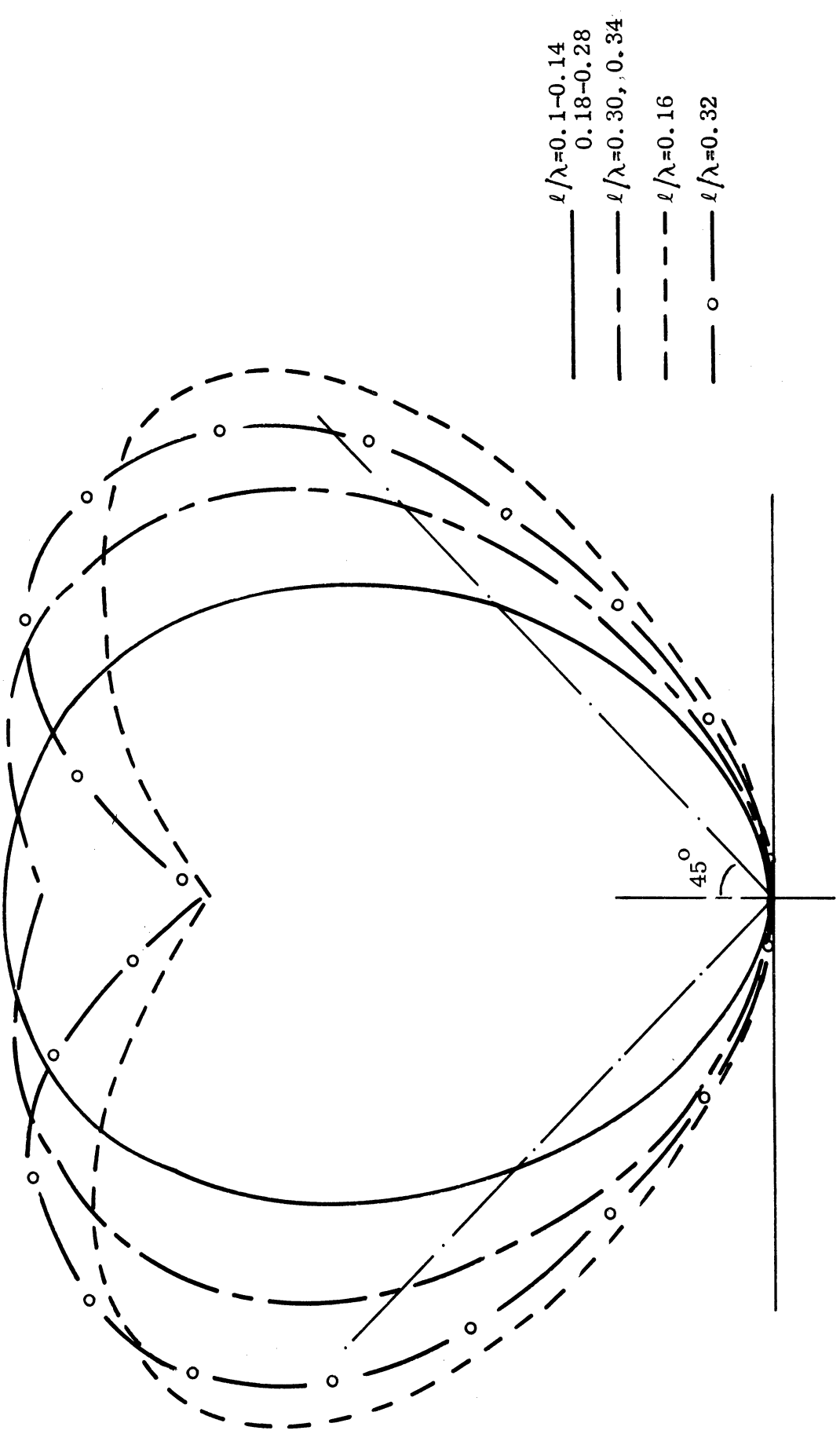

FIG. 3-25: THE FAR FIELD H-PLANE E_y-PATTERN FOR N=10, a/ℓ=0.02, b/ℓ=0.1, d/ℓ=0.075.

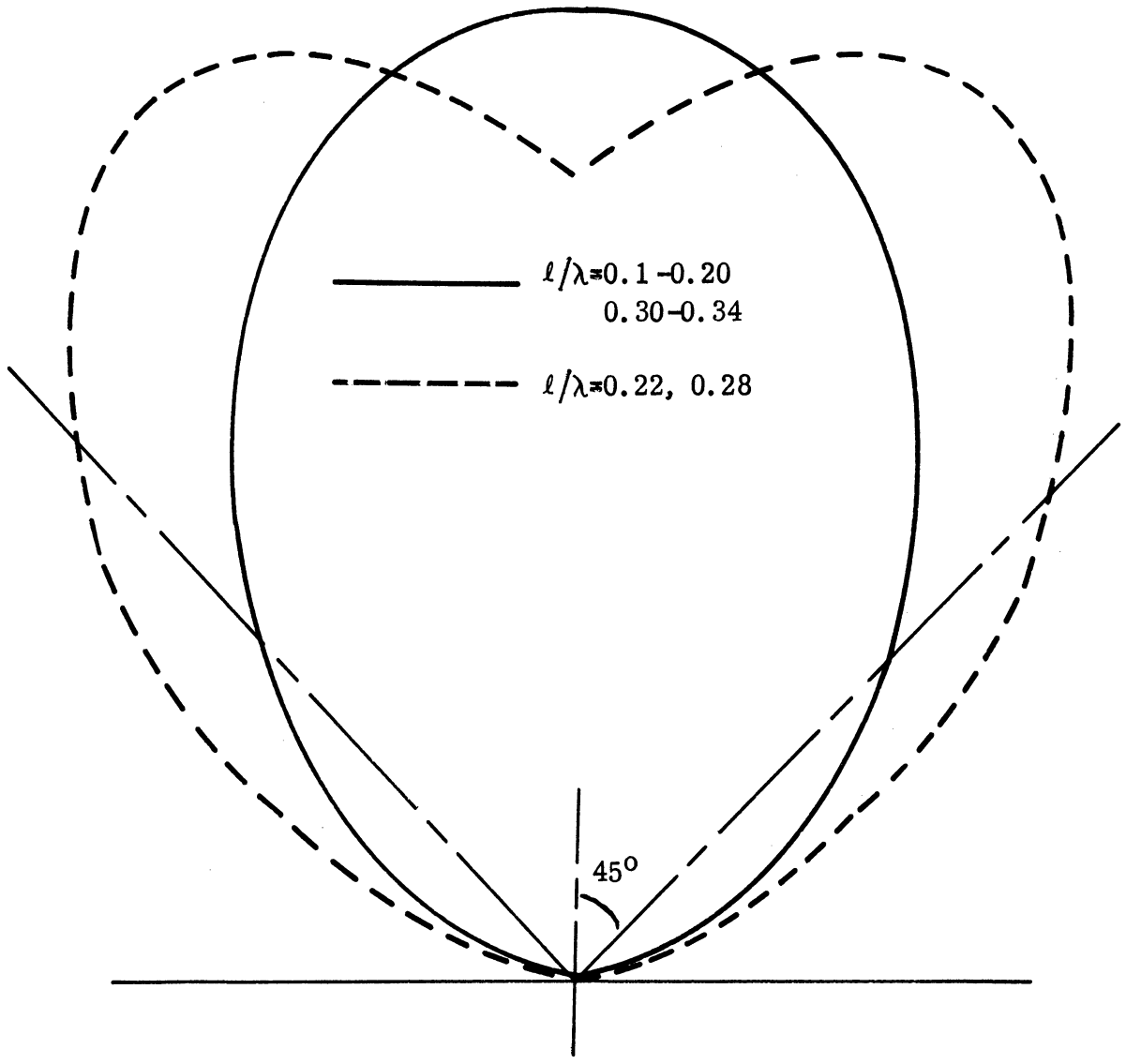

FIG. 3-26: THE FAR FIELD H-PLANE E_y-PATTERN FOR N=6, a/ℓ=0.02, b/ℓ=0.2, d/ℓ=0.075.

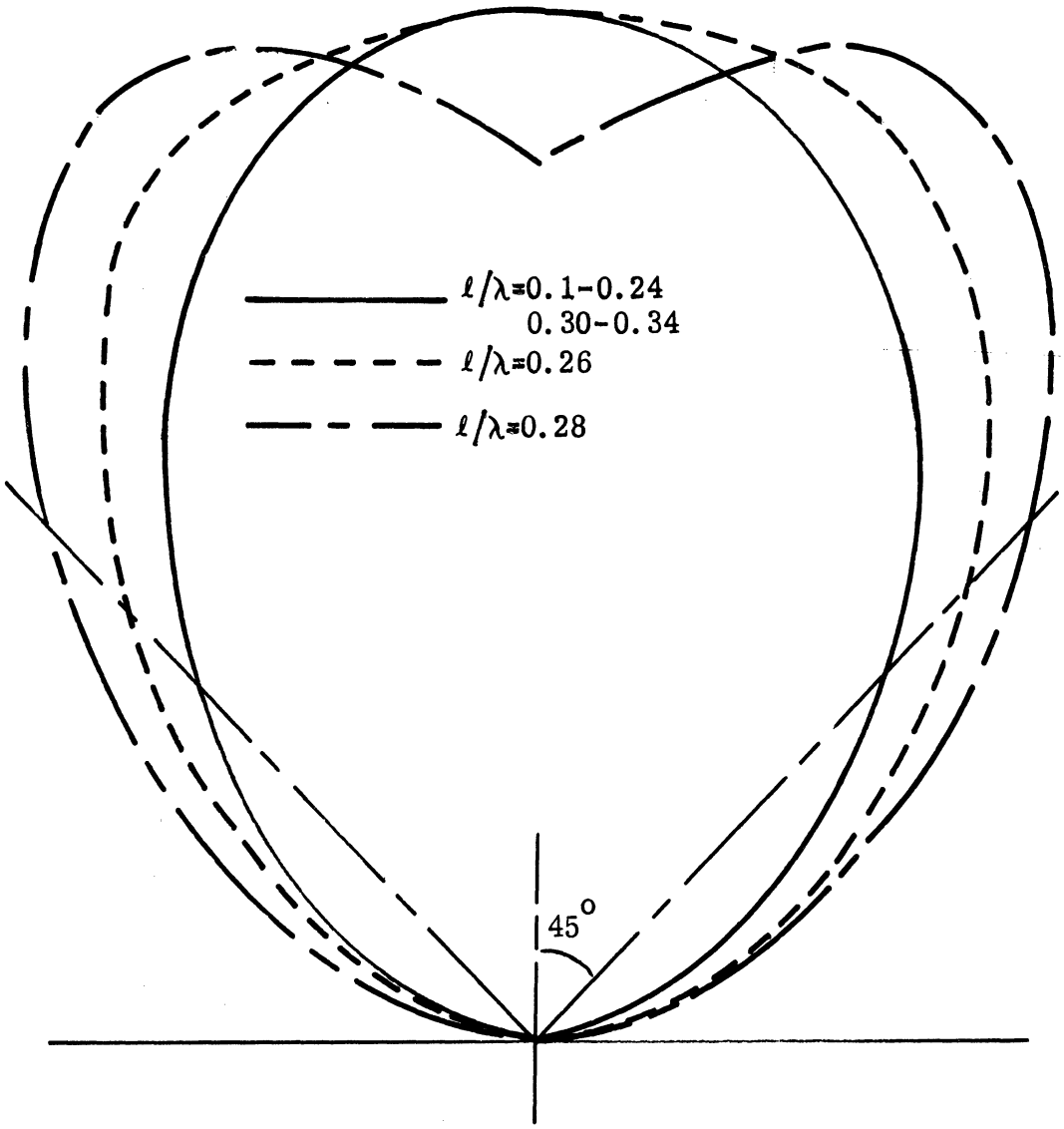

FIG. 3-27: THE FAR FIELD H-PLANE E_y-PATTERN FOR N=10, a/ℓ=0.02, b/ℓ=0.2, d/ℓ=0.075.

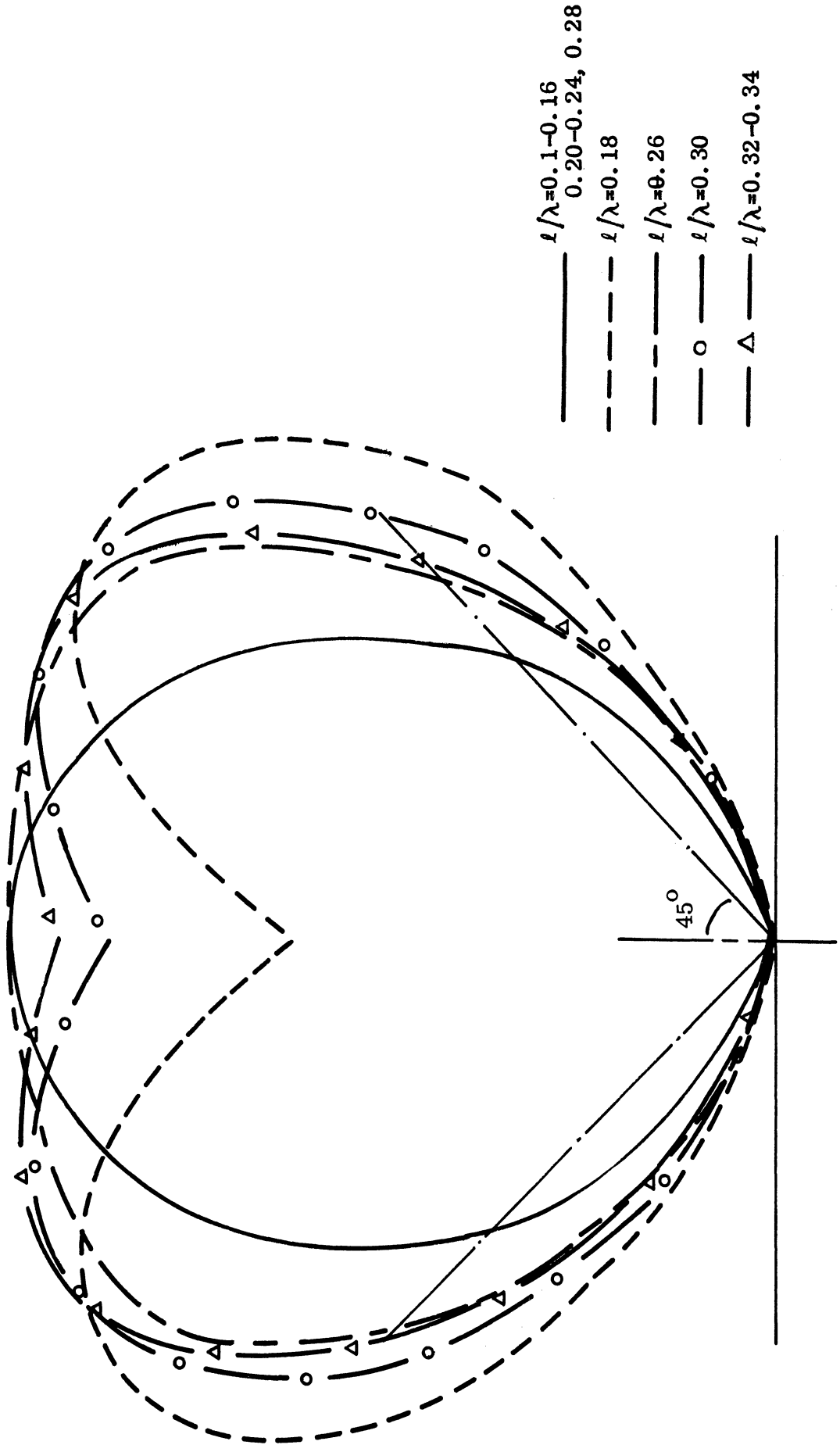

FIG. 3-28: THE FAR FIELD H-PLANE E_y - PATTERN FOR N=6, a/ℓ=0.02, b/ℓ=0.2, d/ℓ=0.225.

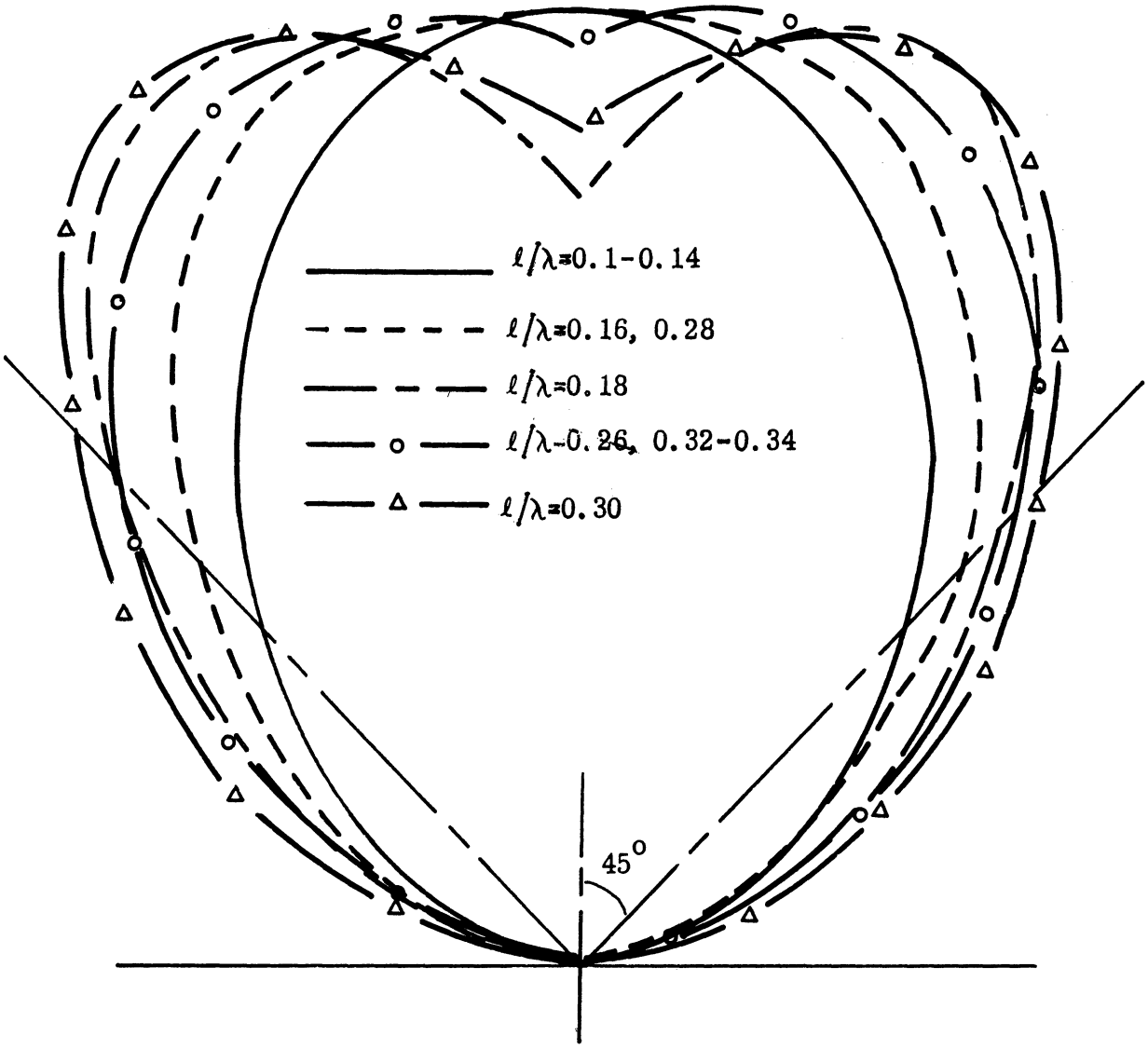

FIG. 3-29: THE FAR FIELD H-PLANE E_y-PATTERN FOR N=10, a/ℓ=0.02, b/ℓ=0.2, d/ℓ=0.225.

for N=6 and 10 reveals that the split is more significant and over a wider frequency range when N=10, which is an indication of the increased significance of the slow wave radiation. However, when the frequency is increased further, the pattern goes back to broadside if b/ℓ is large and d/ℓ is small. This is because of the narrow slow wave bandwidth, corresponding to an above cutoff frequency situation in a closed structure. Therefore, as will be shown experimentally in the next chapter, the radiation can only be of a leaky wave type and is represented by a broadside pattern. An array can be designed for either a broadside or an oblique beam based on the frequency range of operation. If the frequency is kept below the equivalent of a quarter-wavelength of the array element, the broadside radiation is predominant. If the frequency is above the equivalent of a quarter-wavelength of the array element, then a broadband oblique beam can be obtained, if the parameters are properly chosen to obtain a wide slow wave bandwidth.

The above discussion is consistent with the discussion and prediction made in the previous chapter over the slow wave region, where the discussion was based on the dispersion characteristics of an infinite structure.

The contribution of the vertical sections to the radiation pattern are negligible in the broadside case, since the broadside of the array is a null point for the vertical elements. However, for an oblique beam case, the vertical sections will contribute a vertically polarized field to the horizontally polarized field obtained from the horizontal array elements. This will result in a cross-polarization, if the relative field strength of the two are close. This will have to be determined experimentally.

The theoretical far field H-plane E_y-pattern for the antennas A-1, A-2, A-3, B-1 and B-2 (see Chapter IV for specifications) are plotted in Figs. 3-30 through 3-34; these patterns are seen to be predominantly for broadside radiation with cosine square pattern except for some frequencies where the beam splits, indicating a slow wave propagation along the array has taken place in this frequency range.

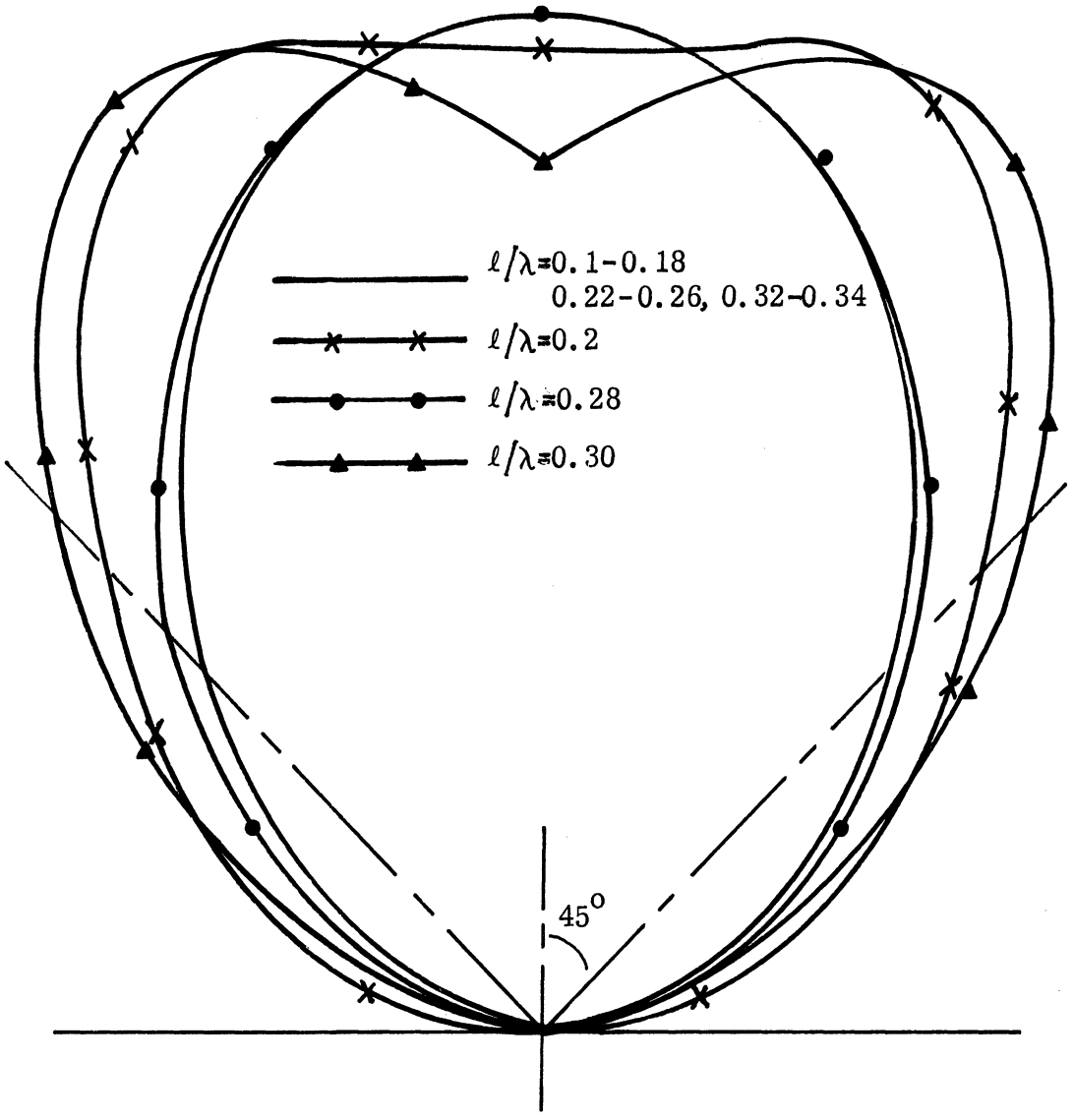

FIG. 3-30: THE THEORETICAL FAR FIELD H-PLANE E_y-PATTERN FOR THE ANTENNA A-1.

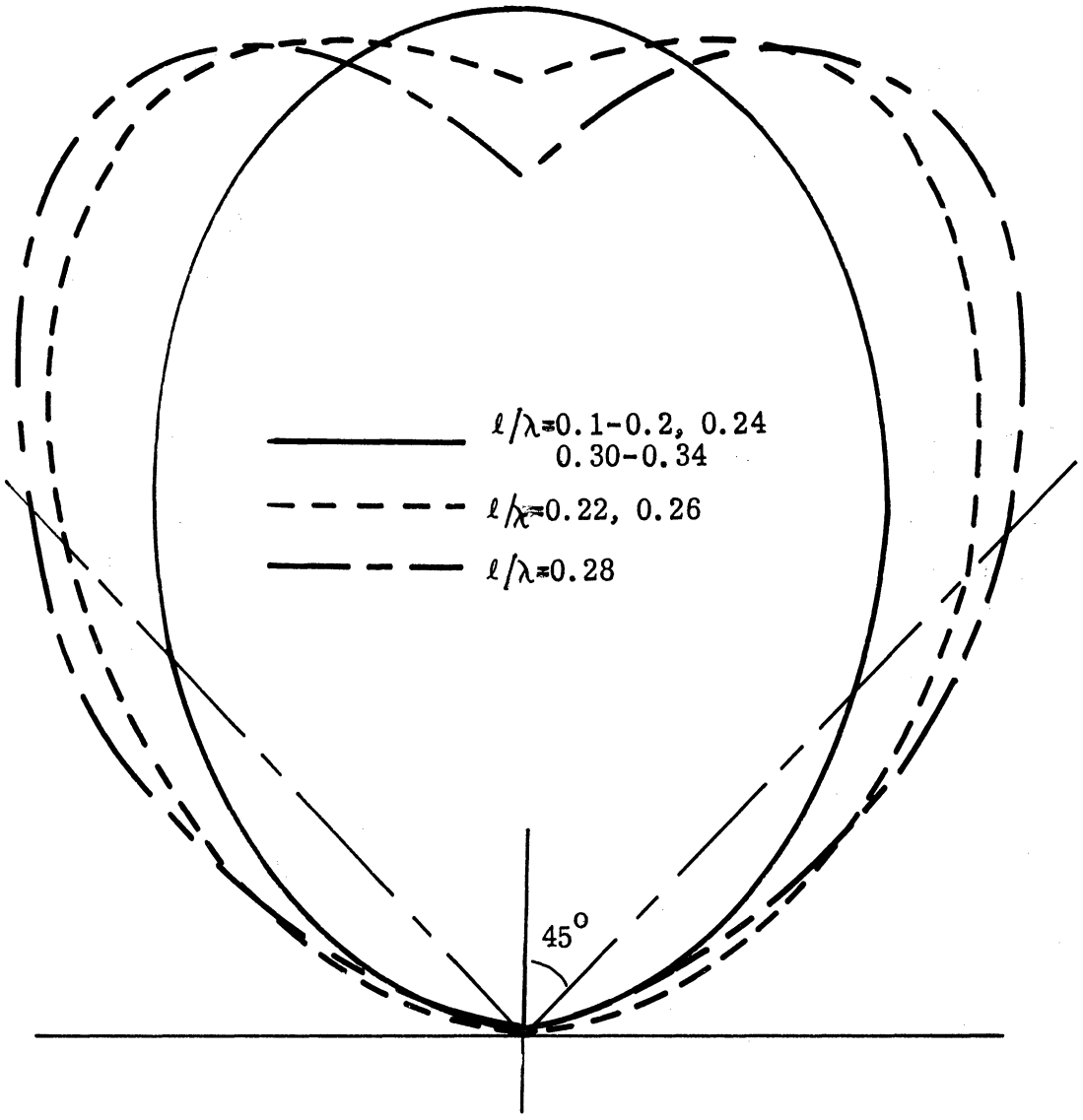

FIG. 3-31: THE THEORETICAL FAR FIELD H-PLANE E_y-PATTERN FOR THE ANTENNA A-2.

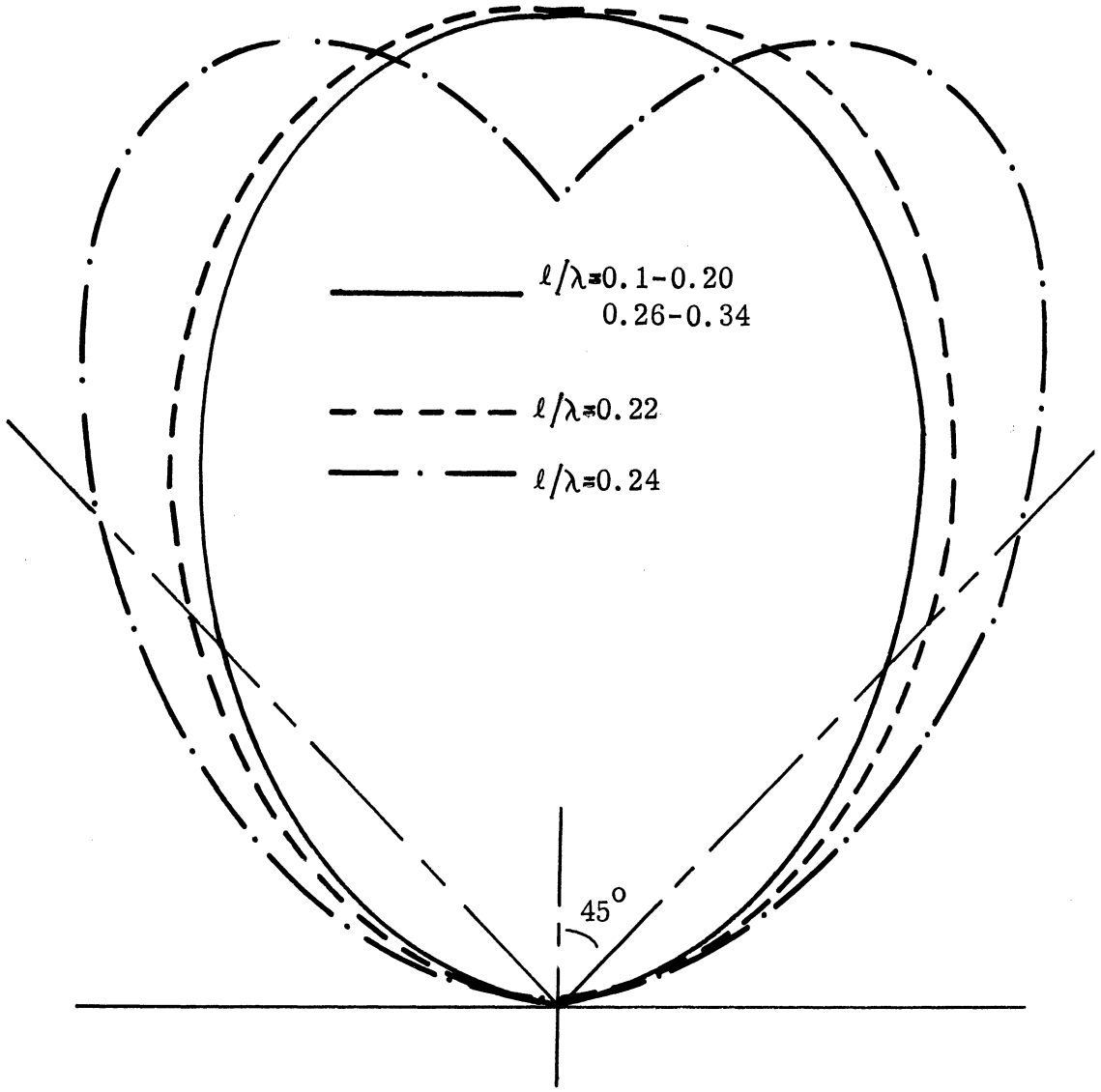

FIG. 3-32: THE THEORETICAL FAR FIELD H-PLANE E_y-PATTERN FOR THE ANTENNA A-3.

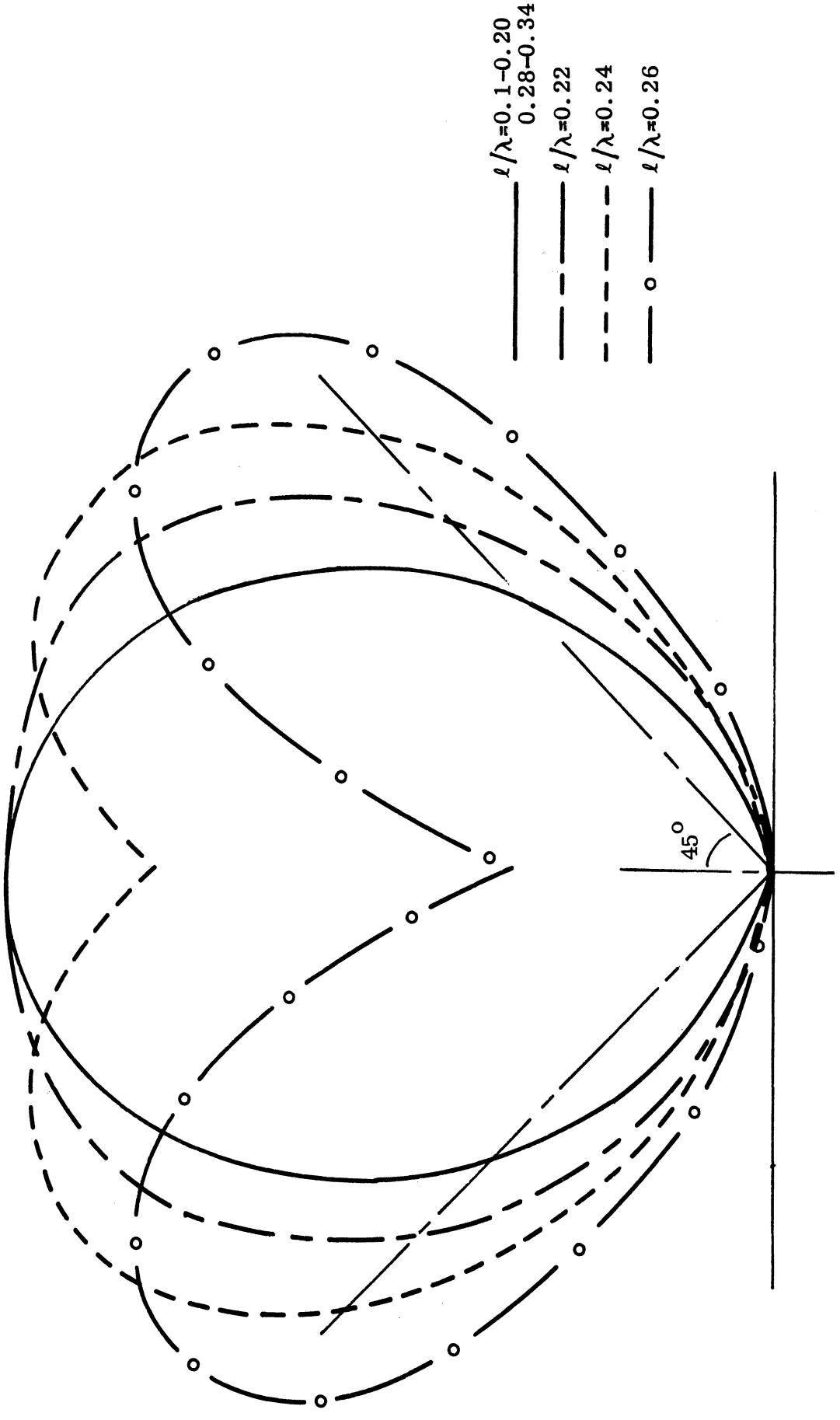

FIG. 3-33: THE THEORETICAL FAR FIELD H-PLANE E_y - PATTERN FOR THE ANTENNA B-1.

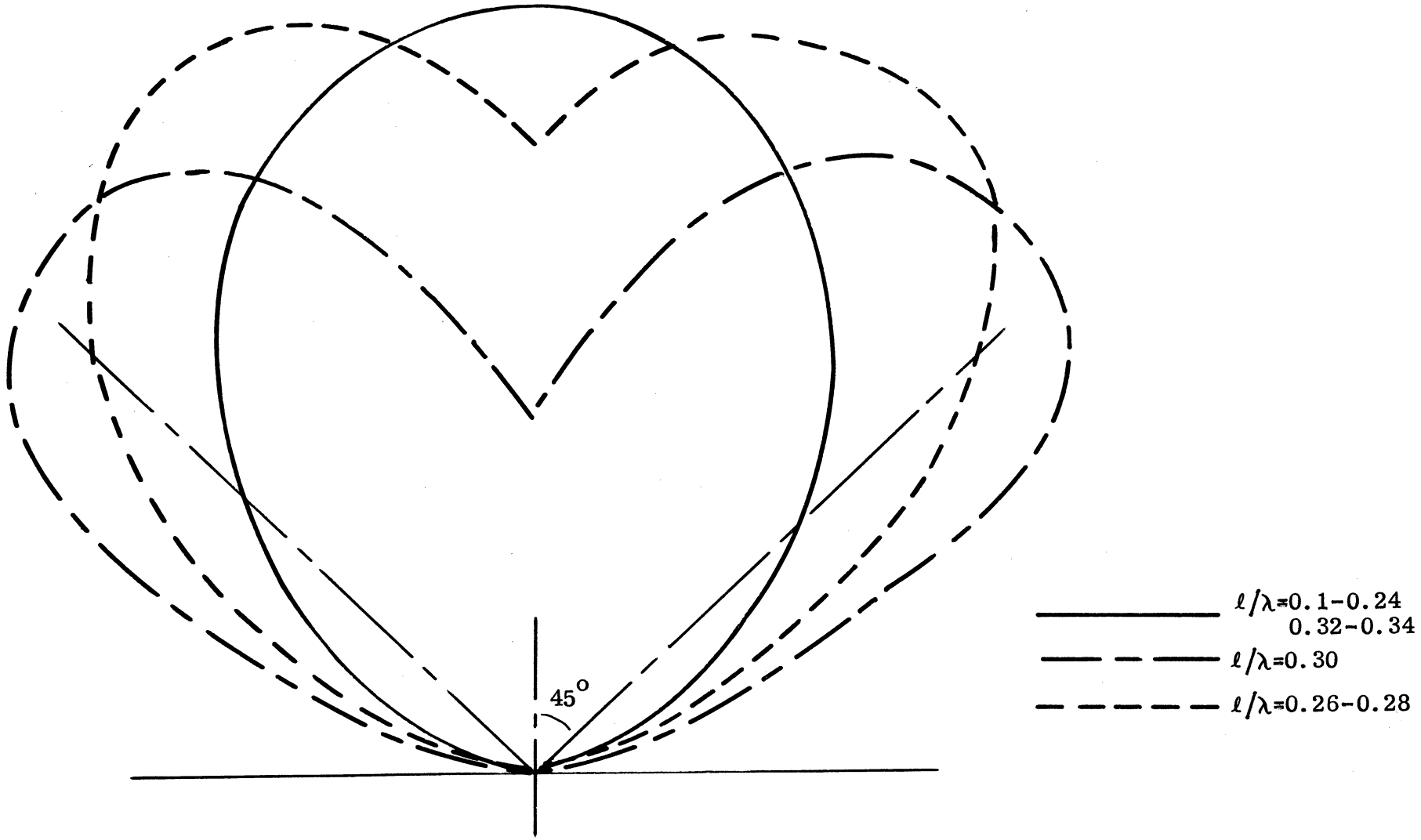

FIG. 3-34: THE THEORETICAL FAR FIELD H-PLANE E_y-PATTERN FOR THE ANTENNA B-2.

3.4 The Angle of Maximum Radiation.

The beam angle for a travelling wave radiator is given by[32]

$$\frac{c}{v} = \sin\phi_m \tag{3.27}$$

where c is the velocity of light, v is the phase velocity of the source and ϕ_m is the angle of the maximum radiation measured from the line perpendicular to the source, or from the broadside of the antenna as shown in Fig. 3-1. Equation (3.27) is true for a source of uniform amplitude distribution and a constant phase velocity v, and gives the far-field expression

$$P(\sin\phi) = \int_0^L e^{-jk_o z' \left(\frac{c}{v} - \sin\phi\right)} dz' \tag{3.28}$$

where L is the length of the source.

Equation (3.27) results from applying the principle of stationary phase (or saddle point) to (3.28). That is,

$$\frac{\partial}{\partial z'} \left[\left(\frac{c}{v} - \sin\phi\right) k_o z'\right] = 0 \quad . \tag{3.29}$$

However, as pointed out by Walter[32], when the source does not have a uniform amplitude distribution, (3.27) is only approximately true when the angle ϕ_m is between 5^o to 70^o. For a larger source length ($L > 5\lambda$), ϕ_m is not too well defined if the angle is either below 5^o or above 70^o. For a shorter source ($L < 5\lambda$), the angle ϕ_m is considerably smaller, especially when the angle ϕ_m is greater than 70^o. It is noticed from (3.27) that the ratio $\frac{c}{v}$ will be greater than unity in the slow wave region. The angle obtained is imaginary in this range but it has been used physically as if it were real; i.e. one can obtain ϕ_m from (3.27)

by taking the inverse of a hyperbolic sine of $\frac{c}{v}$ in the slow wave region.

The beam angle of the interdigital array antenna is expected to be smaller than the expression of (3.27) because the structure is much shorter than 5λ (usually in the order of λ).

Experimental confirmation of Eq. (3.27) is shown in the next chapter, where antenna C-2 is investigated for an interpretation of the radiation mechanisms involved in the interdigital array antenna.

3.5 Discussion.

The input impedance of a finite array is seen to be fairly stable with respect to changes of the parameter values or the number of the array elements. However, the input resistance increases slightly when the parameter d/ℓ is increased and also when the number of the array elements is increased from 13 to 21. On the other hand, the input reactance is not affected by the parameter changes very much, having a resonant frequency a little lower than the equivalent of the quarter-wave wavelength of the array element. The structure is capacitive in the low frequency range and inductive in the high frequency range. The impedance curve is somewhat irregular in its shape and trend, in spite of the assumption of a sinusoidal current distribution along the array elements. This may result from mutual coupling among the array elements with an interdigital boundary condition.

The radiation patterns indicate a fairly wide frequency band for broadside radiation in the low frequency range and a tendency for the beam to split when the slow wave region is reached. As soon as the slow wave pass-band is exceeded, the pattern goes back to a broadside radiation. It is seen that the smaller the value of b/ℓ and the larger the value of d/ℓ, the more the bandwidth of the structure is increased, according to the study of an infinite array. This increase in bandwidth is reflected in the far field pattern as a split beam with a large tilt angle.

Thus, in spite of some uncertainties about the formulation, the far field pattern obtained in this chapter points toward a consistent prediction over

the slow wave bandwidth of the structure. It should be remembered that slow wave phenomena is not well defined in a finite structure. The nature of the radiation mechanism in a finite array can be approximated as a travelling wave type in the pass-band region and a leaky wave type in the higher and lower frequency region. One way to confirm this is to check the angle of maximum radiation for a given travelling wave source, if one can define a constant phase velocity along the array surface. This will be done in the next chapter.

CHAPTER IV

EXPERIMENTAL RESULTS

4.1 Introduction.

Seven experimental models were constructed with the following specifications.

Parameter	Antenna Type						
	A-1	A-2	A-3	B-1	B-2	C-1	C-2
2N+1	13	13	13	21	21	14	17
(2a)*	0.15cm	0.15cm	0.15cm	0.15cm	0.15cm	0.15cm	0.15cm
b	1.2cm	1.8cm	2.4cm	1.2cm	1.8cm	1.8cm	1.2cm
d	1.0cm	1.0cm	1.0cm	1.0cm	1.0cm	2.0cm	2.0cm
ℓ	8.0cm	8.0cm	8.0cm	8.0cm	8.0cm	8.0cm	8.0cm

*equivalent

They are shown in Figs. 4-1 through 4-5. The models were photo-etched from a strip-line material and mounted on a 10" x 15" brass plate and then attached to a 5' x 6' ground screen for all measurements. All models are symmetrically fed, i.e., only the center element was excited, except C-1 and C-2, which were built to study the mechanism of radiation . While the antenna C-2 is fed from the left endof the array, C-1 is actually a combination of two arrays fed at the end of each antenna. Two elements, one from each array and now in adjacent positions, are driven in phase. The strip-line structure was used because of the convenience in construction by means of the photo-etching process. The width of each array element was 0.3 cm which corresponds to an equivalent diameter of 0.15 cm since the thickness is very small relative to the width of the conductor[11] The antenna D-1 was constructed with copper tubes of 0.63 cm diameter, 3 cm above the ground plane, b = 2 cm and a total of five array elements. It is shown in Fig. 4-6 with a magnetic probe above the conductor. The purpose of D-1 is to make the diameter of the element larger for a better measurement of the current distribution along the cylindrical array element.

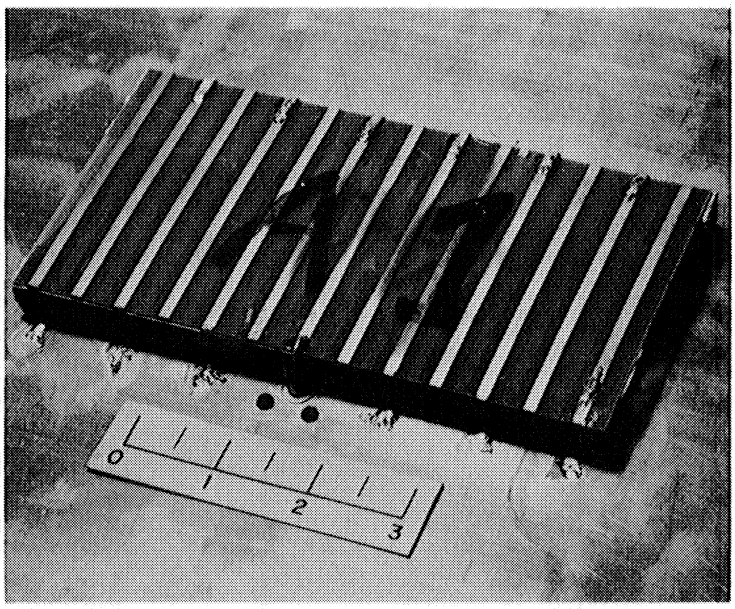

FIG. 4-1: THE INTERDIGITAL ARRAY ANTENNA A-1.
$\ell = 8\,\text{cm}$, $d/\ell = 0.125$, $b/\ell = 0.15$, $a/\ell = 0.01$, $N = 6$.

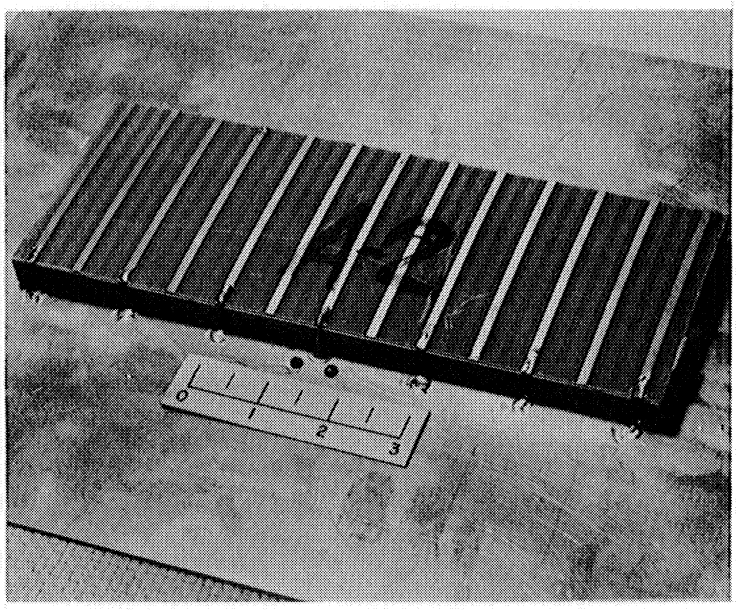

FIG. 4-2: THE INTERDIGITAL ARRAY ANTENNA A-2.
$\ell = 8\,\text{cm}$, $d/\ell = 0.125$, $b/\ell = 0.225$, $a/\ell = 0.01$, $N = 6$.

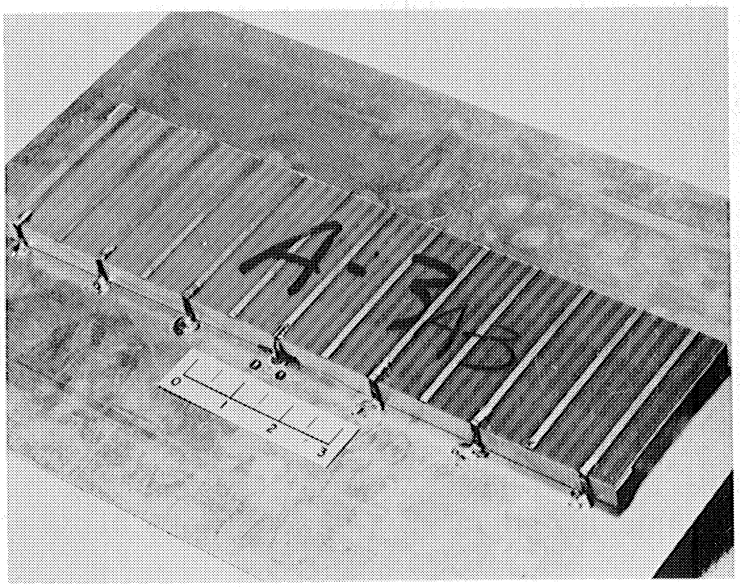

FIG 4-3: THE INTERDIGITAL ARRAY ANTENNA A-3.
$\ell = 8\,\text{cm}$, $d/\ell = 0.125$, $b/\ell = 0.30$, $a/\ell = 0.01$, $N = 6$.

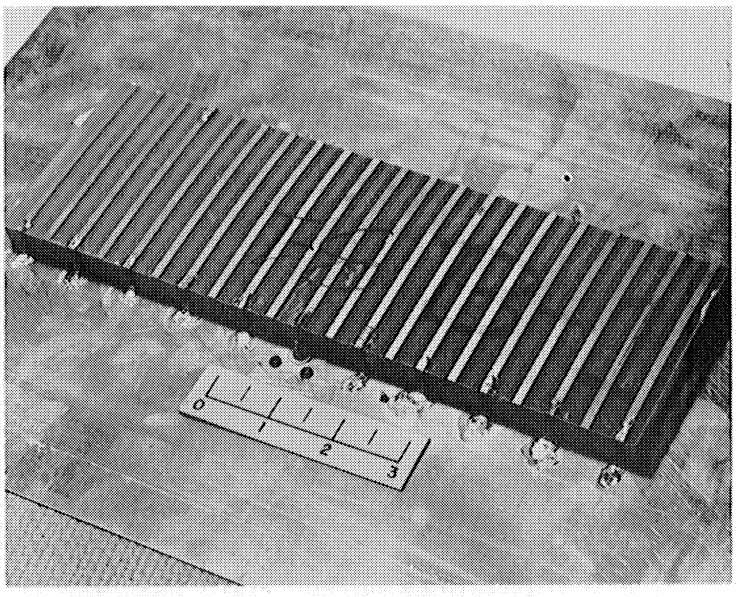

FIG. 4-4: THE INTERDIGITAL ARRAY ANTENNA B-1.
$\ell = 8\text{cm}$, $d/\ell = 0.125$, $b/\ell = 0.15$, $a/\ell = 0.01$, $N = 0$.

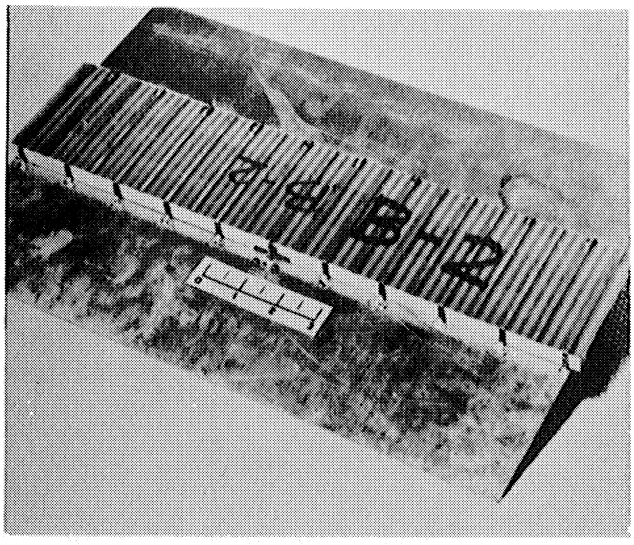

FIG. 4-5: THE INTERDIGITAL ARRAY ANTENNA B-2.
ℓ = 8 cm, d/ℓ = 0.125, b/ℓ = 0.225, a/ℓ = 0.01, N = 10.

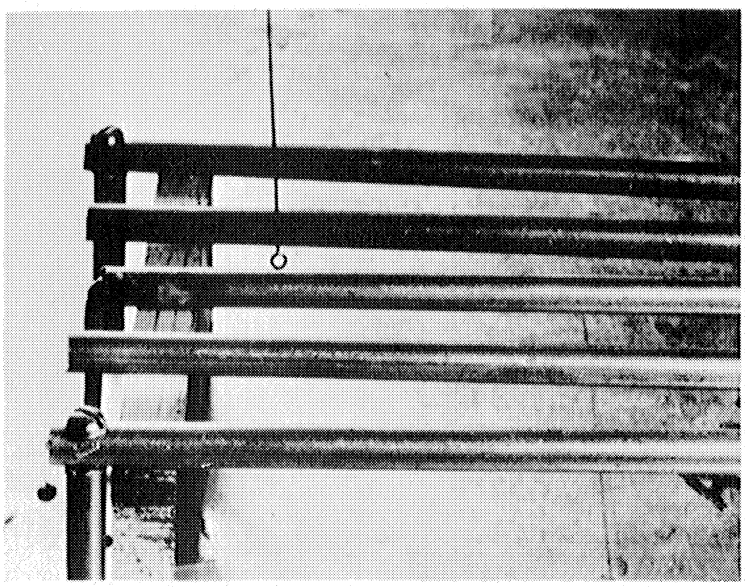

FIG. 4-6: THE INTERDIGITAL ARRAY ANTENNA D-1 WITH A MAGNETIC PROBE ABOVE THE EXCITED ELEMENT.
ℓ = 16 cm, d/ℓ = 0.206, b/ℓ = 0.125, a/ℓ = 0.04, N = 2.

4.2 Near Field Measurements.

The near field measurement facilities involve an anechoic chamber, a magnetic probe with its carriage system, and a receiver-recorder system. A symmetrically shielded vertical loop probe was used throughout the measurements. It has a diameter of 0.33 cm and is made from a coaxial line of 0.084 cm outside diameter. The probe pick-up error due to E-field is very small for all of the frequencies under measurement since the probe is very much smaller than the wavelength of the highest frequency involved (less than 1 per cent).[34]

4.2.1 Near Field Amplitude.

The near field amplitude measurement set-up is shown in Fig. 4-7. The magnetic probe was placed 0.5 cm above the surface along $y=\frac{\ell}{2}$ of the array. A manual control was used to drive the probe synchronously with the pen drive mechanism of the x-y recorder. The recorder output was normalized to the maximum power of the plot. The results are shown in Figs. 4-8 through 4-12.

The study of near field amplitudes shows that when the frequency is low, very little field is present once the first couple of array elements are probed; this suggests that broadside radiation has taken place and the field attenuates very rapidly as it travels along the array surface. However, when the frequency is near 650 MHz, the field is maximum at, or near, the N=3 element, which strongly suggests a slow wave along the array surface and that an oblique radiation is taking place. However, A-1 does not seem to have a sufficient number of elements to establish slow wave propagation. Therefore, it is expected that the radiation pattern will still be very much of a broadside pattern. When the frequency is increased toward 900 MHz, the structure is driven above the slow wave pass-band and the near field amplitude decays very rapidly toward the end of the array. Thus, broadside radiation may take place. The above observation is also true for the A-2 and A-3 antennas, except for the fact that these two are physically longer and thus are able to maintain a better slow wave propagation along the array surface. Therefore, some oblique radiation will take place when the frequency is near and above 650 MHz. The near field patterns for B-1 and B-2 are comparable

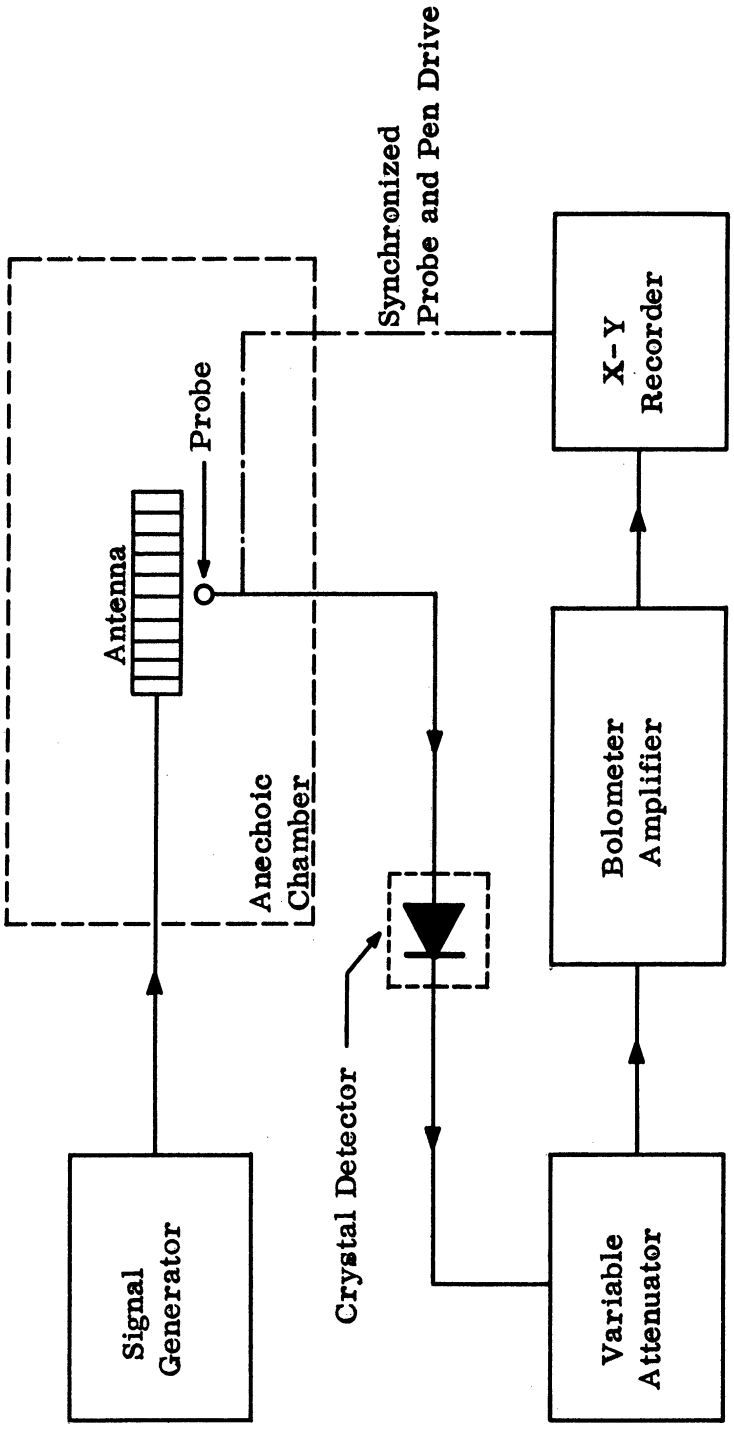

FIG. 4-7: THE EXPERIMENTAL SET-UP FOR THE NEAR FIELD AMPLITUDE MEASUREMENT.

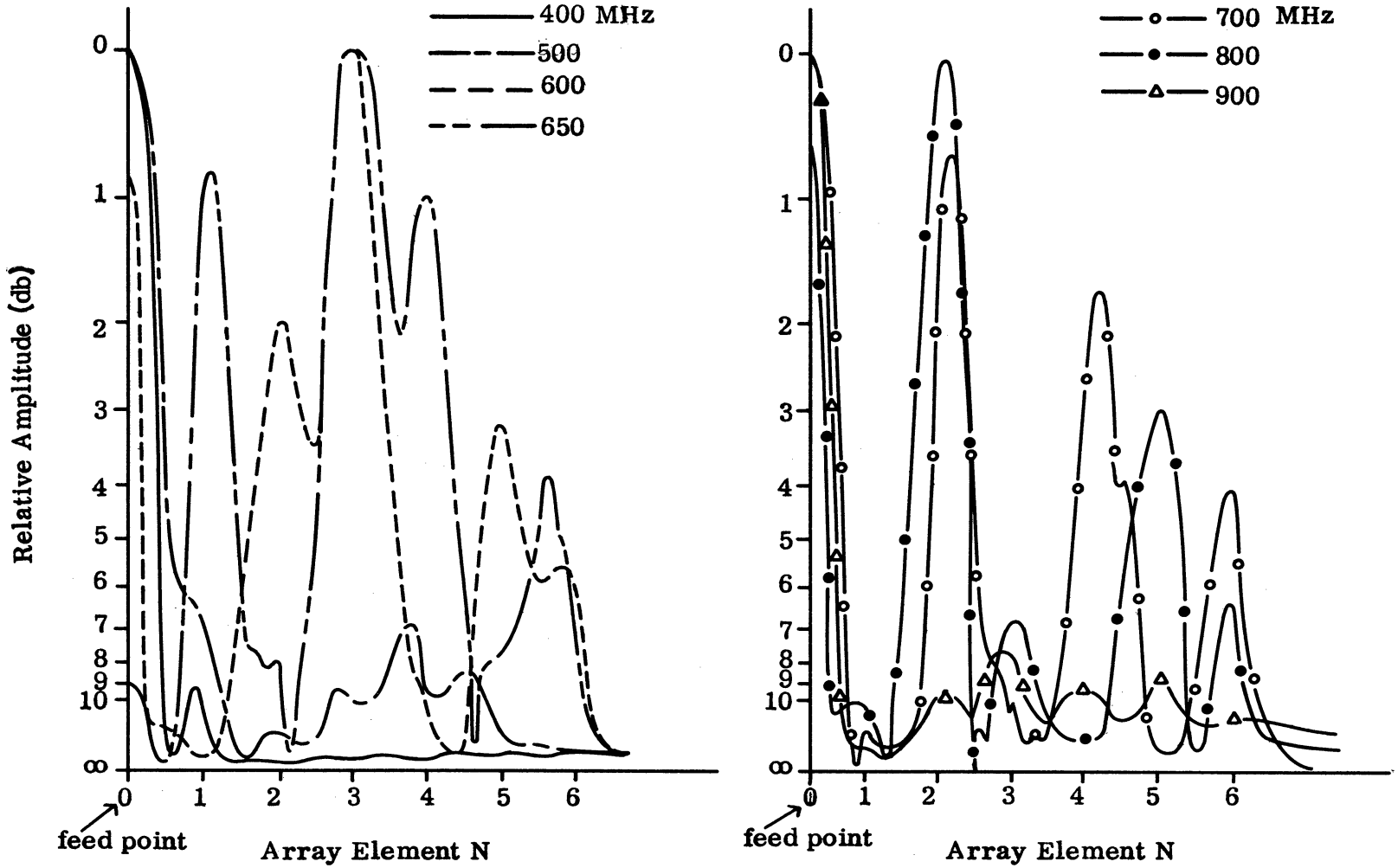

FIG. 4-8: THE NEAR FIELD AMPLITUDE FOR THE ANTENNA A-1.

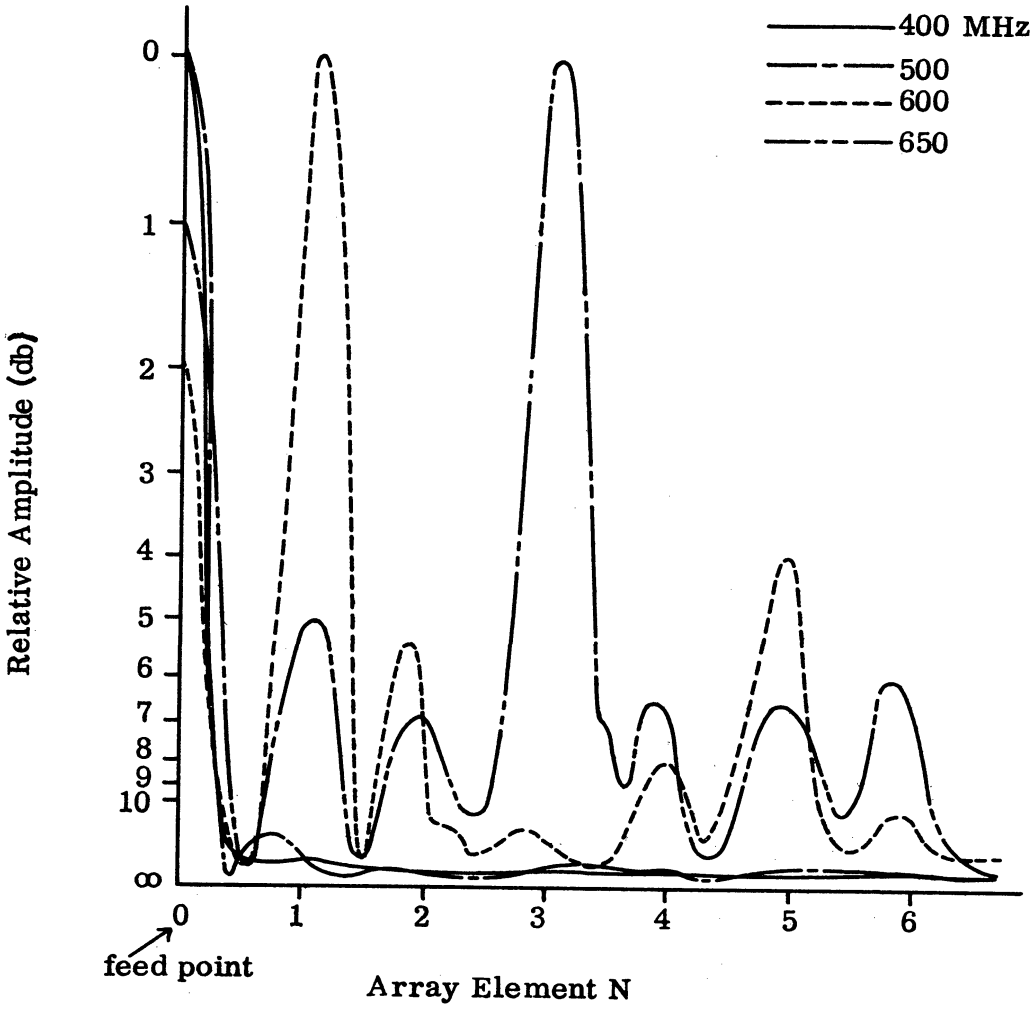

FIG. 4-9 a: THE NEAR FIELD AMPLITUDE FOR THE ANTENNA A-2.

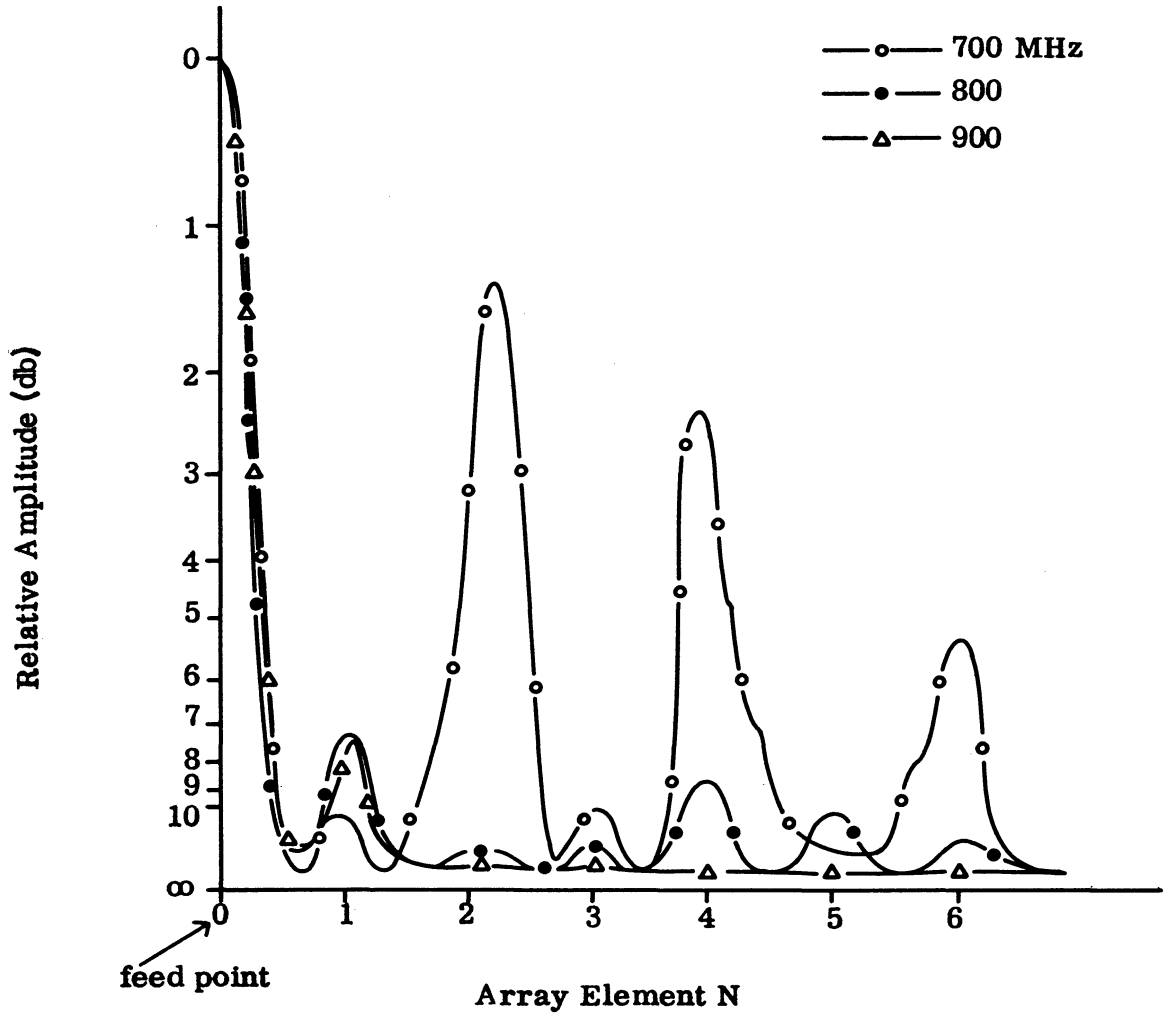

FIG. 4-9b: THE NEAR FIELD AMPLITUDE FOR THE ANTENNA A-2.

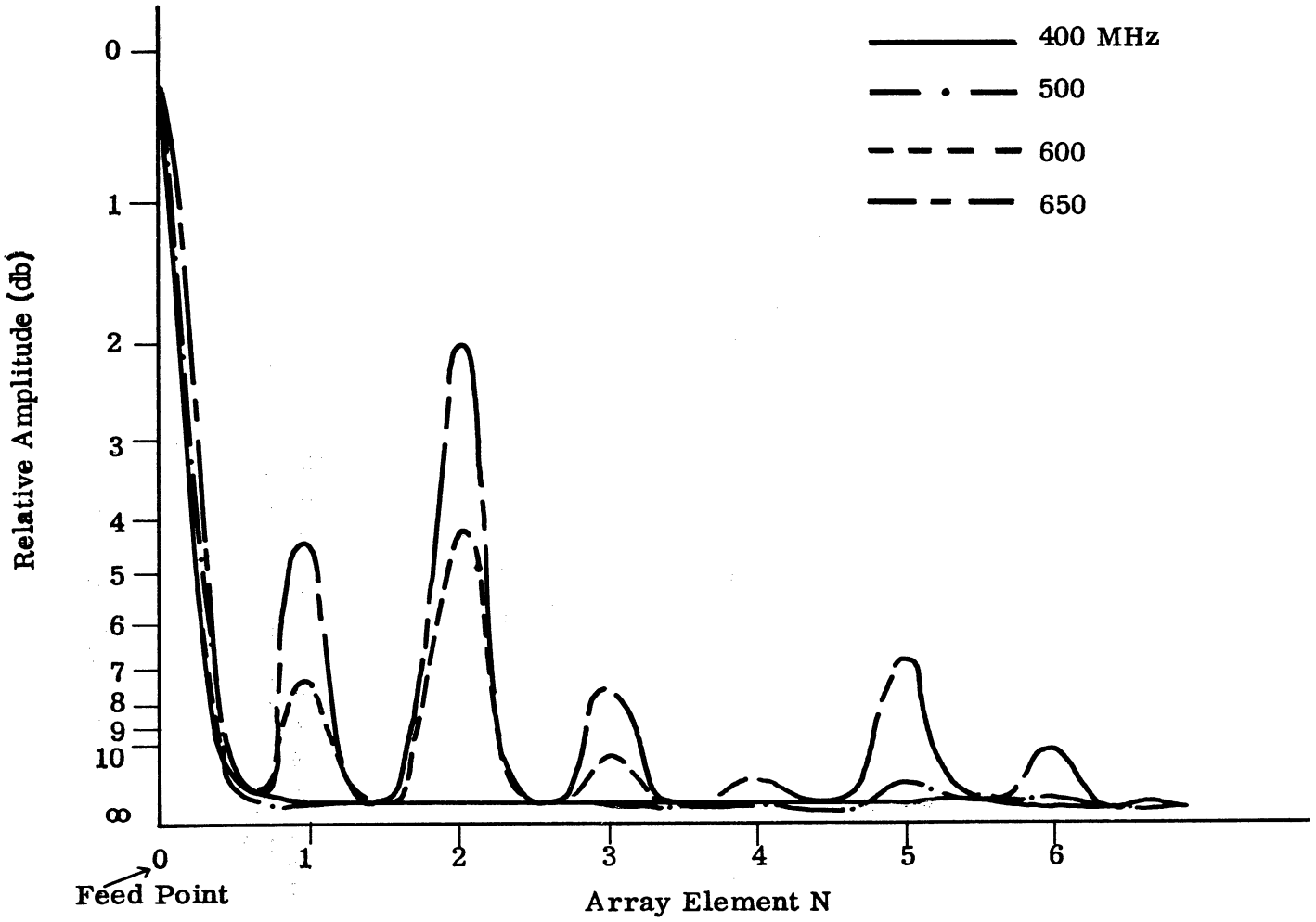

FIG. 4-10a: THE NEAR FIELD AMPLITUDE FOR THE ANTENNA A-3.

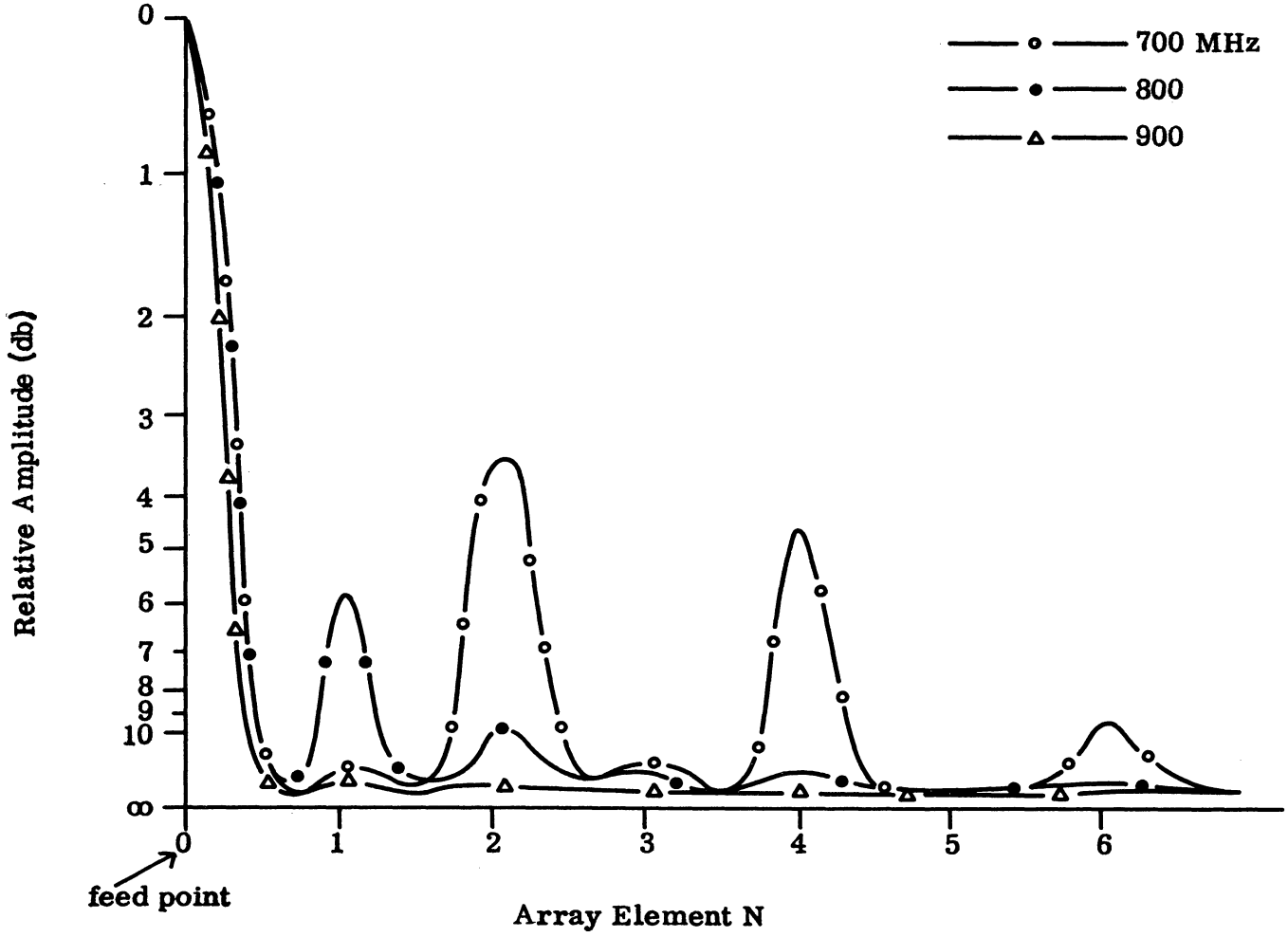

FIG. 4-10b: THE NEAR FIELD AMPLITUDE FOR THE ANTENNA A-3.

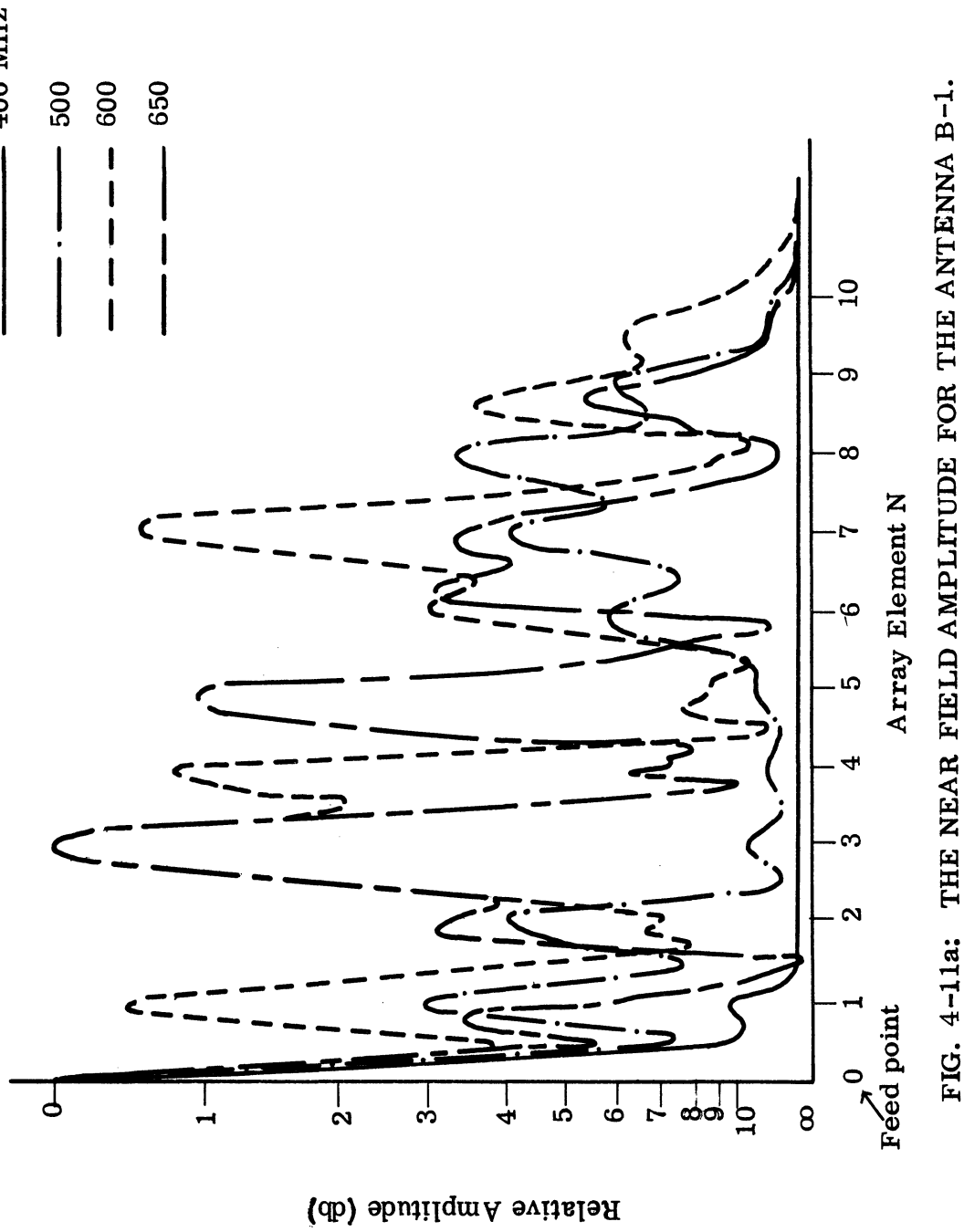

FIG. 4-11a: THE NEAR FIELD AMPLITUDE FOR THE ANTENNA B-1.

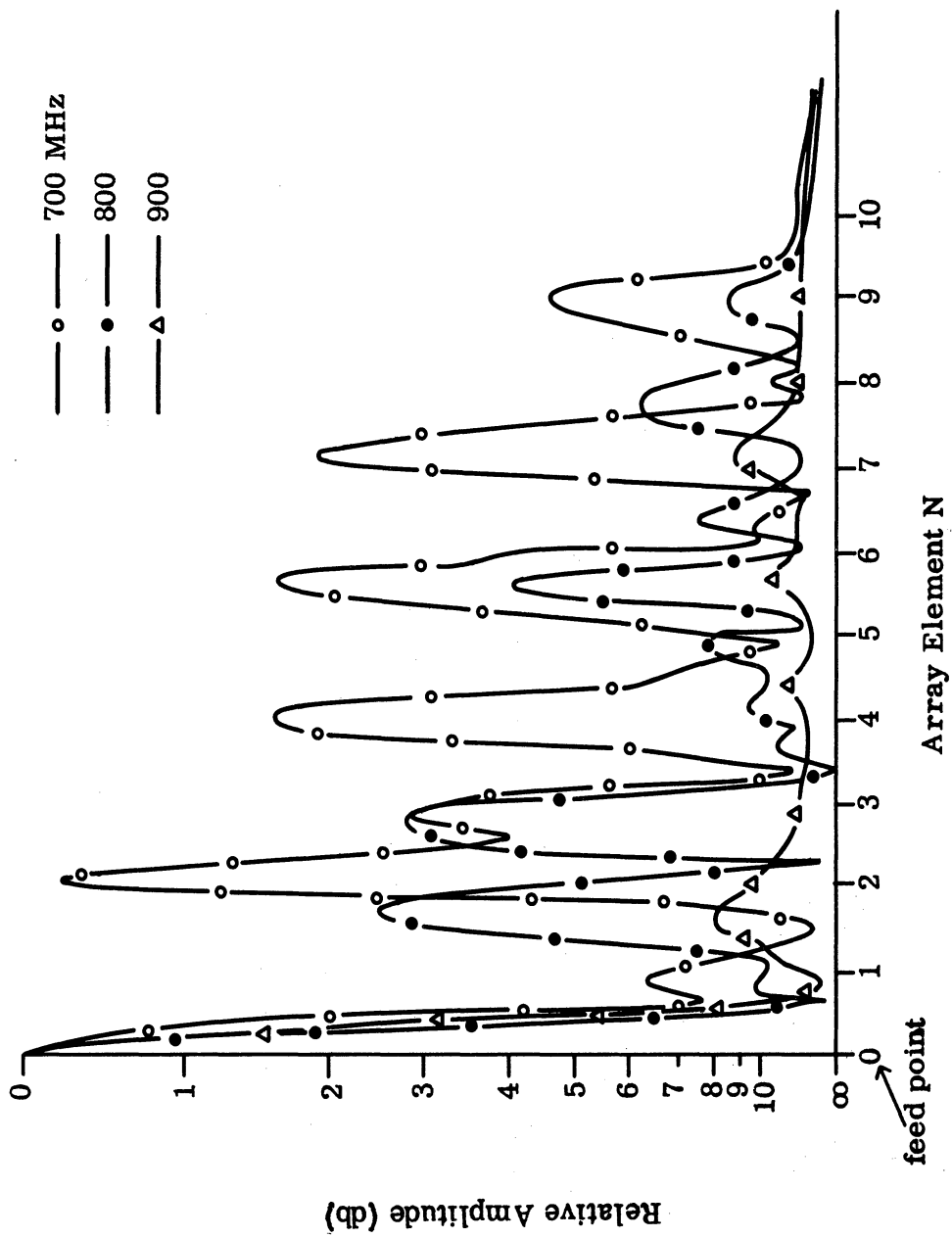

FIG. 4-11b: THE NEAR FIELD AMPLITUDE FOR THE ANTENNA B-1.

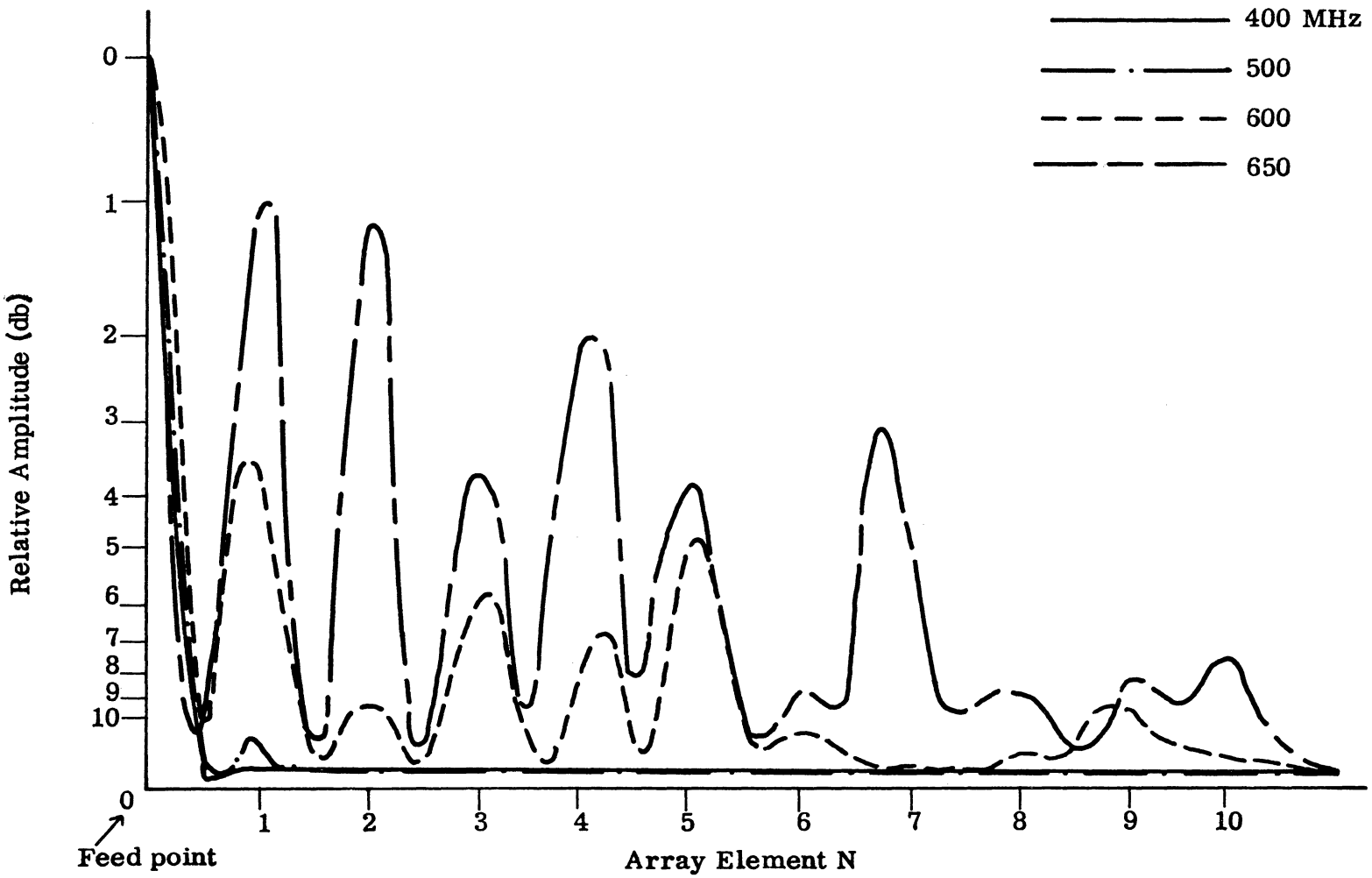

FIG. 4-12a: THE NEAR FIELD AMPLITUDE FOR THE ANTENNA B-2.

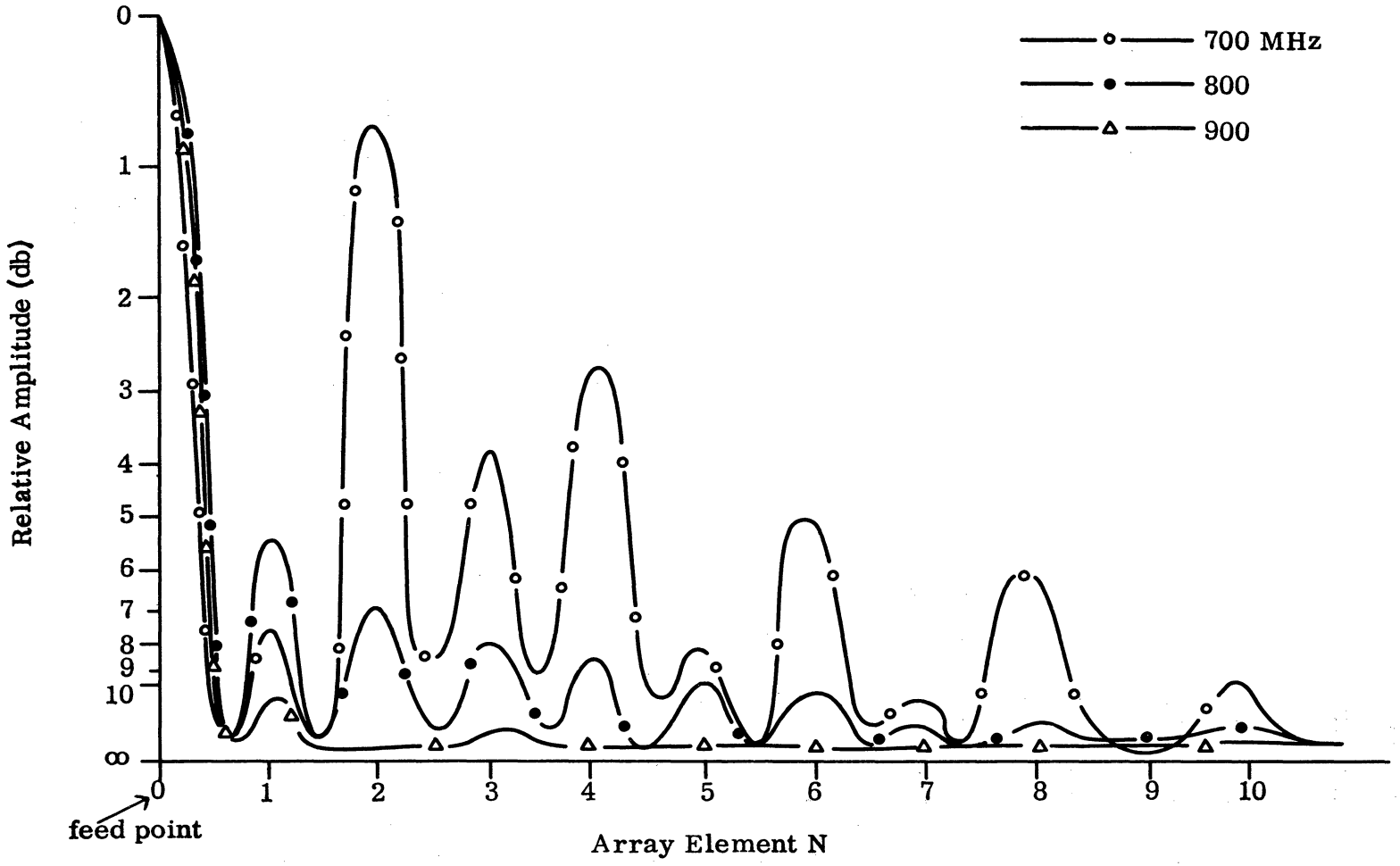

FIG. 4-12b: THE NEAR FIELD AMPLITUDE FOR THE ANTENNA B-2.

to those of A-1 and A-2 except that the number of elements is increased and thus, slow wave propagation will be more efficient and, consequently, better oblique radiation will occur when the frequency is somewhere between 650 MHz and 850 MHz. Here 850 MHz is observed to be the upper limit of the slow wave pass-band. The antenna A-3 has the narrowest bandwidth with the upper frequency of about 800 MHz or less.

4.2.2 Current Distribution.

In order to justify the assumption made in previous chapters, the antenna D-1 was built to check the current distribution along the conducting element. The antenna D-1 is shown in Fig. 4-6 with a magnetic probe above the conducting element. The distance was maintained at about 0.5 mm during the measurement. The near field amplitude along the excited element is shown in Fig. 4-13 and the near field amplitude along the adjacent conductor is shown in Fig. 4-14. One thing is obvious from the observation of these two figures. That is, although it is not perfect, the amplitude of the current along the conductor has a nearly sinusoidal distribution obeying the interdigital boundary conditions. The shape of the current distribution may actually be somewhat different due to the fact that the conductor is only about twice the size of the magnetic probe and the probe-to-element spacing may not have been 0.5 mm uniformly along the conductor. The latter may have been the main reason why the two conductors have quite a different near field amplitude distribution along the conductors. It should be noted here, however, that the near field amplitude was actually a linear power distribution along the conductor and, thus, a direct interpretation of the current distribution has to be done carefully.

To further investigate the current distribution along the array element and to check the proper excitation of the array elements by a single feed arrangement, the near field amplitude was measured along the array edges $y=0$ and $y=l$ for the antenna B-1. The results are shown in Figs. 4-15 and 4-16. The excessive amplitude observed above the feed point is due to the sudden decrease of the probe-to-element spacing caused by the protruding solder joint between the feeding wire and the conducting element. It is noted that along $y=0$ the near field peaks up

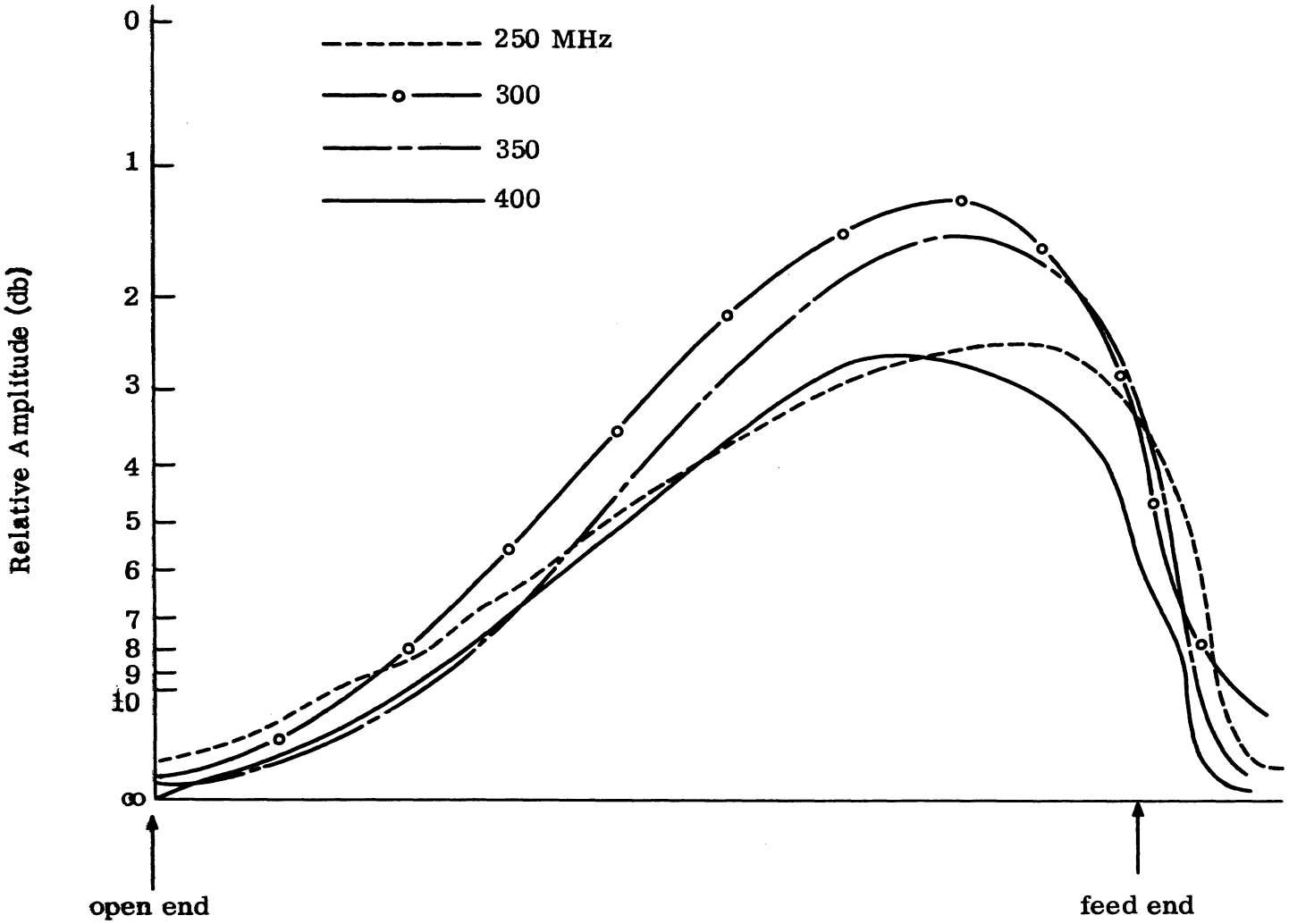

FIG. 4-13: THE NEAR FIELD AMPLITUDE ALONG THE EXCITED ELEMENT OF THE ANTENNA D-1.

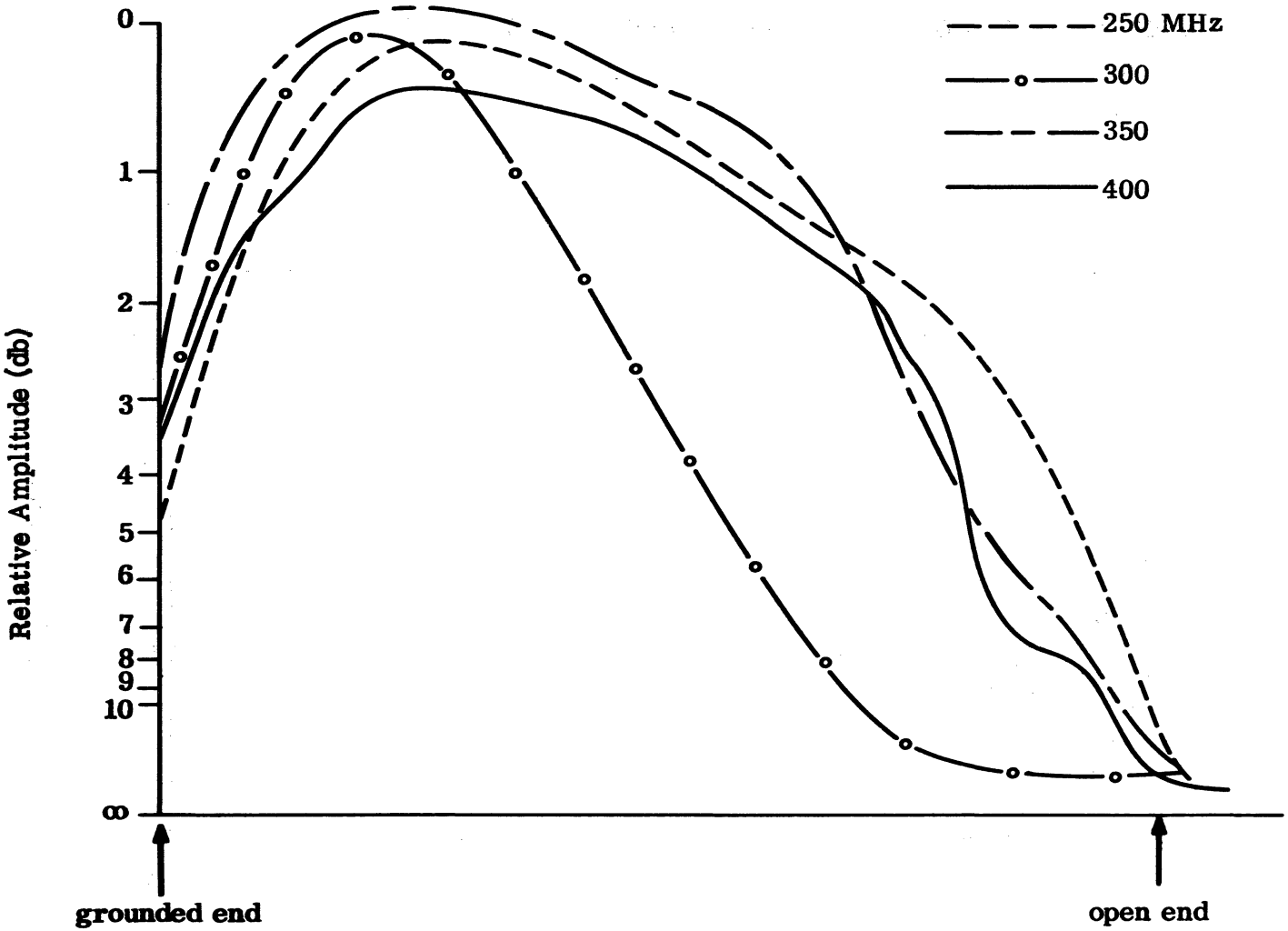

FIG. 4-14: THE NEAR FIELD AMPLITUDE ALONG THE SECOND ELEMENT OF THE ANTENNA D-1.

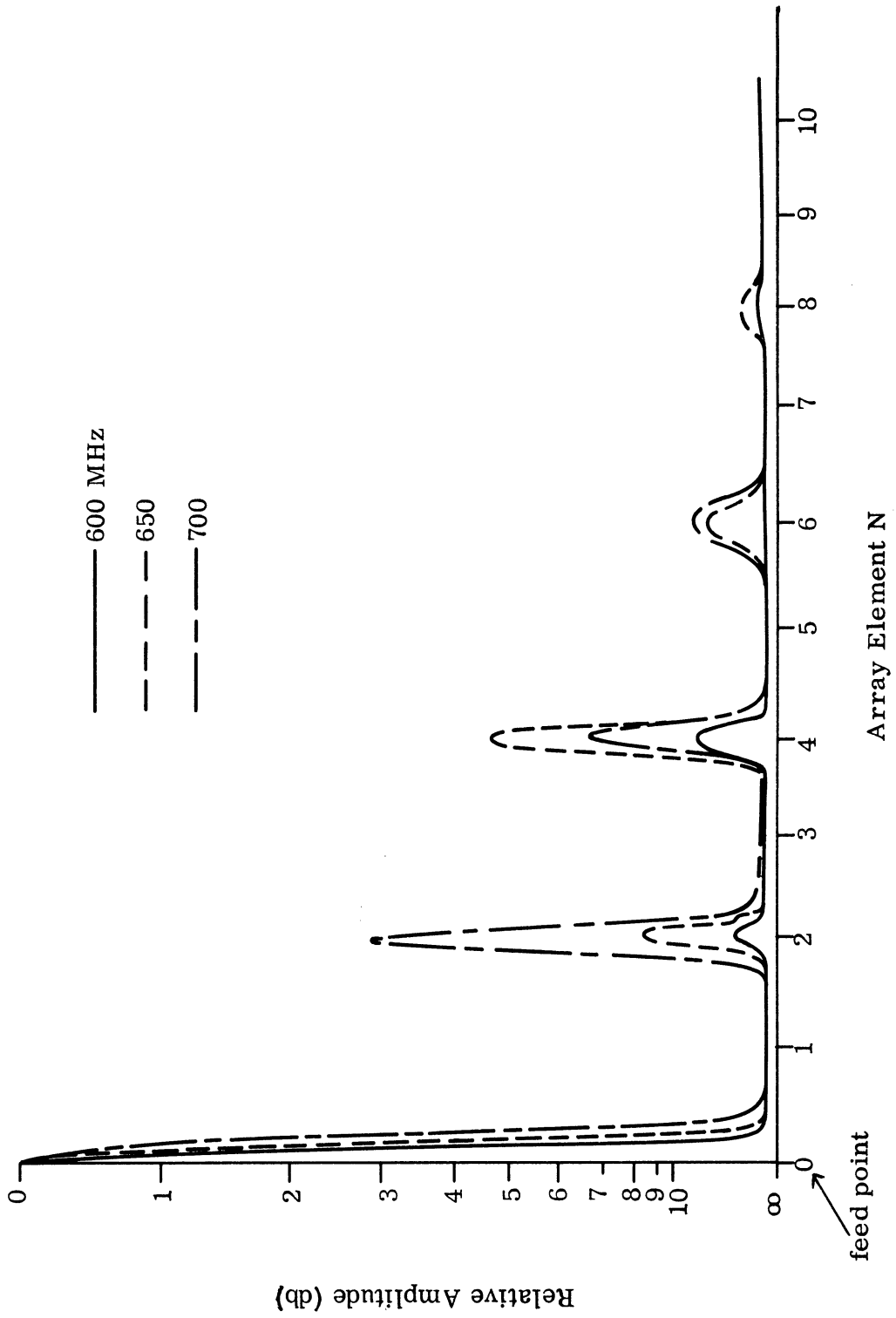

FIG. 4-15: THE NEAR FIELD AMPLITUDE PROBED ALONG y=0 FOR THE ANTENNA B-1. PROBE POSITION: 1.0 mm ABOVE THE ARRAY ELEMENT.

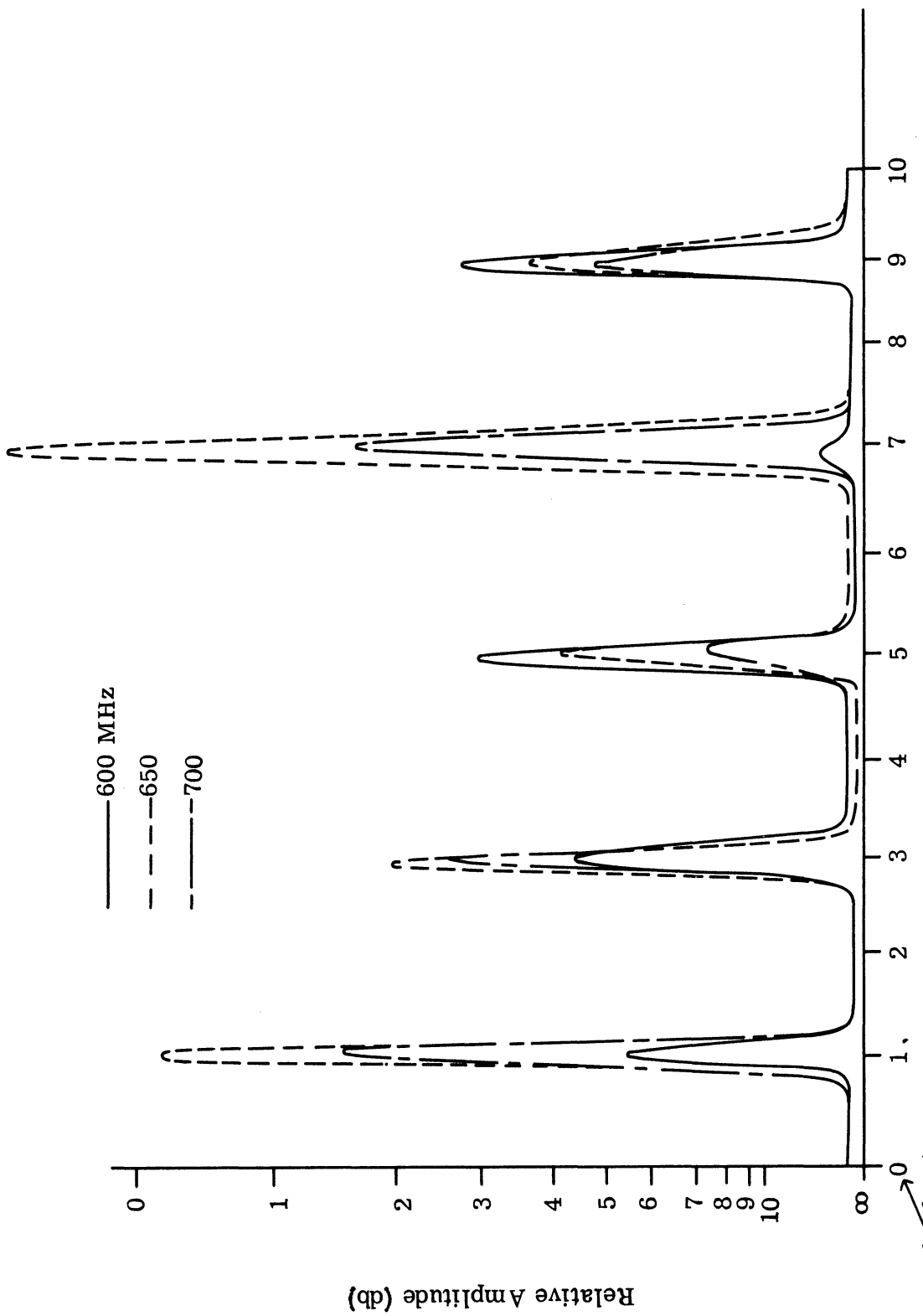

FIG. 4-16: THE NEAR FIELD AMPLITUDE PROBED ALONG $y=\ell$ FOR THE ANTENNA B-1. PROBE POSITION: 1.00 mm ABOVE THE ARRAY ELEMENT.

where the elements are grounded (even elements) and nothing was observed above the ends of odd elements. The reverse is true for $y=\ell$. These results imply (i) both even and odd elements are properly excited; (ii) the current distribution may be sinusoidal subject to the interdigital boundary conditions as observed from the measurement made on antenna D-1.

Slow wave propagation is also observed at 650 MHz from these plots as was discussed in the previous section.

4.2.3 The Near Field Phase Shift.

The near field phase shift was measured with the set-up shown in Fig. 4-17. The attenuators and phase shifter were adjusted to obtain a null on the CRO display, which corresponds to equal amplitude and opposite phase between the reference signal picked up by the directional coupler and the signal picked up by the magnetic probe. Thus, if the net change in phase shifter is recorded and then converted into the angle by dividing the net change with the wavelength of the measuring frequency, the net phase shift angle can be obtained. A trombone-line was modified to provide a convenient phase shifter with its net change readily read out from the attached scale. The probe was put very close (< 0.1 cm) on the middle of the array surface and at the center of the array element for an accurate measurement. The measurements were made for five models, A-1, A-2, A-3, B-1, and B-2, through the frequency range of 400 MHz to 900 MHz. Measurement data are shown in Figs. 4-18 through 4-22, where ψ denotes net phase shift in radians and N denotes the number of array elements counting from the center (which is 0); only half of the antenna was measured because of the assumed symmetry.

An important trend was noted among these phase shift plots; there is a phase decrease along the array at lower frequencies up to 650 MHz when the phase shift suddenly changes to an increasing phase along the array direction. This implies a change in the direction of the phase velocity along the array axis. In other words, at lower frequencies when the antenna is excited in the fast wave region, the phase velocity associated with the decreasing phase along the array

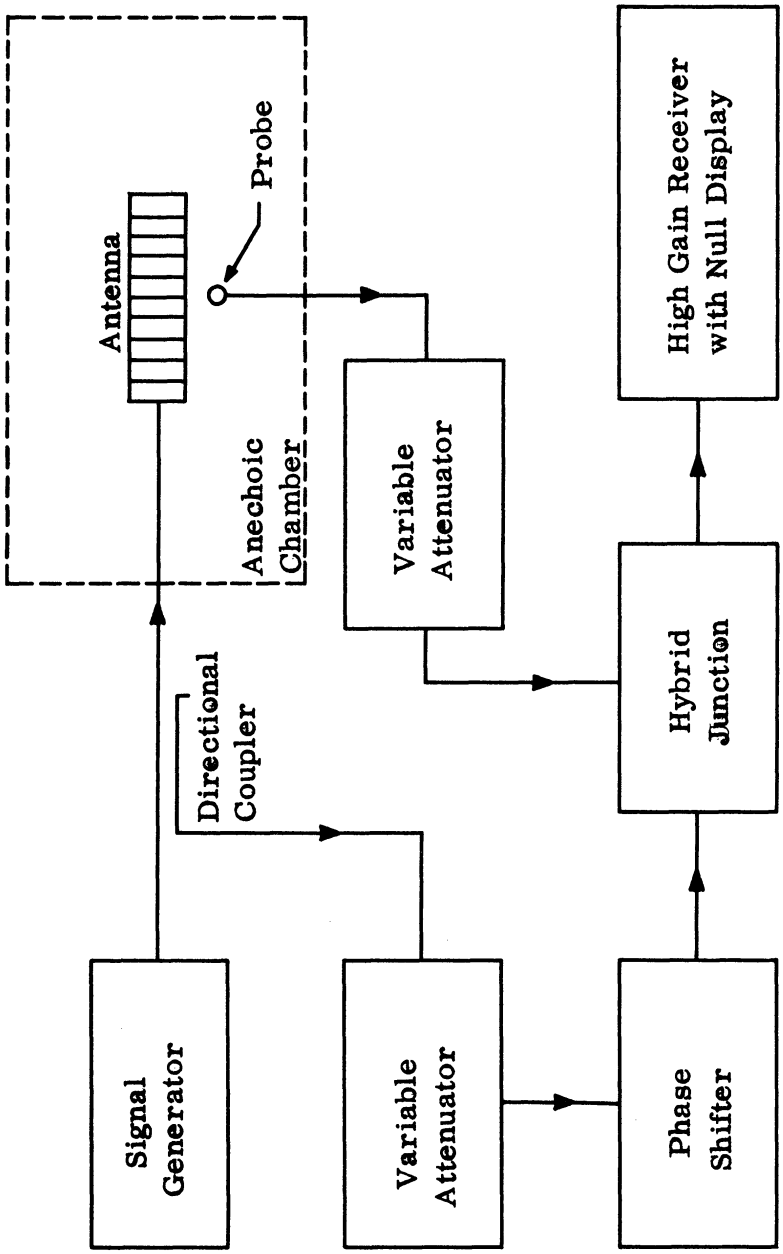

FIG. 4-17: THE EXPERIMENTAL SET-UP FOR THE NEAR FIELD PHASE MEASUREMENT.

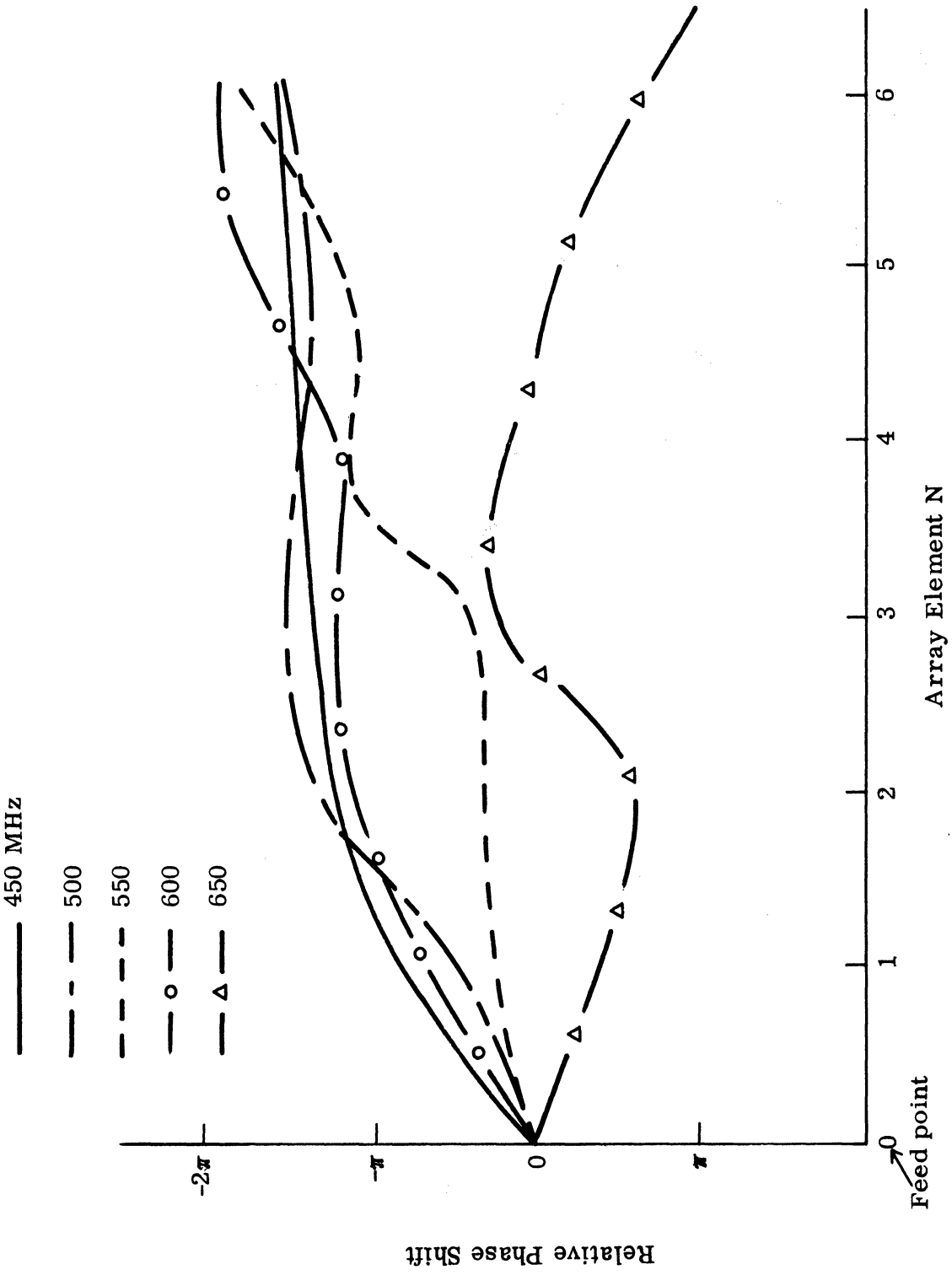

FIG. 4-18a: THE NEAR FIELD PHASE SHIFT FOR THE ANTENNA A-1.

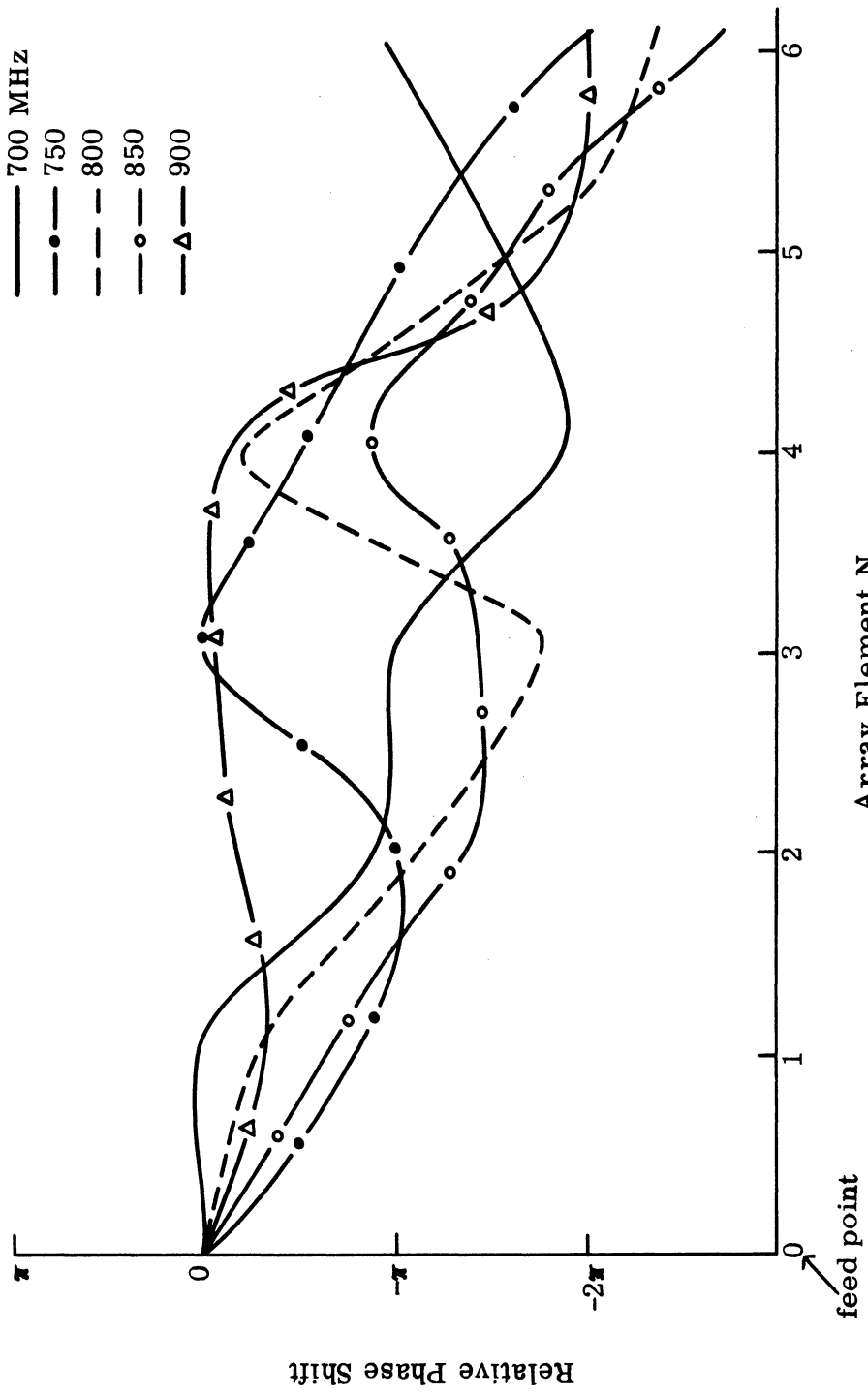

FIG. 4-18b: THE NEAR FIELD PHASE SHIFT FOR THE ANTENNA A-1

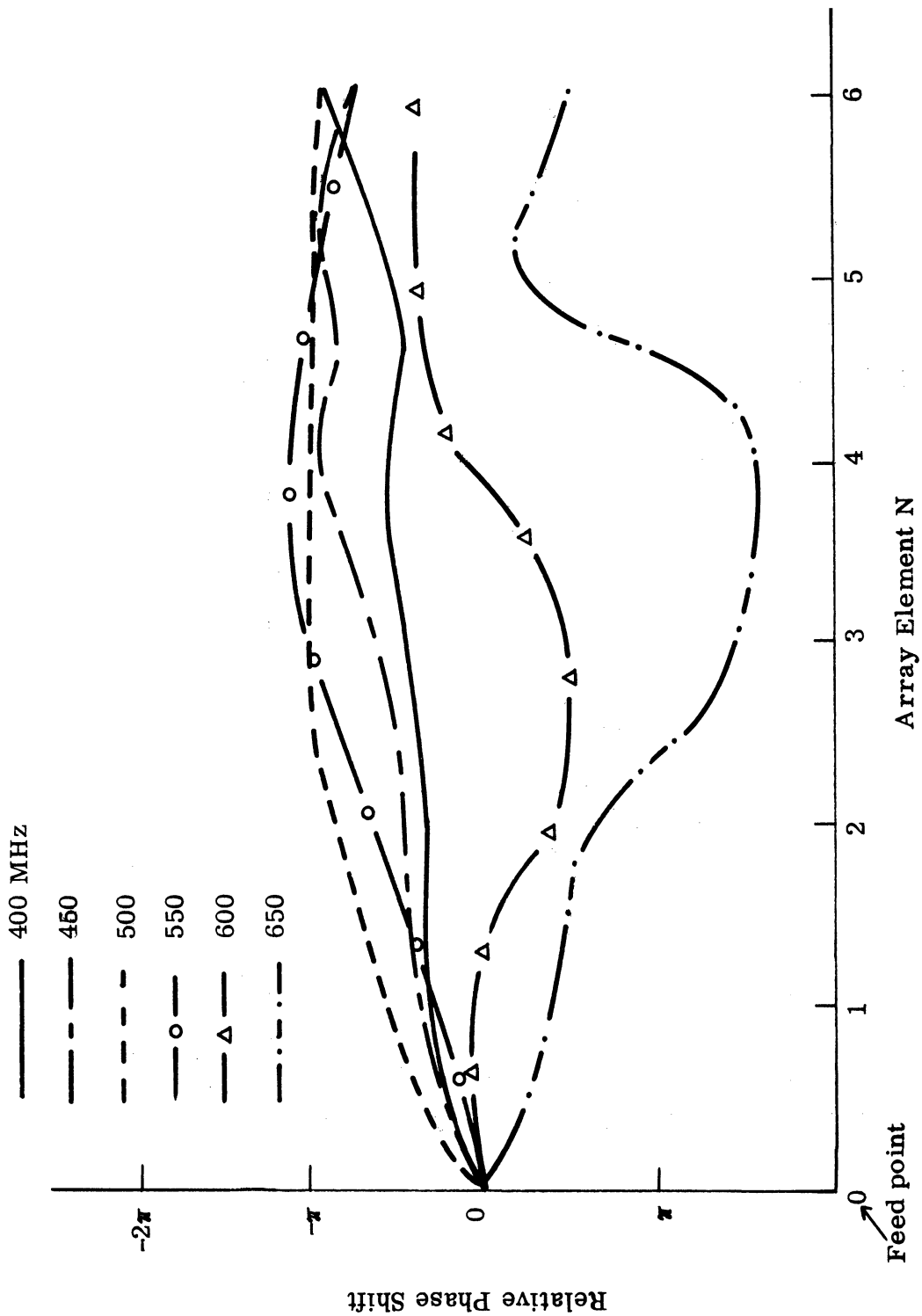

FIG. 4-19a: THE NEAR FIELD PHASE SHIFT FOR THE ANTENNA A-2.

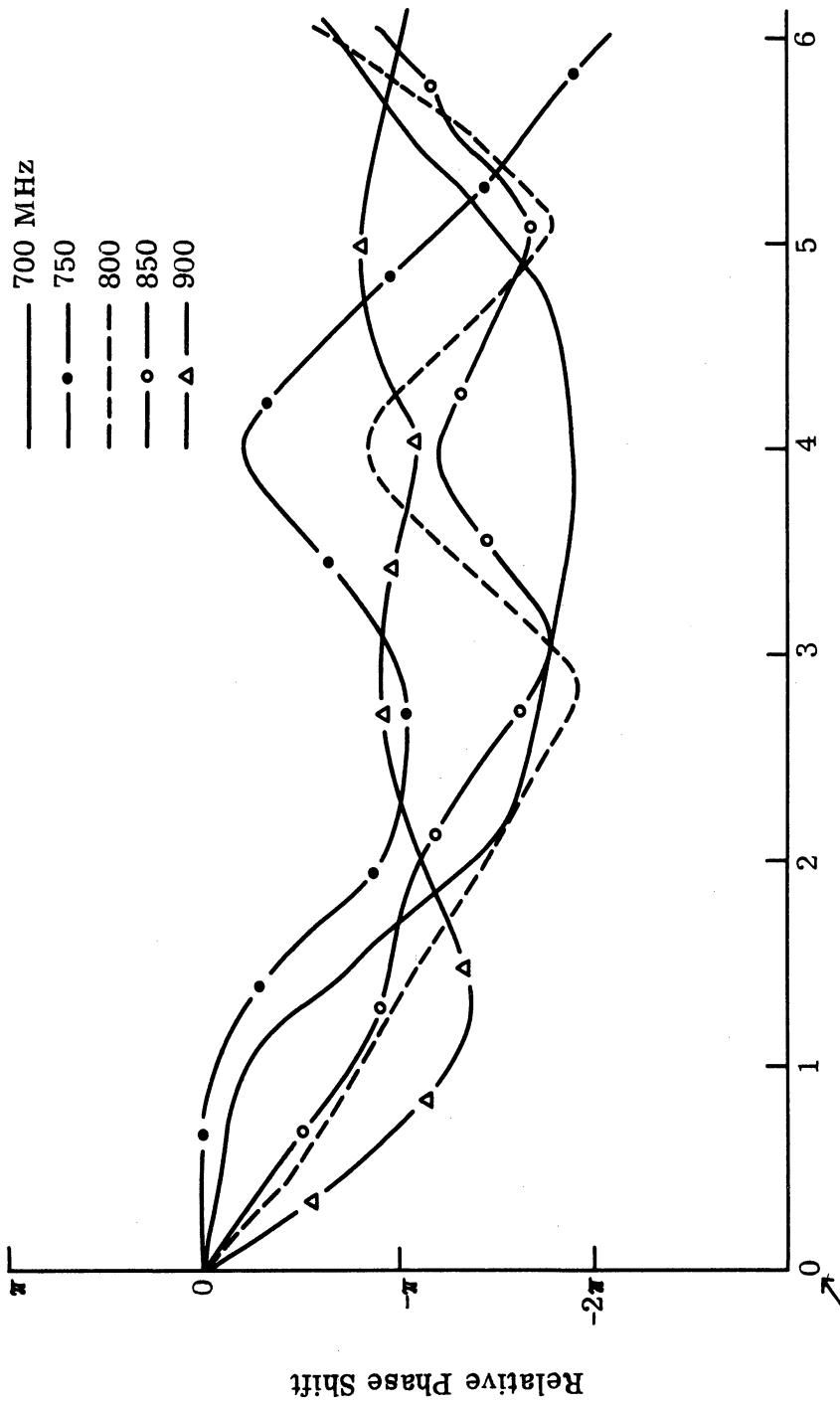

FIG. 4-19b: THE NEAR FIELD PHASE SHIFT FOR THE ANTENNA A-2.

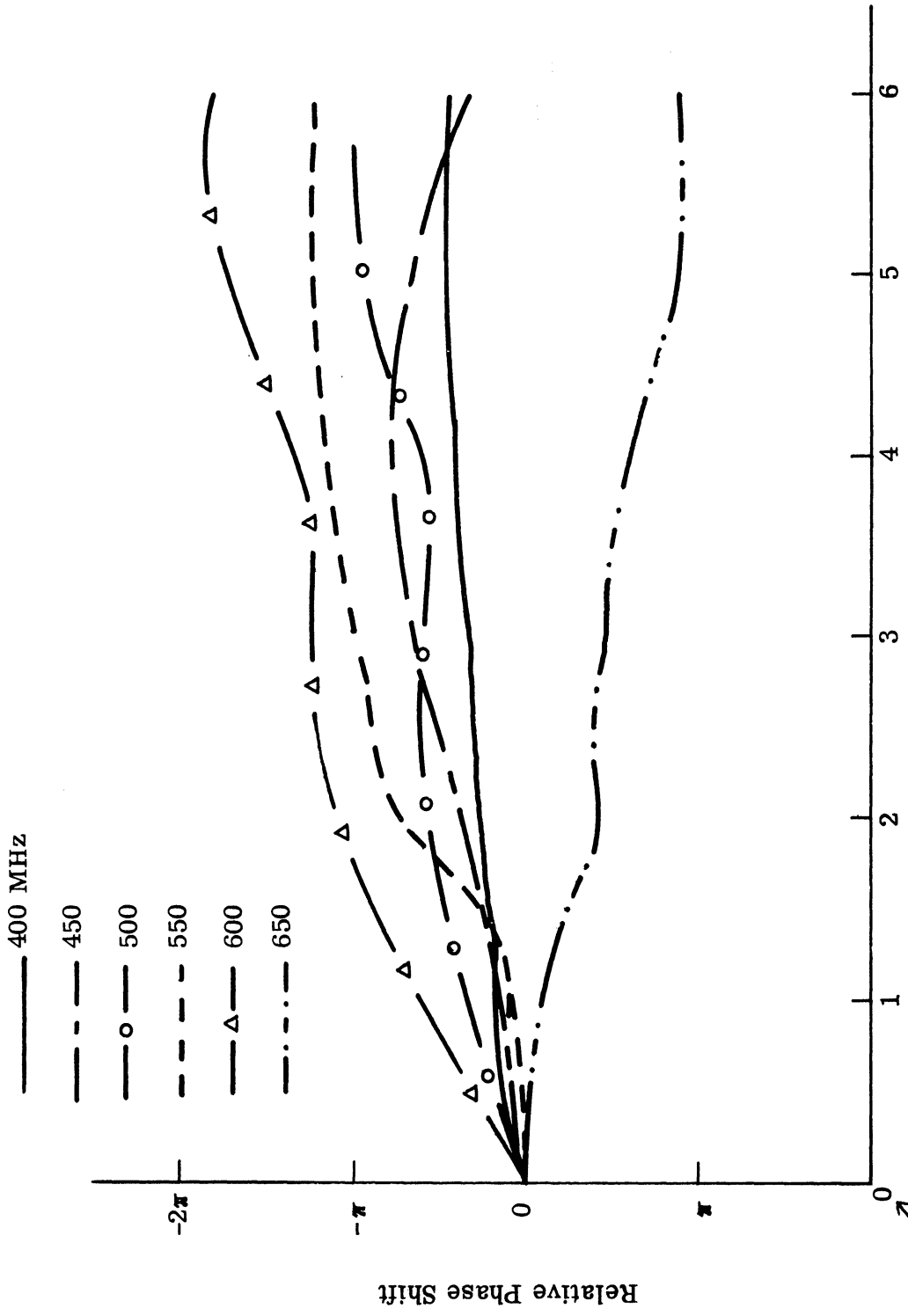

FIG. 4-20a: THE NEAR FIELD PHASE SHIFT FOR THE ANTENNA A-3.

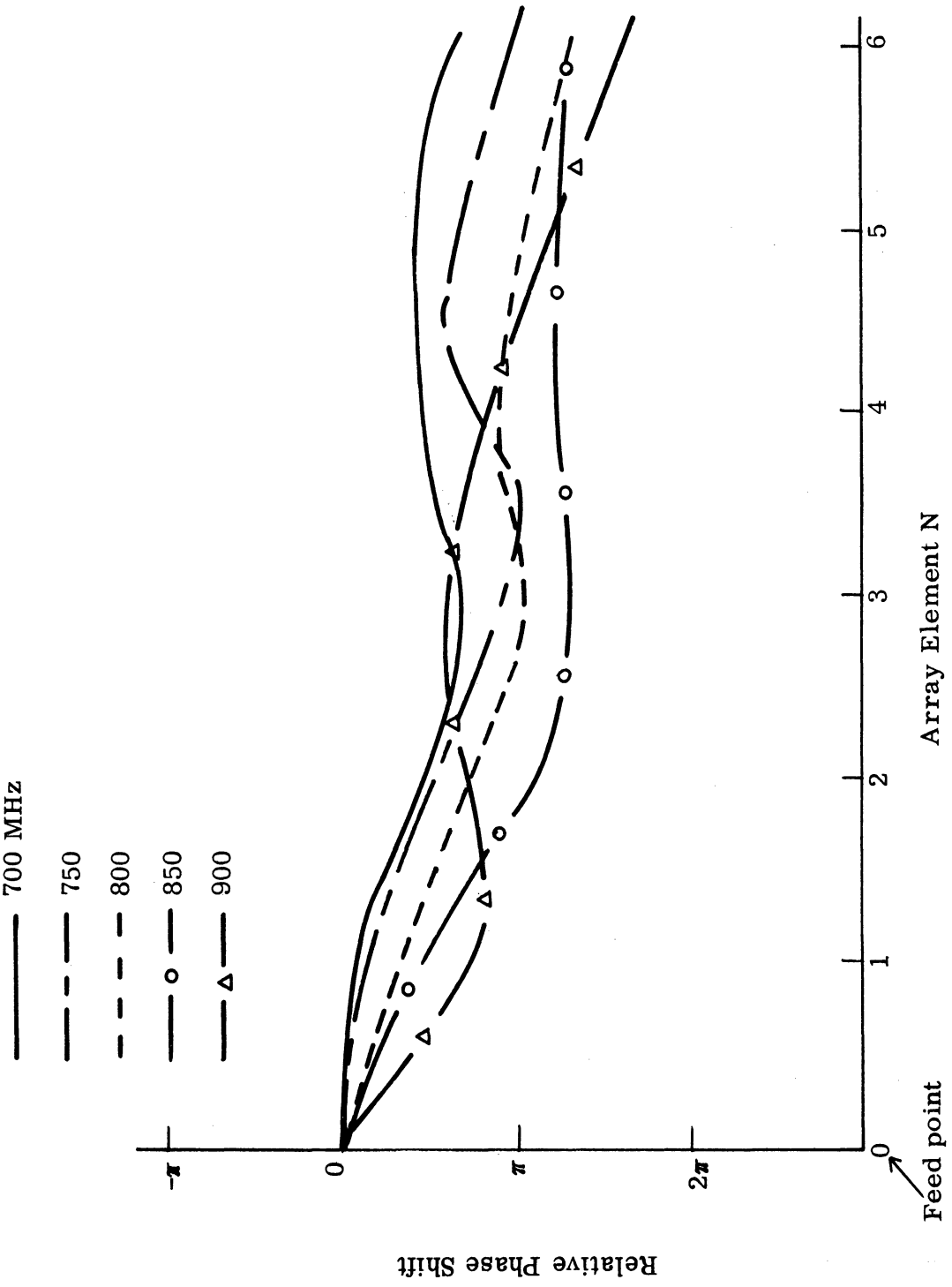

FIG. 4-20b: THE NEAR FIELD PHASE SHIFT FOR THE ANTENNA A-3.

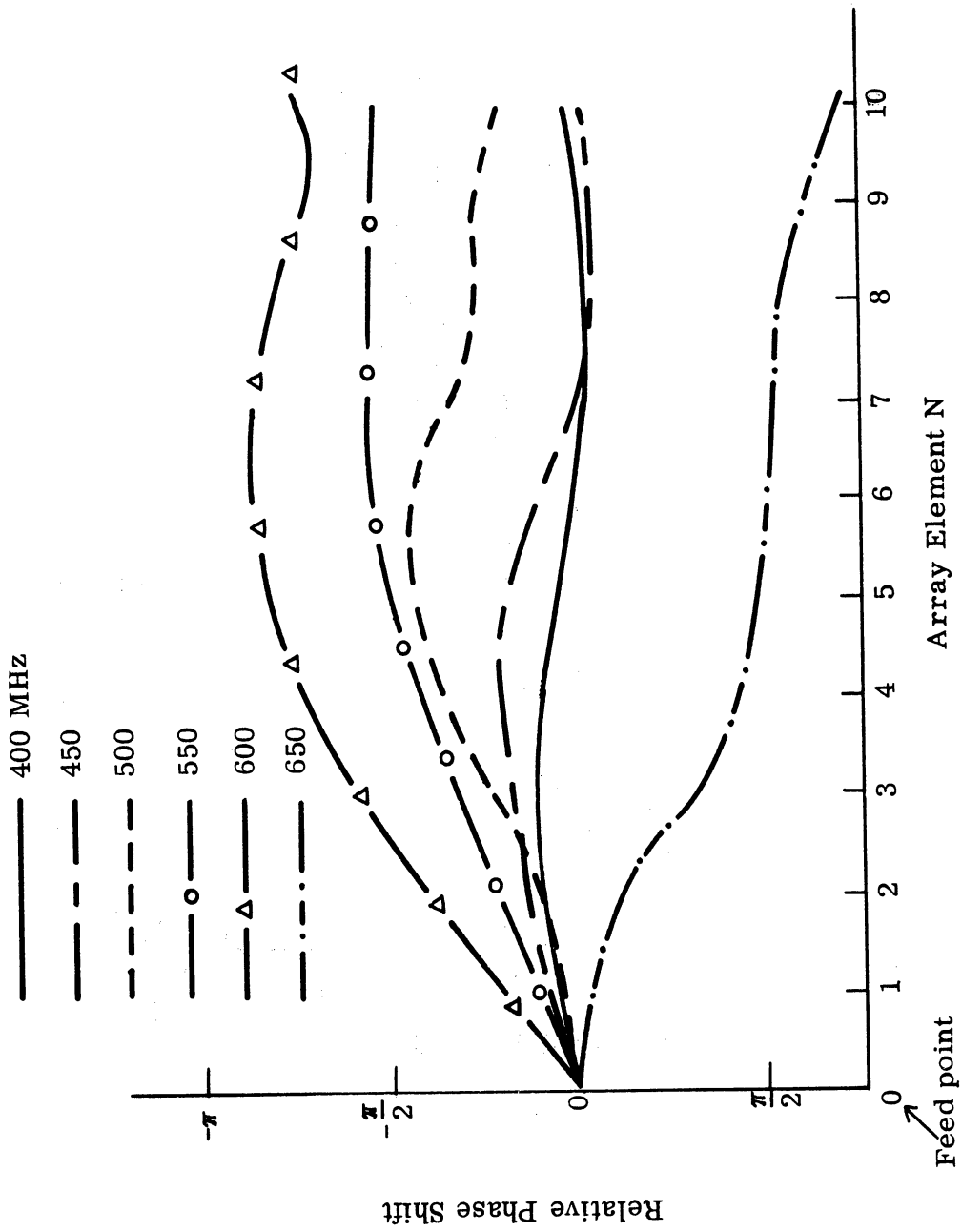

FIG. 4-21a: THE NEAR FIELD PHASE SHIFT FOR THE ANTENNA B-1.

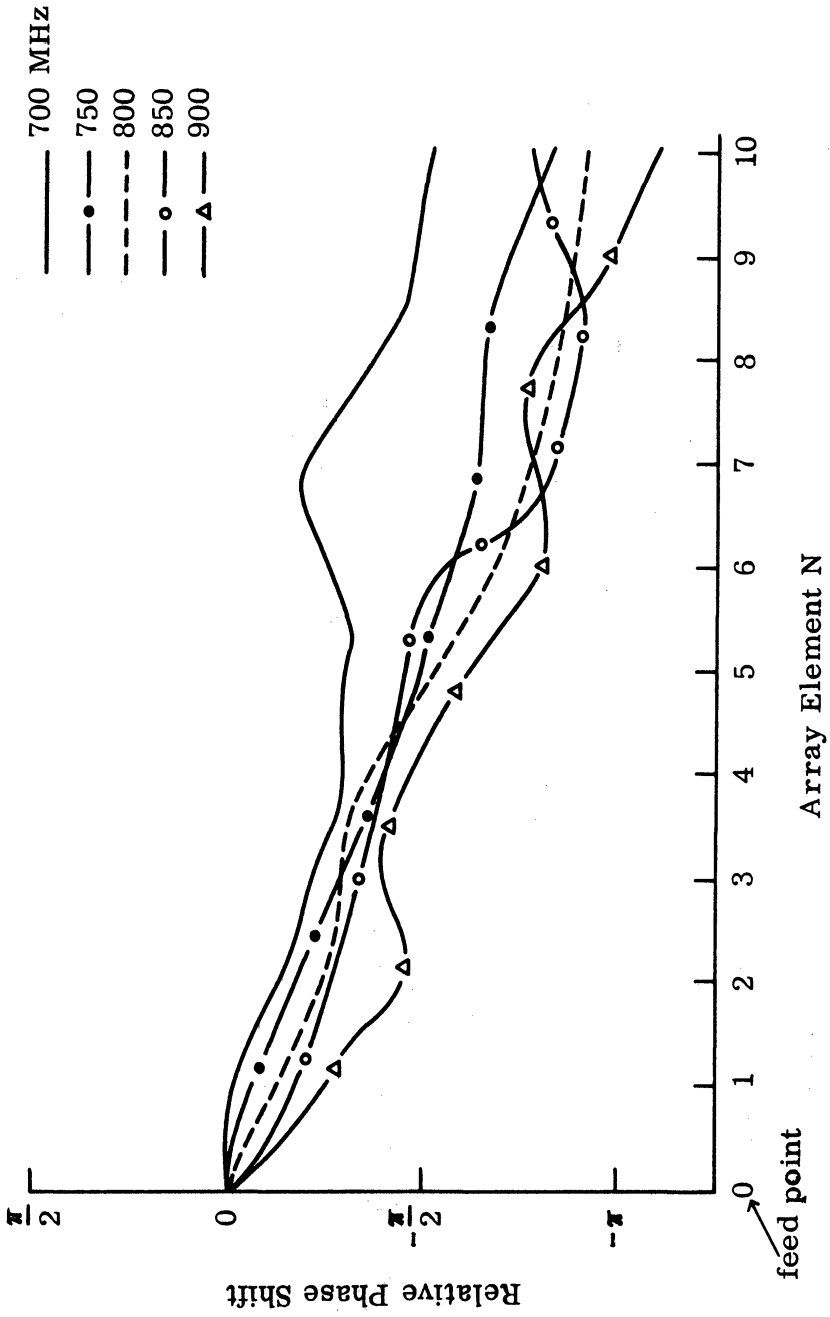

FIG. 4-21b: THE NEAR FIELD PHASE SHIFT FOR THE ANTENNA B-1.

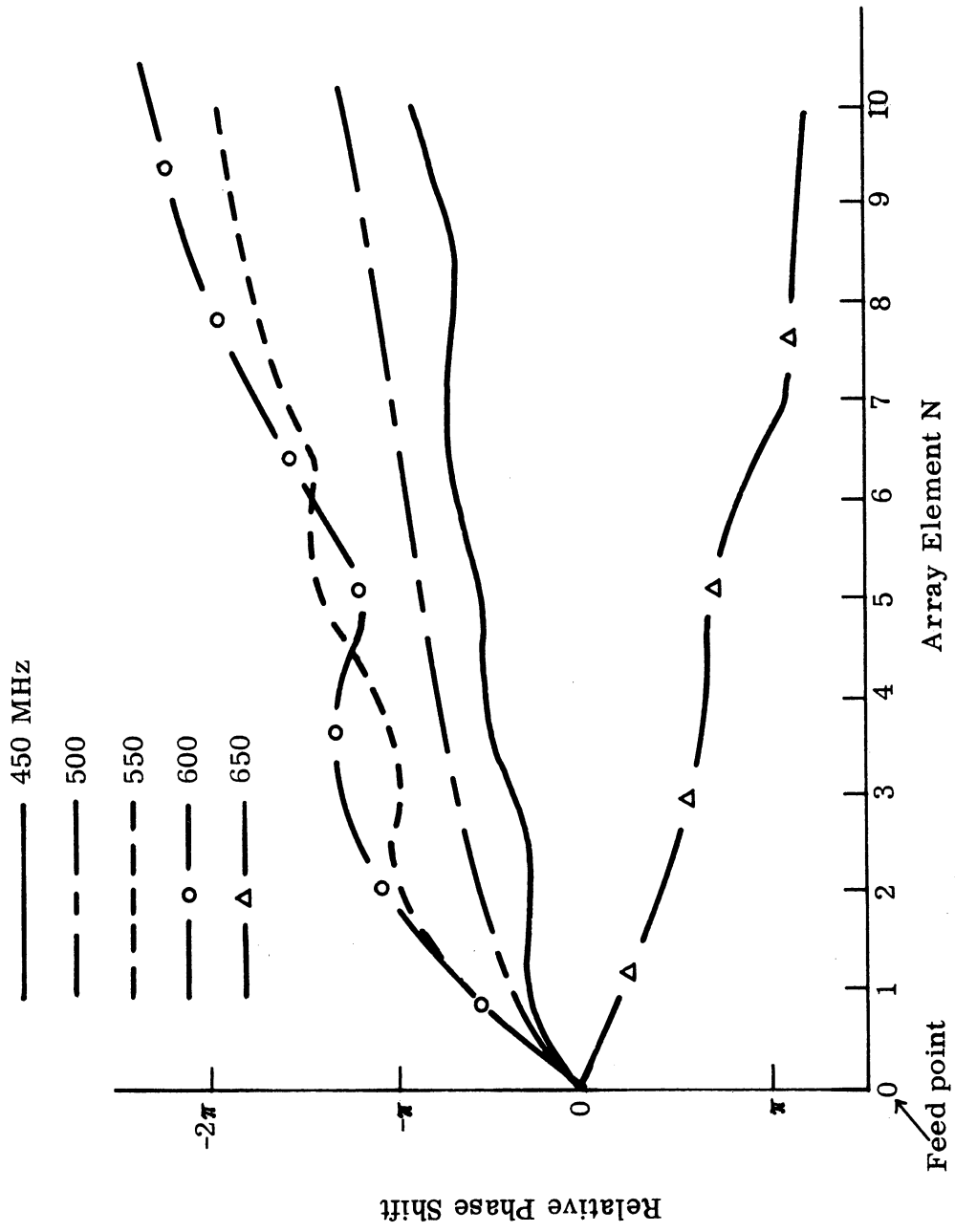

FIG. 4-22a: THE NEAR FIELD PHASE SHIFT FOR THE ANTENNA B-2.

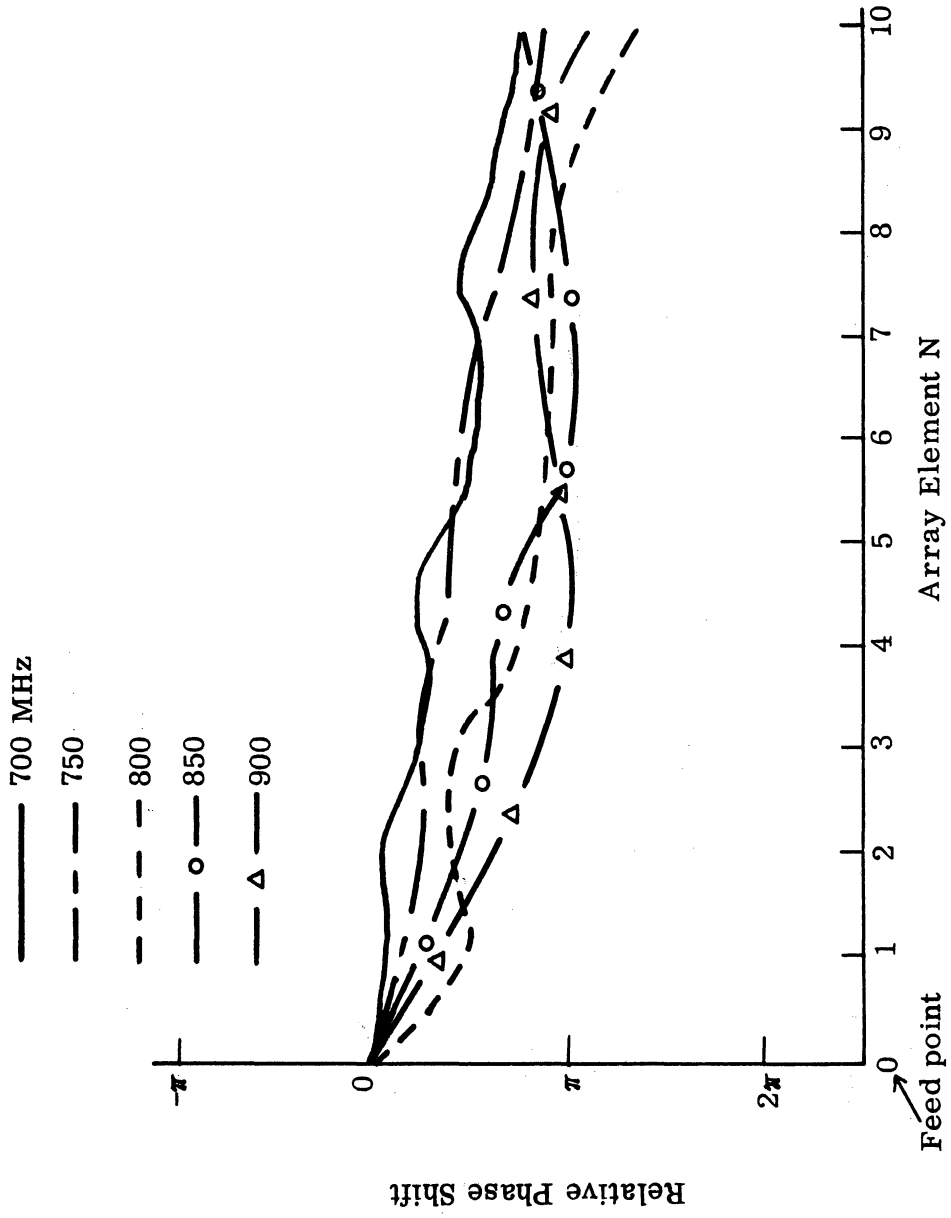

FIG. 4-22b: THE NEAR FIELD PHASE SHIFT FOR THE ANTENNA B-2.

direction is "backward", or directed toward the feed end of the array[7], [17], [18]. Since the dispersion characteristics in the fast wave region require that the phase and the group velocity have to be in the same direction, it is expected that the energy associated with the group velocity will be "backward" also. However, the antenna is fed in such a way that a backward energy flow along the array axis is impossible. Therefore, the radiation mechanism has to be different from the fast wave radiation. It is from this result that the statement in Chapter II was made about the invalidity of the fast wave solution for the theoretical dispersion characteristics. The possible mechanism of radiation in the fast wave region is a "leaky" wave which is defined to be a gradual loss of energy through radiation when the wave is travelling along the array axis. In other words, a complex propagation constant exists along the array axis with its real part equal to that of a free space propagation constant and its imaginary part causing an exponential decay of the amplitude along the array axis. The decay of the amplitude can be seen from the near field amplitude plot in the previous section.

When the antenna is excited above 650 MHz, the phase velocity reverses its direction and becomes "forward" propagation, that is, the phase velocity is along the forward direction of the array axis toward the unexcited end. The energy associated with the group velocity is also along the forward direction of the array for the type of feeding method used in this measurement. Thus, a slow wave solution is valid and a slow wave radiation should take place if the antenna is driven above 650 MHz until the pass-band is exceeded. A leaky wave radiation should take place again once the antenna is driven beyond the pass-band. Since this frequency range is not of present interest, the behavior of the antenna above the slow wave pass-band will not be pursued.

The nonuniform phase shift is probably the result of: (i) probe was not actually at the middle of the array or at the center of the array element, (ii) models were not symmetrically constructed, (iii) drift of the frequency during the measurement, (iv) reflection of the waves at the end of the array, (v) some other experimental errors. It is noted, however, that the phase shift becomes

smoother as the number of array elements is increased from 6 to 10. In order to construct a dispersion curve from these measurements, an average phase shift was obtained by assuming a uniform phase shift and drawing a straight line across the actual phase shift curve. The dispersion curves thus constructed were shown and compared with the theoretical solutions in Figs. 4-23 through 4-25 where the actual resonant frequency of the structure was obtained from the measurement of the single element. It is seen that the experimental results compare fairly well with the theoretical solution except in the fast wave region and above the slow wave pass-band where theoretical solutions are not available numerically.

4.3 The Input Impedance and the VSWR.

The experimental models were placed in an anechoic chamber for an input impedance and a VSWR measurement. The method used was a standard slotted line technique for the impedance measurement. The VSWR was measured by a sweep frequency generator and, thus, continuous values were obtained over a wide frequency range. The frequency marker was integrated into the CRO display for convenience and the reference values of 6.0 and 3.0 were also provided by a standard attenuator. Since the attenuation of the coaxial cable RG 58 may affect the accurate measurement of both input impedance and the VSWR, the feed line was kept very short (less than 3 feet, or less than 1 db within the frequency range) during the entire measurement.

4.3.1 The Single-, Double-, and Triple-Element Antenna.

For a better understanding of the effect of the coupling due to the interdigital boundary conditions, it is natural for one to study the input impedance of a single element antenna first. The physical dimensions of the conducting element and the distance from the ground plane are identical to A-1. The input impedance was measured and plotted in Fig. 4-26. The locus of the input impedance is similar to that of a lossy transmission line. The real part is very small, indicating a weak radiation and some losses, as expected. The resonant frequency is around 700 MHz, which is equivalent to the quarter wavelength of the effective

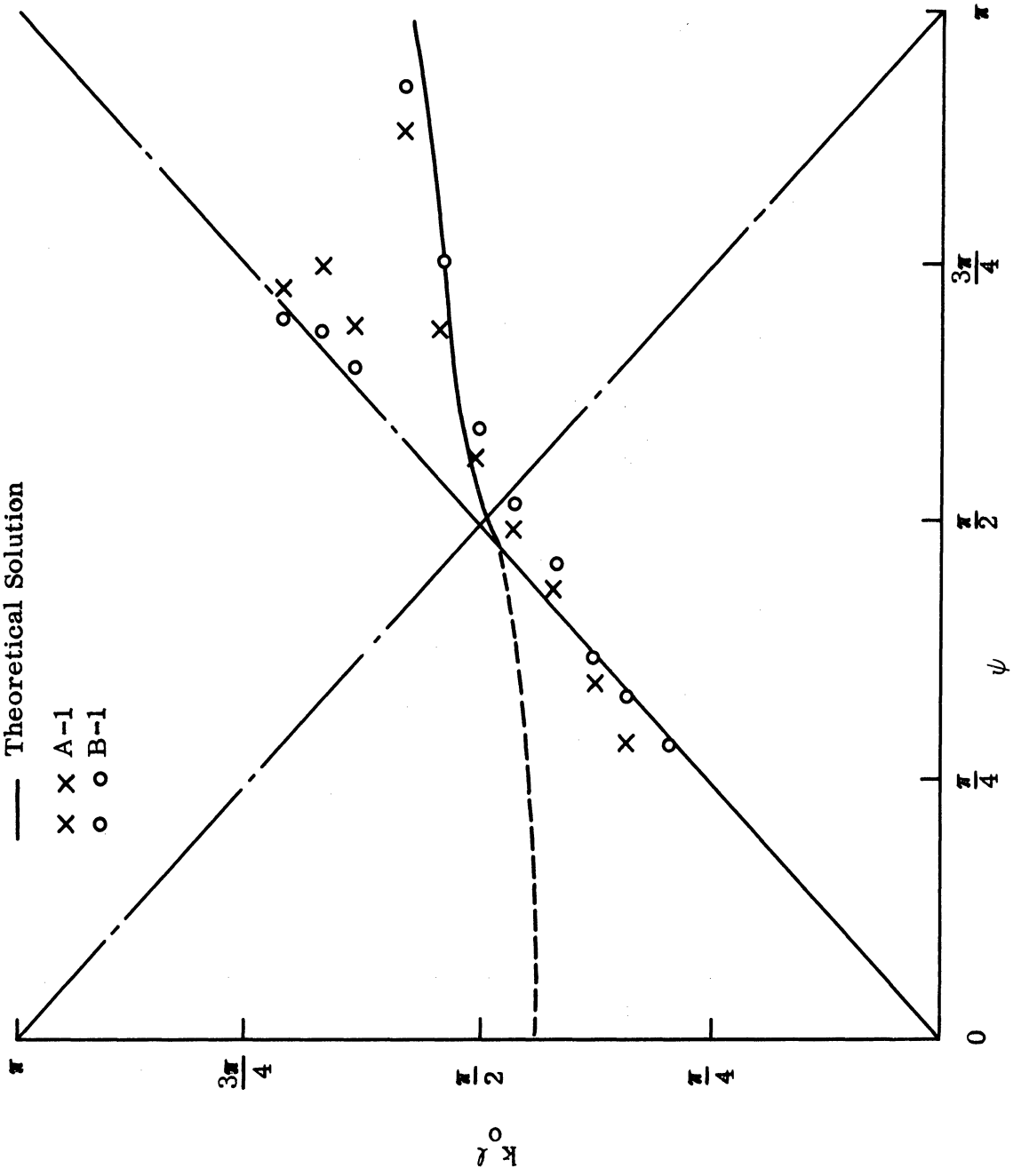

FIG. 4-23: THEORETICAL AND MEASURED DISPERSION CHARACTERISTICS.

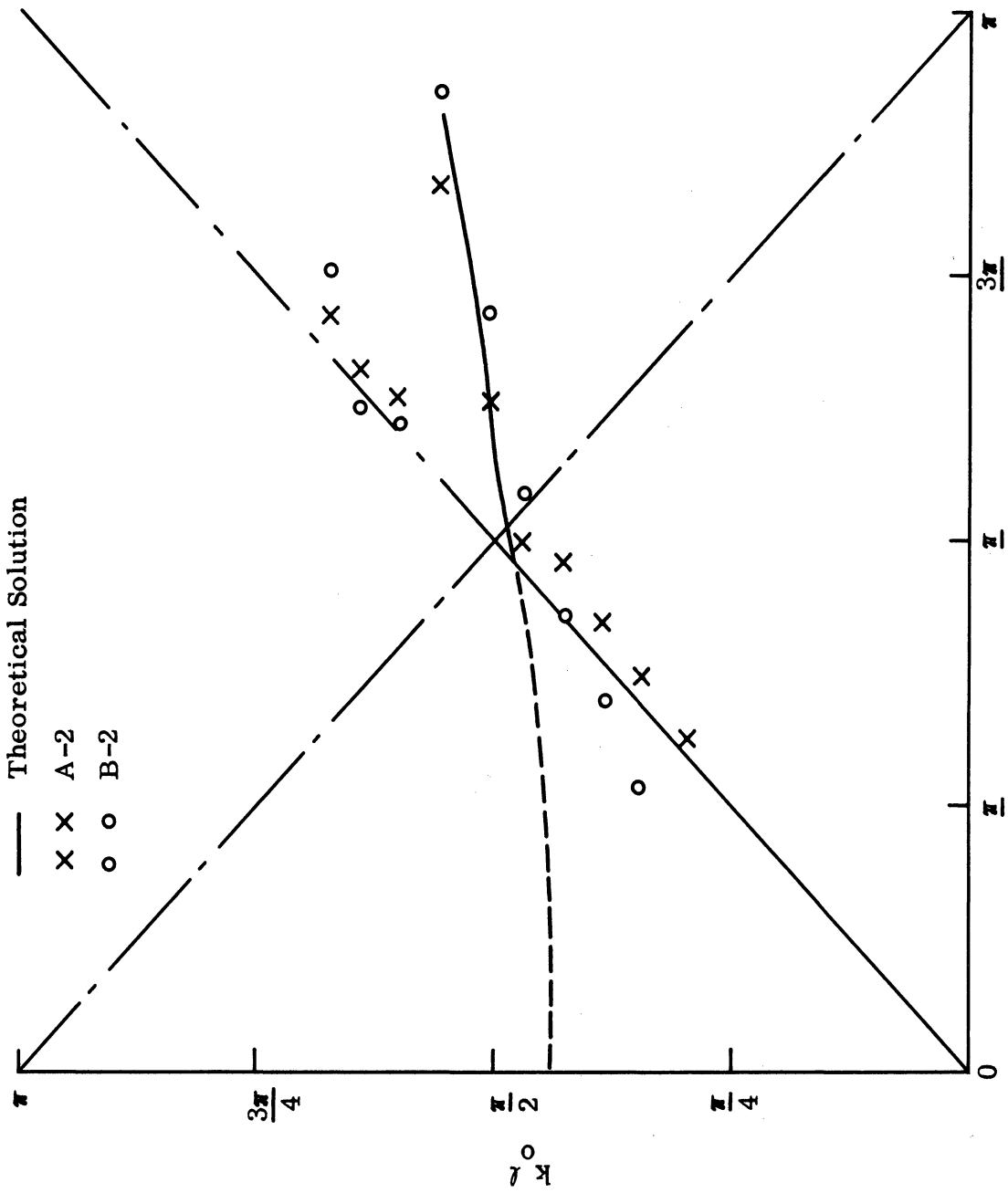

FIG. 4-24: THEORETICAL AND MEASURED DISPERSION CHARACTERISTICS.

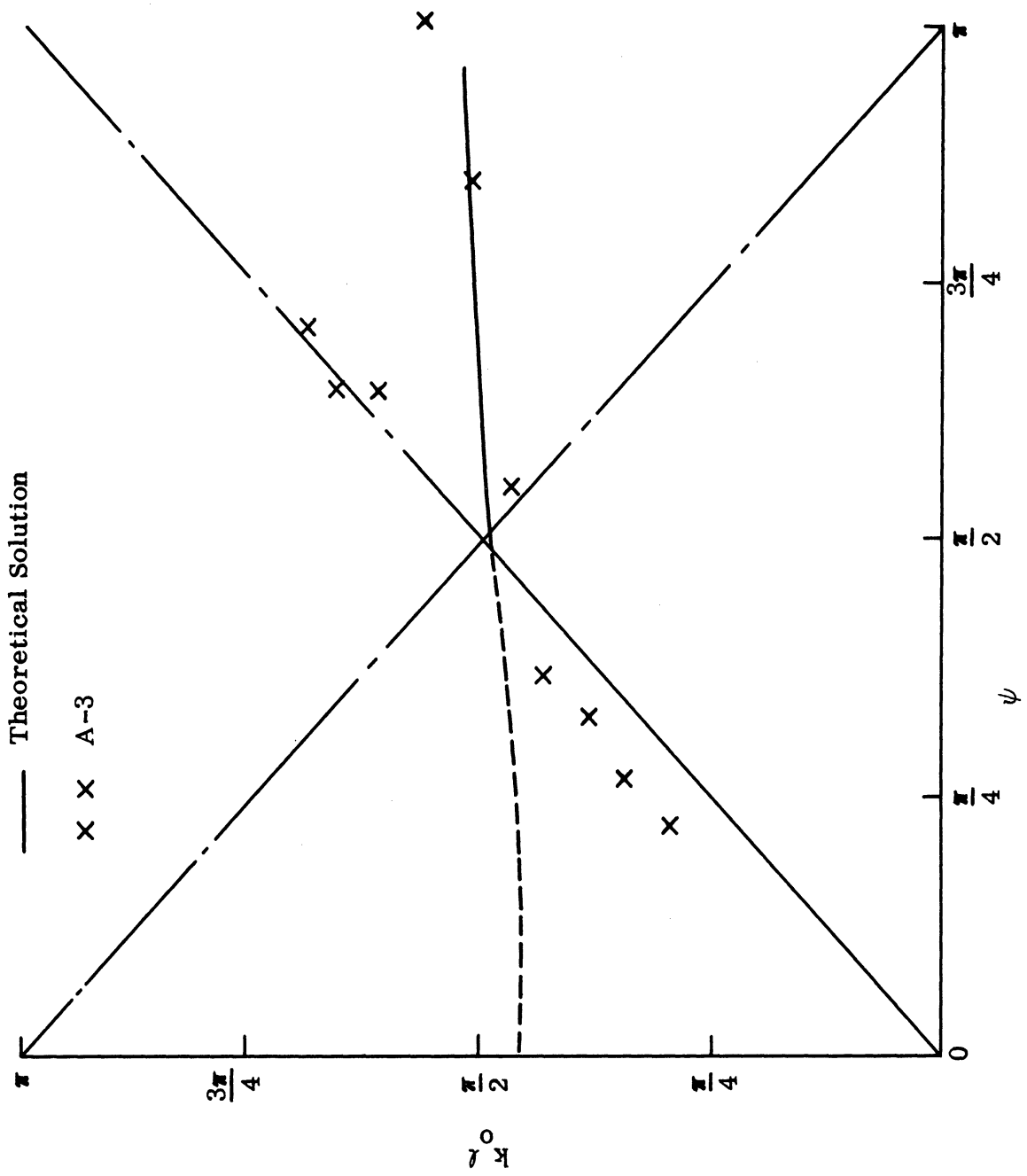

FIG. 4-25: THEORETICAL AND MEASURED DISPERSION CHARACTERISTICS.

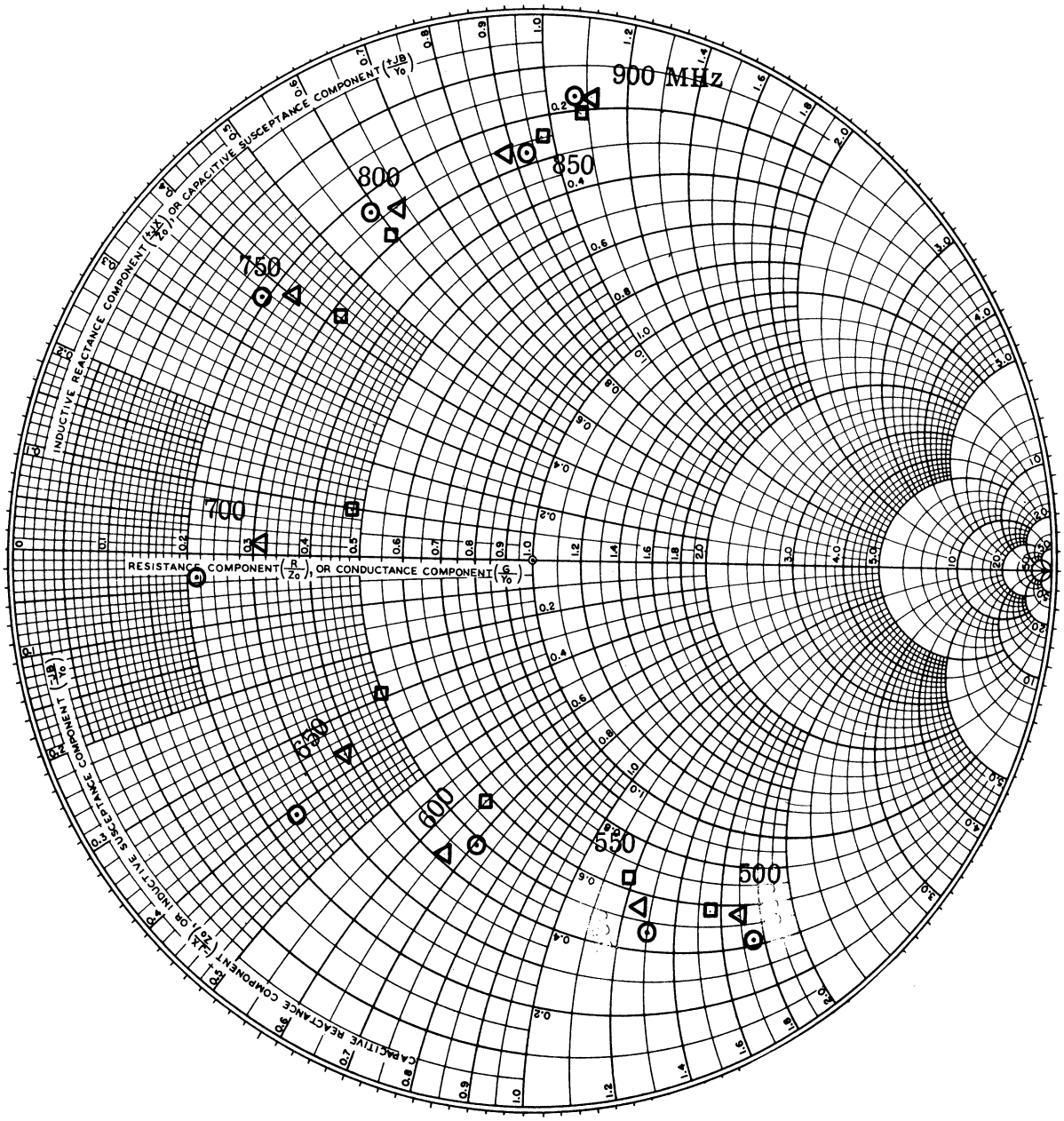

FIG. 4-26: THE INPUT IMPEDANCE FOR SINGLE (⊙), DOUBLE (△) AND TRIPLE (□) ELEMENTS.

length of the vertical plus the horizontal conducting element. The effective length means a ten per cent increase from the actual length of the conducting element to take the true current distribution into consideration.[29]

When a second conducting element is placed near the single element, with the spacing between the elements identical to that of A-1 and grounded on the alternate side, the input impedance locus was moved toward the right of the Smith Chart, meaning some additional radiation and loss due to the second element. Another interesting effect seems to stand out in addition to the increase in radiation. That is, the resonant frequency was decreased somewhat from the original one. This probably is because of the change in the actual current distribution on both elements and thus, more than ten per cent will have to be added to the actual length of the conducting element in order to obtain an effective length. The above two effects are further evidenced when a third element was added along with the alternate boundary conditions. Eventually, when the array element is increased to 13 (A-1), shifts of the input impedance locus and the resonant frequency are advantageous for antenna operation (see Fig. 4-27). That is, a wider band and increased radiation are obtained. The resonant frequency is shifted down to 640 MHz, which is equivalent to a 20 per cent increase in effective length.

Although it is not too obvious from the study of Fig. 4-26, it can be noted that the locus is shrinking toward the center of the Smith Chart as the number of elements is increased from one to three. This is the indication of a wider band structure.

A study was also conducted using VSWR measurements as shown in Fig. 4-28. For the frequency range covered by the sweep frequency generator, it can be observed that the effect of the second and third interdigital elements tends to decrease the overall VSWR gradually. It is also interesting to compare results on one, two, or three elements with the VSWR of the antenna A-1 (see Fig. 4-28d).

Similar measurements were tried without interdigital boundary conditions, that is, grounded on the same side or no grounding at all. The Smith Chart plots

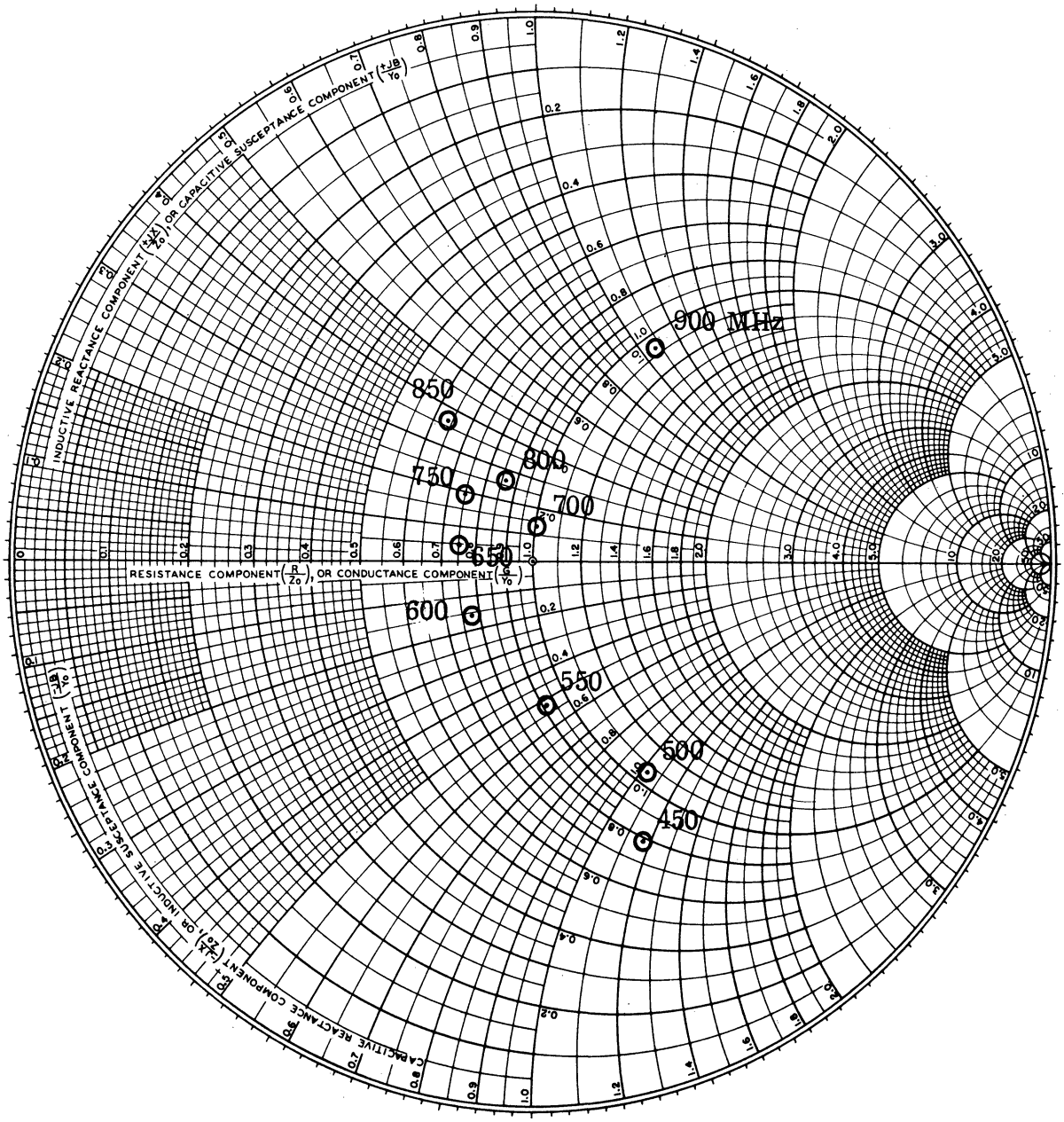

FIG. 4-27: THE INPUT IMPEDANCE FOR THE ANTENNA A-1.

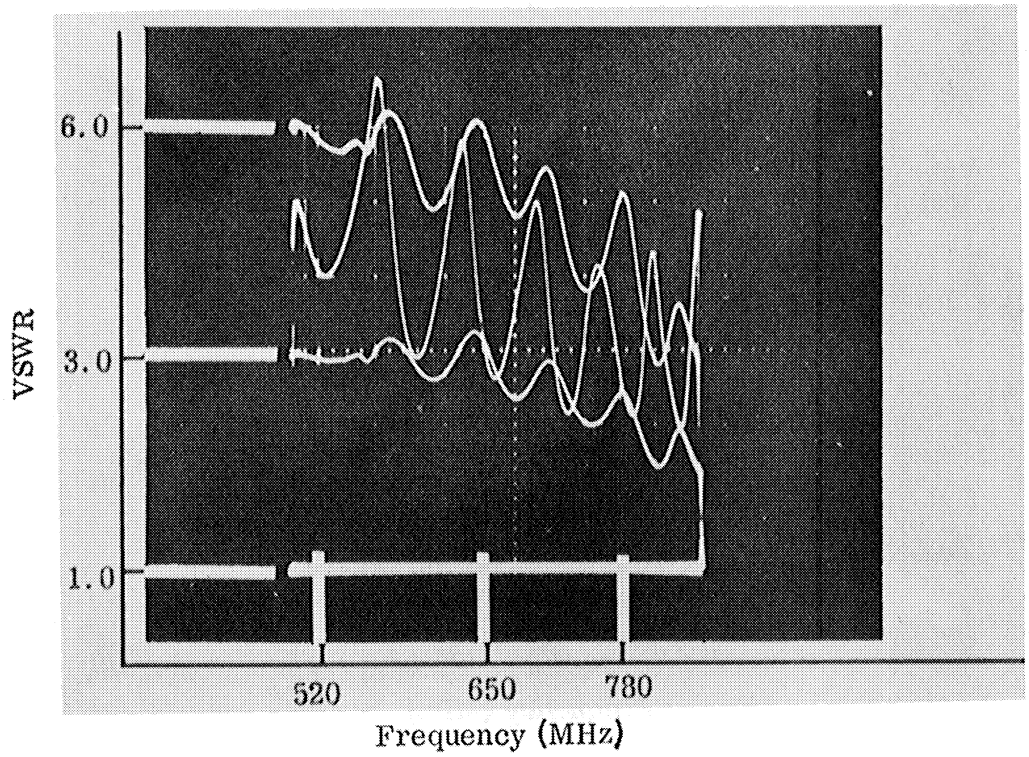

FIG. 4-28a: THE VSWR FOR A SINGLE ELEMENT ANTENNA.

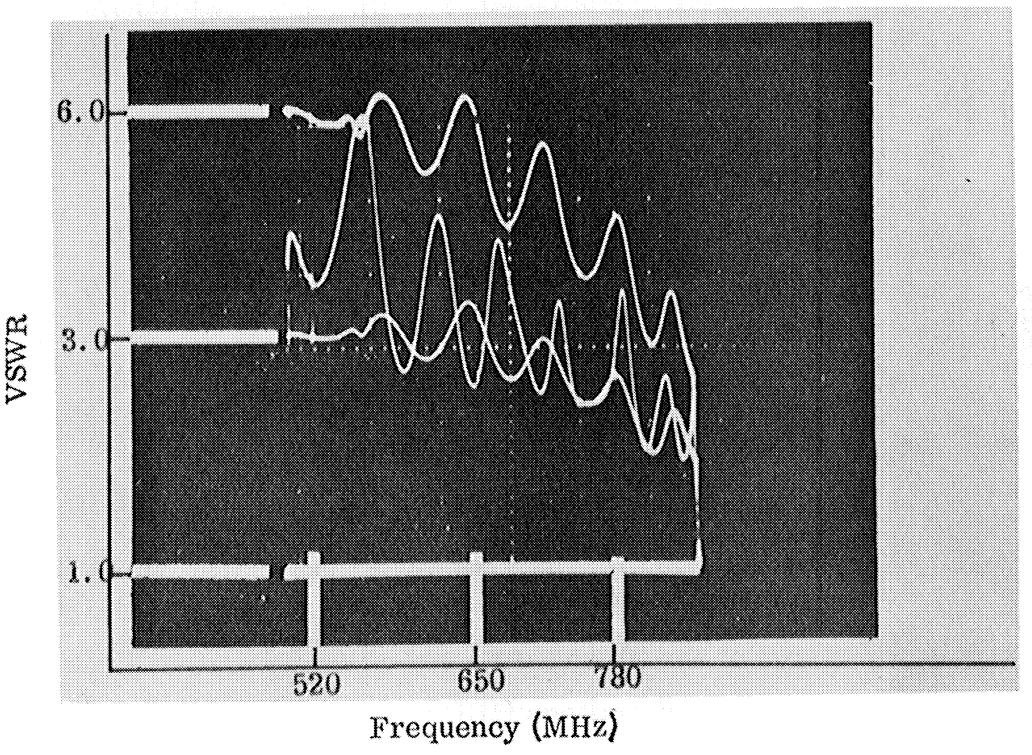

FIG. 4-28b: THE VSWR FOR A DOUBLE ELEMENT ANTENNA.

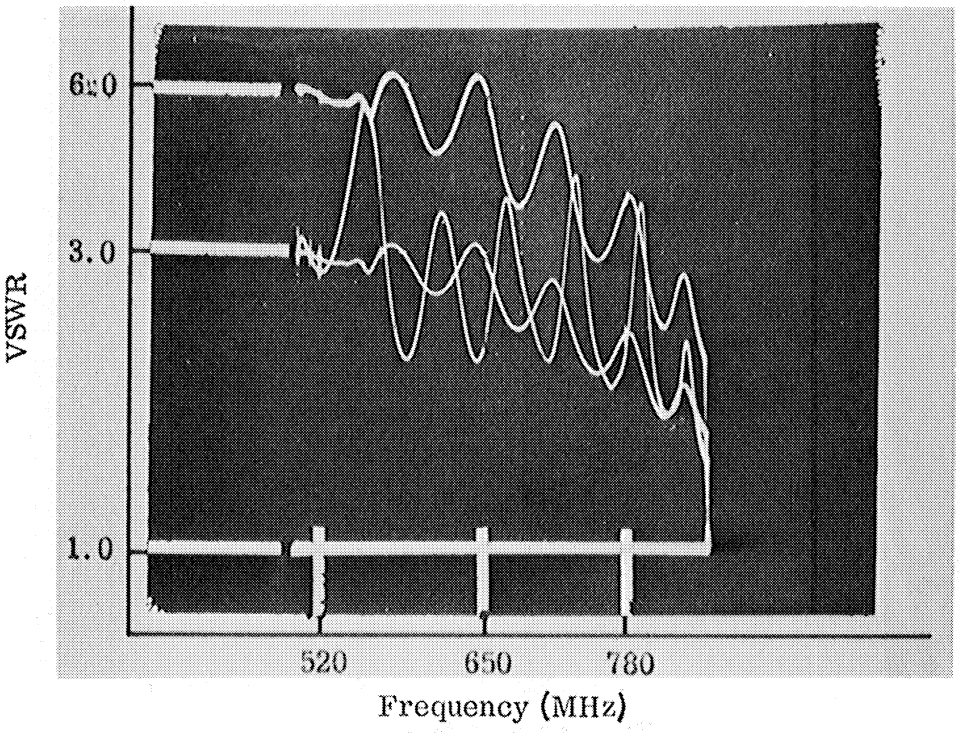

FIG. 4-28c: THE VSWR FOR A TRIPLE ELEMENT ANTENNA.

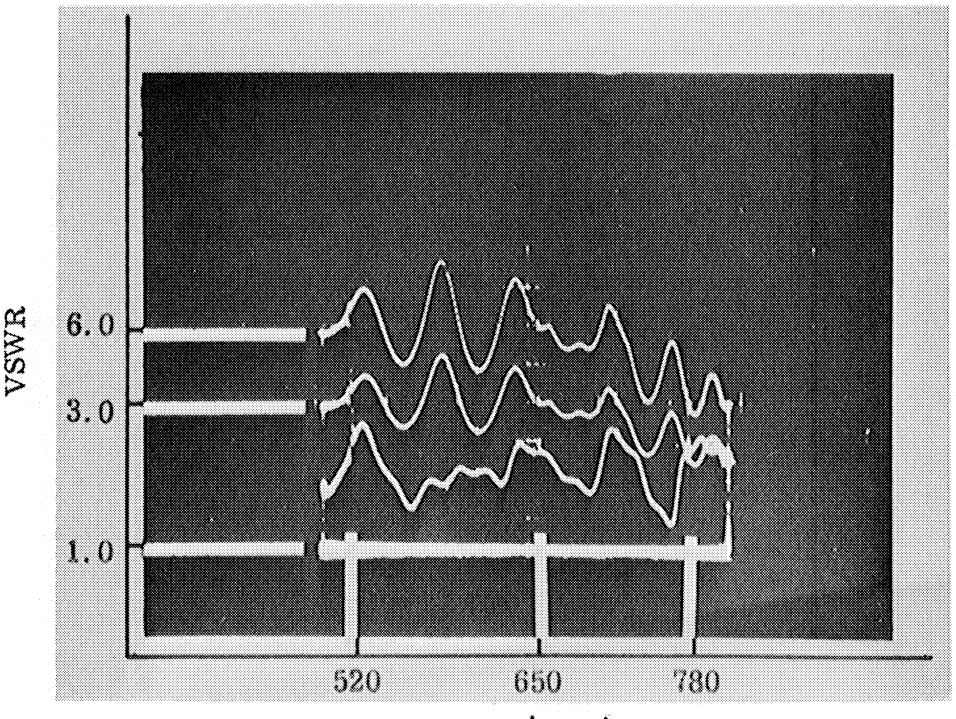

FIG. 4-28d: THE VSWR FOR THE ANTENNA A-1.

do not show significant shifts in the impedance locus by increasing the number of adjacent elements.

To sum up, the addition of the second and third element with an interdigital boundary condition has the following effects:

(a) Lowers the resonant frequency.
(b) Shifts the impedance locus toward the center of the Smith Chart.
(c) Shrinks the impedance locus to become a wider band structure.

4.3.2 The Center-fed Antenna.

The input impedance and the VSWR of the center-fed antennas A-1, A-2, A-3, B-1 and B-2 were taken and compared in this section.

The input impedance of A-1 is already shown in Fig. 4-27 as an extension of the single-element antenna. As was noticed before, the resonant frequency is down to 640 MHz and the VSWR shown in Fig 4-28d indicates a fairly wide band of frequency for which the VSWR is lower than 3 with respect to 50Ω coaxial cable. Based on the above observations, it can be said that the antenna A-1 has a bandwidth of around 280 MHz with a center frequency of 640 MHz. The comparison of the theoretical solution of A-1 and the measured impedance is shown in Fig. 4-29, where it is seen that the theoretical solution fails to coincide with the measured values although it falls into a general range. This perhaps is due to the ambiguity of the theoretical solution and some error in experimental measurement.

The input impedance of A-2 is plotted in Fig. 4-30 and the VSWR is seen in Fig. 4-31. Measurements indicate that the increase in the array spacing has made the antenna into a narrower band structure with its input impedance locus stretched out a little in comparison with the antenna A-1. The resonant frequency is around 630 MHz and the bandwidth is around 250 MHz based on the VSWR of less than 3 with respect to 50Ω coaxial cable. It is seen that the VSWR of A-2 is lower than that of A-1 within the frequency band of operation, which, perhaps is due to a physically longer array structure and thus, a lesser reflection from the end of the array back to the feeding point. The comparison between the theoretical and measured input impedance is shown in Fig. 4-33.

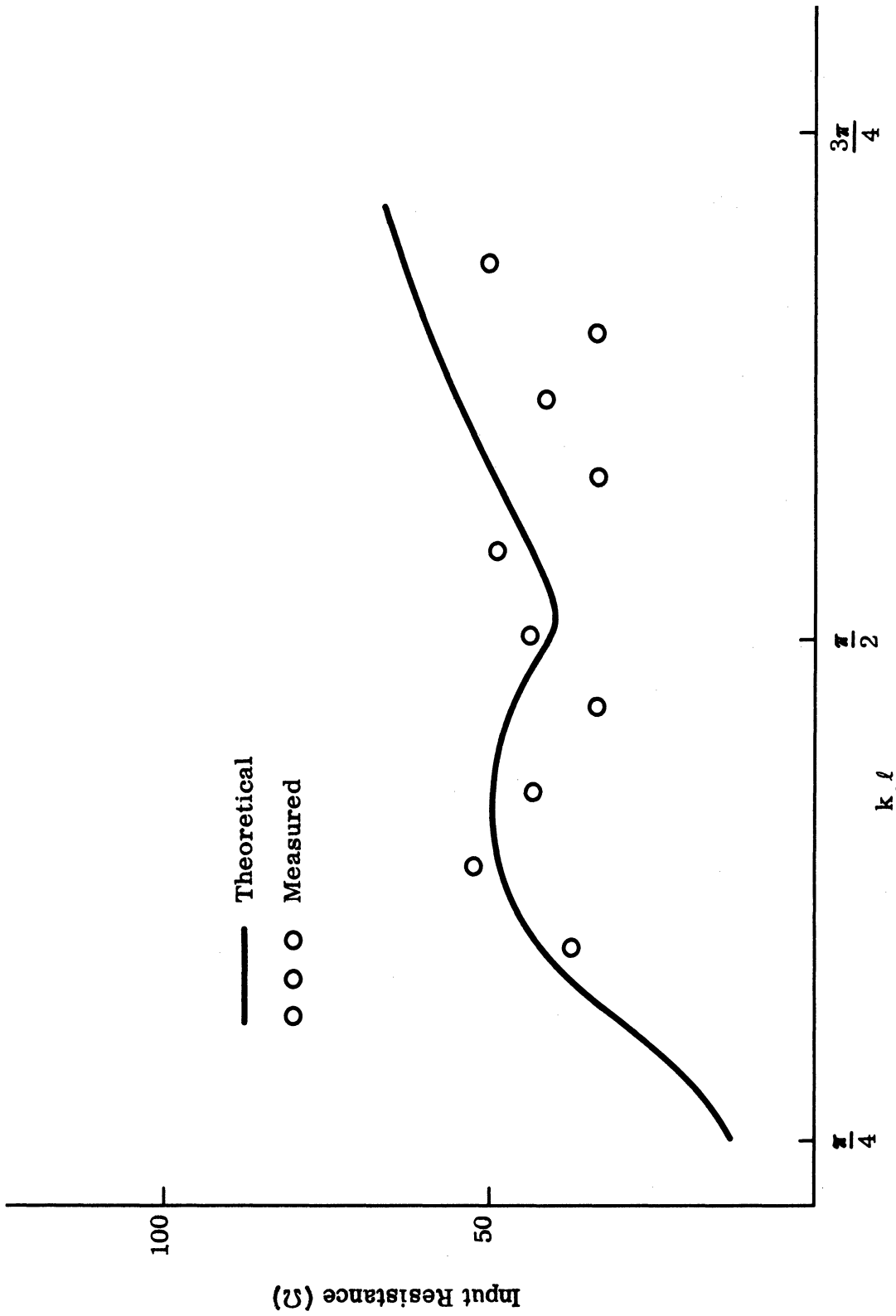

FIG 4-29a: THE INPUT RESISTANCE FOR THE ANTENNA A-1

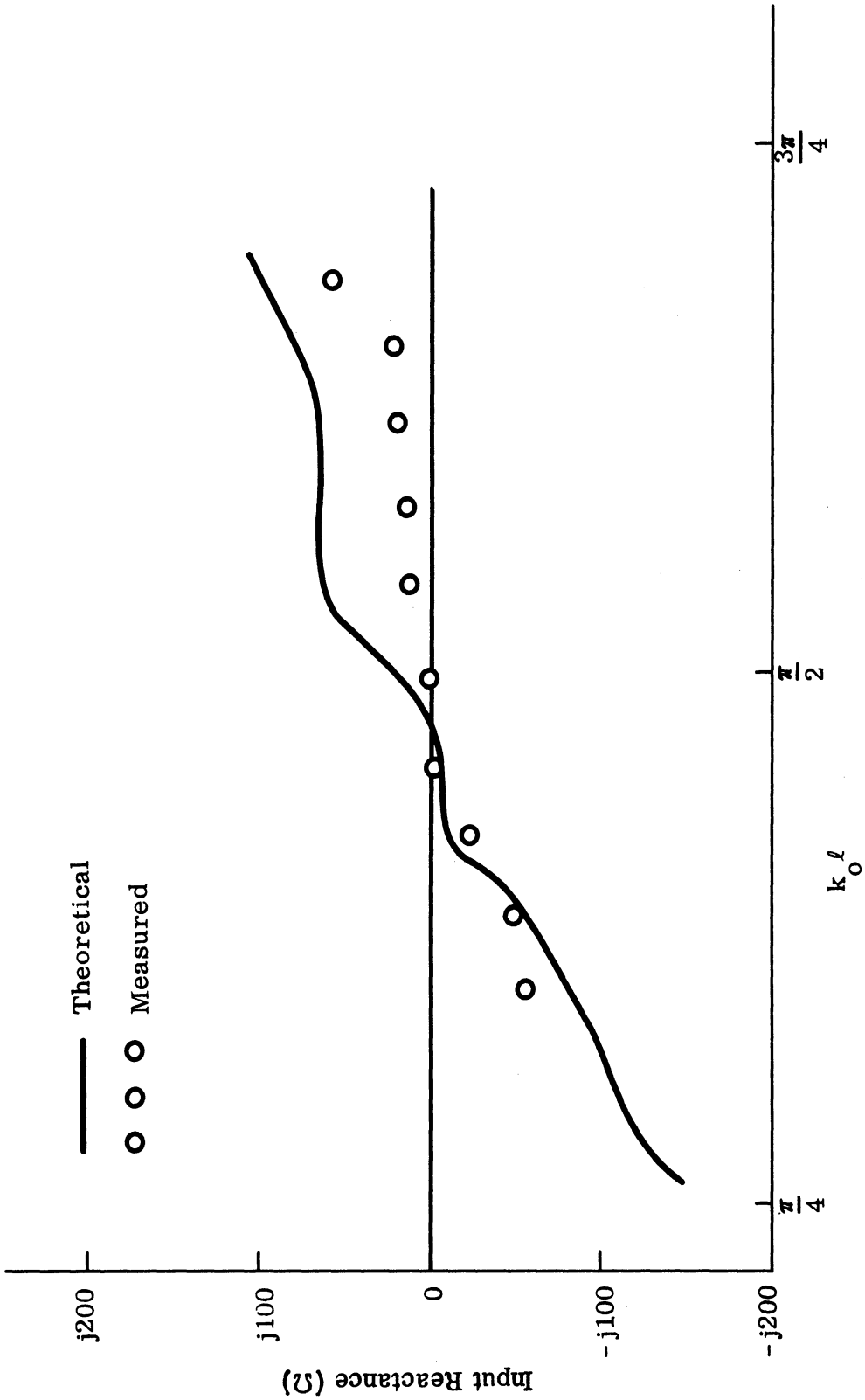

FIG. 4-29b: THE INPUT REACTANCE FOR THE ANTENNA A-1.

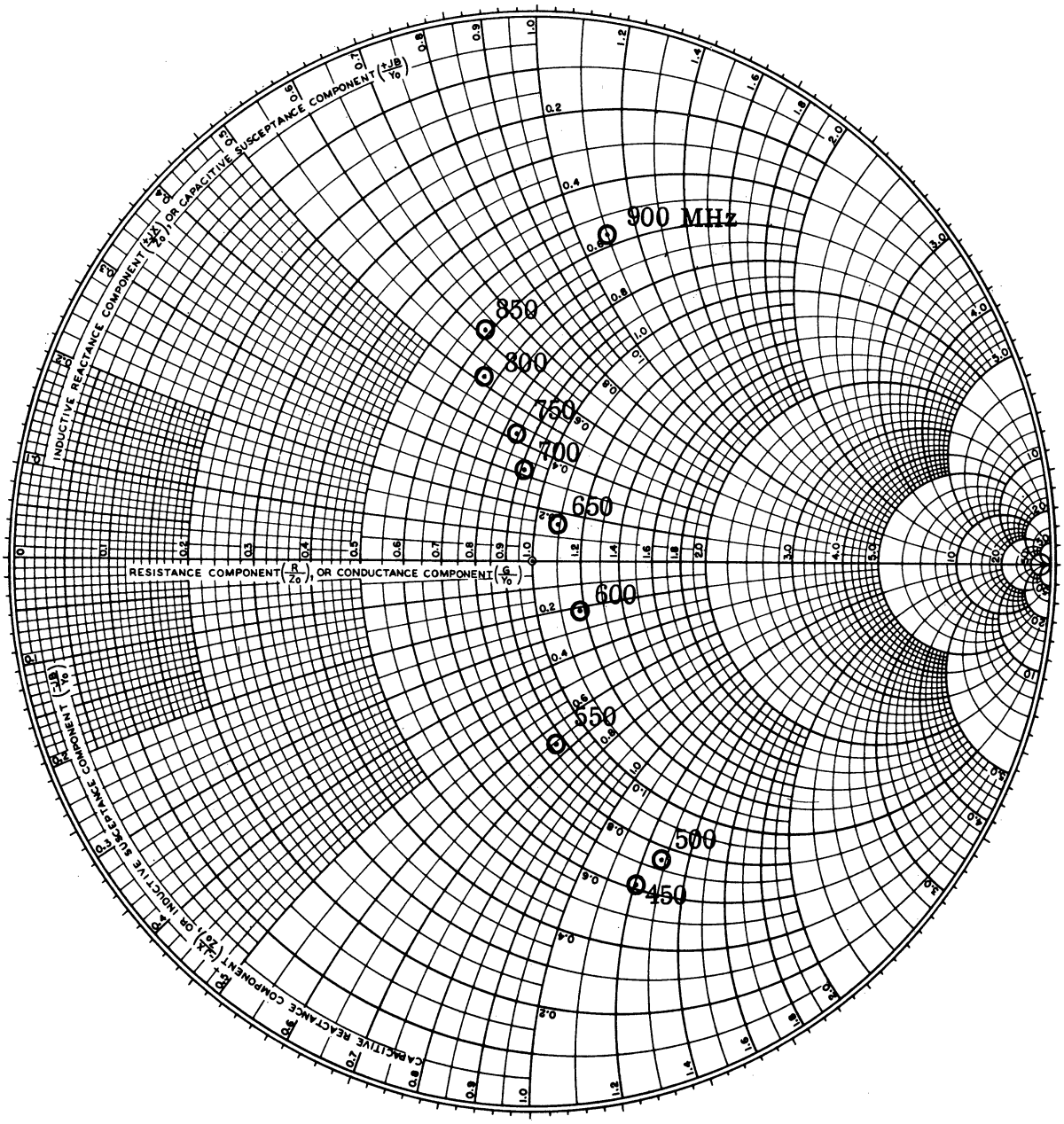

FIG. 4-30: THE INPUT IMPEDANCE FOR THE ANTENNA A-2.

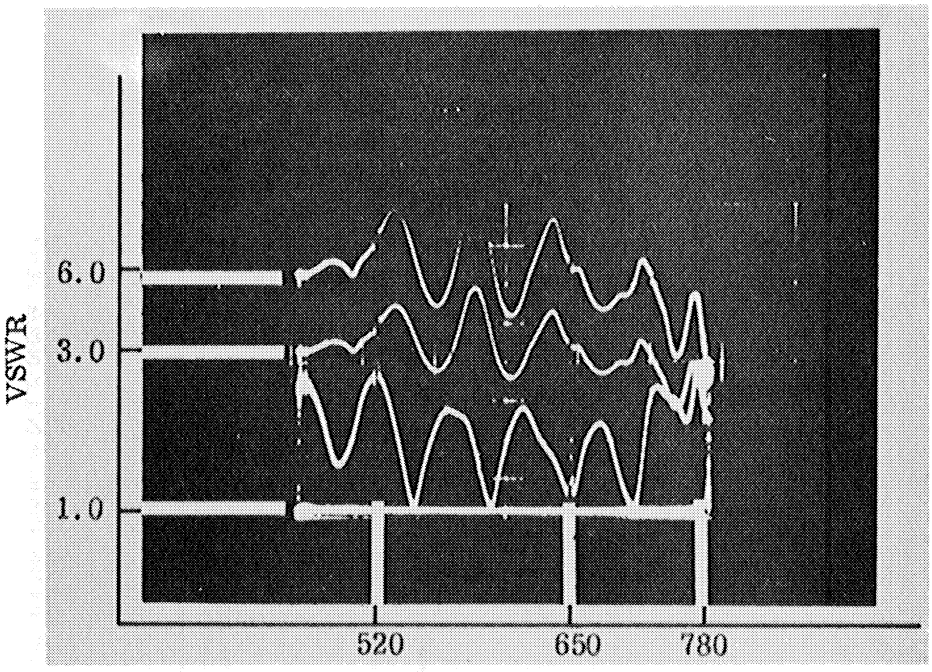

FIG. 4-31: THE VSWR FOR THE ANTENNA A-2.

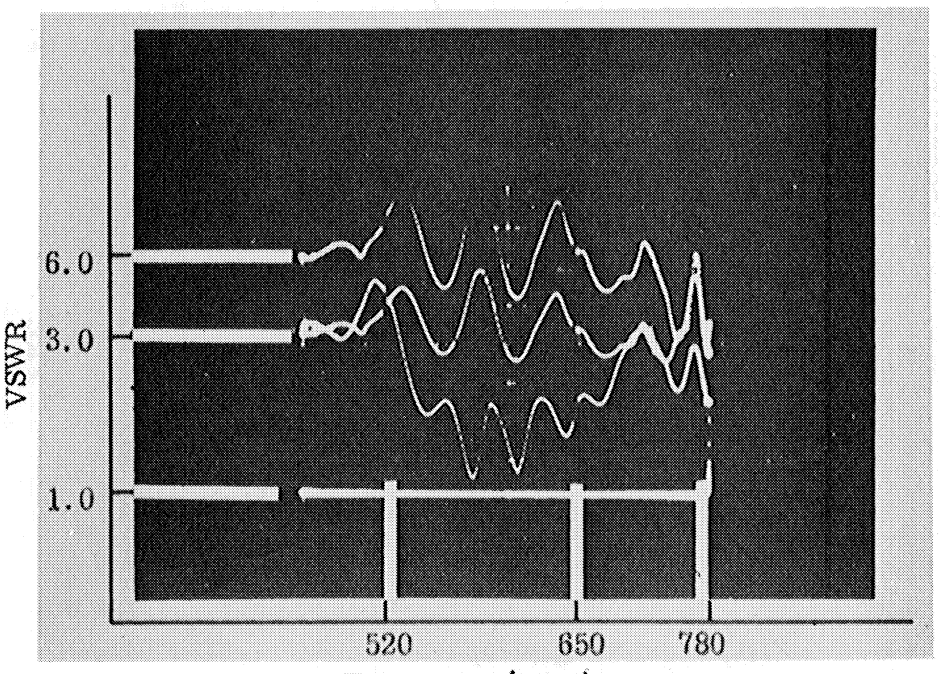

FIG. 4-32: THE VSWR FOR THE ANTENNA A-3.

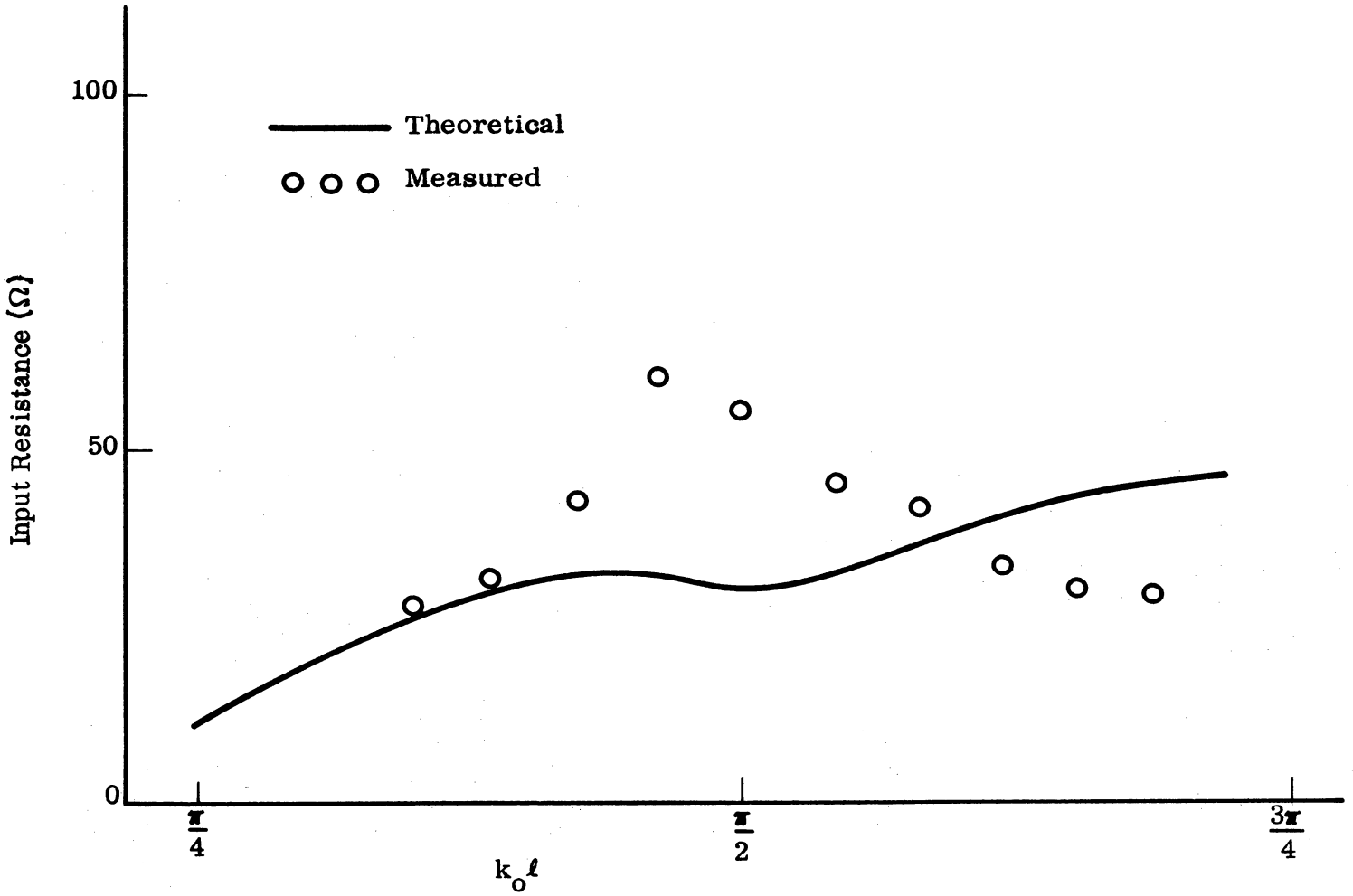

FIG. 4-33a: THE INPUT RESISTANCE FOR THE ANTENNA A-2.

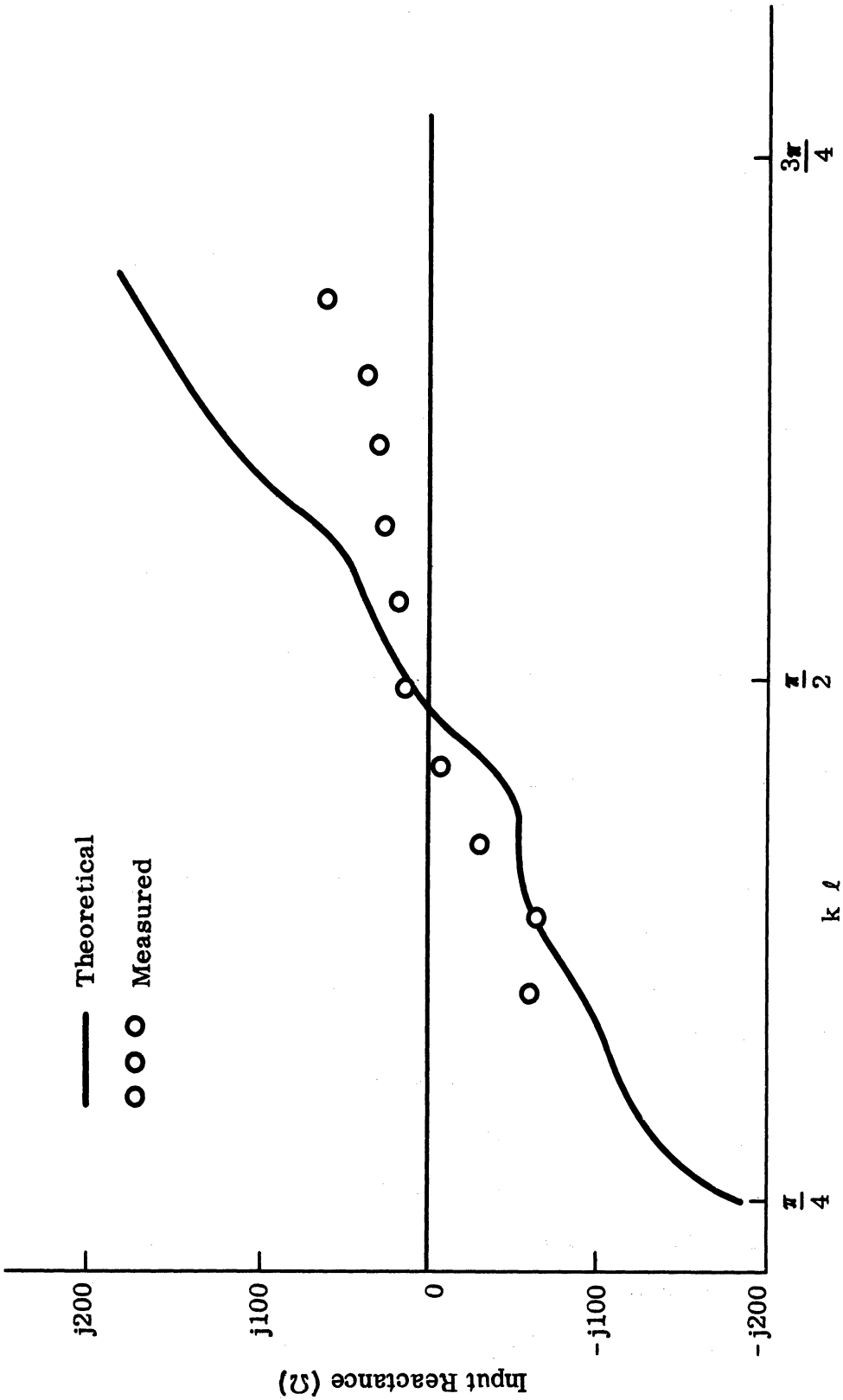

FIG. 4-33b: THE INPUT REACTANCE FOR THE ANTENNA A-2.

When the array spacing is further increased, the input impedance shifts toward the same value as for the single-element antenna, as evidenced from Fig. 4-34, where the input impedance of the antenna A-3 is plotted. The resonant frequency has shifted up to around 700 MHz and the VSWR, shown in Fig. 4-32, indicates a much narrower frequency band. The comparison between the theoretical solution and the measured input impedance is shown in Fig. 4-35.

The input impedance and the VSWR of B-1 and B-2 are shown in Figs. 4-36 through 4-39, where the study reveals, as expected, the increase in the number of array elements from 13 to 21 lowered the VSWR within the frequency band and the band became slightly wider with a shift in resonant frequency of the structure. Therefore, from the above observation, the antennas B-1 and B-2 are slightly better than the antennas A-1 and A-2, respectively. The comparison between theoretical solutions and the measured results again shows the same discrepancy observed in the other three types of antennas. They are shown in Figs. 4-40 and 4-41.

4.3.3 The Asymmetrically-fed Antenna.

The antennas C-1 and C-2 were built as wider frequency band antennas and also for a better understanding of the mechanisms of radiation. The antenna C-1 is actually a combination of two seven-element antennas fed at one end of the array, with the excited element of both antennas brought together next to each other at a spacing of 1.8 cm apart (which is identical to the array spacing of each antenna). Altogether, it looks like one antenna with two center elements being excited from the same feeding wire. The use of this feeding method is a consequence of the investigation and the prediction of the radiation pattern based on the study of the antenna C-2. The input impedances of the antennas C-1 and C-2 are shown in Figs. 4-42 and 4-43. The antenna C-2 is fed from end of the array to investigate the mechanisms of radiation. A wide band is obtained by reducing the array spacing "b" and increasing the distance of the array above the ground plane. It is observed that the input resistances are substantially greater

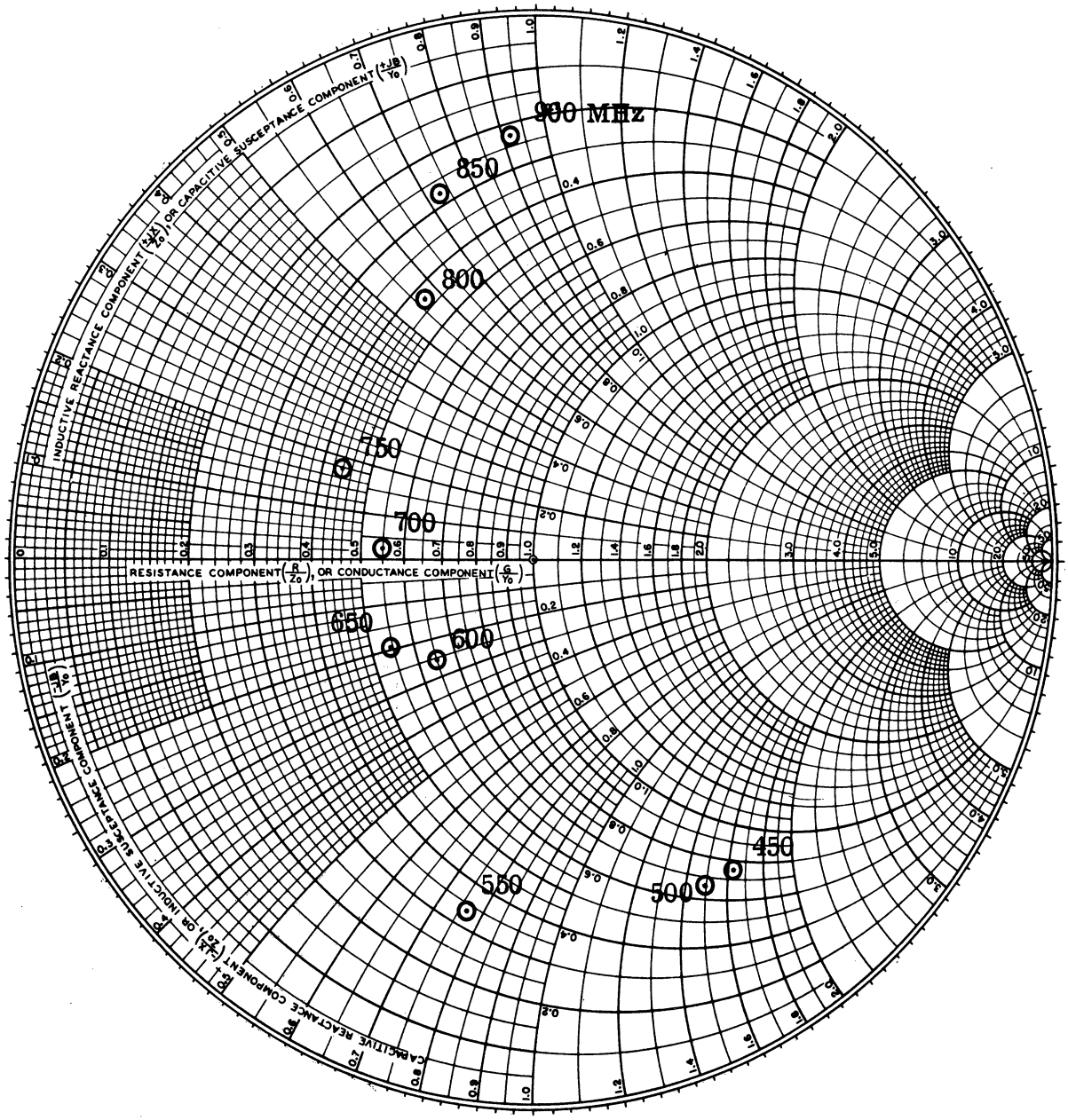

FIG. 4-34: THE INPUT IMPEDANCE FOR THE ANTENNA A-3.

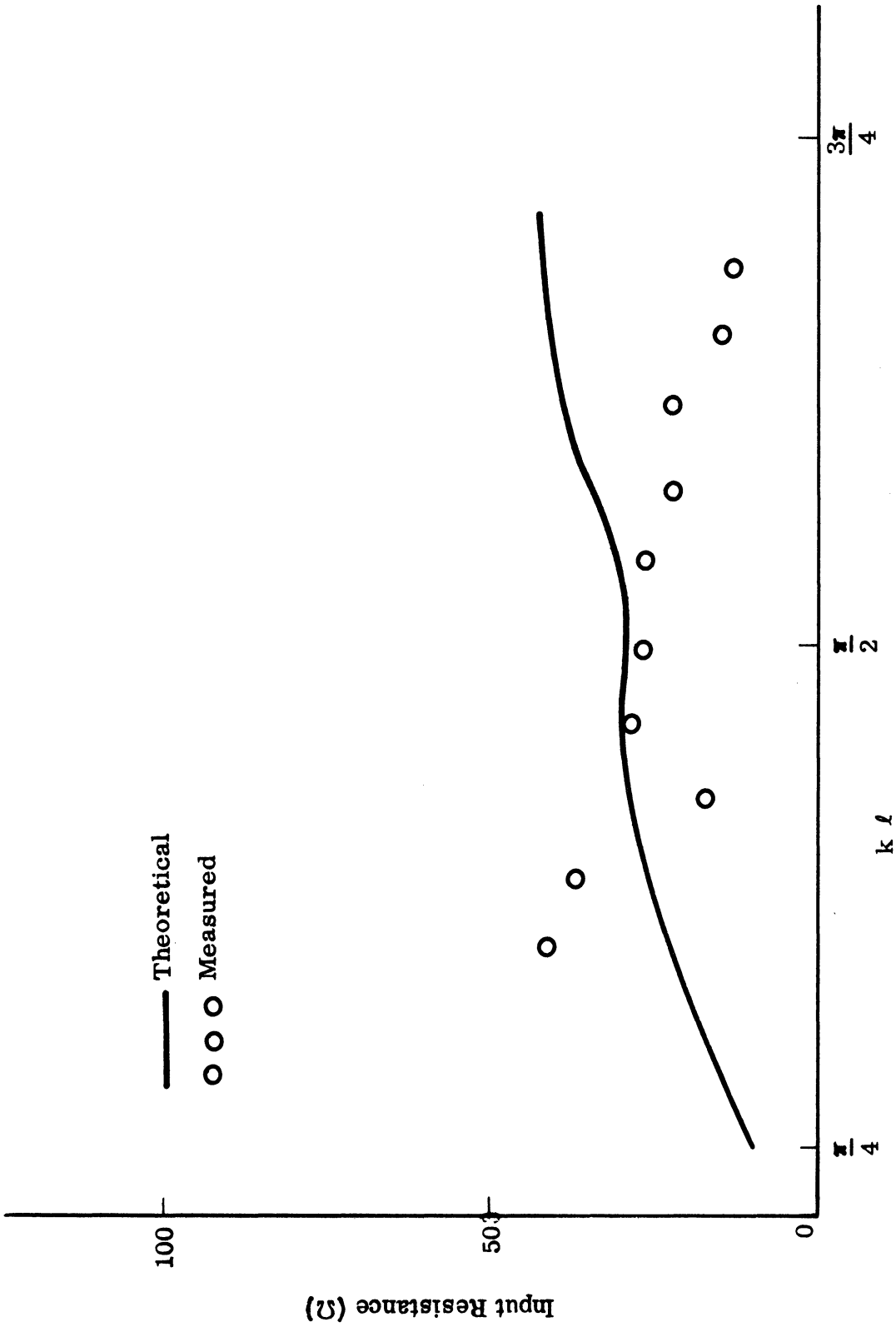

FIG. 4-35a: THE INPUT RESISTANCE FOR THE ANTENNA A-3.

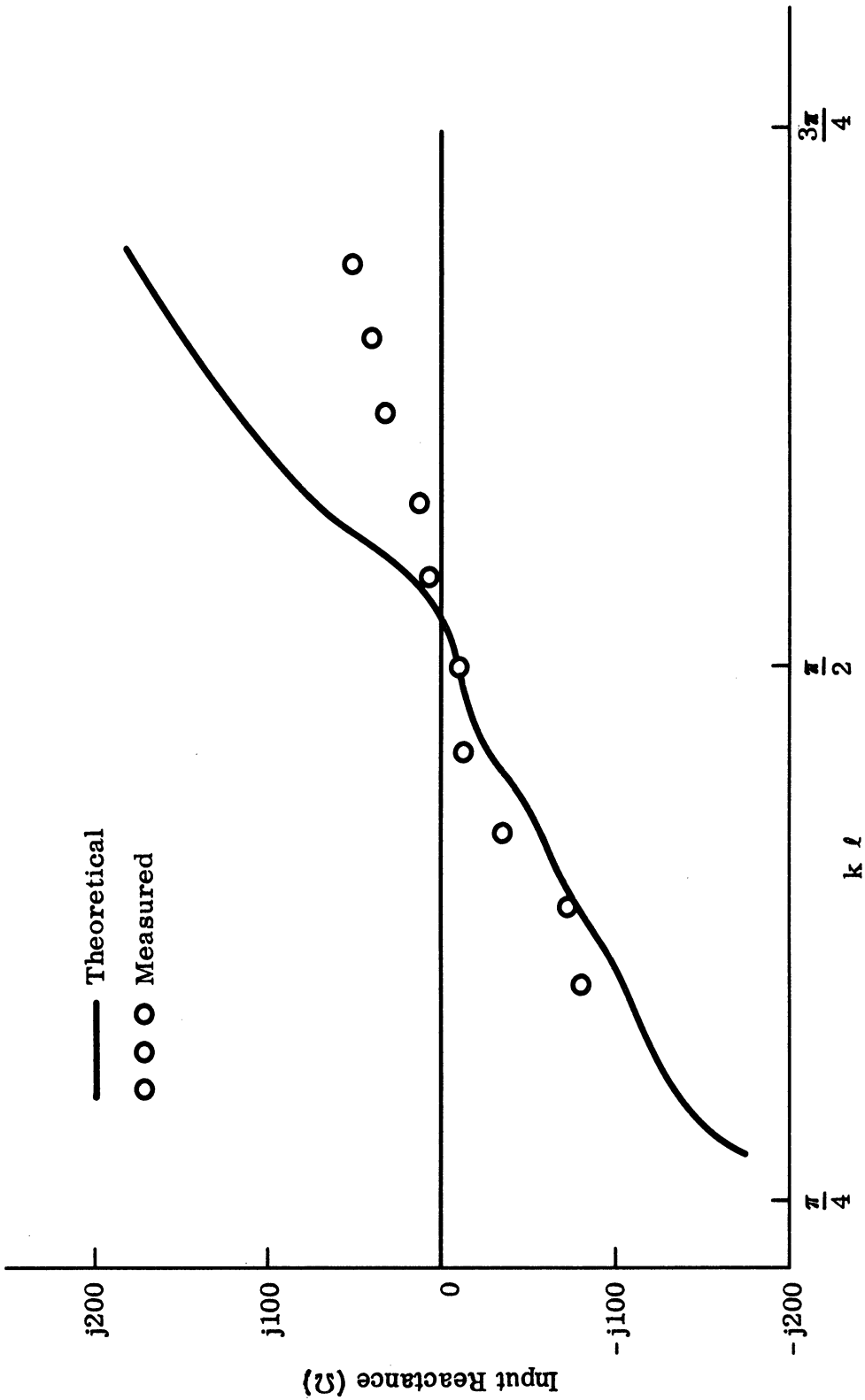

FIG. 4-35b: THE INPUT REACTANCE FOR THE ANTENNA A-3.

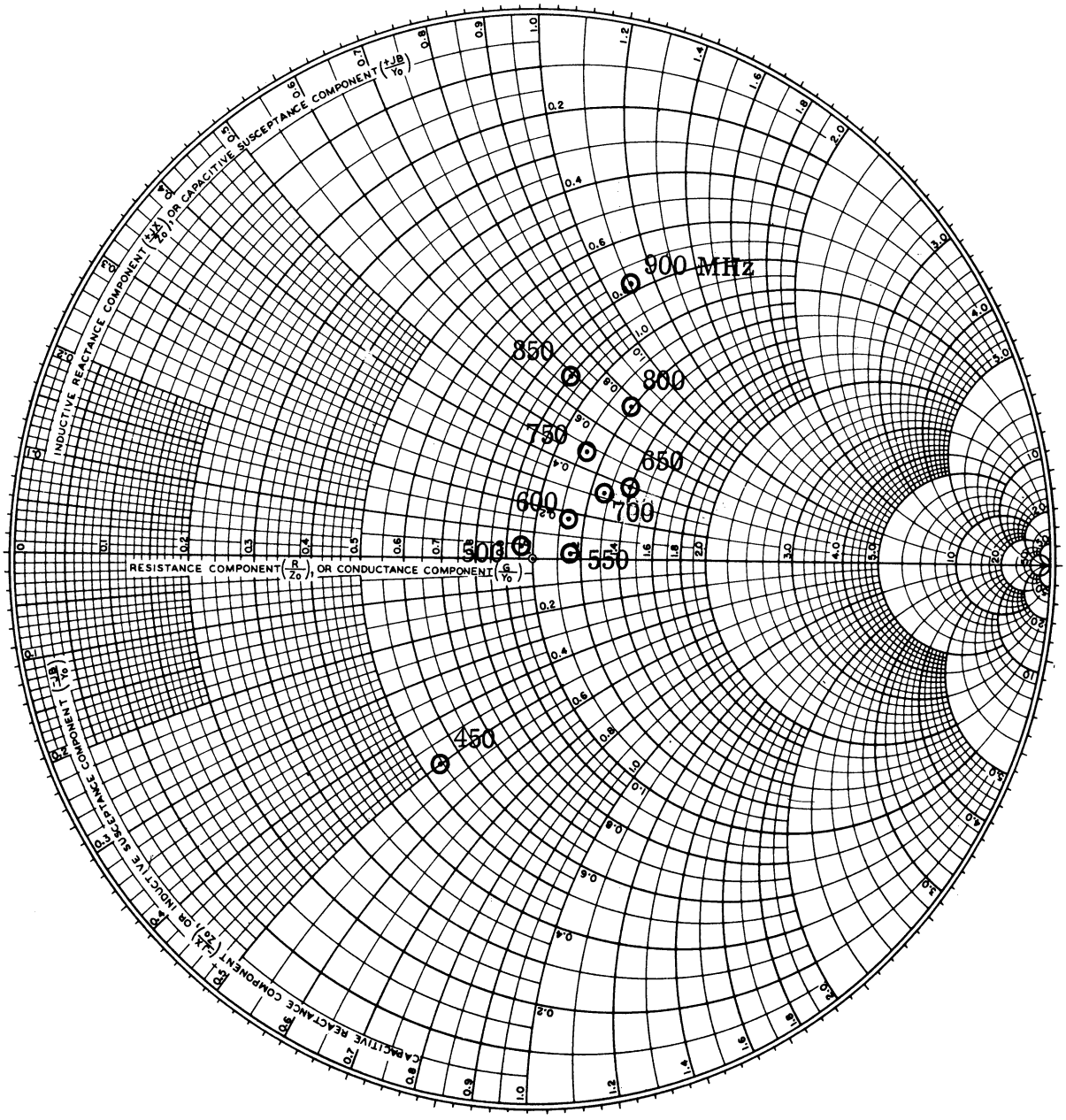

FIG. 4-36: THE INPUT IMPEDANCE FOR THE ANTENNA B-1.

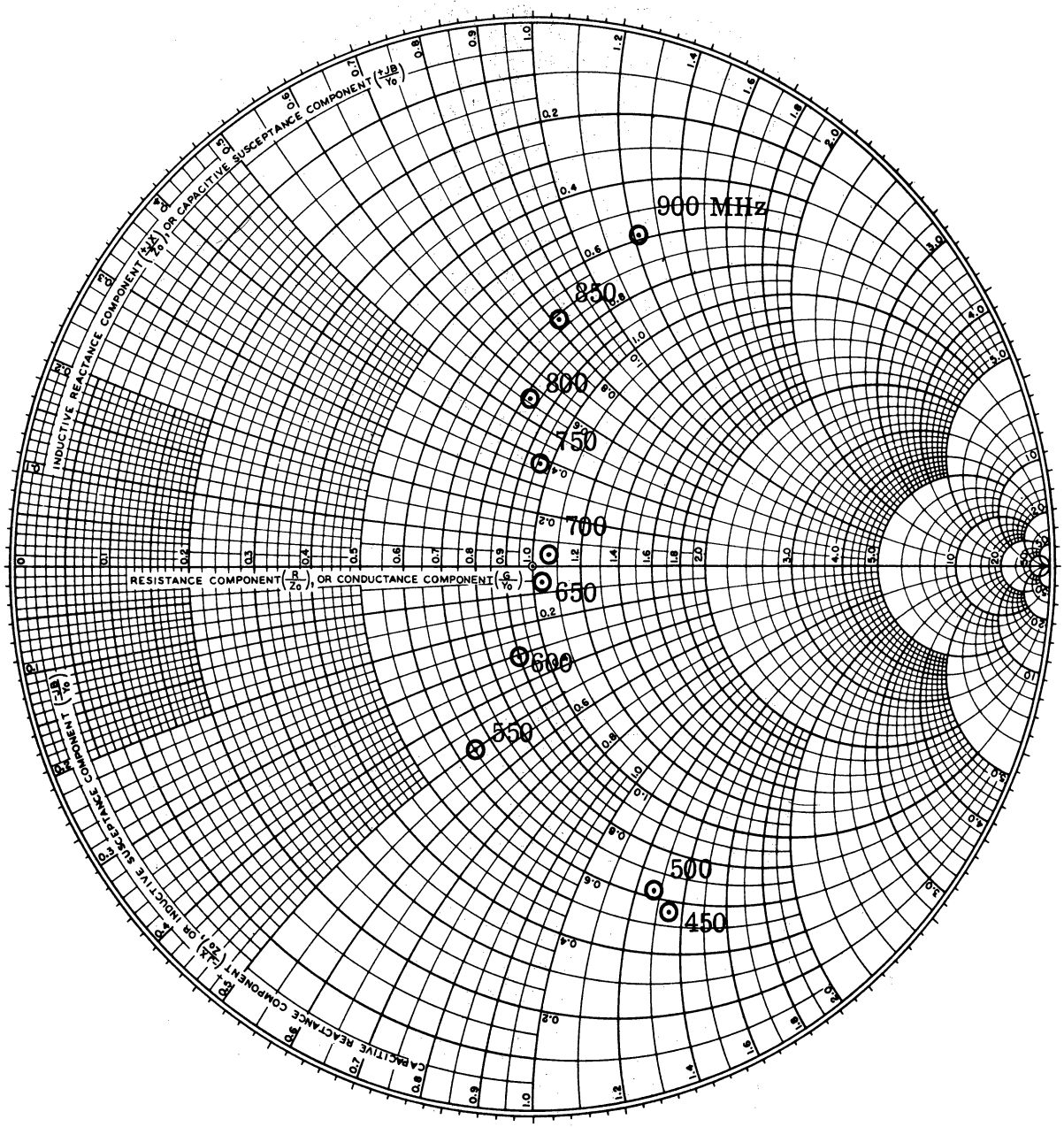

FIG. 4-37: THE INPUT IMPEDANCE FOR THE ANTENNA B-2.

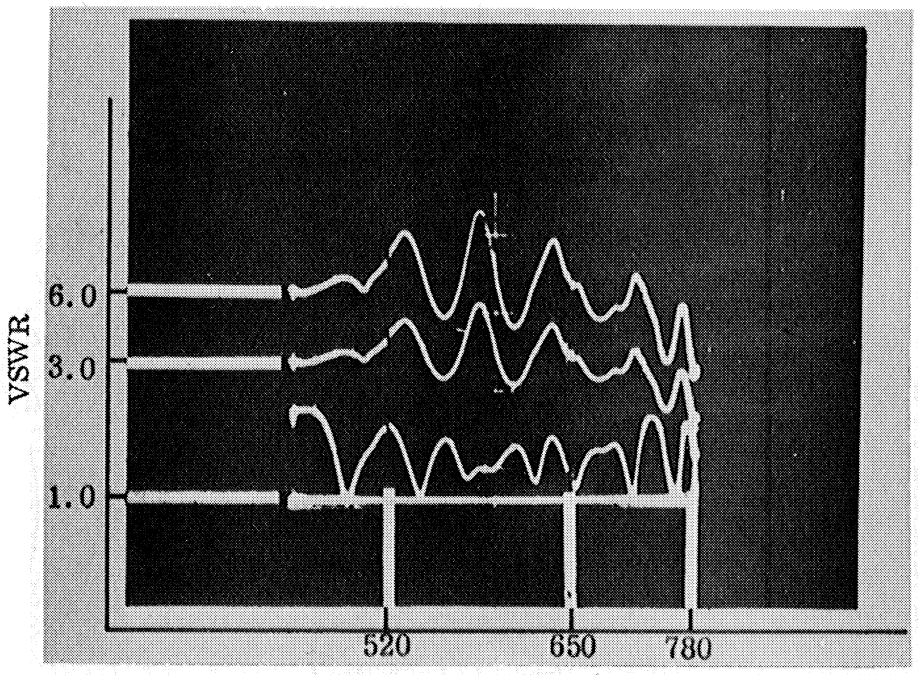

FIG. 4-38: THE VSWR FOR THE ANTENNA B-1.

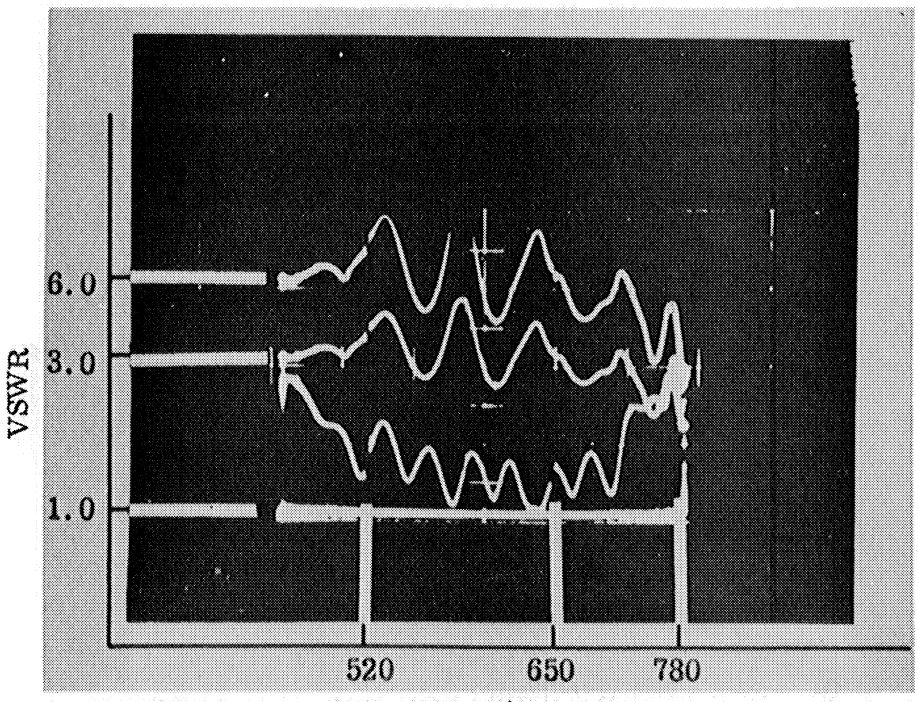

FIG. 4-39: THE VSWR FOR THE ANTENNA B-2.

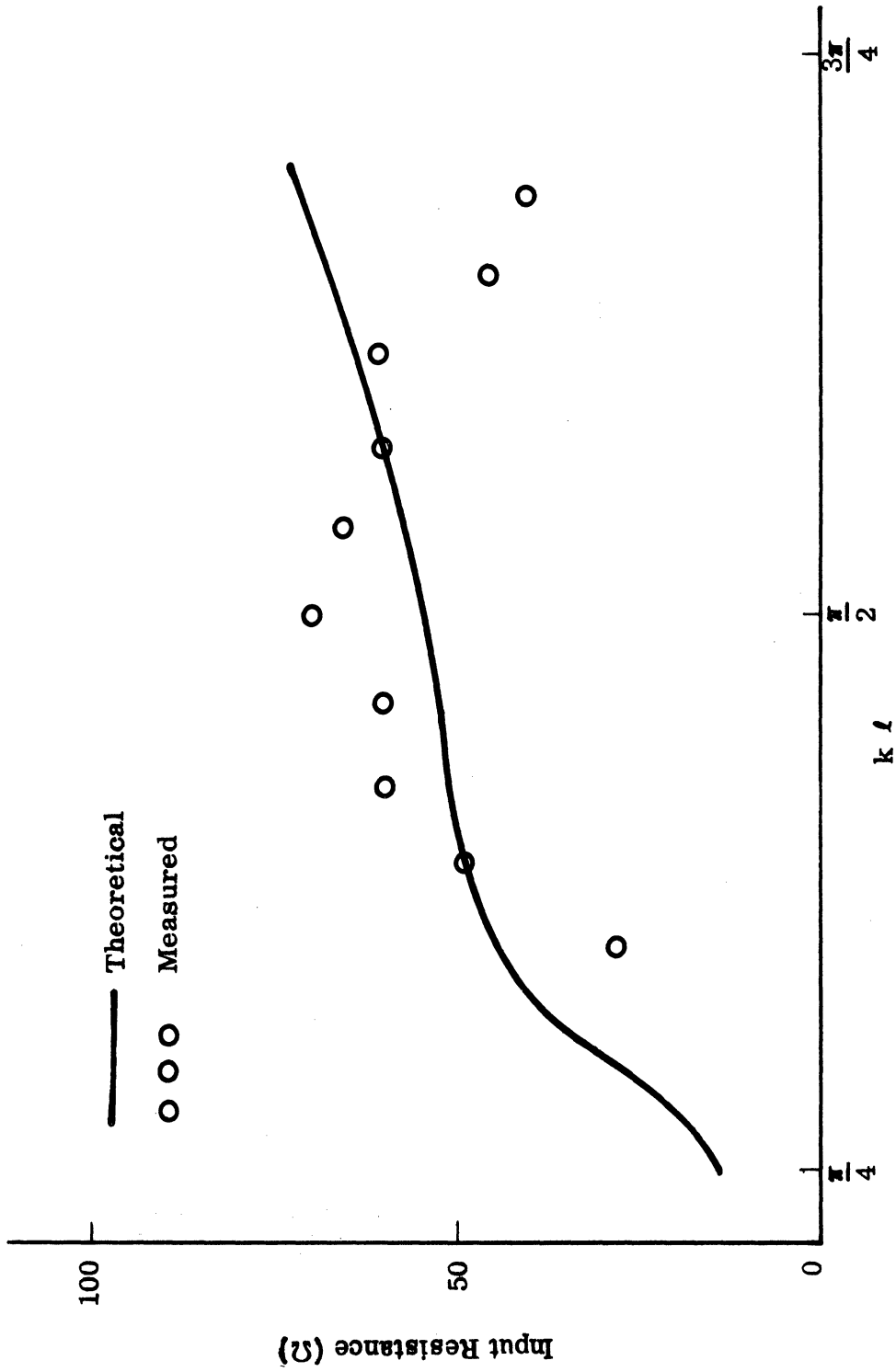

FIG. 4-40a: THE INPUT RESISTANCE FOR THE ANTENNA B-1.

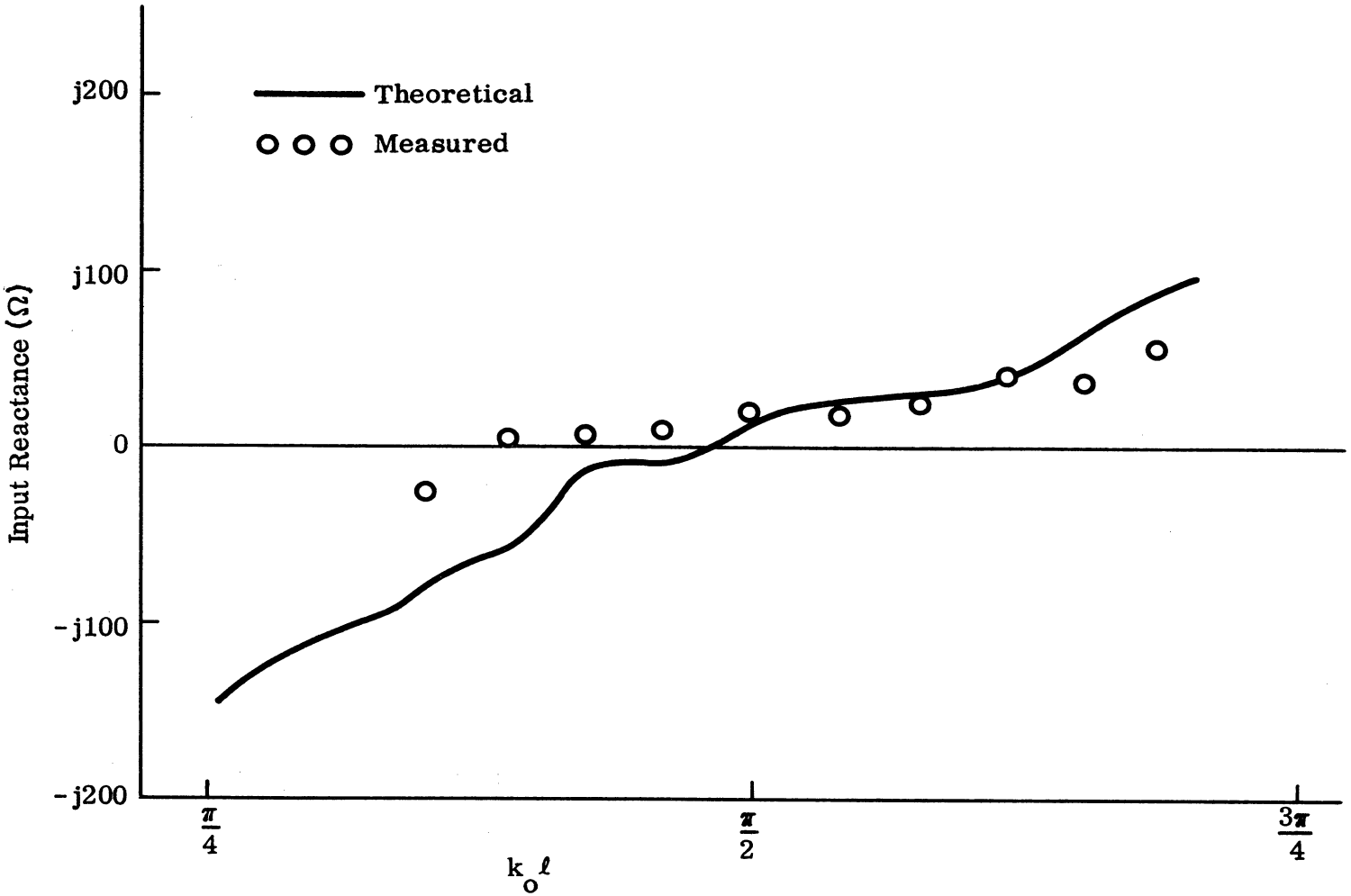

FIG. 4-40b: THE INPUT REACTANCE FOR THE ANTENNA B-1.

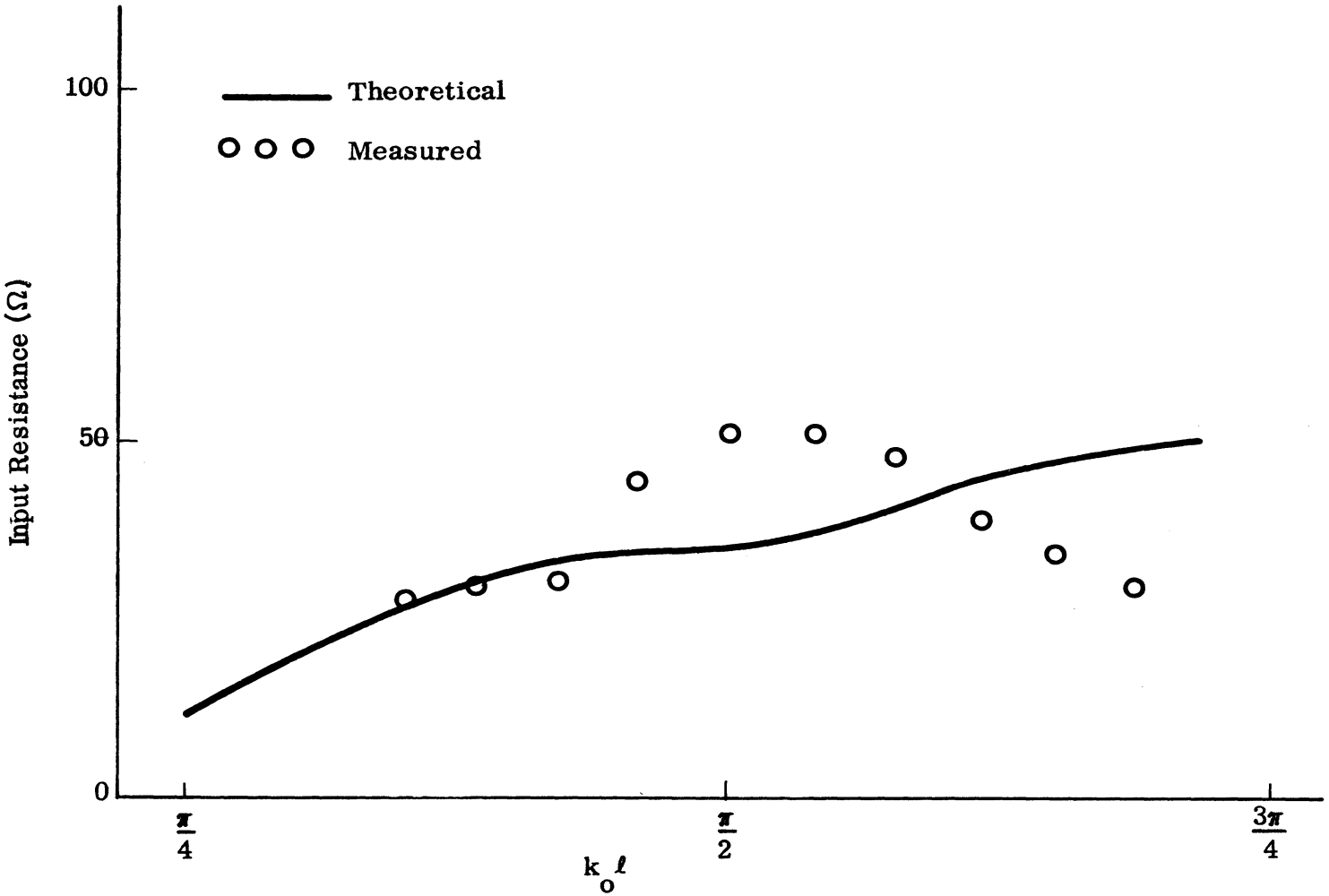

FIG. 4-41a: THE INPUT RESISTANCE FOR THE ANTENNA B-2.

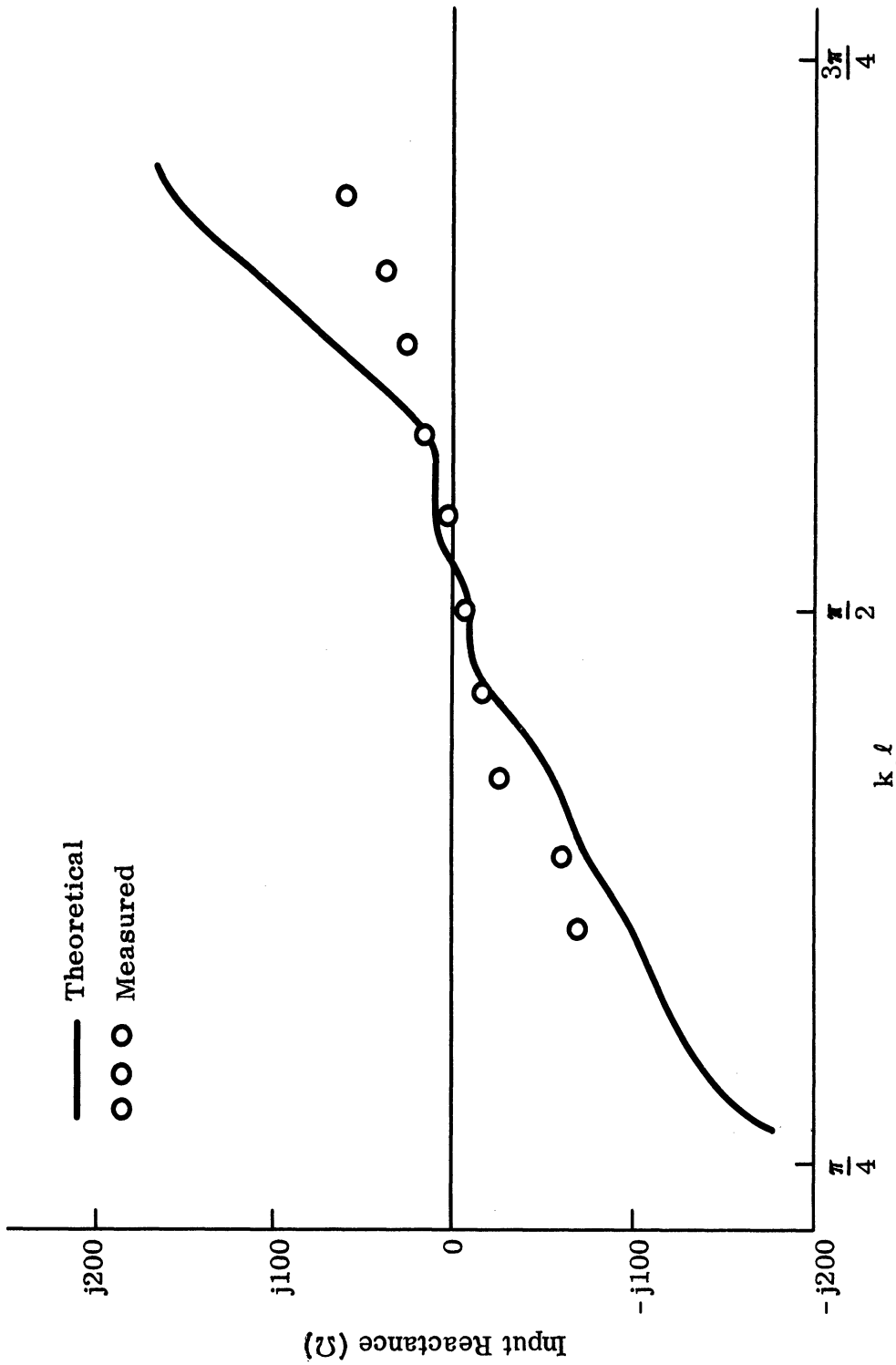

FIG. 4-41b: THE INPUT REACTANCE FOR THE ANTENNA B-2.

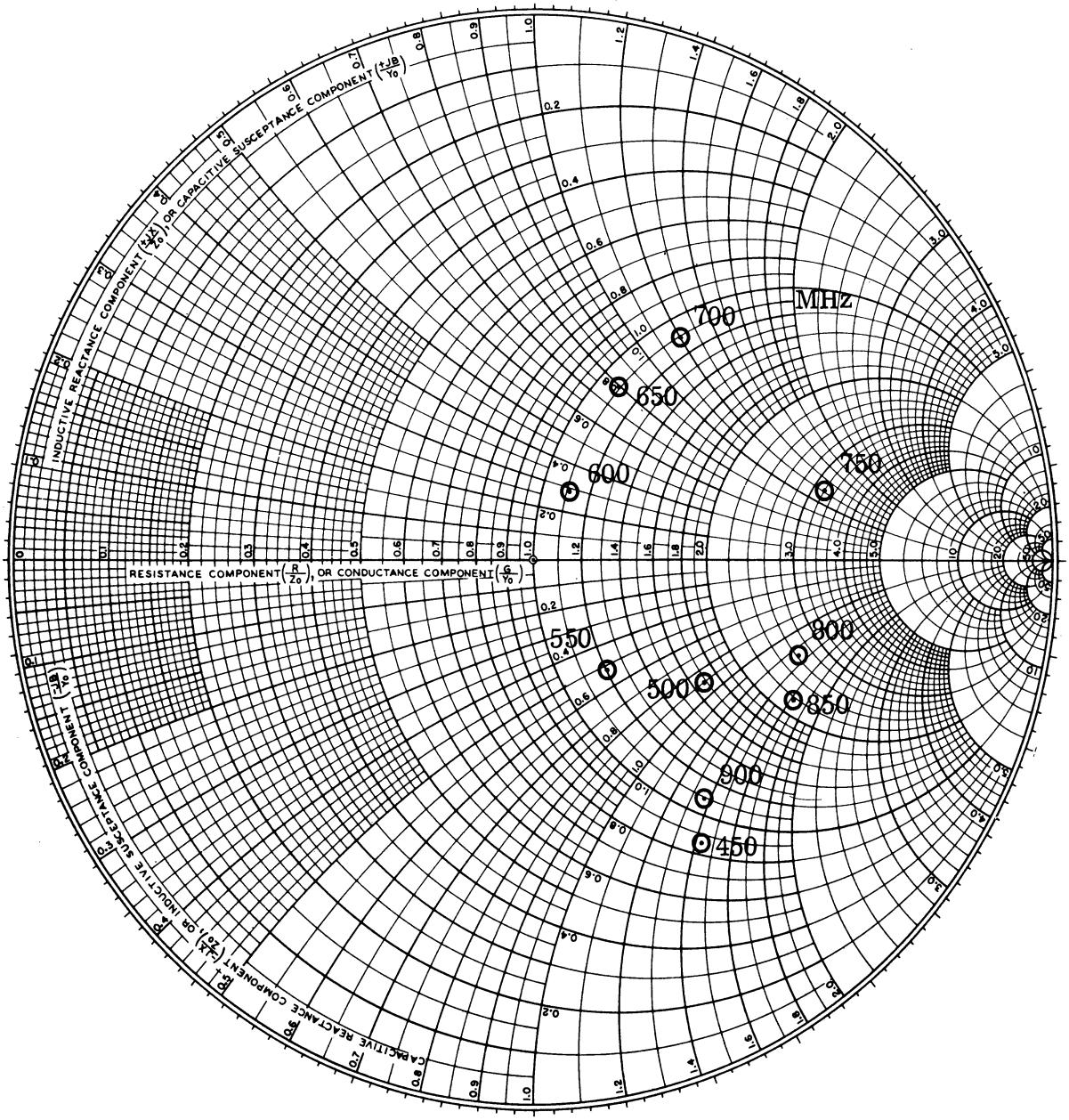

FIG. 4-42: THE INPUT IMPEDANCE FOR THE ANTENNA C-1.

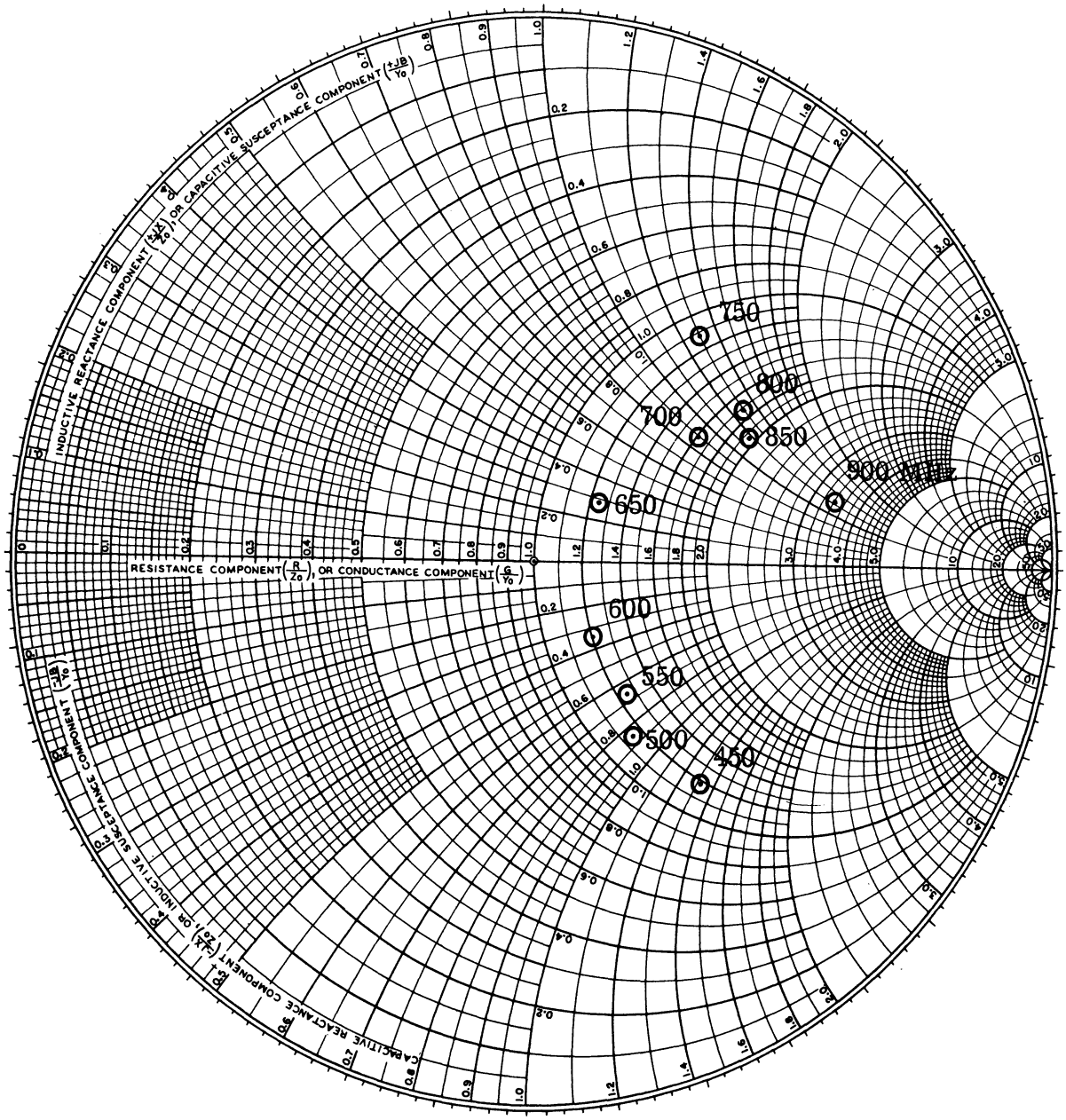

FIG. 4-43: THE INPUT IMPEDANCE FOR THE ANTENNA C-2.

than those of previous models. The reason is due the increase of the distance above the ground plane "d", which can be understood intuitively from the viewpoint of a cylindrical antenna above the ground plane. Furthermore, it is noteiced that the frequency band is also increased significantly and the resonant frequency is slightly lower than for previous models.

4.3.4 Discussion.

The measurements of input impedance and the VSWR for various experimental models are, in general, consistent with the prediction and analysis from the infinite array structure. Discrepancies were observed between the theoretical solution and the experimental results. The exact reasons are not all apparent. Some possibilities are listed below.

(a) The ambiguity involved in the theoretical formulation and the discrepancy between the assumed current distribution and the actual current distribution.

(b) The vertical sections were not included in the analysis but were included in the experimental measurement. The effect of the vertical sections is assumed small for all cases. If they can be treated as two parallel arrays of Hertzian dipoles, the calculated radiation resistance is less than 10Ω within the frequency range of interest. However, they will have to be considered as an additional contribution to the structure in terms of an input impedance.

4.4 The Radiation Pattern.

The radiation patterns of all experimental models were taken at the North Campus Antenna Range on the roof of the Fluids Building. The models were designed to utilize the best frequency band for operation of these facilities.

4.4.1 The Broadside Radiation.

The antennas A-1, A-2, A-3, B-1 and B-2 were primarily designed for a broadside radiation utilizing the "leaky" wave mechanism[32] for a fairly wide band operation. As mentioned before, the broadside radiation was made possible by feeding the antenna through the center element and exciting the structure within the frequency band which lies inside the fast wave region. Thus,

the wave radiates or "leaks" as it travels toward both ends of the array, resulting in a broadside pattern. When the antenna is excited into the slow wave region, the radiation pattern will depend on the electrical length of the array. If the array is less than a slow wave wavelength, it will be difficult to sustain an efficient slow wave propagation and thus, the radiation pattern may still have a broadside tendency instead of an oblique radiation, as will be discussed in the next section. The array length of A-1 is less than a slow wave length for the range of frequency involved and, therefore, a predominantly broadside pattern is expected which is as predicted from the theoretical solutions in a previous chapter. The antenna A-2 is about one slow wave wavelength, and thus, if the frequency is increased above 650 MHz, a beam split will be expected. The antenna A-3 is designed for a very narrow pass band and, thus, a radiation pattern will resemble that of a single element or a predominantly broadside pattern will be observed. When the number of array elements is increased in going from A-1 to B-1, the radiation pattern above 650 MHz must become oblique because the array length is sufficient to support a slow wave propagation along both directions of the array. A similar argument is true for the antenna B-2.

The far field H-plane E_y-patterns were plotted in Figs. 4-44 through 4-48. The above arguments on slow wave propagation are well applied to the experimental results. The experimental patterns are not quite symmetrical because of some errors in construction of the models and possibly because of the error in the recording and plotting devices. The theoretical solutions for the far field patterns were plotted in Figs. 3-30 through 3-34, respectively. Although they do not have a perfect fit with the experimental patterns, the general trend of the beam shift, the half power beam width and the frequency range are fairly consistent. The bandwidth of the antenna based on the far field pattern is quite different from that of the VSWR study, except for the antenna A-1, where both criteria are quite consistent.

Based on the above discussion, a design of a wideband, broadside radiation antenna can be achieved by the following methods.

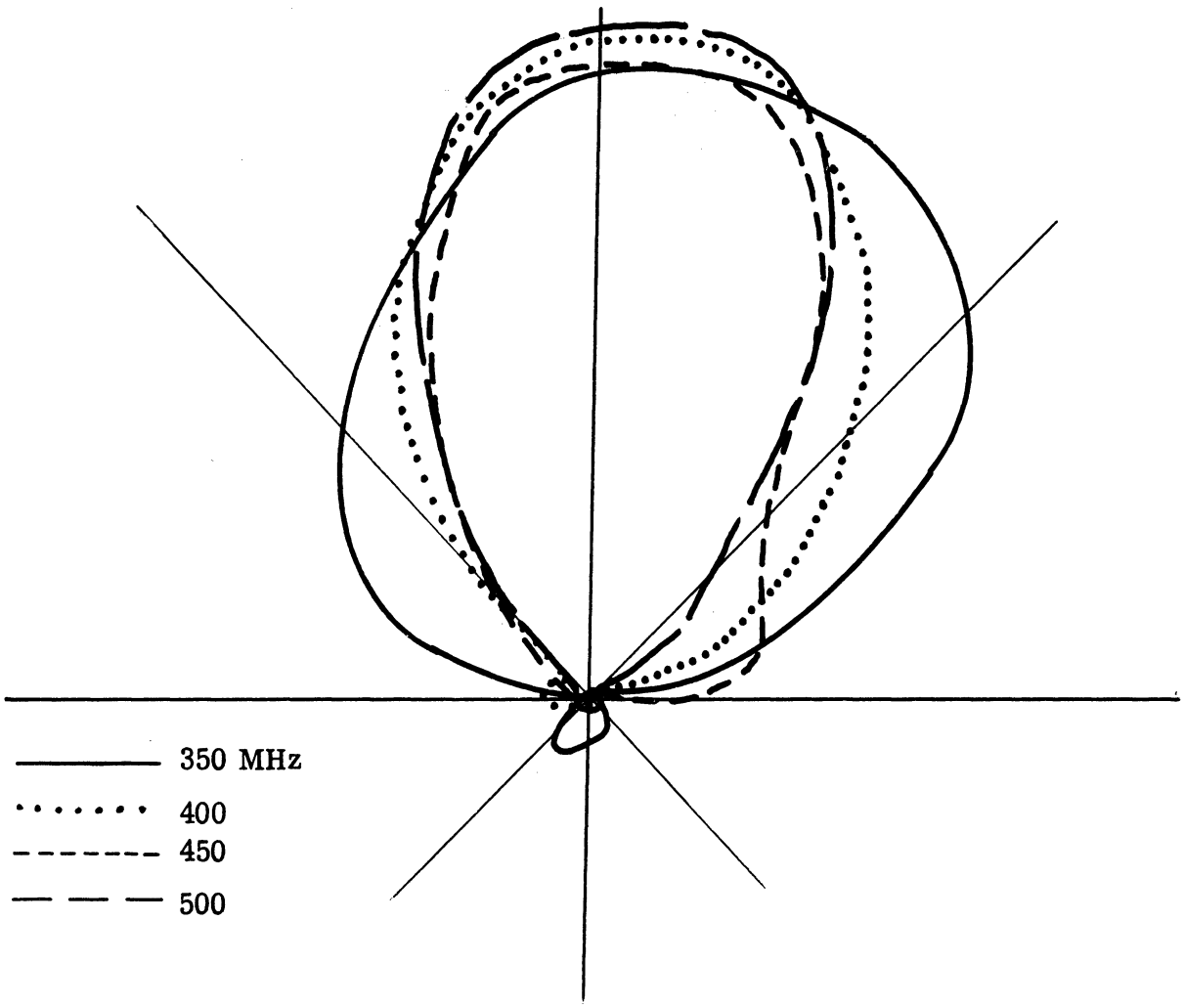

FIG. 4-44a: THE FAR FIELD H-PLANE E_y-PATTERN FOR THE ANTENNA A-1.

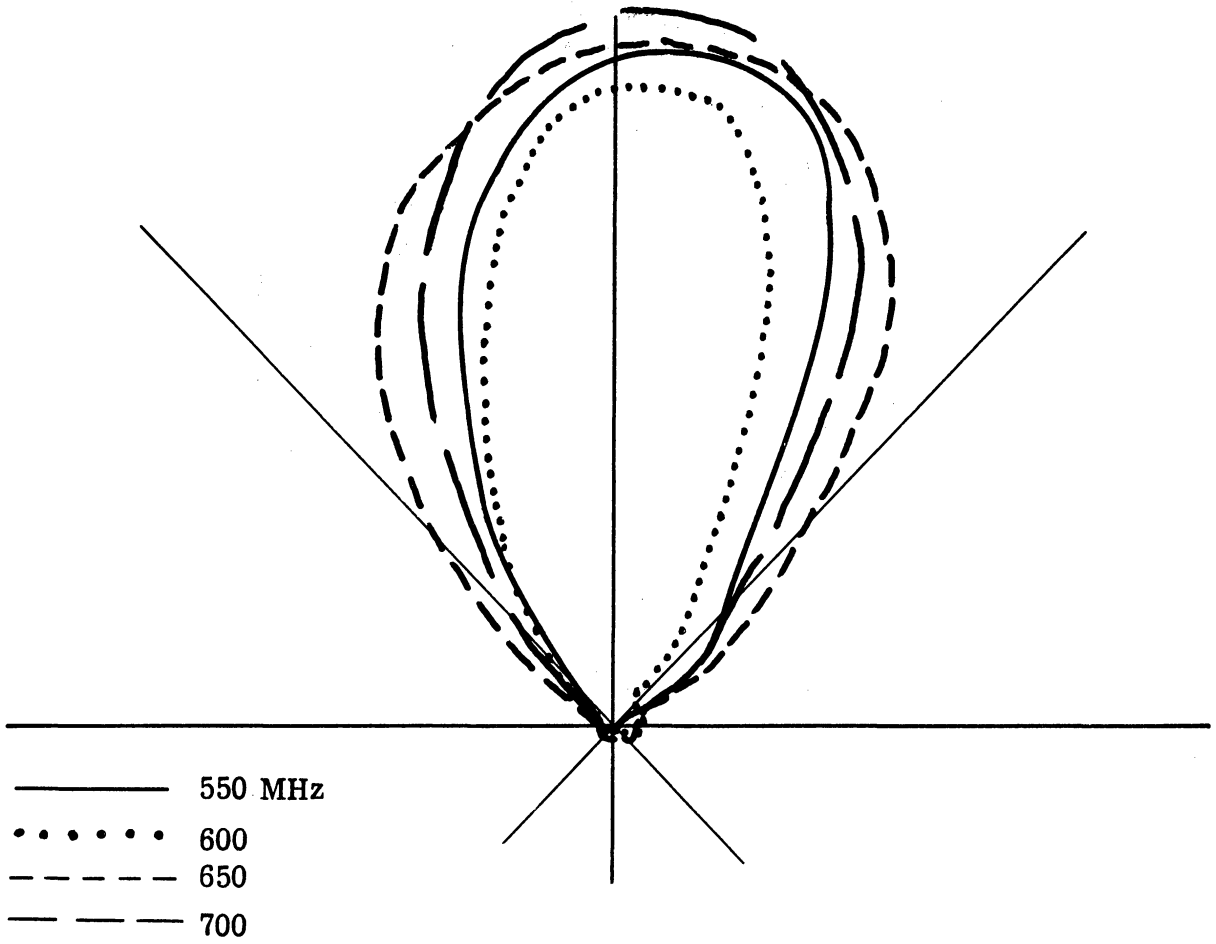

FIG. 4-44b: THE FAR FIELD H-PLANE E_y-PATTERN FOR THE ANTENNA A-1.

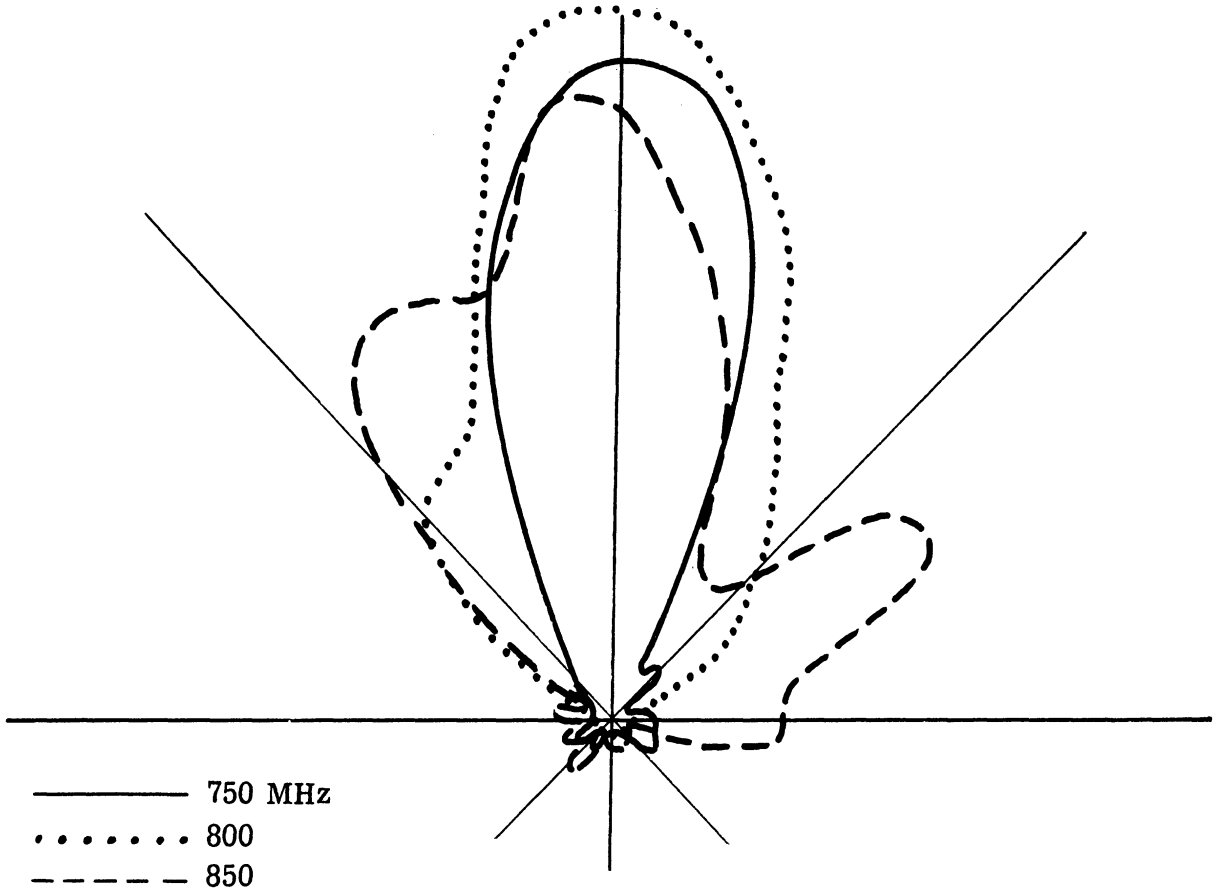

FIG. 4-44c: THE FAR FIELD H-PLANE E_y-PATTERN FOR THE ANTENNA A-1.

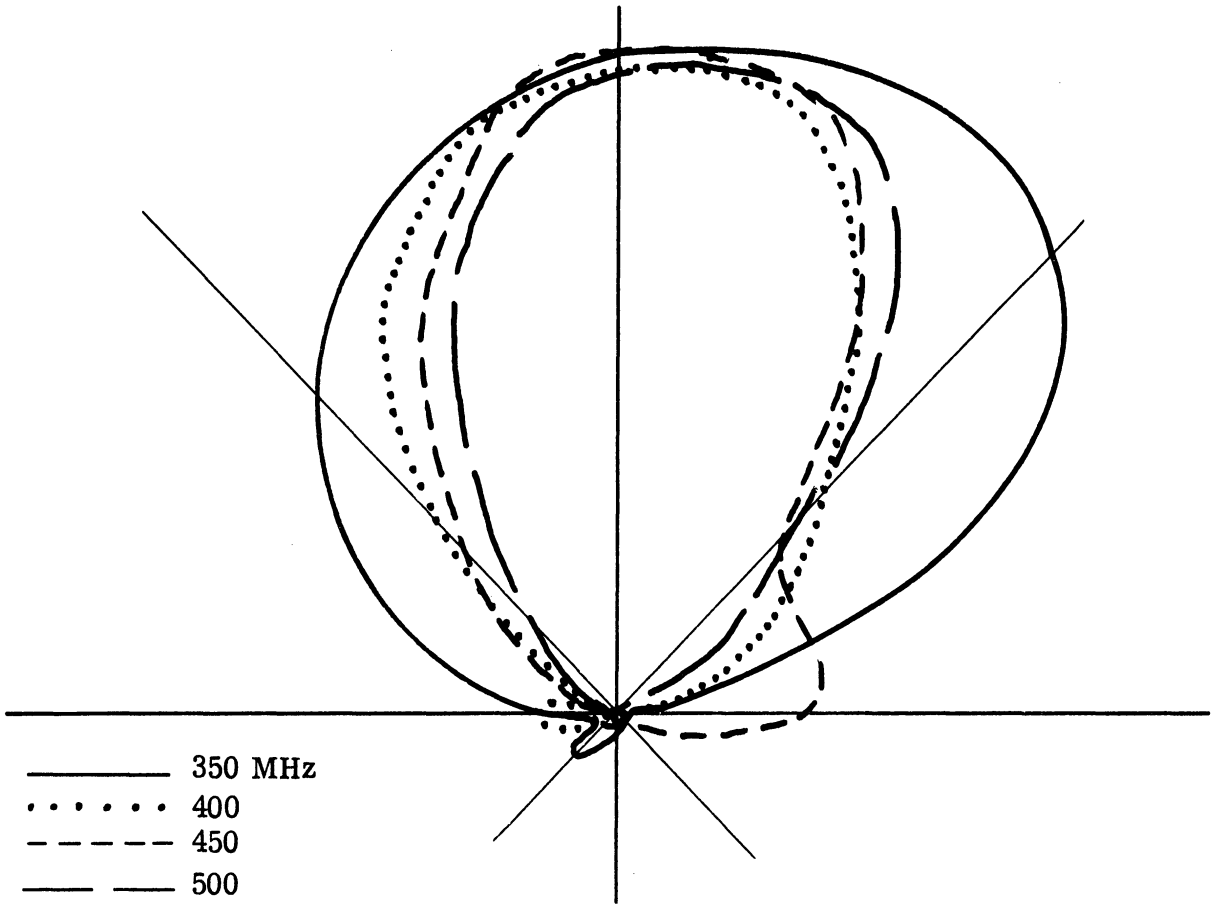

FIG. 4-45a: THE FAR FIELD H-PLANE E_y-PATTERN FOR THE ANTENNA A-2.

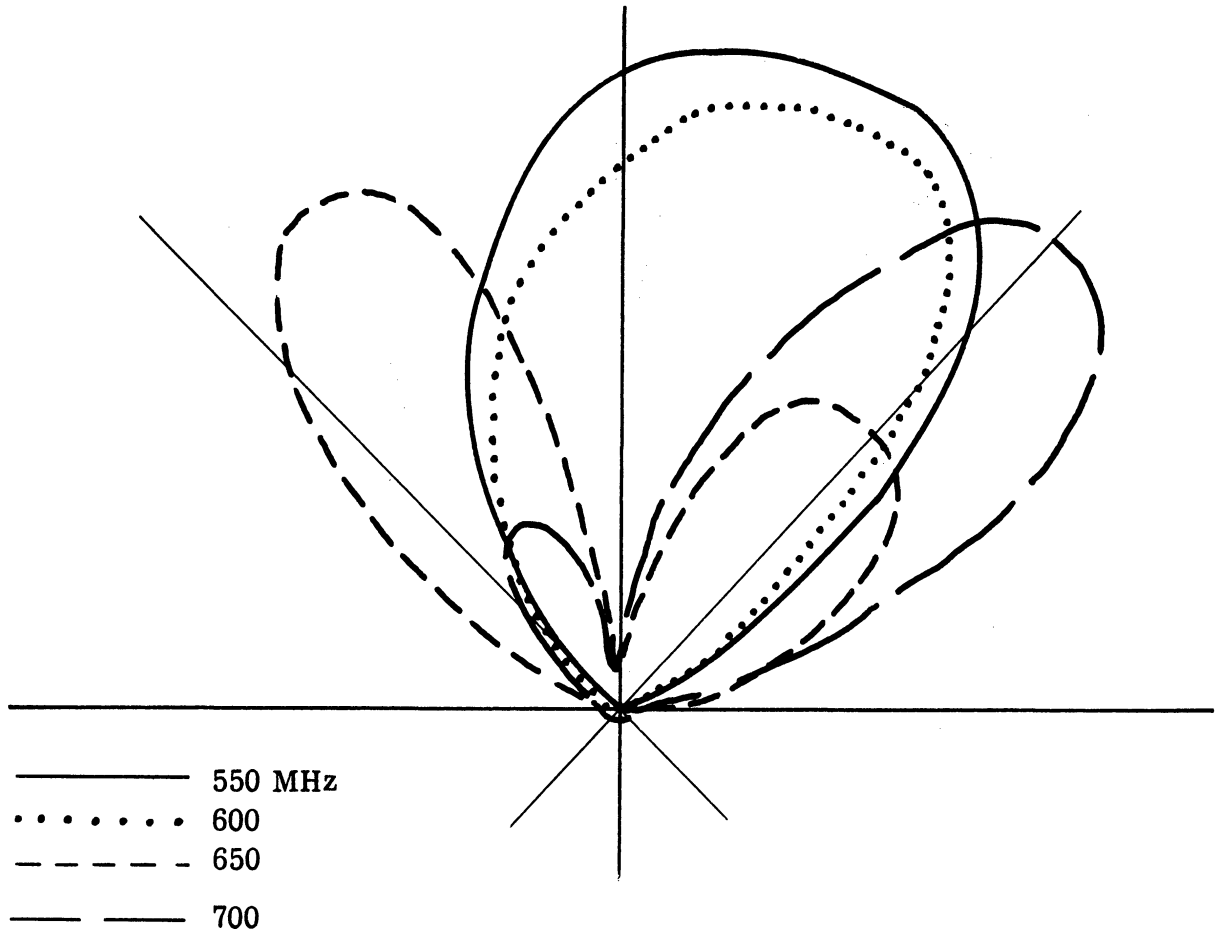

FIG. 4-45b: THE FAR FIELD H-PLANE E_y-PATTERN FOR THE ANTENNA A-2.

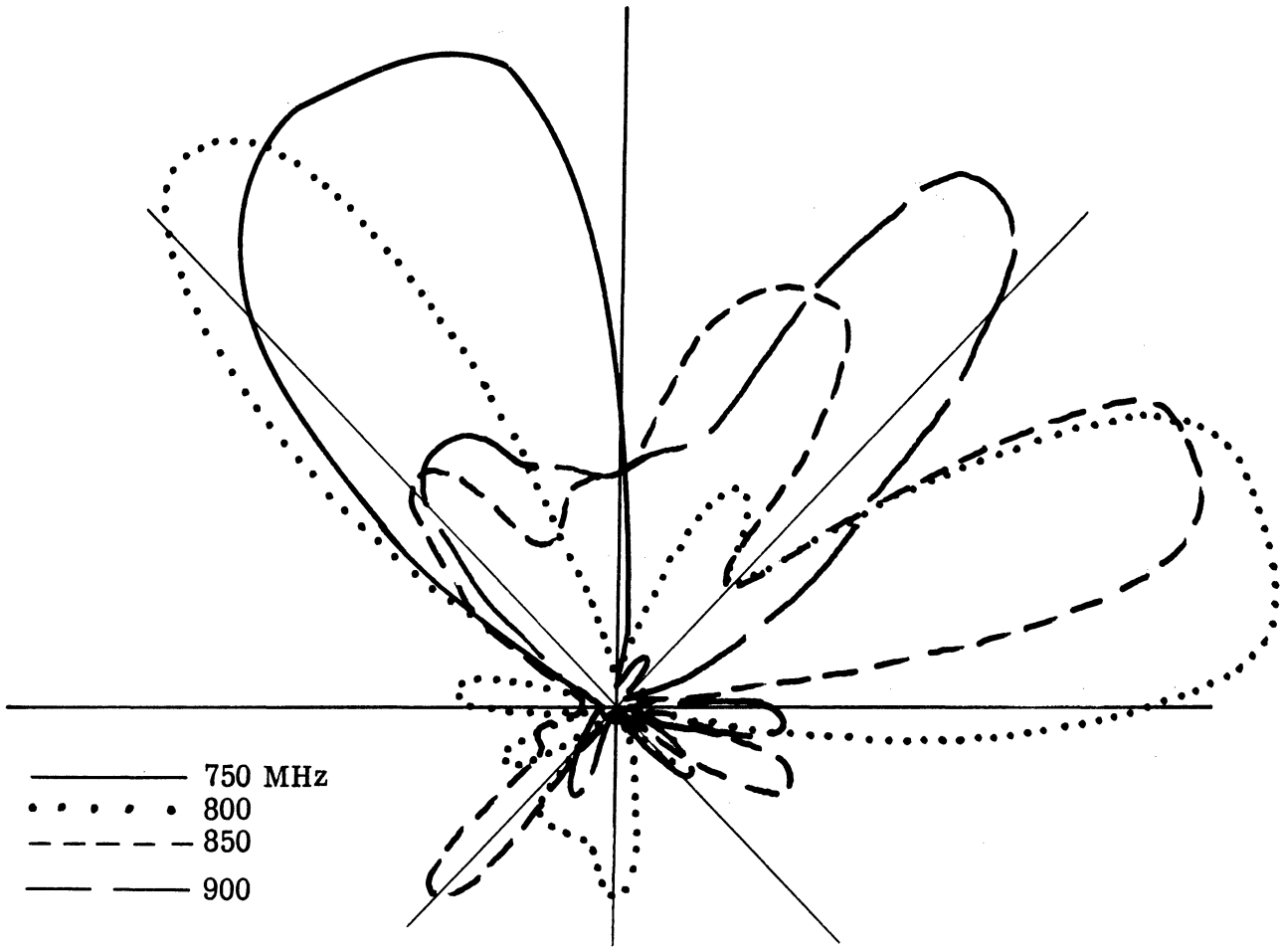

FIG. 4-45c: THE FAR FIELD H-PLANE E_y-PATTERN FOR THE ANTENNA A-2.

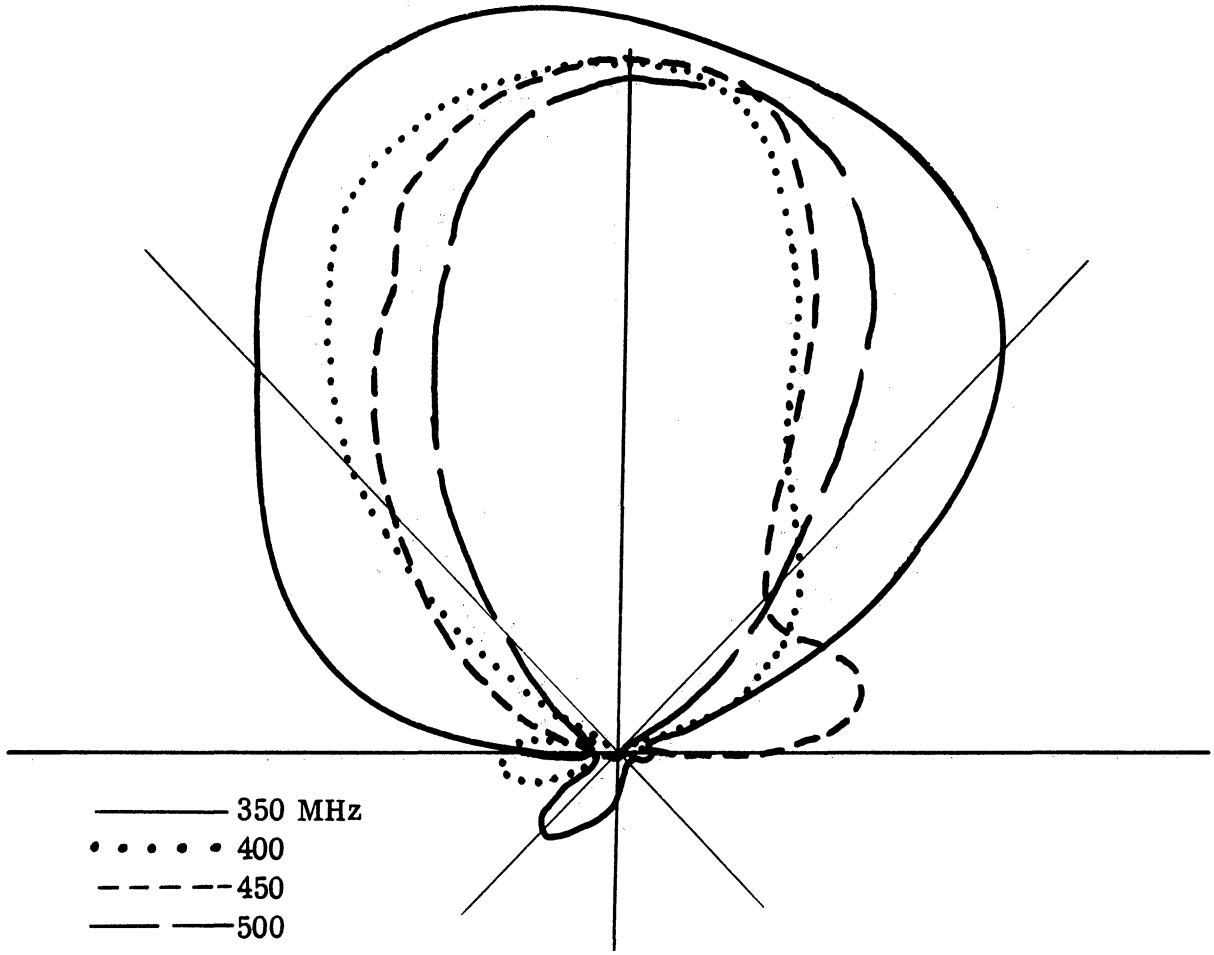

FIG. 4-46a: THE FAR FIELD H-PLANE E_y-PATTERN FOR THE ANTENNA A-3.

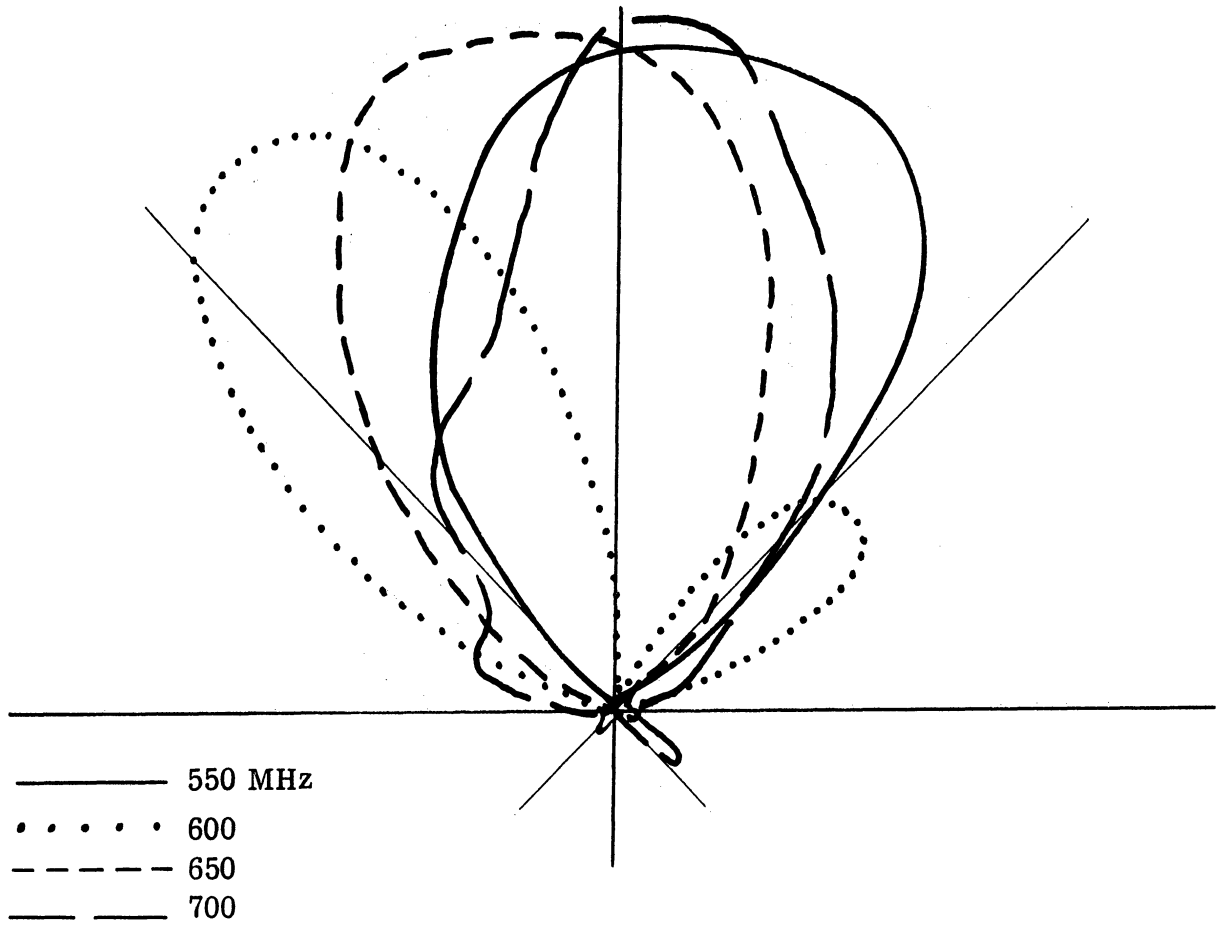

FIG. 4-46b: THE FAR FIELD H-PLANE E_y-PATTERN FOR THE ANTENNA A-3.

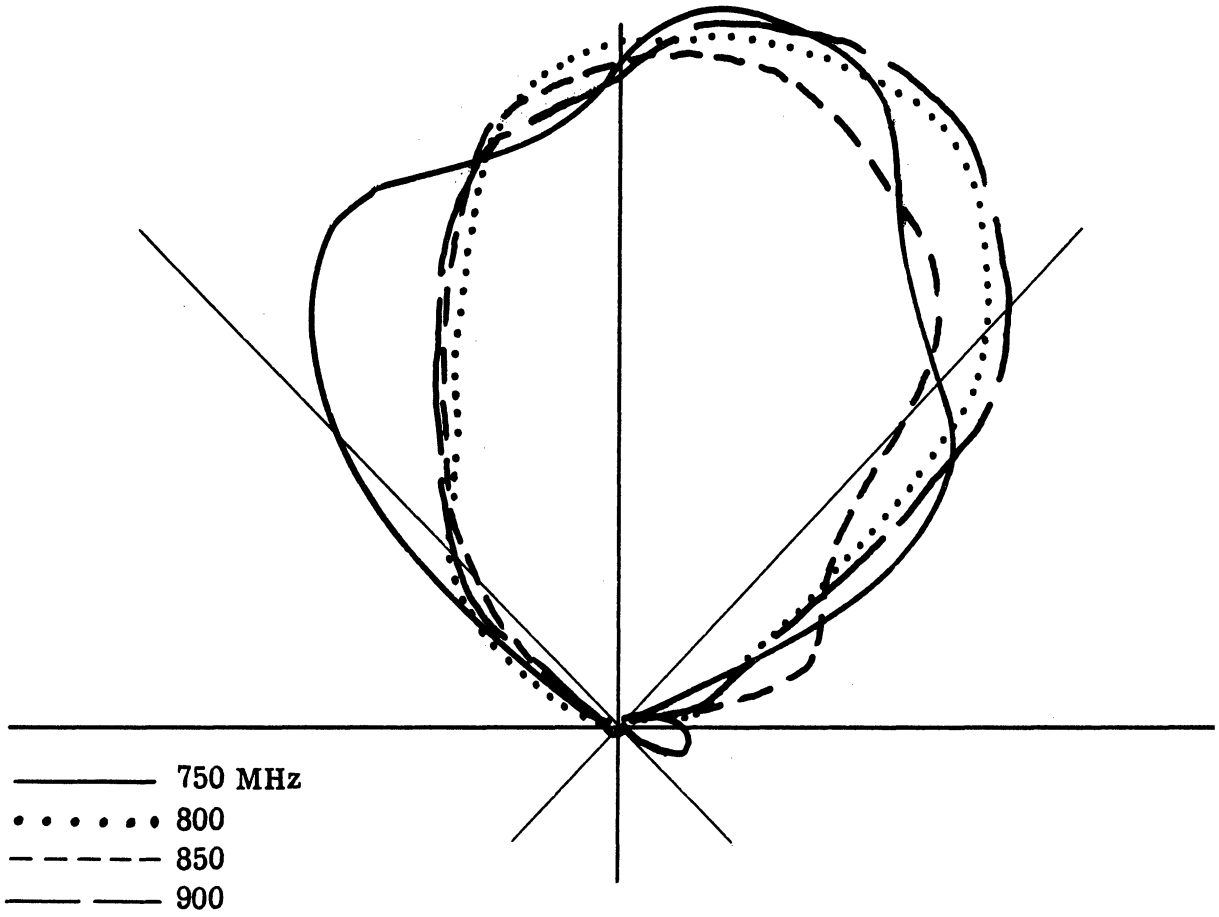

FIG. 4-46c: THE FAR FIELD H-PLANE E_y-PATTERN FOR THE ANTENNA A-3.

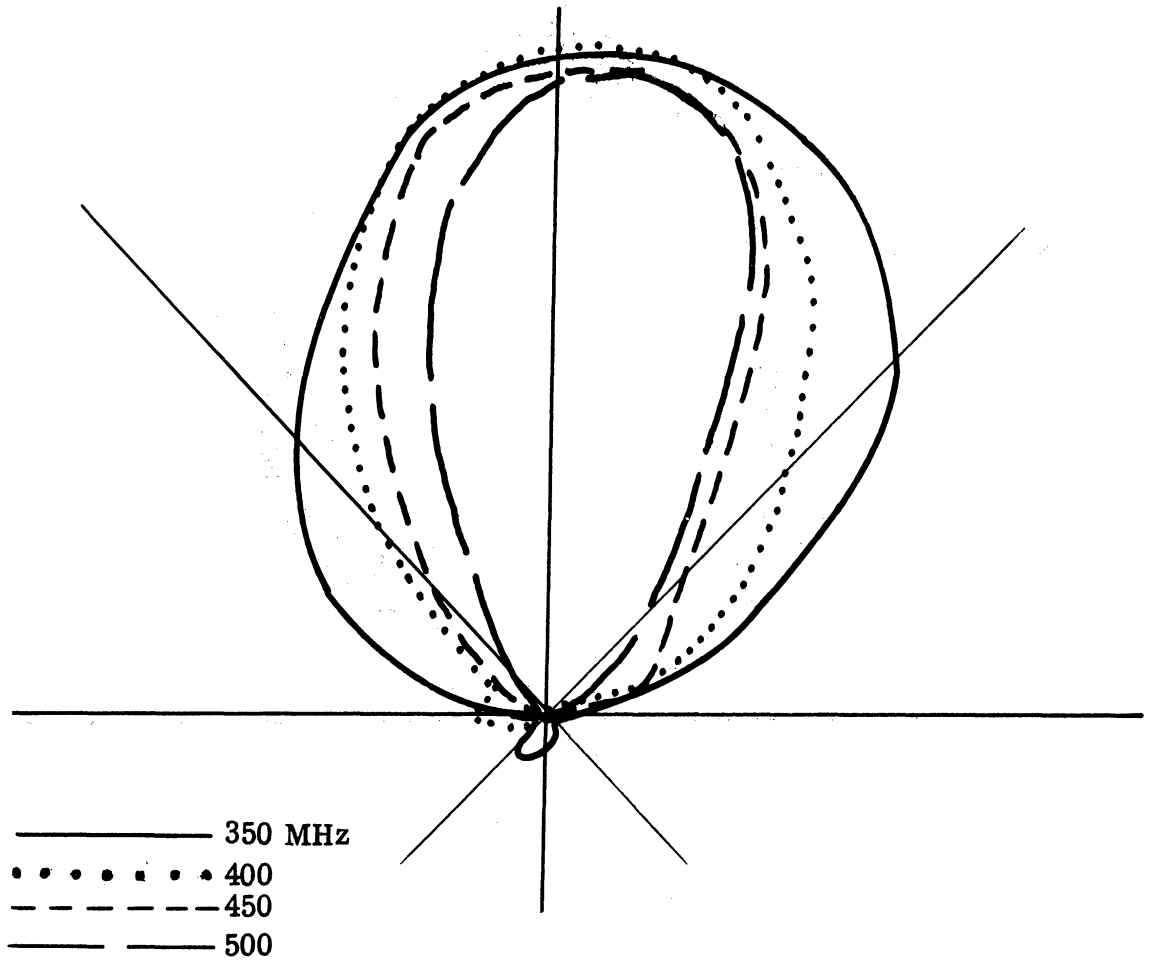

FIG. 4-47a: THE FAR FIELD H-PLANE E_y-PATTERN FOR THE ANTENNA B-1.

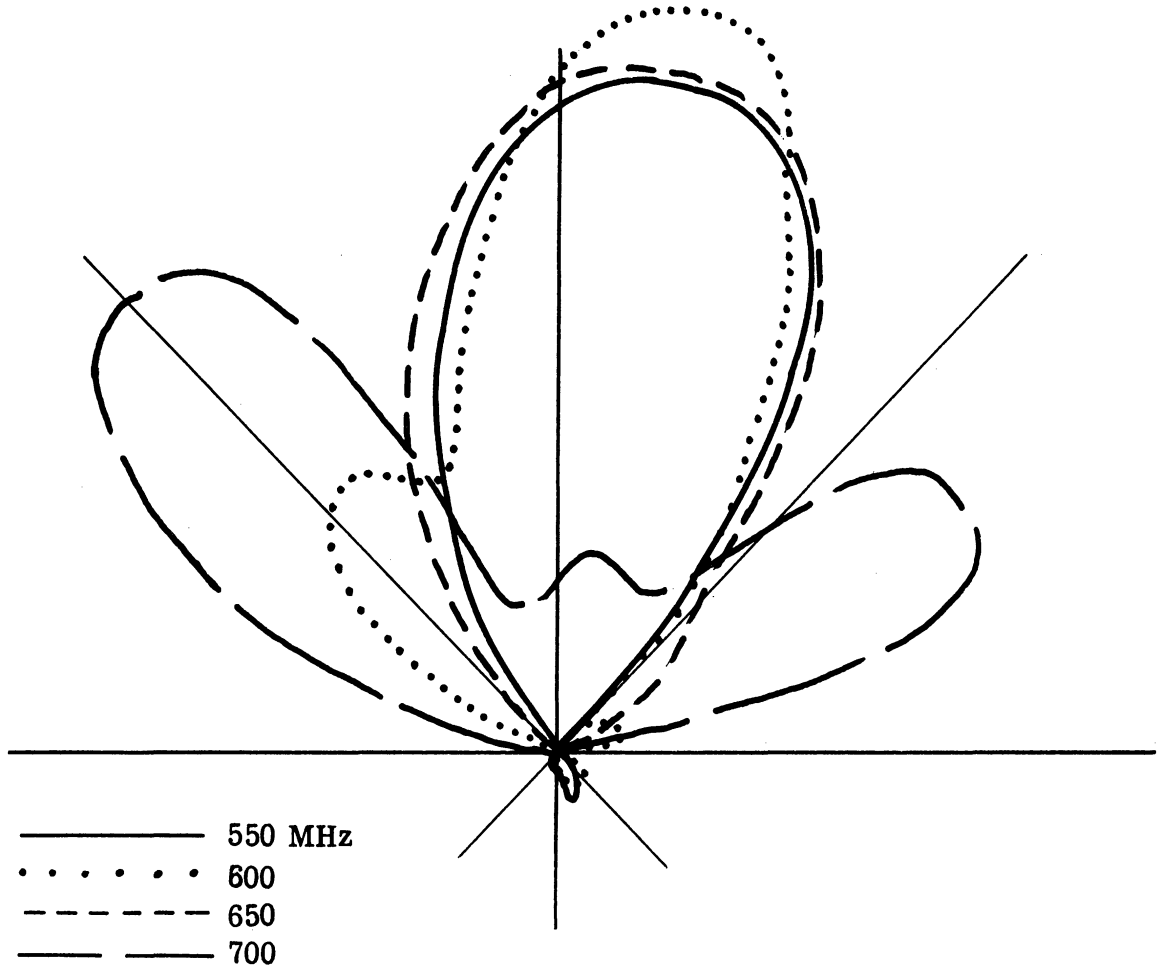

FIG. 4-47b: THE FAR FIELD H-PLANE E_y-PATTERN FOR THE ANTENNA B-1.

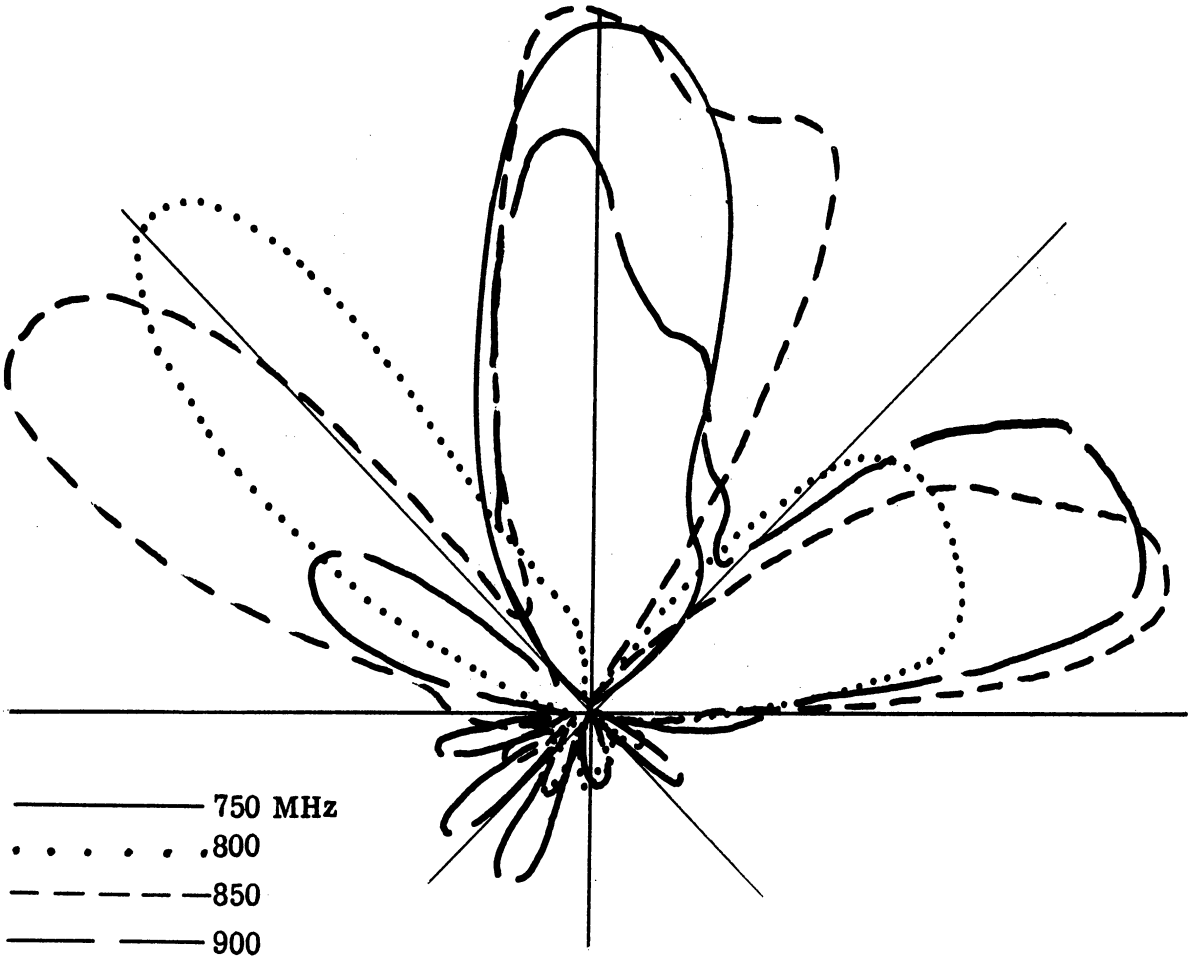

FIG. 4-47c: THE FAR FIELD H-PLANE E_y-PATTERN FOR THE ANTENNA B-1.

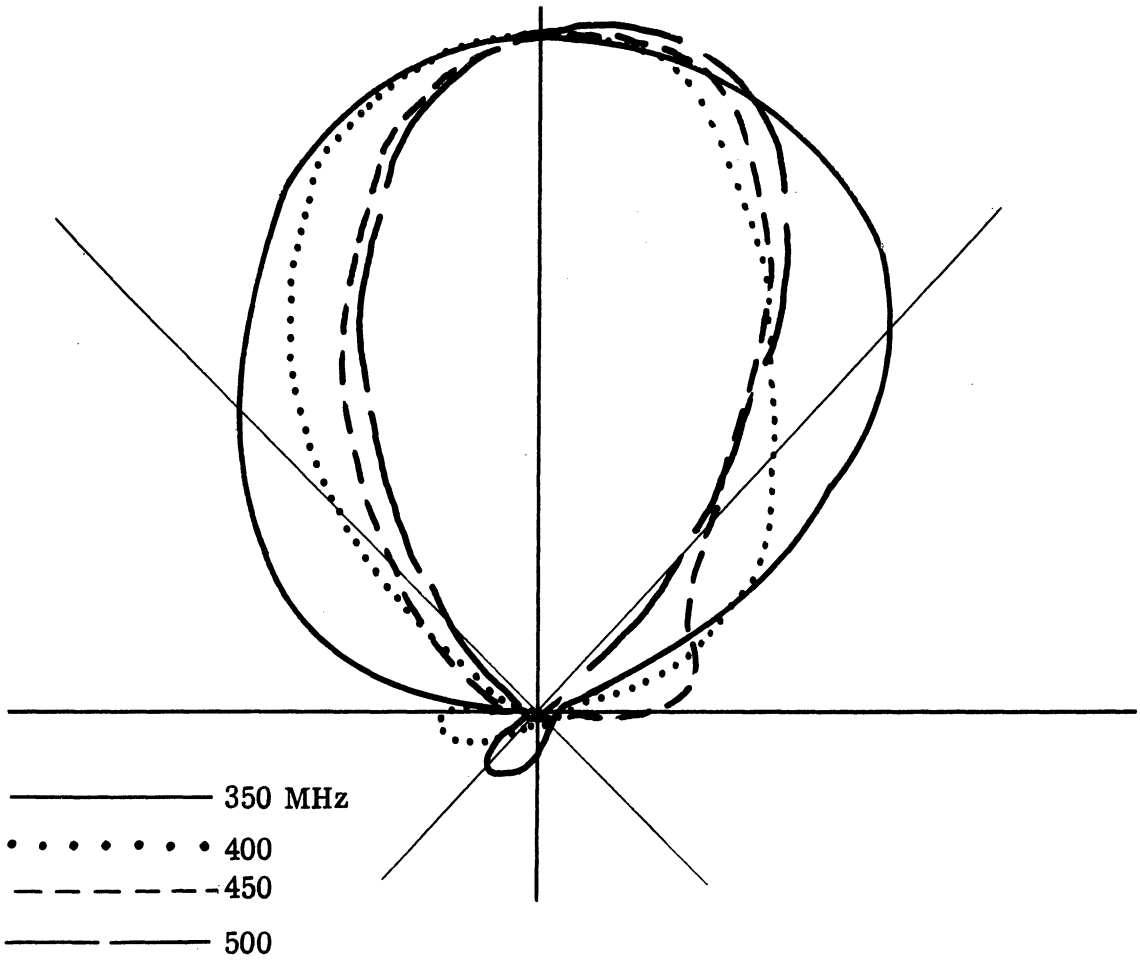

FIG. 4-48a: THE FAR FIELD H-PLANE E_y-PATTERN FOR THE ANTENNA B-2.

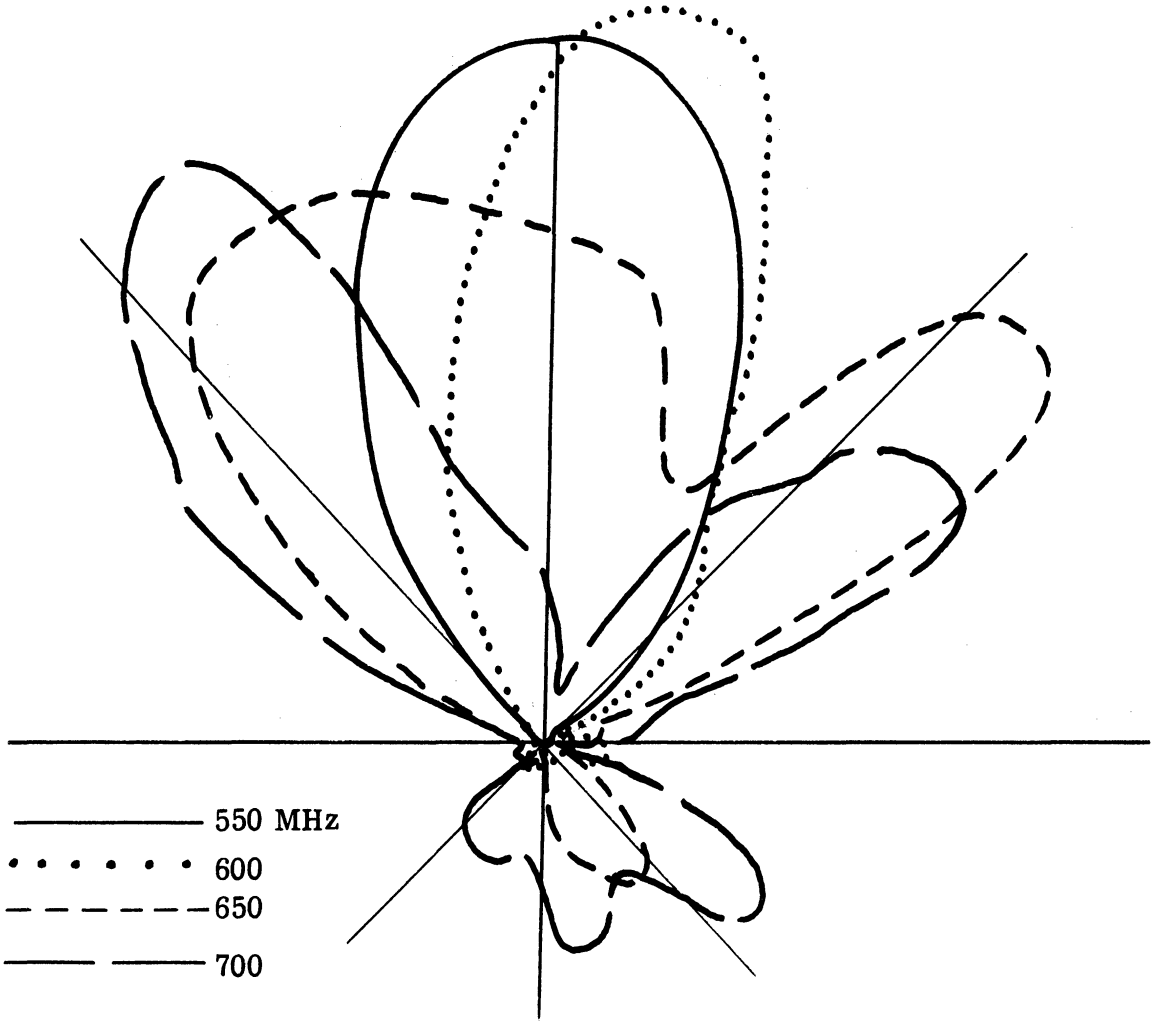

FIG. 4-48b: THE FAR FIELD H-PLANE E_y-PATTERN FOR THE ANTENNA B-2.

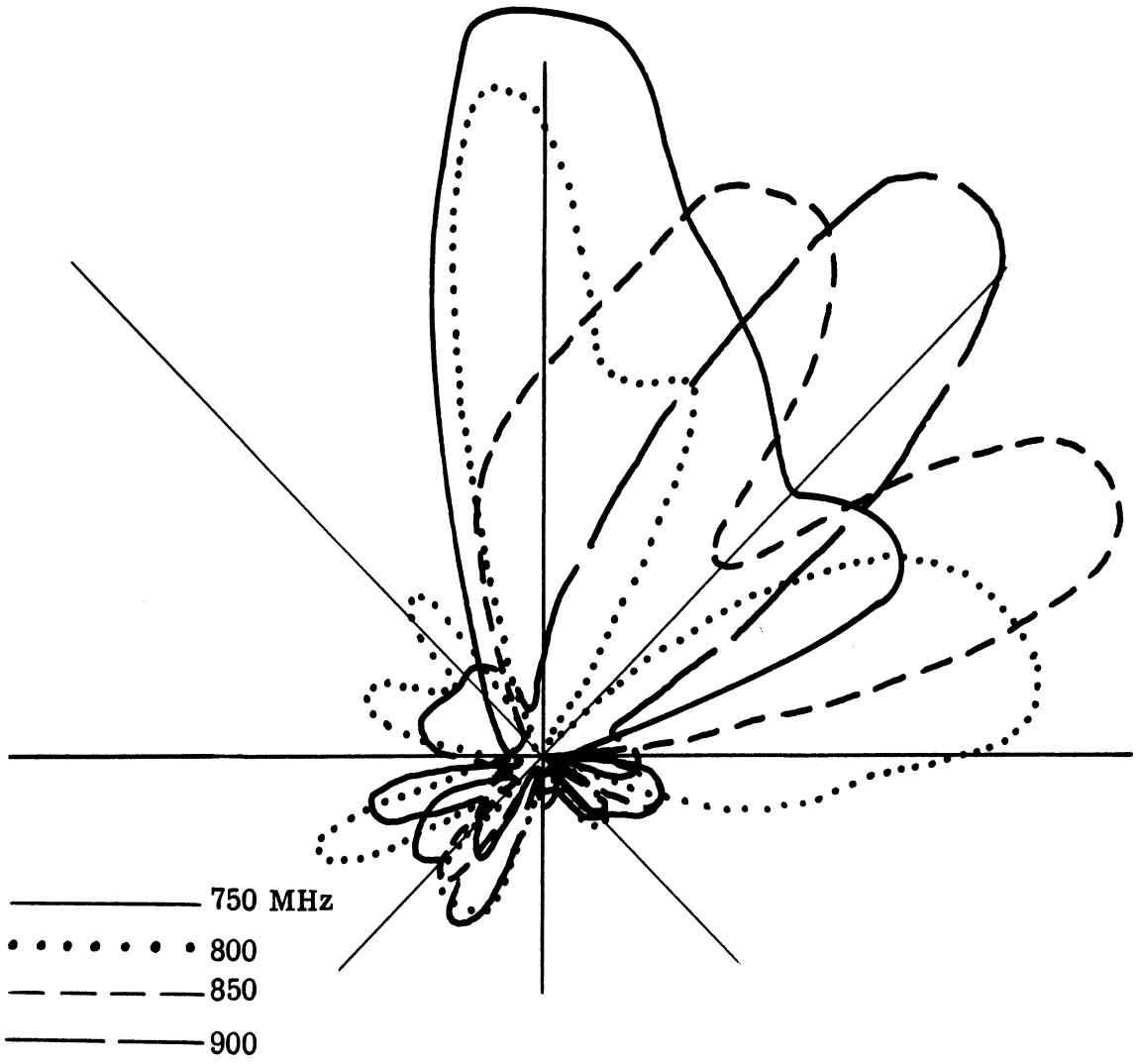

FIG. 4-48c: THE FAR FIELD H-PLANE E_y-PATTERN FOR THE ANTENNA B-2.

(a) Feed the antenna symmetrically at the center of the array.

(b) Increase the bandwidth of the structure by choosing small "b" and large "d".

(c) Make the length of the array shorter than the slow wave wavelength of the structure within the frequency range of operation.

4.4.2 The Oblique Radiation.

A further study of the mechanisms of radiation is attempted here with the construction of antenna model C-2. The number of array elements is 17 and the antenna was fed from one end of the array (left end, see Fig. 4-49a). Thus, if the frequency is increased into the slow wave region, the array will have sufficient length to support the slow wave along the direction of the array. The antenna is made to have a broader frequency bandwidth by an increase in "d" and a decrease in "b", as mentioned in previous section. The far field H-plane E-pattern is plotted in Fig. 4-49. At low frequencies where the structure is excited in its fast wave region, the radiation pattern is seen to be a "leaky" wave type, resulting in a "backward" radiation, or, the radiation pattern is toward the opposite or feed end of the array. This is expected as can be observed in Fig. 4-50, where the dispersion characteristics of the infinite structure are plotted and the appropriate frequencies are indicated by the dots along the curve, and where the points b, ---, ℓ correspond to the patterns (b), ---, (ℓ) in Fig. 4-49. As the frequency is gradually increased toward points e and f, a slow wave is becoming significant, as observed in Fig. 4-49 (e) and (f) where the second beam begins to appear along the direction of the array. This corresponds to the well-known phenomenon of radiation from a slow wave structure.[32] The trend is self-explanatory as the frequency is further increased into the slow wave region. The slow wave radiation becomes predominant and eventually, as seen in (k) and (ℓ) of Fig. 4-49, the beam is totally directed in the forward direction of the array in a typical slow wave radiation. It is noted that a change in radiation mechanism seems to have occurred although the beam tilt angles are not changed significantly when the frequency is varied. This behavior is quite different from what is commonly known as frequency scanning of an array structure.[10]

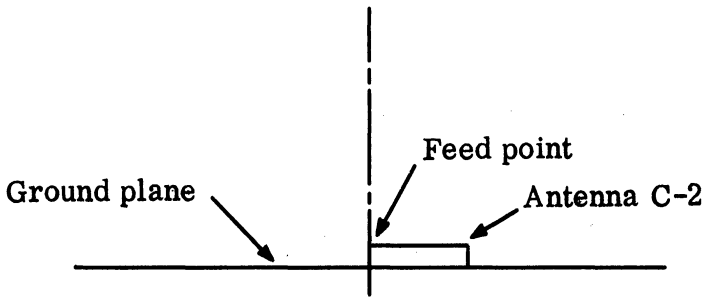

(a) Antenna C-2 Fed at Left End of the Array

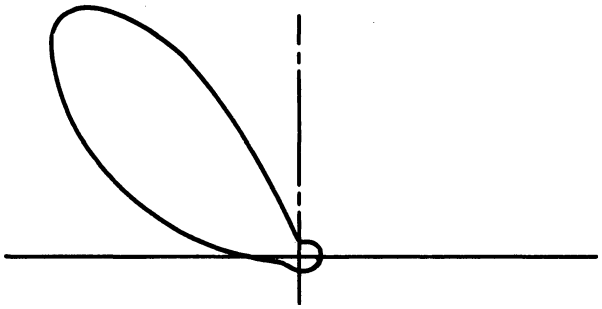

(b) 450 MHz

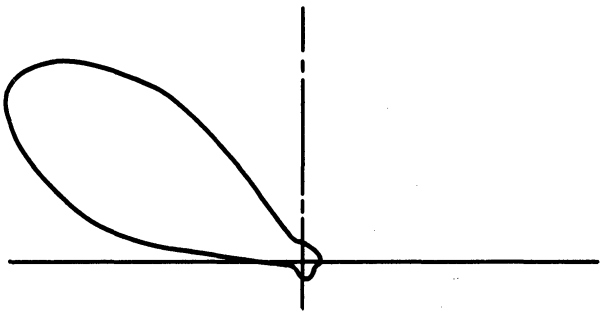

(c) 500 MHz

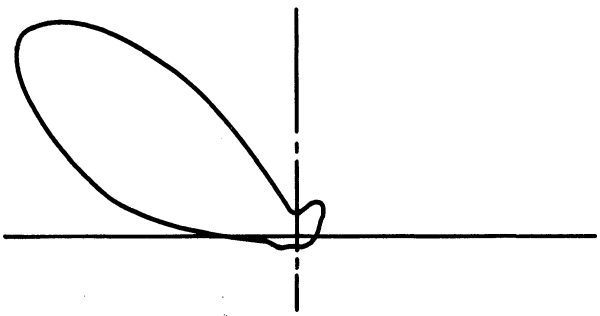

(d) 550 MHz

FIG. 4-49: THE FAR FIELD H-PLANE POWER PATTERN FOR THE ANTENNA C-2 FED AT LEFT END OF THE ARRAY.

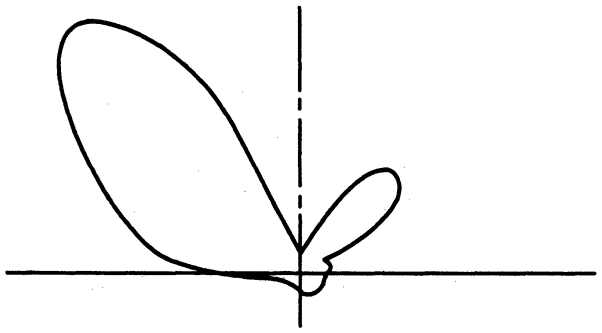

(e) 600 MHz

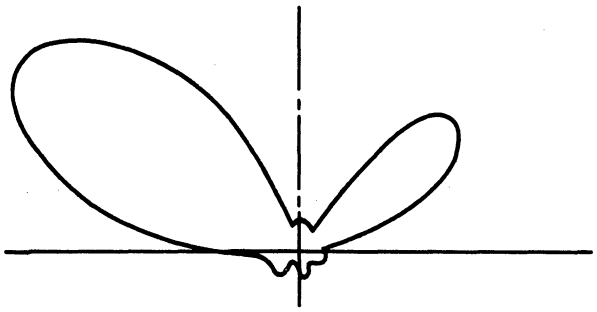

(f) 650 MHz

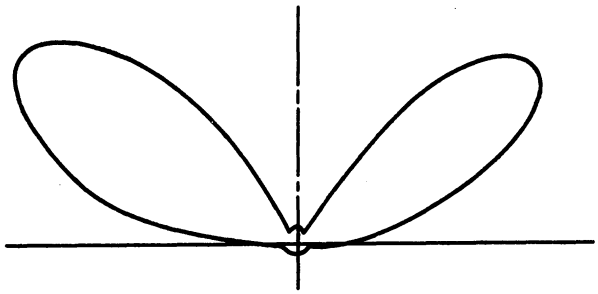

(g) 700 MHz

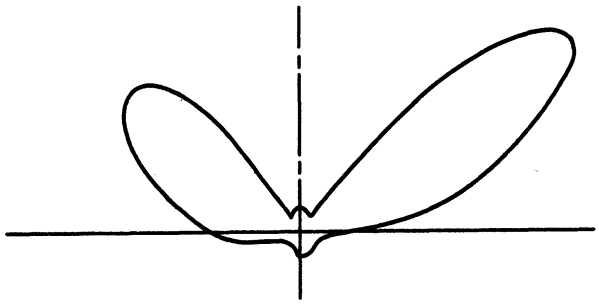

(h) 750 MHz

FIG. 4-49: THE FAR FIELD H-PLANE POWER PATTERN FOR THE ANTENNA C-2 FED AT LEFT END OF THE ARRAY.

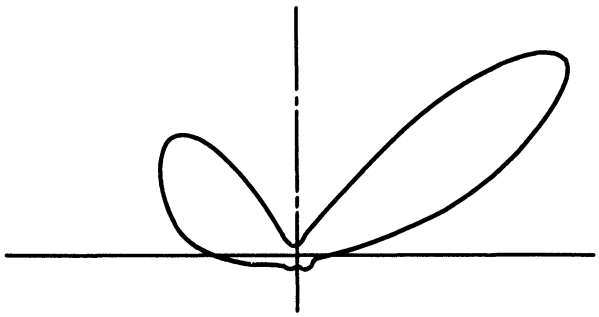

(i) 800 MHz

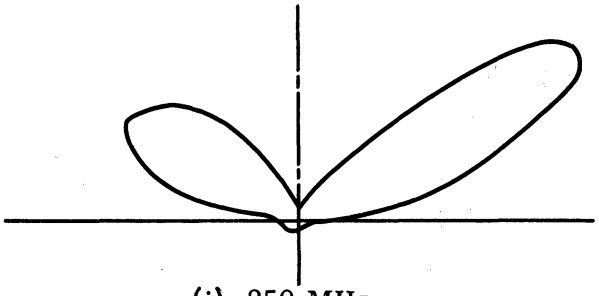

(j) 850 MHz

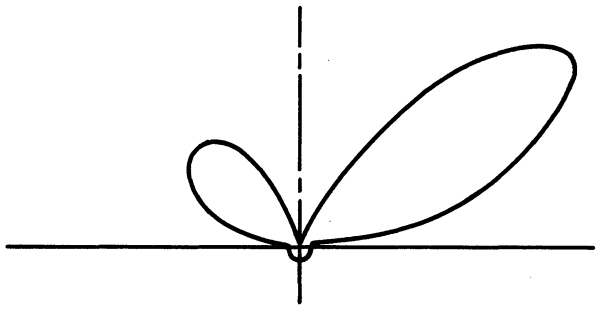

(k) 900 MHz

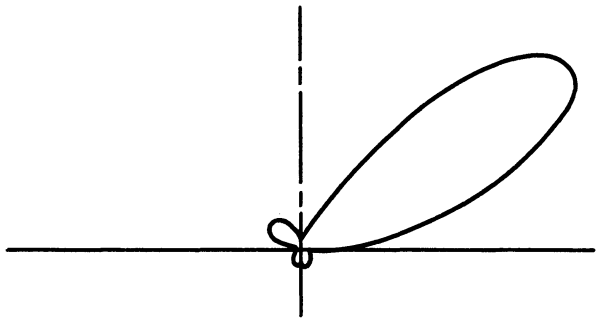

(ℓ) 950 MHz

FIG. 4-49: THE FAR FIELD H-PLANE POWER PATTERN FOR THE ANTENNA C-2 FED AT LEFT END OF THE ARRAY.

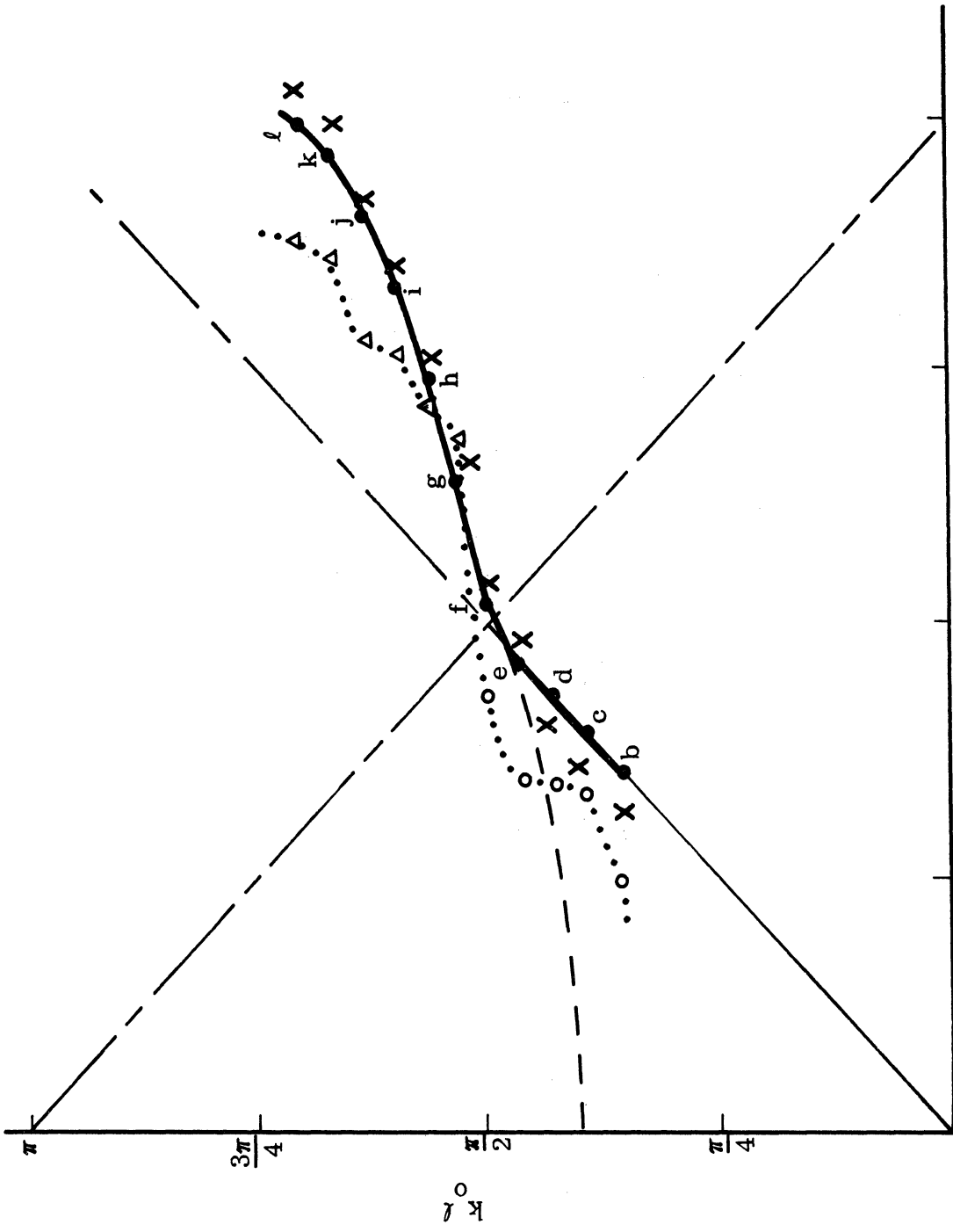

FIG. 4-50: THE DISPERSION CHARACTERISTICS FOR THE ANTENNA C-2.
—— Theoretical; ..... Experimental from Beam Angle (oo Fast Wave, $\Delta\Delta$ Slow Wave). xxxxx Experimental from Phase Measurement.

In scanning structures, the beam is shifted from, say 0^{o} to 180^{o}, gradually through a broadside when the frequency is changed. The broadside is always a null for antenna C-2 while the main beam shifts the direction. A leaky wave structure, such as a slot array fed by a wave guide also has a tendency to scan the beam when the frequency is gradually changed.[32] It is noticed, however, that the array spacing in both a frequency scanning structure and the waveguide fed slot array are in the order of the slow wave wavelength (or guide wavelength) and, thus, a broadside radiation occurs when all array elements or slots are in-phase. But, this in-phase situation is impossible in the interdigital array structure since the array spacing is very much smaller than the slow wave wavelength. As a matter of fact, the whole length of the array is only of the order of the slow wave wavelength.

The angles of maximum radiation in Fig. 4-49 for C-2 were taken as the beam angles of the dominant beam. In a lower frequency range (450~ 650 MHz), the dominant beams were those of leaky wave type in the fast wave region with pattern tilt backward toward the feed of the array. If the expression (3.27) were used by assuming that the beams were produced by a fast wave source, then the angle of maximum radiation could be converted into a ratio of the phase velocity of the source to the velocity of light. This ratio is plotted in Fig. 4-50 along with the theoretical solution. The angle of maximum radiation of the dominant beam in the higher frequency range (700~950 MHz) was also converted into the ratio of the phase velocity of the source to the velocity of light by assuming that the dominant beams were those of a slow wave type since they point toward the forward direction of the array. These data were also plotted in Fig. 4-50 with different symbols. When these two sets of plots were connected by a dotted line in Fig. 4-50 and compared with the theoretical solution, the difference between the two curves was noticeable. However, since the expression (3.27) is only approximate and many experimental errors may enter into the far field pattern, the results seem to agree quite well except in the fast wave region.

The dispersion curve obtained by a near field phase measurement is also shown in the same figures. It is seen that this curve is much closer to the theoretical solution than the one obtained using the beam angle. The comparison points toward an argument previously stated, that is, the radiation mechanism involved in the fast wave region is a leaky wave type and not a travelling wave type for an interdigital array antenna.

Since the beam tilt angle, which is defined to be the angle between the main beam and the broad-side direction, has the same value (50^{o}-60^{o}) but opposite direction, it is contemplated that two identical antennas be brought side by side. Then a split beam radiation pattern over a wide frequency band with both beam tilt angle and half power beam angle fairly constant would result. The antenna C-1 has been based on such an anticipation. The far field patterns are shown in Fig. 4-51. A fairly constant half power beam angle of $30^{o} \sim 40^{o}$ was observed. A beam tilt angle of 50^{o}-60^{o} was also observed despite some experimental measurement error as well as imperfections in the construction of the models.

From the above observations and discussions it is seen that an antenna with a single beam with tilt angle in either direction can be designed making use of the following:

(a) Obtain wider bandwidth by choosing larger "d" and smaller "b".

(b) For a backward radiation, excite the structure below the equivalent of the quarter-wave length of the array element for a predominant "leaky" radiation.

(c) For a slow wave type of radiation along the direction of the array, excite the structure at a frequency above the equivalent of the quarter-wavelength of the array element.

A symmetrical dual beam antenna, such as C-1, can also be designed with much wider frequency band since both mechanisms of radiation can be implemented. A 2:1 band-width can be designed easily if the parameters "b" and "d" are properly chosen.

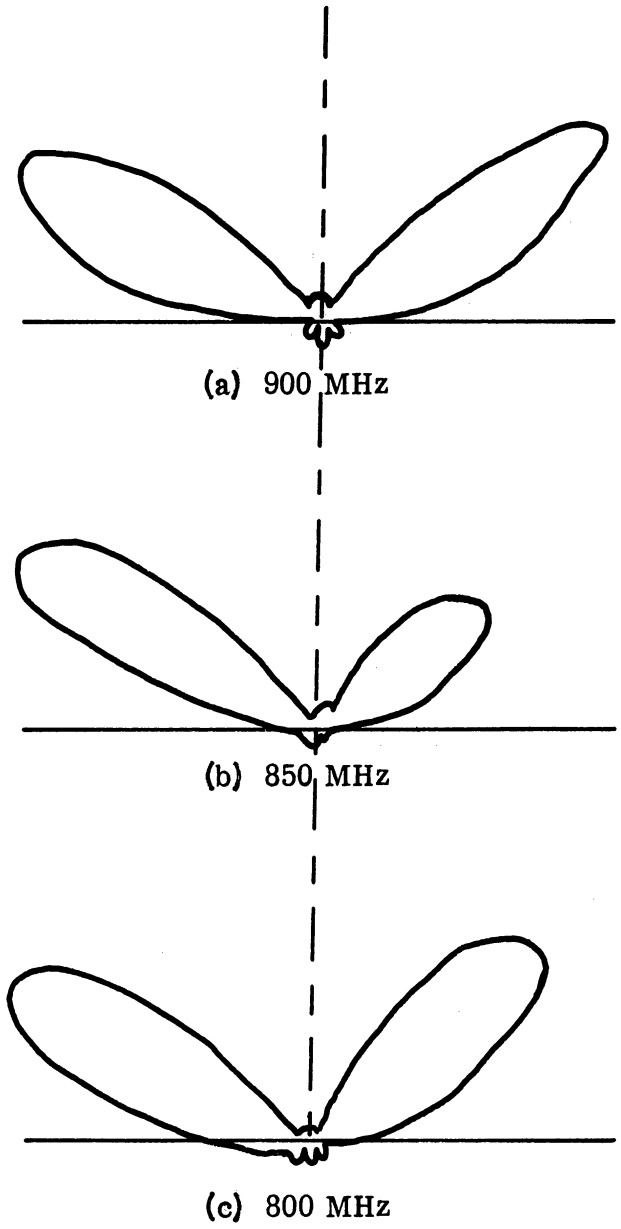

FIG. 4-51: THE FAR FIELD H-PLANE POWER PATTERN FOR THE ANTENNA C-1.

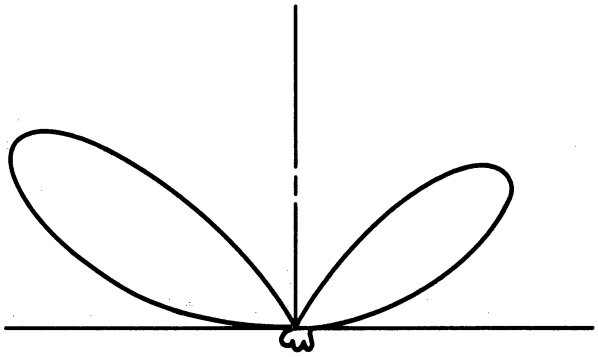

(d) 750 MHz

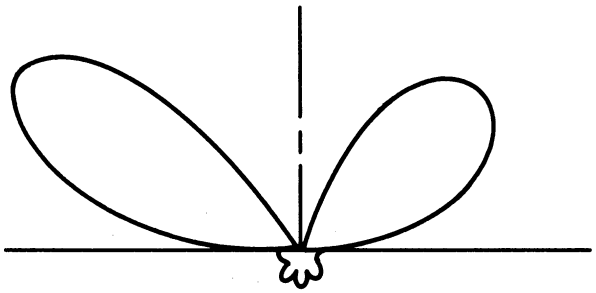

(e) 700 MHz

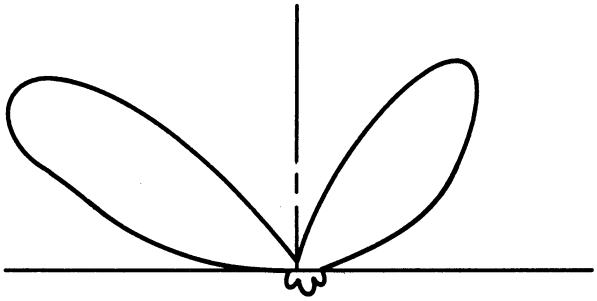

(f) 650 MHz

FIG. 4-51: THE FAR FIELD H-PLANE POWER PATTERN FOR THE ANTENNA C-1.

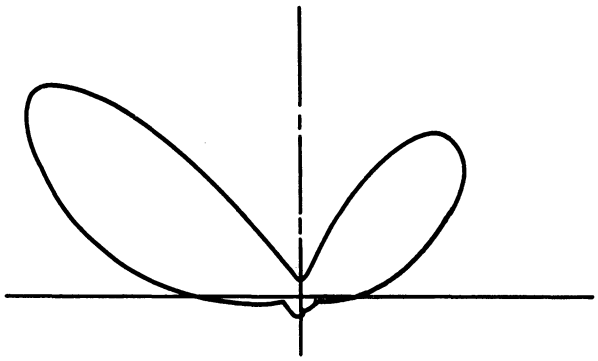

(g) 600 MHz

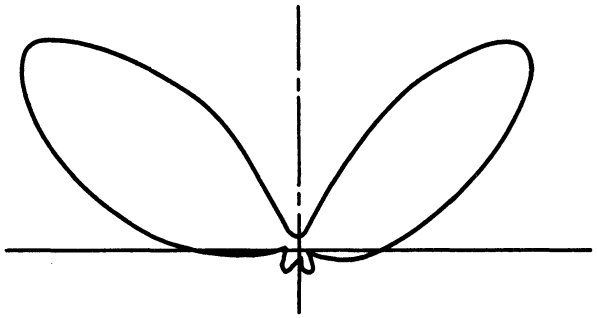

(h) 550 MHz

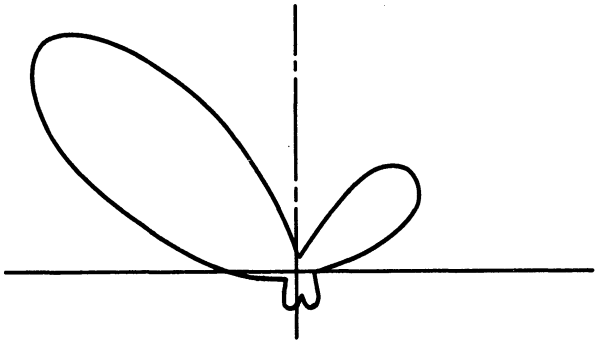

(i) 500 MHz

FIG. 4-51: THE FAR FIELD H-PLANE POWER PATTERN FOR THE ANTENNA C-1.

4.4.3 Effect of the Vertical Section of Element.

In all of the above discussion, the vertical section of the element has been neglected for some reasons. First of all, they are secondary in a sense that the radiation is determined primarily by the horizontal array element because of relative size and closer array spacings.

However, the effect of the vertical section will have a certain effect on the radiation pattern of the structure. As mentioned in a previous chapter, the vertical sections can be thought of as two staggered and parallel Hertzian dipole arrays with currents determined by the horizontal array element currents. Since the vertical sections will yield vertically polarized endfire radiation[20], the broadside pattern of the horizontally polarized radiation is not affected. However, their radiation will combine with the horizontally polarized oblique radiation. The field strength of the vertical polarization is much weaker (0~10 db) than the horizontal polarization because of small size and a relatively great distance between the sections. Of course, this particular polarization can be used to advantage if one designs an antenna for oblique radiation.

The vertically polarized patterns are shown in Figs. 4-52 through 4-56. It is noted that the pattern changes from a very weak (10~20 db below horizontal pattern) radiation toward an endfire radiation at higher frequencies, where the field strength is a little greater (0~10 db below the horizontal polarization). The term endfire was used here even though the actual radiation pattern is only half of the endfire. The other half is "hidden" behind the ground plane. The patterns shown in Figs. 4-52 through 4-56 are quite satisfactory in terms of the earlier assumption to treat them as two staggered and parallel Hertzian dipole array.

The effect of the vertical section can be minimized if a recessed mounting is used to "flush mount" the antenna. It is also possible to use some other methods, to be explored in the future, to minimize the effect of the vertical section both in terms of input impedance and the radiation pattern. This is another reason why the vertical section of the element is considered only to be of secondary effect.

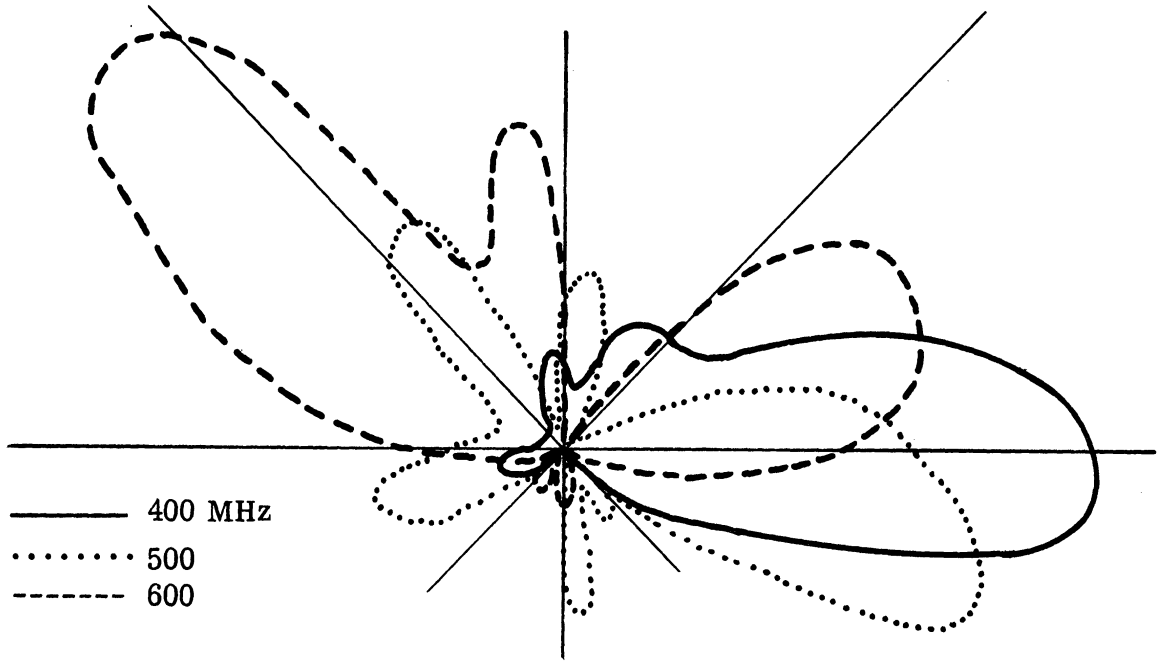

(a)

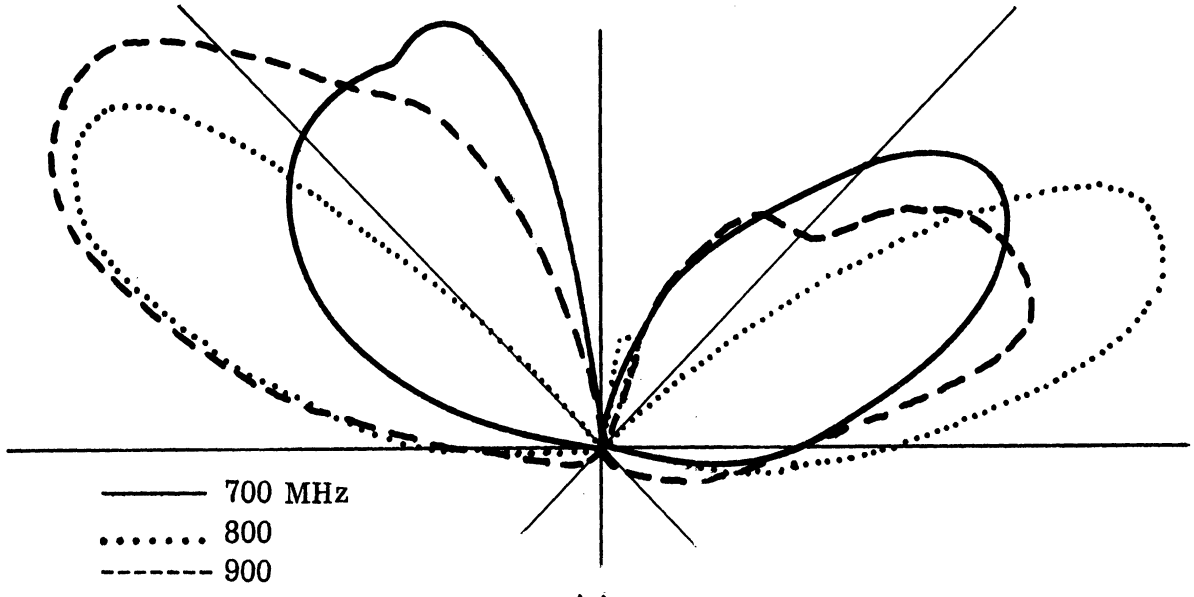

(b)

FIG. 4-52: THE FAR FIELD H-PLANE E_z-PATTERN FOR THE ANTENNA A-1.

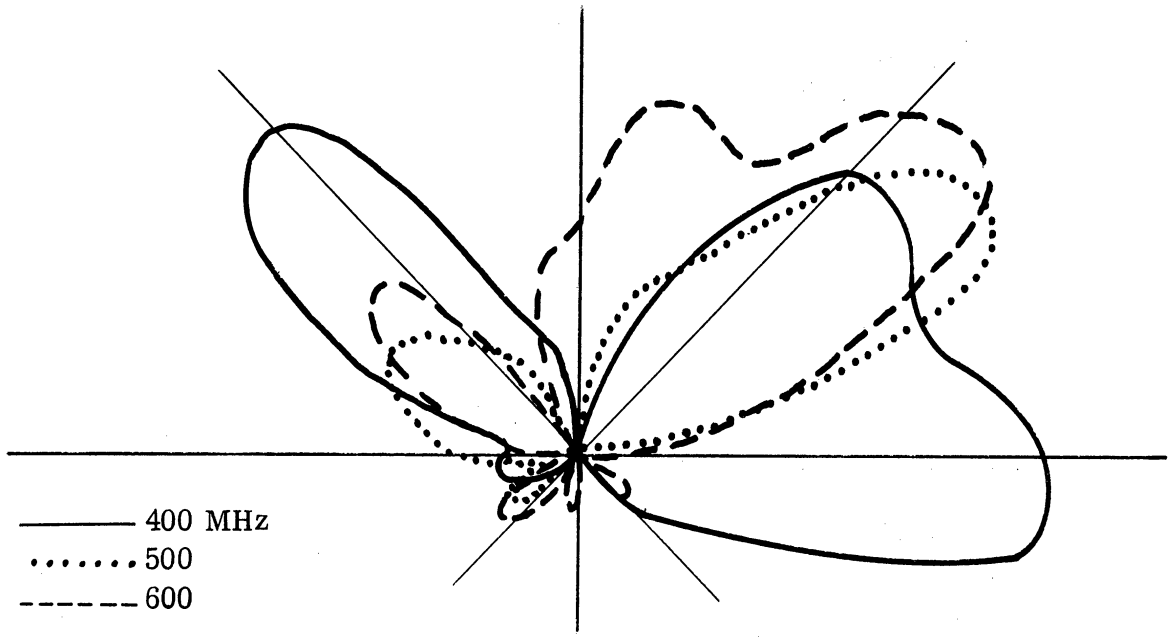

(a)

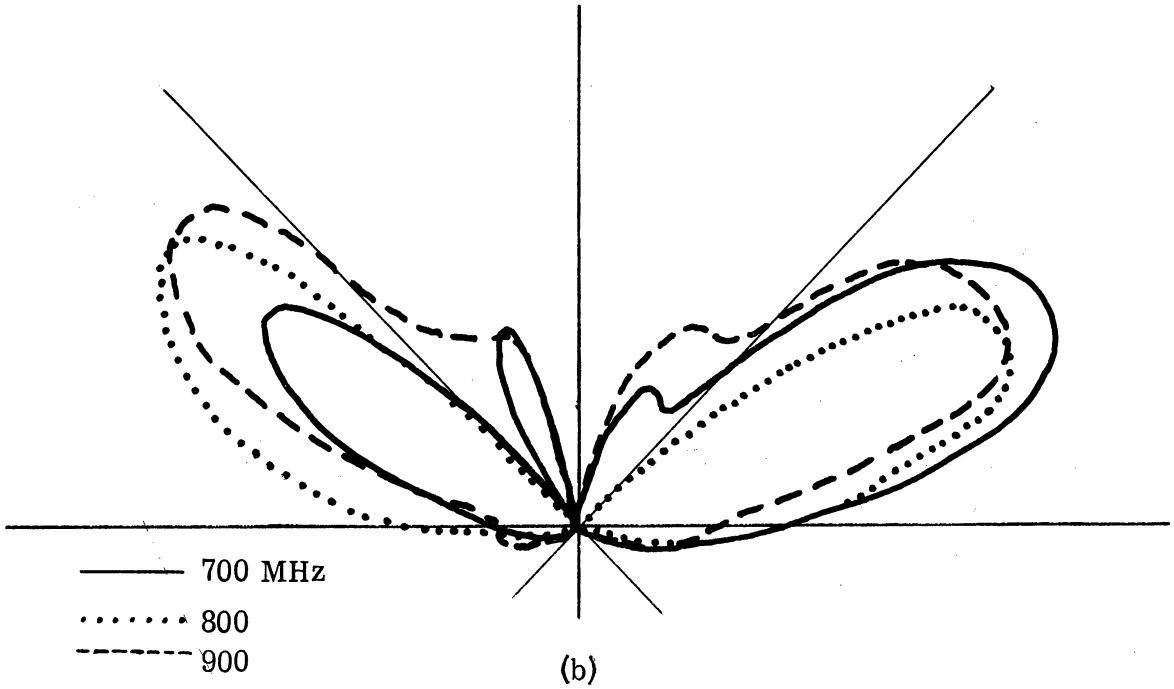

(b)

FIG. 4-53: THE FAR FIELD H-PLANE E_z-PATTERN FOR THE ANTENNA A-2.

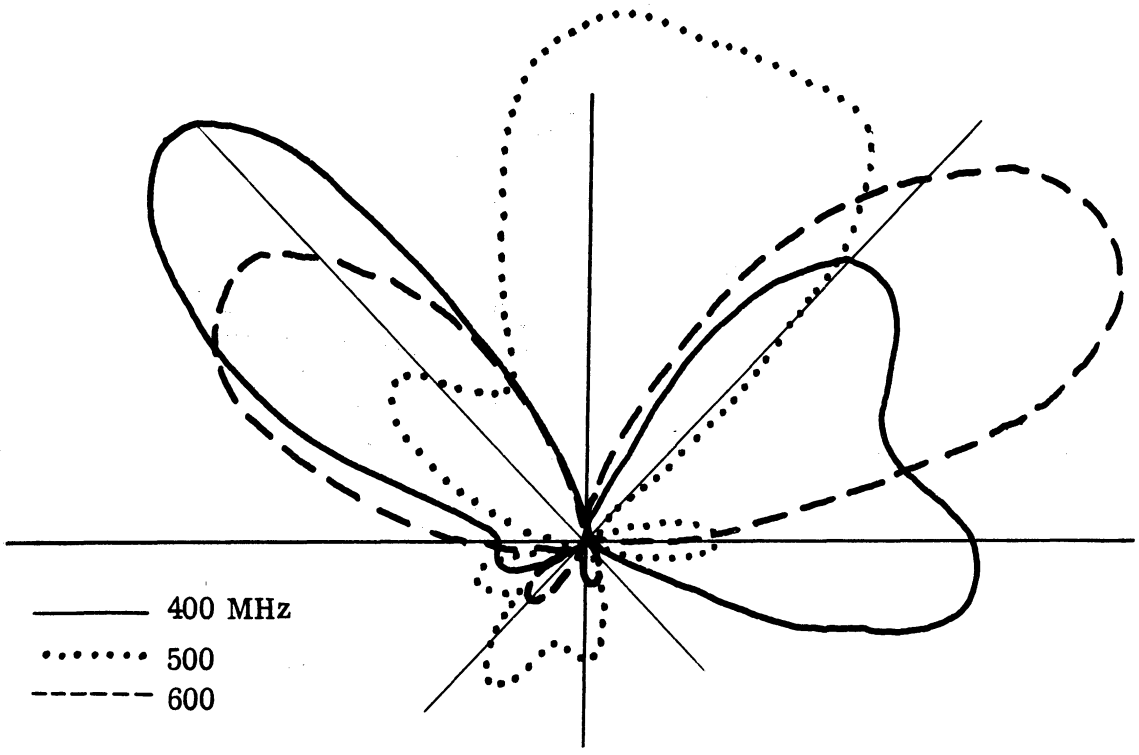

(a)

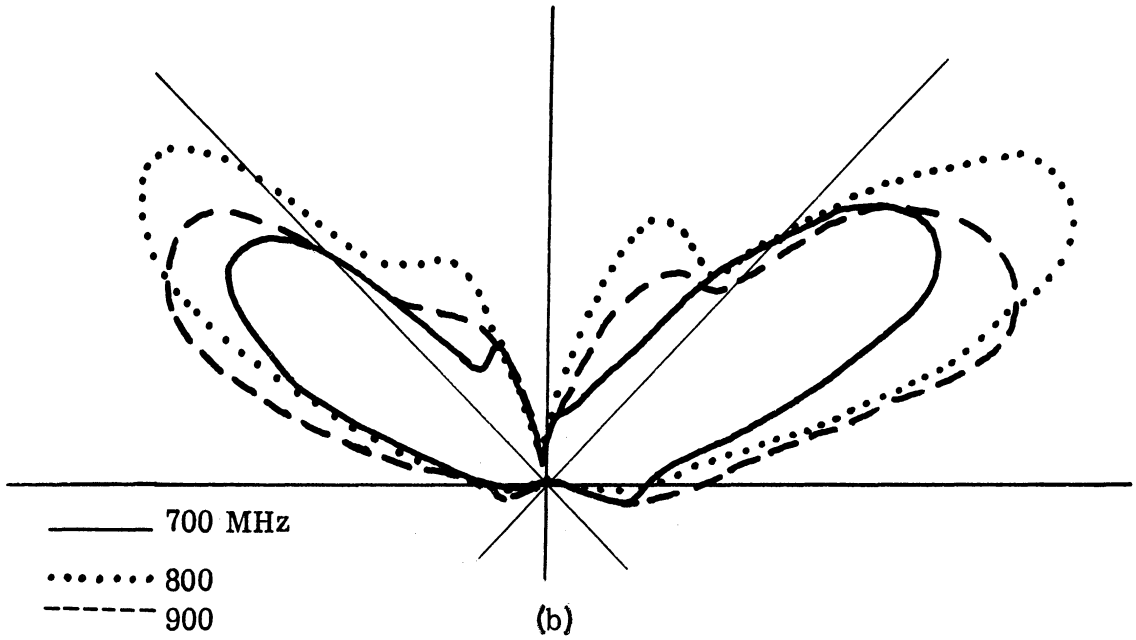

(b)

FIG. 4-54: THE FAR FIELD H-PLANE E_z-PATTERN FOR THE ANTENNA A-3.

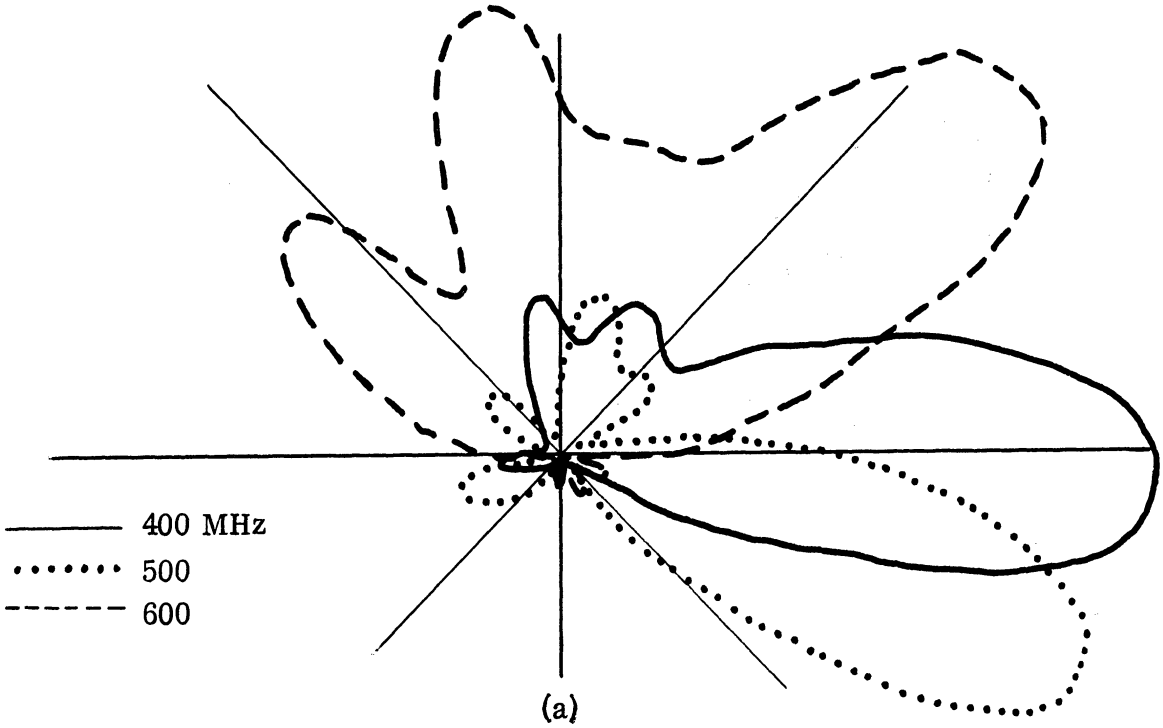

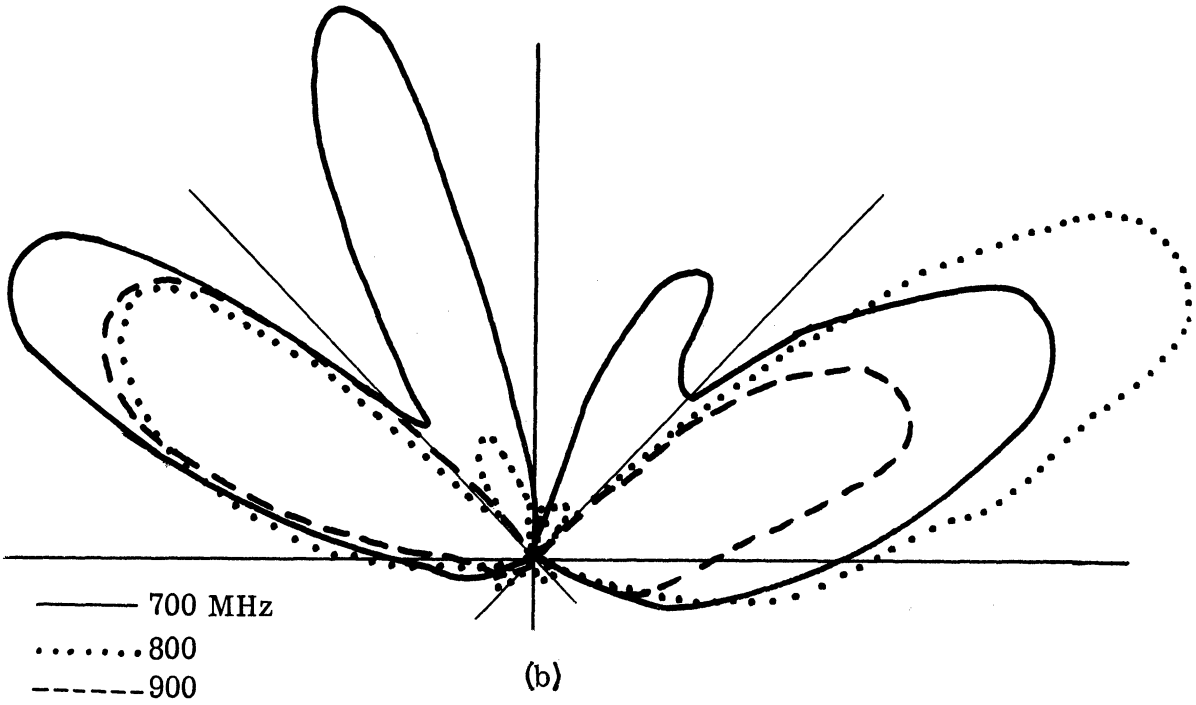

FIG. 4-55: THE FAR FIELD H-PLANE E_z-PATTERN FOR THE ANTENNA B-1.

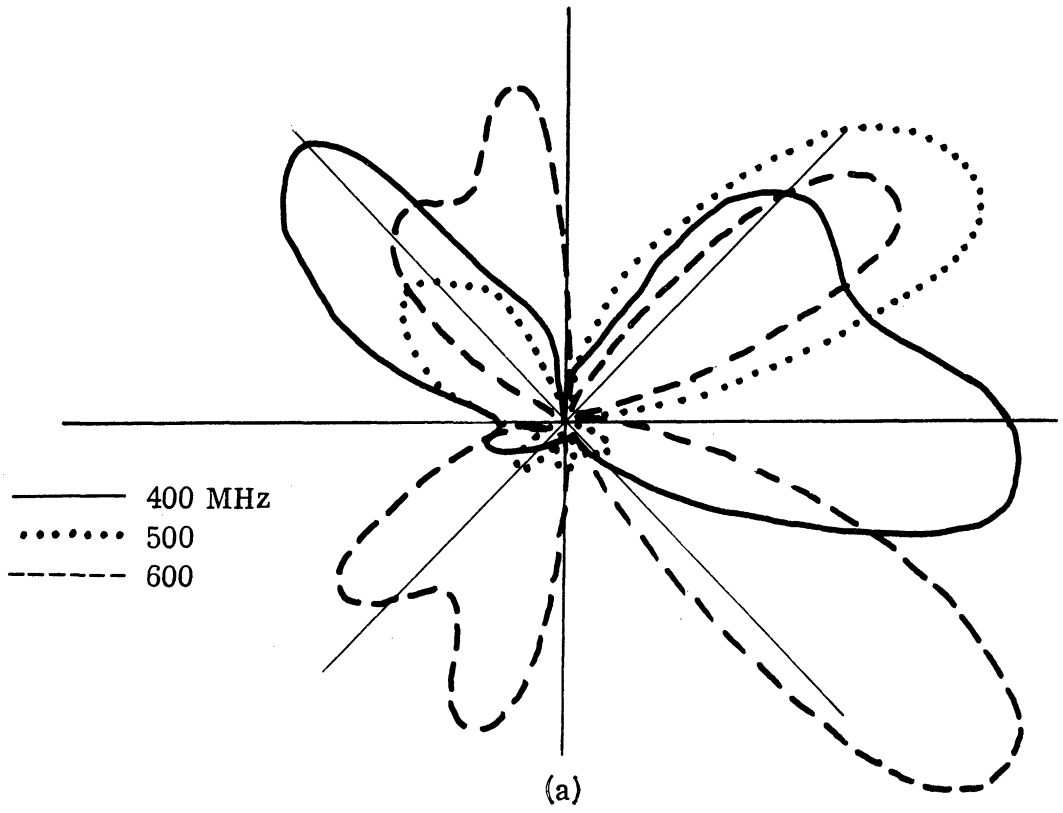

(a)

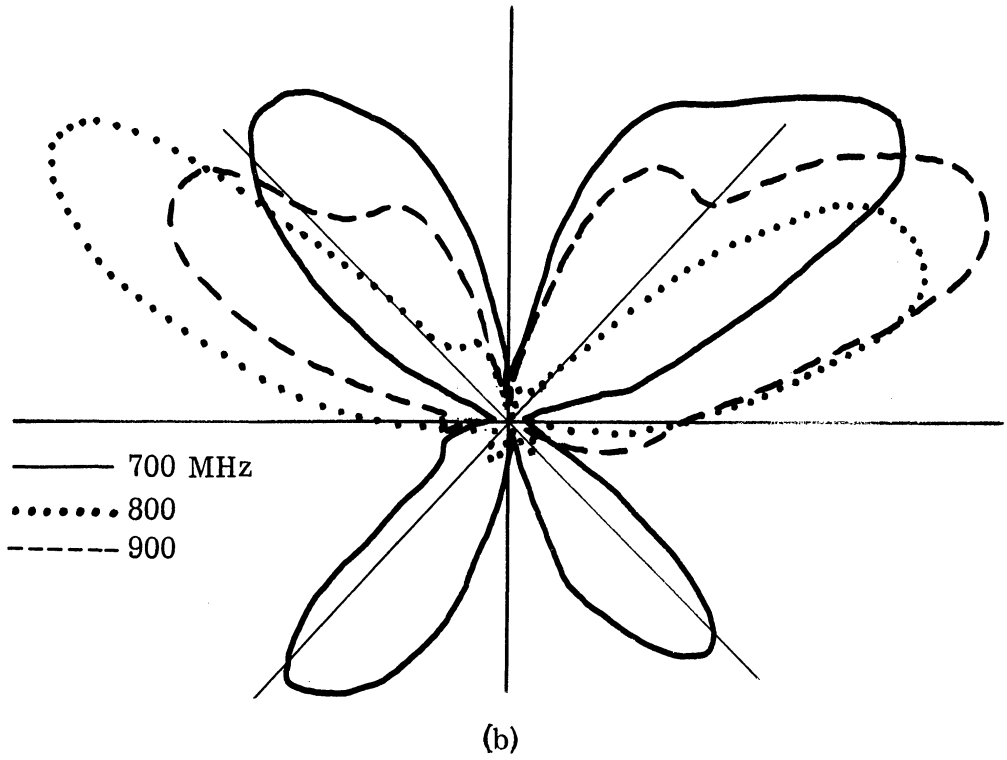

(b)

FIG. 4-56: THE FAR FIELD H-PLANE E_z-PATTERN FOR THE ANTENNA B-2.

4.4.4 Discussion.

The radiation pattern of the interdigital array antenna is found to be predictable over a fairly wide frequency band. The mechanism of radiation is considered to be of two types. The "leaky" backward wave in the fast wave region and the "slow" forward wave in the slow wave region. The theory fails to have a complete fit over the entire range of experimental results, but the general trend, the half power beam angle, and the frequency band are quite consistent with the measured patterns. Since the experimental models constructed were not quite symmetrical, the measured patterns were seen to be non-symmetrical with respect to the center of array.

Different types of mechanisms involved in the radiation can be utilized separately or jointly, depending on the particular type of the radiation pattern and the bandwidth of the antenna desired. The choice of the parameters "b" and "d" must be made consistent with the required bandwidth, input impedance and VSWR of the structure. An antenna properly designed will be wideband with respect to radiation pattern and input impedance.

CHAPTER V

CONCLUSIONS AND FUTURE RECOMMENDATIONS

5.1 Conclusions.

Several conclusions can be drawn from the discussions of the previous chapters.

First of all, the application of the antenna-wave theory concept to obtain the dispersion characteristics was found to be quite close to the solutions obtained by Bolljahn and Matthaei[2], Fletcher[8] for a closed structure, although the direct comparisons were difficult for the reasons mentioned in Chapter II. Some interesting trends of the dispersion characteristics of the interdigital array were also compared with those of the Yagi-Uda structure. Thereby, it was seen that for given parameter values, the interdigital array antenna has a much wider bandwidth than that of a Yagi-Uda array. The theory used was only approximate since the current distribution along the conducting elements was assumed to be a sinusoidal one obeying the interdigital boundary condition. However, the experimentally measured dispersion characteristics are found to be fairly close to the theoretical ones. It is also found that the dispersion characteristics can be used to explain the mechanisms of the radiation quite satisfactorily.

The analysis of a finite array was not as good as that of the infinite array mainly because of the uncertainty of the actual current distribution along the array elements which was again assumed to be a sinusoidal one obeying the interdigital boundary conditions. Hallén's first order current distribution was used in the excited element in order to obtain a better expression of the input impedance. Many other current distributions were tried numerically for a best result. In spite of this effort, the theoretical results were not in complete agreement with the experimental measurements. However, the input impedance and the radiation patterns based on analysis were close enough to make some limited predictions possible and help explain the experimentally obtained data.

The experimental study of the input impedance reveals a shift of the impedance locus on Smith Chart when the antenna parameters were changed. The resonant frequency of the structure was found to be about 20 per cent lower than the equivalent of the quarter-wavelength of the array element. This is taken as a change in actual current distribution due to the mutual coupling of the adjacent elements. From the circuit point of view, the excited element has been "loaded" down by the adjacent elements both capacitively and inductively, thus lowering the resonant frequency. The theoretical analyses were not able to predict this since the current distribution was already assumed to be sinusoidal along the array elements.

It is found through the experiment that there are two dominant mechanisms involved in the radiation of an interdigital array antenna. When the frequency is below the equivalent of the quarter wavelength of the array element, the radiation is of a "leaky" wave nature. Strickly speaking, a "leaky" wave concept is used only in an infinite structure such as in a waveguide fed slot array. The term is used here to define, loosely, the phenomenon of continuous radiation as the wave travels along the direction of the array. When the frequency is above the equivalent of the quarter wavelength of the array element, the radiation becomes a slow wave type. The two different mechanisms result in backward and forward radition patterns respectively with respect to the direction of the axis of the array. The axis of the array is taken perpendicular to each radiating element of the array. Therefore, an antenna can be designed for a desired radiation pattern if the desired mechanism is excited with proper arrangement of feeding location.

Models were built for a broadside and a tilted beam application. The broadside models (A-1, A-2, A-3, B-1, B-2) were found to have a half power angle of 30^{o} to 60^{o} over 25 to 40 per cent bandwidth where the bandwidth is defined to be the frequency range in which the main beam is directed broadside from the surface of the ground plane. The tilt beam models C-1 have a rabbit-ear pattern with half power angle of 20^{o} to 40^{o} and a beam tilt angle of 30^{o} to 40^{o} well over a 2:1 frequency range. The physical size of the antennas ranges from 14 cm. x

8 cm. x 1 cm. for A-1 to 36 cm. x 8 cm. x 1 cm. for B-2 which should be compared with a typical cavity-backed slot antenna. For the same frequency the size of the slot is about 25 cm. x 13 cm. x 13 cm., which is considerably larger than the antenna A-1 (about 4 to 1 in volume and 3 to 1 in aperture area) and slightly larger than the antenna B-2 (about 2 to 1 in volume and comparable in aperture area).

The wideband characteristics, in terms of the input impedance and the VSWR, were noted to be consistent with the wideband characteristics in terms of the far field pattern. In general, it was found that a 2:1 frequency range can be designed easily in terms of both a far field pattern and an input impedance.

The vertical sections of elements which are necessary in providing an interdigital boundary condition were found to have a little influence in terms of the input impedance and the far field pattern. The radiation resistances of the vertical sections of elements were found to be, at most, 5Ω each, if they are assumed to be Hertzian dipoles. The far field patterns were vertically polarized directed along the axis of the array in an endfire radiation. The far field was found to be much weaker than the far field of the horizontal array elements (which is horizontally polarized) by 10 to 20 db and is, therefore, considered insignificant.

As a summary conclusion it is found that an interdigital array antenna has the advantages of being comparatively broadband, having a low profile, being of small electrical size and permitting versatile feeding arrangements while its main disadvantages are a low input resistance and a small amount of cross polarization caused by the vertical sections.

5.2 Future Recommendations.

A further improvement of the present structure is possible through some modifications:

(i) A dielectric and/or magnetic loading: The loading of the antenna will reduce the resonant frequency of the array and thus reduce the physical size of the structure.

(ii) Lumped inductive or capacitive loading: These types of loading at alternate ends of each element will change the current distribution along the array element and may result in modified performance characteristics.

(iii) Recessed mounting: This will permit a flush mount and thus minimize the effect of the vertical sections on its far field pattern.

Alternate approaches to the theoretical analysis of the present problem for a finite array would be of much interest.

REFERENCES

1. Blass, J. and S.J. Rabinowitz, (1957), "Mutual Coupling in Two-Dimensional Arrays," IRE Wescon, Part I, 134-150.

2. Bolljahn, J.T. and G.L. Matthaei, (March 1962), "A Study of the Phase and Filter Properties of Arrays of Parallel Conductors between Ground Planes," Proc. IRE, 54, 299-311.

3. Brillouin, L., (1946), Wave Propagation in Periodic Structures, McGraw Hill, New York.

4. Butcher, P.N., (March 1957), "A Theoretical Study of Propagation Along Tape Ladder Lines," Proc. IEE, 194, Part B, 169-176.

5. ——— (March 1957), "The Coupling Impedance of Tape Structure," Proc. IEE, 104, Part B, 177-187.

6. Carter, P.S., (June 1932), "Circuit Relations in Radiating Systems and Applications to Antenna Problems," Proc. IRE, 20, 1004-1042.

7. Ferris, J.E., J.A.M. Lyon, G.G. Rassweiler, D.L. Smith, P.R. Wu and W.E. Zimmerman, (June 1966), "Broadband Antenna Techniques Study-Interim Report No. 1," Technical Report ECOM-TR-01263-4, The University of Michigan Radiation Laboratory Report 07260-1-T, 175.

8. Fletcher, R.C., (August 1952), "A Broadband Interdigital Circuit for Use in Traveling-wave Type Amplifiers," Proc. IRE, 40, 951-958.

9. Hallén, E., (November 1938), "Theoretical Investigations into the Transmitting and Receiving Qualities of Antennae," Nova Acta Regiae Societatis Scientiarum Upsaliensis, Ser. IV, 11, No. 4, 1-44.

10. Jasik, H., (1961), Antenna Engineering Handbook, McGraw-Hill, New York.

11. King, R.W.P., (1956) Theory of Linear Antennas, Harvard University Press, Cambridge, Massachusetts.

12. King, R.W.P. and S.S. Sandler, (May 1964), "The Theory of Broadside Arrays and the Theory of Endfire Arrays," Trans. IEEE, AP-12, 269-280.

13. King, R.W.P and C.W. Harrison, Jr., (June 1944), "Mutual and Self-Impedance for Coupled Antennas," J. Appl. Phys., 15, 481-495.

14. King, R.W.P. and C.W. Harrison, Jr., (October 1944), "The Distribution of Current Along a Symmetrical Center-driven Antenna," Proc. IRE, 32, 548-567.

15. King, R.W.P. and D. Middleton, (January 1946), "The Cylindrical Antenna; Current and Impedance," Quart. Appl. Math., 3, 302-335.

16. Kraus, J.D., (1950), Antennas, McGraw-Hill, New York.

17. Lyon, J.A.M., N.G. Alexopoulos, C.C. Chen, A.M.Kazi, G.G.Rassweiler, D.L. Smith and P.R. Wu, (May 1966), "A Study of a UHF-VHF Antenna-Final Report," AFAL TR-66-101, The University of Michigan Radiation Laboratory Report 07140-1-F, 169.

18. Lyon, J.A.M., N.G. Alexopoulos, A.M.Kazi, D.L.Smith and P.R.Wu, (May 1966), "Study and Investigation of a UHF-VFH Antenna-Quarterly Report No. 1," The University of Michigan Radiation Laboratory Report 07848-1-Q, 39.

19. Mailloux, R.J., (July 1965), "Antenna and Wave Theories of Infinite Yagi-Uda Arrays," Trans. IEEE, AP-13, 499-506.

20. ———(September 1965), "Excitation of a Surface Wave Along an Infinite Yagi-Uda Array," Trans. IEEE, AP-13, 719-724.

21. ———(March 1966), "The Long Yagi-Uda Array," Trans. IEEE, AP-14, 128-137.

22. Mei, K.K., (May 1965), "On the Integral Equations of Thin Wire Antennas," Trans. IEEE, AP-13, 374-378.

23. Nielsen, K.L., (1956), Methods in Numerical Analysis, The MacMillan Co., New York.

24. Pierce, I.R., (1955), "Propagation in Linear Arrays of Parallel Wires," Trans. IRE, ED-2, No. 1, 13.

25. Sengupta, D.L., (July 1959), "On the Velocity of Wave Propagation Along an Infinite Yagi Structure," Trans. IRE, AP-7, 234-239.

26. ———(January 1960), "On Uniform and Linearly Tapered Long Yagi Antennas," Trans. IRE, AP-8, 11-17.

27. Serracchioli, F. and C.A. Levis, (December 1959), "The Calculated Phase Velocity of Long Endfire Uniform Dipole Arrays," Trans. IRE, AP-7, S424-S434.

28. Schelkunoff, S.A., (1952), Advanced Antenna Theory, New York, Wiley.

29. Schelkunoff, S.A. and H.T. Friis, (1952), Antennas; Theory and Practice, New York, Wiley.

30. Tai, C.T., (April 1948), "Coupled Antennas," Proc. IRE, 36, 487-500.

31. ———(July 1955), "A New Interpretation of the Integral Equation Formulation of Cylindrical Antennas," Trans. IRE, AP-3, 125-127.

32. Walter, C.H., (1965), Traveling Wave Antennas, McGraw, New York.

33. Watkins, D.C., (1958), Topics in Electromagnetic Theory, Wiley, New York.

34. Whiteside, H., (October 1962), Electromagnetic Field Probes," Harvard University Cruft Laboratory Technical Report No. 377.

DISTRIBUTION LIST AF33(615)-3609 Proj. 07848

Destination	Number of Copies
Adams-Russell Company Library - Antenna Section 280 Bear Hill Road Waltham, Mass. 02154	1
Aero Geo Astro Security Officer Edsall and Lincolnia Blvd. Alexandria, Va.	1
Aerospace Corporation Robert C. Hansen 2400 E. El Segundo Blvd. Los Angeles, Calif. 90045	1
Cutler-Hammer Division, Airborn Instruments Labs. Librarian - Antenna Section Walt Whitman Road Melville, L.I., New York 11729	1
All Products Company Mr. James Buzbee Mineral Wells, Texas	1
Americal Electronic Laboratories, Inc. Antenna Section Box 552 Lansdale, Pa.	1
Andrew Alfred Consulting Engineers Librarian - Antenna Section 299 Atlantic Ave. Boston, Mass. 02110	1
AVCO Res. and Adv. Development Division Research Library 201 Lowell Wilmington, Mass. 01887	1
AVCO Electronic and Ordnance Division Technical Library 2630 Glendale-Milford Road Cincinnati, Ohio 45241	1
Bell Aircraft Corporation Technical Library - Antennas Buffalo, New York 14205	1
Bell Telephone Laboratories Inc. Technical Reports Library - Room 2A165 Whippany, New Jersey 07961	1

Bendix Radio Division
Technical Library - Dept. 462-4
East Joppa Road
Baltimore, Md. 21204 1

Bendix Research Laboratories
Technical Library
20800 10 1/2 Mile Road
Southfield, Michigan 48076 1

Boeing/Wichita - Antenna Systems Staff Unit
Technical Library
3801 South Oliver
Wichita, Kansas 67201 1

Boeing Aerospace Division
Technical Library - Antenna and Radomes
Box 3707
Seattle, Washington 98124 1

Bunker-Ramo Corporation, Defense Systems Div.
8433 Fall Brook Avenue
Canoga Park, California 91304 1

Canoga Electronics - Advanced Programs Dept
Box 2086
Canoga Park, California 91306 1

Chance-Vought Aircraft, Inc.
BuAer Representative
Technical Library - Antenna Section
Box 1500
Arlington, Texas 75222 1

Collins Radio Research Division
Technical Library
5200 C NE
Cedar Rapids, Iowa 52406 1

Collins Radio Corporation
Dr. Robert L. Carrel - Antenna Section
Dallas, Texas 75207 1

Dalmo Victor Company
Technical Library - Antennas
1515 Industrial Way
Belmont, California 1

Dorne and Margolin, Inc.
Technical Library - Antenna Section
29 New York Avenue
Westbury, L.I., N.Y. 11591 1

Douglas Aircraft MSSD Technical Library
Antenna Section
3000 Ocean Park Blvd.
Santa Monica, Calif. 90406 1

Dynatronics, Inc.
Technical Library - Antennas
Hwy 17 and 92 N. Castlebury
Orlando, Florida 1

Electronic Communications Research Division
Technical Library
1830 York Road
Timonium, Md. 1

Emerson and Cuminb, Inc.
E. J. Luoma
869 Washington St.
Canton, Mass. 02021 1

Fairchild Aircraft and Missiles Division
Technical Library - Antennas
Hagerstown, Maryland 1

Fairchild Hiller Corporation
Technical Library
1455 Research Blvd.
Rockville, Md. 20850 1

General Dynamics/Convair
Technical Library - Antennas
Grants Lane
P.O. Box 748
Fort Worth, Texas 76101 1

General Electric Electronics Laboratory
Technical Library
Electronics Park
Syracuse, New York 13201 1

General Electric Light Military Electronics Dept.
901 Broad Street
Utica, New York 13503 1

General Electric General Engineering Laboratory
Building 371, Room 478
Schenectady, New York 12305 1

General Electronics Laboratories, Inc.
Technical Library - Antennas
18 Ames Street
Cambridge, Mass 1

General Precision Laboratory
Technical Library - Antennas
63 Bedford Road
Pleasantville, N. Y. 1

Goodyear Aircraft Arizona Division
Antenna Department
Box. 85
Litchfield Park, Arizona 85340 1

Grumman Aircraft Engineering Corporation
Technical Library - Avionics Engineering
South Oyster Bay Road
Bethpage, N. Y. 1

Hallicrafters Company
Technical Library - Antennas
4401 West Fifth Avenue
Chicago, Illinois 60624 1

Hoffman Laboratories, Inc.
4501 North Arden Drive
El Monte, California 91734 1

Hughes Aircraft Corporation
Technical Library - Antennas
Centinela and Teale Streets
Culver City, California 90232 1

Hughes Aircraft Communications and Videosonics Div.
Antenna Section
1901 West Malvern Avenue
Fullerton, California 1

ITT Federal Laboratories
Technical Library - Antennas
500 Washington Ave.
Nutley, N. J. 07110 1

Laboratory for Electronics, Inc.
Antenna Department
1079 Commonwealth Avenue
Boston, Mass. 02115 1

Ling-Temco-Vought Military Electronics Div.
Librarian - Antennas
1200 Jupiter St.
Garland, Texas 1

Litton Systems, Amecom Division
Technical Library - Antennas
1140 E. W. Highway
Silver Spring, Md. 20910 1

Lockheed Marietta Division
South Cobb Drive
Marietta, Georgia 30061 1

Lockheed Electronic and Armaments System Office
P. O. Box 551
Burbank, California 91503 1

The Martin/Denver Division Headquarters
Antenna Laboratory Mail Nr. T-0453
P. O. Box 179
Denver, Colorado 80201 1

The Martin/Orlando Company
Technical Library - Microwaves
Box 5837
Orlando, Florida 1

The Martin/Baltimore Company
Technical Library - Antennas
Baltimore, Md. 21203 1

Maxon Electronics Corporation
Sunrise Highway
Great River, L. I., New York 11739 1

McDonnell Aircraft Corporation
Technical Library - Antennas
Box 516
St. Louis, Missouri 63166 1

Melpar, Inc.
Technical Library - Antennas
3000 Arlington Blvd.
Falls Church, Va. 22047 1

MITRE Corporation
Technical Library
Electronic Warfare Department D-21
Middlesex Turnpike
Bedford, Mass. 01730 1

Motorola Western Military Electronics Division
8201 E. McDowell
Scottsdale, Arizona 85252 1

North American Aviation, Inc.
Technical Library - Dept. 56
International Airport
Los Angeles, California 90009 1

North American Aviation, Autonetics Division
System Technology Department
3370 Miraloma Avenue
Anaheim, California 92803 1

North American Aviation/Columbus Division
Technical Library - Engineering Dept.
4300 E. Fifth Avenue
Columbus, Ohio 43216 1

Northrop/Norair Division
3901 West Broadway
Technical Information (3924-3)
Hawthorne, California 90250 1

Northrop/Ventura
Technical Information Center
1515 Rancho Conejo Blvd.
Newbury Park, Calfironia 91320 1

Philco Communications and Electronics
Government and Industrial Division
Technical Library - Antennas
4700 Wissachickon Ave.
Philadelphia, Pa. 19144 1

Radiation Systems, Inc.
Engineering Department
440 Swann Avenue
Alexandria, Va. 1

Radiation Products Division
Technical Library
Box 37
Melbourne, Fla. 31511 1

RCA Missile and Service Radar Division
Manager, Antenna Engineering Skill Center
Marne Highway
Moorestown, New Jersey 08057 1

Rantec Corporation
Librarian - Antenna Laboratory
24003 Ventura Blvd.
Calabasas, California 91302 1

Raytheon Equipment Division
Library - Mr. J. Portsch
P. O. Box 520
Waltham, Mass. 02154 1

Raytheon Missile Systems Division
Research Library
Hartwell Street
Bedford, Mass. 1

Raytheon Space and Information Systems Div.
528 Boston Post Road
Sudsbury, Mass. 1

Sanders Associates
Librarian - Antennas
95 Canal Street
Nashua, New Hampshire 1

Sichak Associates.
Mr. W. Sichak
518 Franklin Ave.
Nutley, New Jersey 1

HRB Singer Corporation
Attn: Library - Antennas
Box 60, Science Park
State College, Pa. 16801 1

Southwest Research Institute
Librarian - Antenna Laboratory
8500 Culebra Road
San Antonio, Texas 78206 1

Space Technology Laboratory
Research Library
One Space Park
Redondo Beach, California 90278 1

Sperry Gyroscope Division
Librarian - Antenna Laboratory
Great Neck, L. I., New York 11020 1

Sperry Microwave Electronics Division
Librarian - Antenna Laboratory
Box 1828
Clearwater, Florida 1

Stanford Research Institute
Librarian - Antennas
333 Ravenswood Street
Menlo Park, California 94025 1

Sylvania Electronic Products
Librarian - Antennas
Box 188
Mountain View, California 1

Sylvania Electronic Systems Division
Librarian - Antennas and Microwaves
40 Sylvan
Waltham, Mass 02154 1

Teledyne Communications System Division
12964 Panama Street
Los Angeles 66, California 1

Texas Instruments, Inc.
Librarian - Antennas
13500 N. Central Expressway
Dallas, Texas 75209 1

A. S. Thomas, Inc.
Librarian - Antennas
355 Providence Highway
Westwood, Mass. 02091 1

Westinghouse Aerospace Division
P. O. Box 746
Baltimore, Md. 21203 1

Wheeler Laboratories
Librarian - Antennas
Box 561
Smithtown, New York 11787 1

AFCRL C. J. Sletten CRD L G Hanscom Field Bedford, Mass. 01731	2
AFETRL - Technical Library Patrick AFB, Bla. 32925	1
AFMDC - Technical Library Holloman AFB, New Mexico 88330	1
APGC, Hq. 3208 Test Group Eglin AFB, Fla. 32542	1
ASD - ASEP B. Brooks Wright-Patterson AFB, Ohio 45433	1
RADC - EMATA, Griffiss AFB, New York 13442	1
RADC EMLT-1 Griffiss AFB, New York 13442	1
RADC EMIAD - R F Davis Griffiss AFB, New York 13442	1
SEG - SEAEM Mr. Mulligan Wright-Patterson AFB, Ohio 45433	1
SEG - SEACC Y. E. Stahler Wright-Patterson AFB, Ohio 45433	1
SEG - SEPIE Wright-Patterson AFB, Ohio 45433	1
AFSC - SCSE Andrews AFB, Wash. D. C. 20331	1
RTD - RTGS Bolling AFB, Washington, D. C. 20332	1
Hq, USAF, AFRDR, Lt. Col. B. Lieber Washington, D. C. 20330	1
Hq, USAF AFXSAI, Air Battle Analysis Center Dep. Dir. Plans for War Plans Washington, D. C. 20330	1
RTD RTHR Bolling AFB, Washington, D. C. 20332	1
FTD TD-EE Wright-Patterson AFB, Ohio 45433	1

U. S. Army Electronics Command
SIGRA/NAI
Ft. Monmouth, N J 1

U. S. Army White Sands Missile Range
Technical Library ORDBS-OM RR-312
White Sands, New Mexico 88002 1

Ballistic Research Laboratory
Technical Library - Antennas
Aberdeen Proving Ground, Md. 21005 1

Harry Diamond Laboratories
Connecticut Ave., and Vann Ness Street, NW
Attn: 240
Washington, D. C. 20438 1

U S Army Electronics R and D Activity
SELWS-ED
White Sands Missile Range, N. Mexico 88002 1

USAFSS
ESD/ESG Mr. A. Martinez
San Antonio, Texas 78241 1

Director, Surveillance Dept.
Evans Area
Technical Document Center
Belmar, New Jersey 1

ONR Branch Office
Box 39
FPO, New York 09510 1

Chief, Bureau of Ships
Code 312
Main Navy Building
Washington, D. C. 20360 1

Naval Research Laboratory
Code 5200
Washington, D. C. 20390 1

U S Naval Air Test Center
WSST-54, Antenna Section
Patuxent River, Md. 20910 1

Materials Laboratory
New York Naval Shipyard
Code 932
Brooklyn, N. Y. 11201 1

U. S. Navy Electronics Laboratory
Code 3220 - Library
San Diego, California 92152 1

U. S. Naval Ordnance Test Station
Mr. J. A. Mosko - Code 4021
China Lake, California 93557 1

U. S. Naval Ordnance Laboratory
Technical Library
Corona, California 91720 1

Office, Assist. Sec'y Def. R and D
Technical Library 3E1065, Pentagon
Washington, D. C. 20330 1

Air University Library
3T-AUL-59-30
Maxwell AFB, Alabama 36112 1

NASA Goddard Space Flight Center
Antenna Branch
Greenbelt, Md. 20771 1

V. DeSanti, Exchange Section DCD
Scientific/Technical Information Facility
P O Box 5700
Bethesda, Md. 1

GIT Engineering Experiment Station
Technical Library - Electronics Division
Atlanta, Ga. 30313 1

JHU Applied Physics Laboratory
8621 Georgia Avenue
Silver Springs, Md. 20910 1

JHU Carlyle Barton Laboratory
Charles and 34th Streets
Baltimore, Md. 22218 1

MIT-Lincoln Laboratory
Document Room
Box 73
Lexington, Mass. 02173 1

New Mexico State University
Antenna Department
Physical Science Dept.
University Park, New Mexico 1

U. S. Army Electronics Command
SIGRA/NAI
Ft. Monmouth, N J 1

U. S. Army White Sands Missile Range
Technical Library ORDBS-OM RR-312
White Sands, New Mexico 88002 1

Ballistic Research Laboratory
Technical Library - Antennas
Aberdeen Proving Ground, Md. 21005 1

Harry Diamond Laboratories
Connecticut Ave., and Vann Ness Street, NW
Attn: 240
Washington, D. C. 20438 1

U S Army Electronics R and D Activity
SELWS-ED
White Sands Missile Range, N. Mexico 88002 1

USAFSS
ESD/ESG Mr. A. Martinez
San Antonio, Texas 78241 1

Director, Surveillance Dept.
Evans Area
Technical Document Center
Belmar, New Jersey 1

ONR Branch Office
Box 39
FPO, New York 09510 1

Chief, Bureau of Ships
Code 312
Main Navy Building
Washington, D. C. 20360 1

Naval Research Laboratory
Code 5200
Washington, D. C. 20390 1

U S Naval Air Test Center
WSST-54, Antenna Section
Patuxent River, Md. 20910 1

Materials Laboratory
New York Naval Shipyard
Code 932
Brooklyn, N. Y. 11201 1

Northeastern University
Dodge Library
Boston, Mass. 02115 1

Ohio University
Technical Library - EE Dept.
Athens, Ohio 1

Ohio State University Research Foundation
Technical Library - Antenna Laboratory
2024 Neil Ave.
Columbus, Ohio 43210 1

Ohio State University Antenna Laboratory
Technical Library
1320 Kinnear Road
Columbus Ohio 43212 1

PIB Microwave Research Institute
Professor A. A. Oliner
55 Johnson St.
Brooklyn, N. Y. 11201 1

Stanford Electronics Laboratory
Librarian - Antennas
Stanford, California 94025 1

Syracuse University
Dr. Jose Perihi - Electrical Engineering Dept.
Syracuse, N. Y. 13210 1

University of Dayton Research Institute
Professor Douglas Hanneman
300 College Park
Dayton, Ohio 45409 1

University of Southern California
W. V. Trusch - EE Dept.
University Park
Los Angeles, California 90007 1

University of Texas - EE Res. Lab.
Route 4
Box 189
Austin, Texas 1

AF 33(615)-3609 Proj. 07848

Cornell Aeronautical Laboratory Research Library Buffalo, New York 14221	1
University of Illinois EE Res. Laboratory Engineering Experiment Station Urbana, Illinois	1
Air Force Avionics Laboratory AVWE-3 Wright-Patterson AFB, Ohio 45433	5 +reproducible
Defense Documentation Center Alexandria Virginia 22314	20 + card
	163 + reproducible

UNCLASSIFIED

Security Classification

DOCUMENT CONTROL DATA - R&D

(Security classification of title, body of abstract and indexing annotation must be entered when the overall report is classified)

1. ORIGINATING ACTIVITY (Corporate author)	2a. REPORT SECURITY CLASSIFICATION
The University of Michigan Radiation Laboratory Department of Electrical Engineering Ann Arbor, Michigan 48108	Unclassified
	2b. GROUP

3. REPORT TITLE

A Study of an Interdigital Array Antenna

4. DESCRIPTIVE NOTES (Type of report and inclusive dates)

Quarterly Report No. 5 1 February through 31 March 1967

5. AUTHOR(S) (Last name, first name, initial)

Pei Rin Wu

6. REPORT DATE	7a. TOTAL NO. OF PAGES	7b. NO. OF REFS
May 1967	193	34

8a. CONTRACT OR GRANT NO.	9a. ORIGINATOR'S REPORT NUMBER(S)
AF 33(615)-3600 b. PROJECT NO. 6278 c. Task 01 d.	7848-5-Q
	9b. OTHER REPORT NO(S) (Any other numbers that may be assigned this report) Quarterly Report No. 5

10. AVAILABILITY/LIMITATION NOTICES

Subject to special Export Controls (DoD Dir. 203. 4A FR 400-10); not to be disseminated to OTS. Qualified requestors may obtain copies from DDC.

11. SUPPLEMENTARY NOTES	12. SPONSORING MILITARY ACTIVITY
	Air Force Avionics Laboratory Research and Technology Division, AFSC Wright-Patterson AFB, Ohio 45433

13. ABSTRACT An interdigital array antenna has been devised and studied in this work as a useful antenna for certain applications. The theory of the linear antenna was used in the theoretical analysis to obtain the dispersion relation for a source free infinite interdigital array. In carrying out this analysis, the antenna-wave theory concept was used. This is essential if Floquet's Theorem is to be applied along with the antenna theory. The approximate solutions were obtained numerically through the use of the digital computer. The input impedance and the radiation pattern were also formulated for a finite array of 2N+1 elements with a voltage source applied between the ground plane and the grounded end of the center element of the array. The expressions were then computed numerically, through the computer, for an approximate solution.

It is found that an interdigital array antenna has a fairly wide frequency band for its broadside radiation at low frequencies. The field is polarized in a plane parallel to the plane containing the elements and perpendicular to the axis of the array along which the elements are spaced. The input resistance has been found to be 50Ω. However, when the frequency is increased and the length of each array element exceeds one quarter free space wavelength, the radiation pattern becomes twin lobed symmetrical about the broadside axis with the input resistance flustuating between 50Ω and 100Ω.

Several experimental models with 13, 14, 17 and 21 array elements were constructed and tested. The comparison between the theoretical dispersion characteristics and the experimental results after a correction for overall resonant length is close within the experimental error. The agreement between the theoretical solution and the experimental measurement of input impedance is reasonably good since the theory is based on an assumed current distribtuion. The vertical sections were not considered in the analysis. In view of this, an extended effort was given to experimental studies to determine the mechanism of the radation and the input impedance characteristics for both broadside and twin lobe radiation.

DD FORM 1 JAN 64 1473

UNCLASSIFIED

Security Classification

14. KEY WORDS	LINK A		LINK B		LINK C	
	ROLE	WT	ROLE	WT	ROLE	WT
Interdigital Antennas Digital Broadside Arrays Miniaturized Antennas						

INSTRUCTIONS

1. ORIGINATING ACTIVITY: Enter the name and address of the contractor, subcontractor, grantee, Department of Defense activity or other organization *(corporate author)* issuing the report.

2*a*. REPORT SECURITY CLASSIFICATION: Enter the overall security classification of the report. Indicate whether "Restricted Data" is included. Marking is to be in accordance with appropriate security regulations.

2*b*. GROUP: Automatic downgrading is specified in DoD Directive 5200.10 and Armed Forces Industrial Manual. Enter the group number. Also, when applicable, show that optional markings have been used for Group 3 and Group 4 as authorized.

3. REPORT TITLE: Enter the complete report title in all capital letters. Titles in all cases should be unclassified. If a meaningful title cannot be selected without classification, show title classification in all capitals in parenthesis immediately following the title.

4. DESCRIPTIVE NOTES: If appropriate, enter the type of report, e.g., interim, progress, summary, annual, or final. Give the inclusive dates when a specific reporting period is covered.

5. AUTHOR(S): Enter the name(s) of author(s) as shown on or in the report. Enter last name, first name, middle initial. If military, show rank and branch of service. The name of the principal author is an absolute minimum requirement.

6. REPORT DATE: Enter the date of the report as day, month, year; or month, year. If more than one date appears on the report, use date of publication.

7*a*. TOTAL NUMBER OF PAGES: The total page count should follow normal pagination procedures, i.e., enter the number of pages containing information.

7*b*. NUMBER OF REFERENCES: Enter the total number of references cited in the report.

8*a*. CONTRACT OR GRANT NUMBER: If appropriate, enter the applicable number of the contract or grant under which the report was written.

8*b*, 8*c*, & 8*d*. PROJECT NUMBER: Enter the appropriate military department identification, such as project number, subproject number, system numbers, task number, etc.

9*a*. ORIGINATOR'S REPORT NUMBER(S): Enter the official report number by which the document will be identified and controlled by the originating activity. This number must be unique to this report.

9*b*. OTHER REPORT NUMBER(S): If the report has been assigned any other report numbers *(either by the originator or by the sponsor)*, also enter this number(s).

10. AVAILABILITY/LIMITATION NOTICES: Enter any limitations on further dissemination of the report, other than those imposed by security classification, using standard statements such as:

(1) "Qualified requesters may obtain copies of this report from DDC."

(2) "Foreign announcement and dissemination of this report by DDC is not authorized."

(3) "U. S. Government agencies may obtain copies of this report directly from DDC. Other qualified DDC users shall request through _____."

(4) "U. S. military agencies may obtain copies of this report directly from DDC. Other qualified users shall request through _____."

(5) "All distribution of this report is controlled. Qualified DDC users shall request through _____."

If the report has been furnished to the Office of Technical Services, Department of Commerce, for sale to the public, indicate this fact and enter the price, if known.

11. SUPPLEMENTARY NOTES: Use for additional explanatory notes.

12. SPONSORING MILITARY ACTIVITY: Enter the name of the departmental project office or laboratory sponsoring *(paying for)* the research and development. Include address.

13. ABSTRACT: Enter an abstract giving a brief and factual summary of the document indicative of the report, even though it may also appear elsewhere in the body of the technical report. If additional space is required, a continuation sheet shall be attached.

It is highly desirable that the abstract of classified reports be unclassified. Each paragraph of the abstract shall end with an indication of the military security classification of the information in the paragraph, represented as *(TS), (S), (C), or (U)*.

There is no limitation on the length of the abstract. However, the suggested length is from 150 to 225 words.

14. KEY WORDS: Key words are technically meaningful terms or short phrases that characterize a report and may be used as index entries for cataloging the report. Key words must be selected so that no security classification is required. Identifiers, such as equipment model designation, trade name, military project code name, geographic location, may be used as key words but will be followed by an indication of technical context. The assignment of links, rules, and weights is optional.